AD _____

Armed Services Technical Information Agency

ARLINGTON HALL STATION
ARLINGTON 12 VIRGINIA

FOR

MICRO-CARD

CONTROL ONLY

CONFIDENTIAL

(2)

35097

APR 2 1958 ENG. PUBLICATIONS CONTROL NO.

R245-9

RYAN AERONAUTICAL COMPANY

LINDBERGH FIELD — SAN DIEGO, CALIFORNIA

CONFIDENTIAL

COPY NO. 9

6-80

R-792L

THE

ING

04.

LAW.

REPORT NO. 9220-2

1 October 1957

ESTIMATED PERFORMANCE, STABILITY AND CONTROL

RYAN MODEL 92 VERTICAL TAKE-OFF AIRPLANE

Contract Nonr 2139(00)

Prepared by: H. S. Price
H. S. Price
Aerodynamics Engineer

Approved by: N. W. Tillinghast Jr.
N. W. Tillinghast Jr.
Unit Chief, Dynamics

Prepared by: W. C. Parks
W. C. Parks
Aerodynamics Engineer

Approved by: R. A. Fuhrman
R. A. Fuhrman
Chief, Technical Section

Checked by: H. R. Burnett
H. R. Burnett
Aerodynamics Group Engineer

Approved by: F. Landgraf
F. Landgraf
Project Engineer

Checked by: N. W. Tillinghast
N. W. Tillinghast
Research Group Engineer

No. of Pages: 185

No. of Figures: 107

TABLE OF CONTENTS

LIST OF FIGURES

LIST OF TABLES

1.0 SUMMARY

This report presents the estimated performance, stability and control characteristics of the Ryan Model 92 research airplane. The Model 92 is a vertical and short field take-off airplane built to explore the full-scale flight characteristics of aircraft utilizing the deflected propeller slipstream principle.

The Model 92 has a maximum speed limitation of 185 knots, true airspeed, at sea level. This limitation has been imposed due to the dynamic pressure loads on the airframe. The data shown in this report indicate that a maximum speed of 195 knots, true airspeed, is possible at 25,000 feet.

Vertical take-off is made with forward and aft flaps deflected 35° (maximum deflection) and at military power setting. The model has vertical take-off capabilities up to 2940 pounds gross weight using military power on an ICAO standard day at sea level.

Performance transition characteristics were unknown at the time of this writing; consequently, no techniques or procedures have been analyzed.

Short field take-off characteristics are excellent since the thrust-to-weight ratio at military rated power (ICAO S.L. std. day) is 1.57. Operating in this power setting, the model requires only 90 feet ground distance from brake release to wheels off. Operating in normal rated power, the model requires 98 feet and in 50 percent normal rated power the model requires 287 feet. These figures are based on a gross weight of 2352

pounds on an ICAO standard day. On an Army-Navy-Hot Day, (103°F), the take-off distance is increased to 176 feet at the military power setting. The short field take-off calculations assumed the forward flap deflected 10 degrees and the aft flap deflected 11.6 degrees

The airplane is statically and dynamically stable in the conventional flight regime, though exhibiting a loosely coupled roll and sideslip motion in the lateral-directional mode. The damping of this short-period oscillation and the handling characteristics of the airplane can be improved by adding end plates to the horizontal tail and by extending the span of the existing wing-tip end plates.

In hovering flight the airplane motions are characterized by an unstable pitch oscillation and an aperiodic divergence in the lateral-directional mode. The pitch oscillation can be stabilized by increasing the pitch rate damping using an artificial damping device. Stabilization of the pitch oscillation makes the pitching motion easy to control and permits controlled flight to be maintained for extended periods of time.

The jet exhaust control nozzle provides adequate pitch and yaw control for trim in low speed flight. The induced yawing moments resulting from use of the hovering roll control in transition flight can be minimized by phasing this control out at low forward speeds following vertical take-off (below 30-40 knots).

2.0 INTRODUCTION

This report was written under the auspices of Item 4, Annex A, of MIL-C-5011A, Contract Nonr 2139(00) to assist pilot familiarization and present estimated performance, stability and control characteristics.

The Ryan Model 92 is a high-wing monoplane powered by a single Lycoming T-53 gas turbine engine located in the fuselage. Two three-bladed counter-rotating Hartzell propellers mounted on wing pylons are driven by the engine through a system of gears and shafting. Vertical take-off and landing is accomplished by redirecting the propeller slip-stream downward by deflecting the two large-chord, slotted wing flaps.

The performance portion of this report has been analyzed in four major divisions: (1) vertical take-off, (2) short field take-off, (3) transition, and (4) missions. Excellent research data was available for the vertical and short field take-off regimes; however, the transition flight regime investigation was seriously hampered by a lack of data for specific application to the Model 92. A wind tunnel test program, which is in progress at the Forrestal Research Institute, Princeton University, may provide much of the data necessary to adequately describe the transition flight regime of the Model 92.

The stability and control analysis is divided into three major sections which embrace the conventional, hovering, and transition flight regimes. Both stability and control characteristics in the conventional and hovering flight regimes are analyzed, whereas in the transition flight

regime consideration is given only to the control required for trim.

In conventional flight, aerodynamic control is obtained through the operation of an elevator, rudder and slot-lip ailerons. Normal control stick forces are provided by the aerodynamic hinge moments of each of these controls. The horizontal stabilizer is adjustable in flight for longitudinal trim.

For hovering and low-speed transition flight, pitch and yaw control are obtained from the reaction of the engine exhaust gases ejected from a controllable nozzle at the tail of the airplane. The exhaust nozzle is mechanically connected to and operates in conjunction with the elevator and rudder. Roll control in hovering flight is provided by differentially varying the pitch of the two propellers. Means are provided for phasing the hovering roll control in or out during transition. All of the maneuvering controls are operated by movement of the pilot's control stick and rudder pedals.

The conventional airplane stability and control characteristics were based on theoretical methods for estimating aerodynamic derivatives and from NACA wind tunnel test data.

Estimation of the hovering stability derivatives was based largely upon tests by NACA of propellers and models utilizing the deflected slipstream principle. Hovering control characteristics were based on test data obtained by the Contractor.

A three-view drawing of the Ryan Model 92 airplane is shown in Figure 2.1.

THREE-VIEW DRAWING - RYAN MODEL 92

Figure 2.1

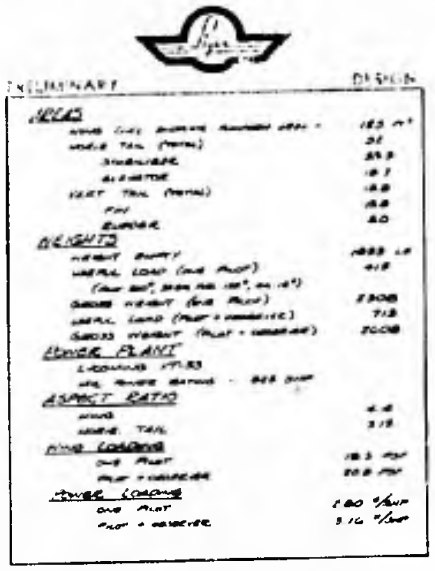

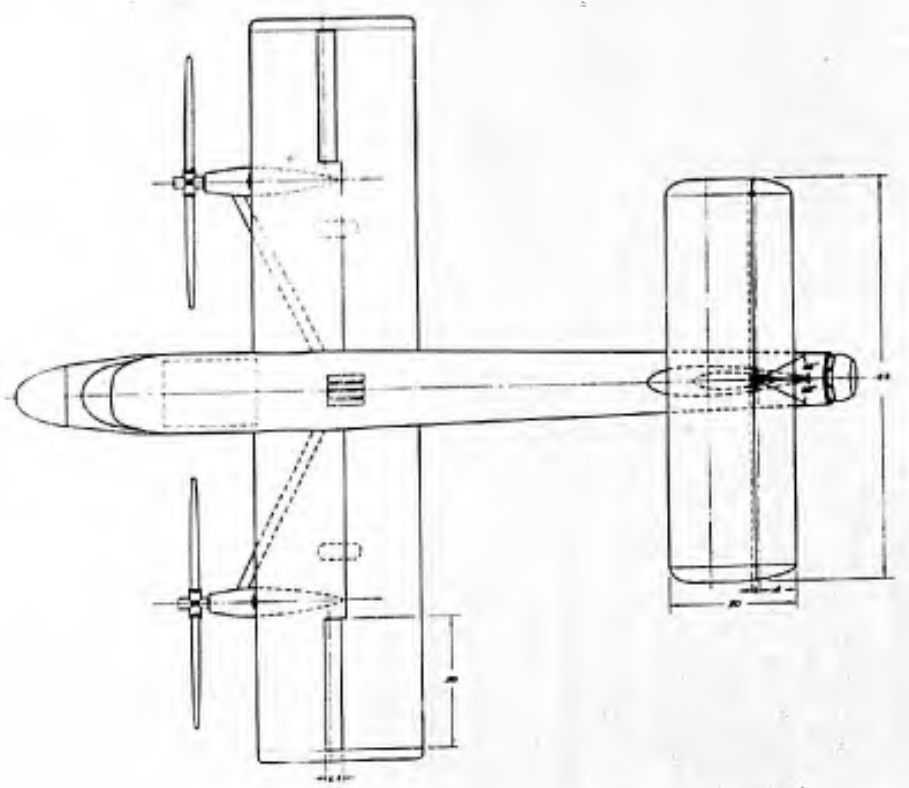

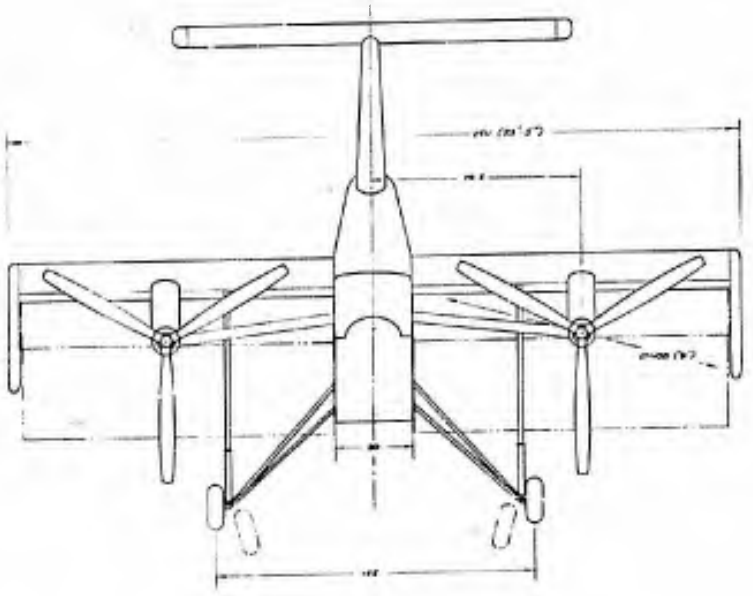

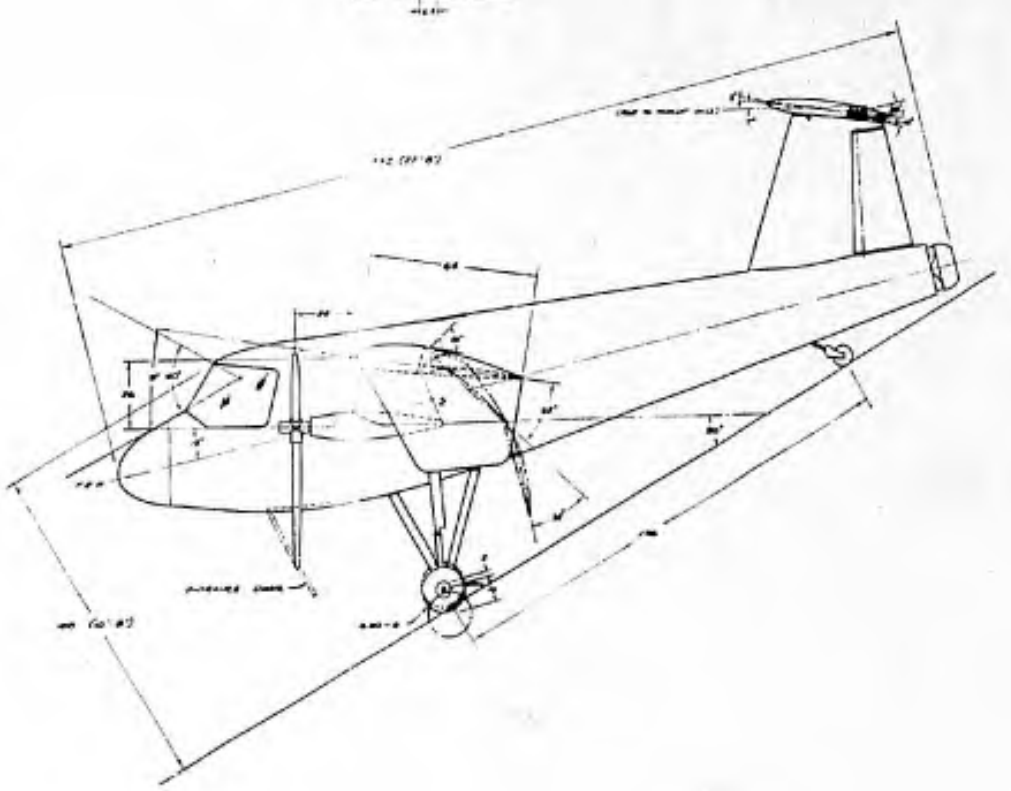

3.0 METHOD OF APPROACH

The method of approach used in analyzing the Model 92 required (1) defining the physical characteristics of the configuration, and (2) analyzing the configuration to determine its performance, stability and control characteristics.

3.1 Configuration Characteristics

3.1.1 Physical Characteristics

Wing

Area, theoretical planform, sq. ft.	125.00
Span, ft.	23.42
Aspect ratio	4.40
Mean aerodynamic chord, ft.	5.34
Taper ratio	1.00
Dihedral, deg.	0.00
Incidence, root and tip, with reference to fuselage reference line, deg.	22.00
Sweepback, quarter chord line, deg.	0.00
Airfoil, root, normal to L.E.	NACA 4418
Airfoil, tip, normal to L.E.	NACA 4418
Aileron hinge line, from wing L.E., percent of wing chord	42.00
Aileron area, one, sq. ft.	2.25
Aileron chord, normal to hinge line, ft.	0.542
Aileron span, along hinge line, ft.	4.16
Aileron deflection normal to axis of rotation, deg.	Up 50.00 Dwn 7.00

Flaps

Forward Flap

Area, planform, each, sq. ft.	33.95
Span, each, ft.	10.31
Aspect ratio, each	3.23
Mean aerodynamic chord, each, ft.	3.29
Taper ratio, each	1.00
Flap deflection normal to axis of rotation, deg.	Up 0.00 Dwn 35.00

Aft Flap

Area, planform, each, sq. ft.	30.75
Span, each, ft.	10.31
Aspect ratio, each	3.56
Mean aerodynamic chord, each, ft.	2.98
Taper ratio, each	1.00
Flap deflection normal to axis of rotation, deg.	Up 0.00 Dwn 35.00

Wing End Plates

Area, planform, each, sq. ft.	13.38
Span, each, ft.	3.20
Aspect ratio	0.83
Mean geometric chord, ft.	4.17
Taper ratio	0.55
Airfoil, root and tip, normal to L.E.	Circular L.E. with slab sides

Horizontal Tail

Area, theoretical planform, sq. ft.	52.00
Span, ft.	12.75
Aspect ratio	3.11
Mean aerodynamic chord, ft.	4.16
Taper ratio	1.00
Dihedral, deg.	0.00
Sweepback, quarter chord line, deg.	0.00
Airfoil, root and tip, normal to L.E.	NACA 0012
Elevator hinge line, percent tail chord	30.00
Elevator area, total, aft of hinge line, sq. ft.	15.50
Elevator chord, normal to and aft of hinge line, ft.	1.25
Elevator span, ft.	12.50
Elevator deflection, normal to axis of rotation, deg.	Up 20.00 Dwn 10.00
Incidence angle range measured with respect to propeller shaft axis, deg.	0 to +10

Vertical Tail

Area, sq. ft.	18.80
Span, ft.	4.48
Aspect ratio	1.07
Mean aerodynamic chord, ft.	4.20
Taper ratio	0.57
Sweepback, quarter chord line relative to top of fuselage, deg.	17.00
Airfoil root and tip, parallel to fuselage top contour	NACA 0018
Rudder, aft of hinge line, percent tail chord	31.20

Vertical Tail (Cont'd)

Rudder area, aft of hinge line, sq. ft.		5.00
Rudder chord, normal to hinge line, ft.		1.31
Rudder deflection, normal to axis of rotation, deg.	Left	25.00
	Right	25.00
Rudder height, ft.		3.75

Fuselage

Length, ft.	27.67
Maximum basic depth, ft.	5.44
Maximum basic width, ft.	2.56

Miscellaneous

Maximum height, ft. (static ground position)	10.67
Maximum length, ft.	27.67

Wetted Areas

Wing, sq. ft.	223.00
Flaps, sq. ft.	249.00
Horizontal Tail, sq. ft.	102.00
Vertical Tail, sq. ft.	37.00
Fuselage, sq. ft.	355.00
Pylons, gear boxes and drives, sq. ft.	40.00

3.1.2 Weights

The estimated weight and center of gravity data is as follows:

	WEIGHT, LBS.	c.g. LOCATION FUSELAGE STATION, IN.	c.g. LOCATION FUSELAGE WATER LINE, IN.
Weight Empty	1926.9	151.6	78.75
Gross Weight	2351.9	143.5	77.58

3.1.3 Power Plant

The power characteristics of the Model 92 required analysis from the standpoint of (1) the engine, and (2) the propellers.

3.1.3.1 Engine. The Model 92 contains the single YT-53-L-1 described in Reference 1. The engine output was determined at the output shaft by the following equation: (See Section 4.1.2.1)

$$BHP_{(output)} = SHP_{(spec)} (1 - 0.09)$$

Specification SHP was obtained from Reference 1.

The BHP at each propeller was determined by the following equation: (See Section 4.1.2.1)

$$BHP_{(prop)} = \frac{BHP_{(output)}}{2} (1 - 0.0125)$$

3.1.3.2 Propeller. The Model 92 has two three-bladed counter-rotating propellers whose blade-form curves are shown in Figure 8.1. These propellers are 9 feet, 2 inches in diameter and were manufactured by Hartzell Propeller, Incorporated. The propeller efficiency and resulting thrust were determined by the method contained in Reference 2.

3.1.4 Aerodynamic Characteristics

The lift and drag characteristics of the Model 92 were calculated for the flaps-up and down configurations by the methods shown in the following sections.

3.1.4.1 Drag Coefficient. The drag coefficient for the flaps-up

configuration was determined by a summation of the drag coefficients of the individual components. The component drag increments were obtained in the following manner:

(a) Wetted areas were determined for all the components.

(b) Equivalent drag areas were calculated by the methods of Reference 3.

(c) Incremental drag coefficients were calculated by the methods of References 3, 4, and 5.

(d) The drag coefficient for flaps-up and power-off was then found by a summation of all the calculated increments.

The drag coefficient increment for flap deflections was calculated by the methods shown in Reference 4.

3.1.4.2 Lift Coefficient. The lift coefficient for the flaps-up configuration was determined from the section characteristics of the NACA 4418 (Reference 6) and applied to the specific wing by standard aerodynamic practices.

The incremental lift coefficient due to flap deflection was calculated by the methods shown in Reference 4.

3.1.5 Thrust

Thrust required and thrust available are defined in the following sections.

3.1.5.1 Thrust Required. In level flight, the thrust required was

determined from the following equilibrium equations:

$$F_{nr} \sin\left(\alpha+i_{F_n}\right) + C_L qS - W = 0$$

$$F_{nr} \cos\left(\alpha+i_{F_n}\right) - C_D qS = 0$$

For the level flight regime, the wing angle of attack is used as the criteria and consequently the angle of thrust is a minus 9 degrees. (The symbols are defined in Section 6.0).

Solving for the lift coefficient gives:

$$C_L = \frac{W}{qS} - C_D \tan\left(\alpha+i_{F_n}\right)$$

In order to evaluate the thrust required from the above expression, in which the angle of attack is a variable, an iteration method of solution by an IBM 650 digital computer was utilized.

3.1.5.2 Thrust Available. The installed thrust available and corresponding fuel flow rates were determined in accordance with the methods contained in References 1 and 2.

The effect of individual engine and airframe characteristics on specification fuel flow was accounted for by a 5 percent increase as a service tolerance for all performance calculations.

3.2 Performance Characteristics

Performance characteristics were analyzed by the following methods

to determine maximum speed, stall speeds, rate of climb, service ceiling, climb to altitude, endurance, and range.

3.2.1 Flight Envelope

3.2.1.1 Maximum Speed. The maximum speed in level flight was determined by the intersection of the thrust required and available curves.

3.2.1.2 Stall Speed. The power-on stall speed for no flap deflection was determined from the following equation:

$$V_T = \sqrt{\frac{W - F_n \sin\left(\alpha + i_{F_n}\right)}{178\,\rho\left(C_{L_{MAX}}\right)_{TRIM}}}$$

Solving for stall speed involves successive approximations, since C_L, α, and F_n vary with true airspeed. Values for stall speed were assumed and corresponding values of $C_{L_{MAX}}$ were calculated. The intersection of the locus of these points with the $\left(C_{L_{MAX}}\right)_{TRIM}$ curve is the stall speed.

The power-off stall speed for no flap deflection was determined from the following expression:

$$V_T = \sqrt{\frac{W}{178\,\rho\left(C_{L_{MAX}}\right)_{TRIM}}}$$

Solving for the power-off stall speed involves the same iterative procedure as for power-on stall speed.

3.2.2 Rate of Climb

Rates of climb or descent were computed from the following expression:

$$R/C = 101.4\, V_T \left[\frac{F_{na}}{W} \cos i_{F_n} - \frac{C_D}{C_L} \left(\cos \gamma - \frac{F_{na}}{W} \sin i_{F_n} \right) \right] \left[\frac{1}{1 + \frac{(1.69)^2}{g} V_T \frac{dv}{dh}} \right]$$

Rates of climb were calculated only for the flaps undeflected configuration.

3.2.3 Service Ceiling

Service ceilings for the Model 92 were not determined due to the lack of engine data above 25,000 feet and are not considered important for this aircraft.

3.2.4 Climb to Altitude

3.2.4.1 Climb Schedule. The climb schedule was obtained from the rates of climb curves and may or may not be the peaks of the curves. The ease with which a pilot may fly a given climb schedule dictates the climb schedule within limits.

3.2.4.2 Time to Climb. The time to climb from one altitude to another altitude was determined from:

$$t = \frac{h_2 - h_1}{x \left(\frac{r}{c} \right)_1}$$

3.2.4.3 Fuel Used in Climb. The fuel used in climbing from one altitude to another altitude was determined from:

$$W_{fh} = \left[(W_f)_1 - \left\{ (W_f)_1 - (W_f)_2 \right\} Z \right] t$$

3.2.4.4 Horizontal Distance Gained in Climb. The horizontal distance

gained in climbing from one altitude to another altitude was determined from:

$$S_{N.M.} = \left[V_3 \cos \gamma_3 - (V_c \cos \gamma_3 - V_4 \cos \gamma_4)\ Z \right] \frac{t}{60}$$

3.2.5 Endurance

Endurance was obtained by the following sequence:

(a) The time and fuel used in a climb were part of the results of the IBM 650 computations.

(b) Subtracting the amount of fuel used in climb gave the fuel remaining for cruise.

(c) Knowing the power setting and the fuel flow, the endurance in minutes was calculated for the cruising fuel.

(d) Adding the time used in climb to the cruise time results in the total endurance.

3.2.6 Range

Range was obtained by the following sequence:

(a) The horizontal distance and fuel used in a climb were part of the results of the IBM 650 computations.

(b) Subtracting the amount of fuel used in a climb gave the fuel remaining for cruise.

(c) Knowing the power setting and the fuel flow, the range in terms of nautical miles was calculated for the cruising fuel.

(d) Adding the distance gained in climb to the distance made in cruise results in the total range.

3.2.7 Wing Angle of Attack in Climb

The wing angle of attack in a climb was obtained from the same group of calculations on the IBM 650 digital computer which produced the rates of climb.

3.3 Take-Off Characteristics

3.3.1 STO

Short take-off characteristics were calculated for flaps deflected (forward flap 10^{o}, aft flap 11.6^{o}) by the following expression:

$$S_G = \frac{V_1 - V_o}{6}\left[\frac{V_o}{a} + 4\left(\frac{V_{1/2}}{a}\right) + \frac{V_1}{a}\right] + \frac{V_2 - V_1}{6}\left[\frac{V_1}{a} + 4\left(\frac{\frac{V_1 + V_2}{2}}{a}\right) + \frac{V_2}{a}\right]$$

Hot day calculations were based on ANA standard hot day data (103^{o}F at Sea Level).

3.3.2 VTO

Vertical take-off characteristics were calculated from the data of References 7, 8, 9, 10 and 11. The VTO capabilities are based on the experimental result that 80 percent of the thrust is turned into lift after leaving ground effects.

Hot day calculations were based on ANA standard hot day data which specifies 103^{o}F at sea level.

3.3.3 Transition Characteristics

The transition characteristics of the Model 92 were not known at the time of this writing. Consequently, no attempt has been made to analyze

this flight regime.

3.4 Stability and Control

The stability and control characteristics of the Model 92 airplane are based upon experimental test data and theoretical methods of estimation. The methods for determining the stability and control of the airplane in conventional and hovering flight and a brief treatment of the trim problem in transition flight are presented in this section.

3.4.1 Conventional Flight

The major aerodynamic and physical characteristics used in the conventional flight static stability and control analysis are given in Table 3.1.

3.4.1.1 Longitudinal Static Stability and Control

The stick-fixed, static longitudinal stability level of the airplane is given by

$$\left(\frac{dC_m}{dC_L}\right)_{airplane} = \left(\frac{x_{c.g.}}{\bar{c}} - \frac{x_{a.c.}}{\bar{c}}\right)_{wing} + \left(\frac{dC_m}{dC_L}\right)_{\substack{fuse.\\nac.}} + \left(\frac{dC_m}{dC_L}\right)_{power} + \left(\frac{dC_m}{dC_L}\right)_{t} \qquad (1)$$

The stability contributions of the fuselage, nacelles and power were determined by the methods outlined in References 3 and 12. The contribution of the horizontal tail may be expressed by

$$\left(\frac{dC_m}{dC_L}\right)_t = - \frac{\left(C_{L_\alpha}\right)_t}{\left(C_{L_\alpha}\right)_w} \bar{V} \eta_t (1 - d\epsilon/d\alpha) \frac{\left(C_{L_\alpha}\right)_w}{\left(C_{L_\alpha}\right)_{total}} \qquad (2)$$

where the downwash parameter, $d\epsilon/d\alpha$, was estimated from the charts of Reference 13.

The neutral point was found by setting equation (1) equal to zero and solving for $\frac{x_{c.g.}}{\bar{c}}$.

Due to the large size of the horizontal tail relative to the wing, the wing lift curve was corrected to include the tail lift by the following expression

$$\left(C_{L_\alpha}\right)_{total} = \left(C_{L_\alpha}\right)_w + \left(C_{L_\alpha}\right)_t \frac{S_t}{S_w} \qquad (3)$$

The static longitudinal stability of the airplane with the longitudinal controls free is given by equations (1) and (2) with the tail term rewritten as follows:

$$\left(\frac{dC_m}{dC_L}\right)_t = - \frac{\left(C_{L_\alpha}\right)_t}{\left(C_{L_\alpha}\right)_w} \bar{V}\, \eta_t\, (1 - d\epsilon/d\alpha) \frac{\left(C_{L_\alpha}\right)_w}{\left(C_{L_\alpha}\right)_{total}} \left(1 - \frac{C_{h_\alpha \tau}}{C_{h_\delta}}\right)$$

$$+ \frac{C_{h_\alpha} (1 - d\epsilon/d\alpha)}{C_{h_\delta} \left(C_{L_\alpha}\right)_w} \frac{dT_n}{d\delta_e} \frac{\ell_n C_L}{W \bar{c}} \frac{\left(C_{L_\alpha}\right)_w}{\left(C_{L_\alpha}\right)_{total}} \qquad (4)$$

The first term of the above expression gives the tail contribution to stability with the elevator free and the second term represents the effect of the tail exhaust nozzle which is mechanically connected to and "floats" with the elevator. The stick-free neutral point was found in the same manner as for the stick-fixed condition.

The elevator hinge moment coefficients were based on the two-dimensional wind tunnel data of Reference 14.

The section data was corrected for wind tunnel effects and trailing edge angle as indicated in Reference 14 and finally corrected to three-dimensional flow by the method given in Reference 3.

The general expression for longitudinal stick force is taken from equation (6-48) of Reference 3.

$$F_s = K \frac{1}{2} \rho V^2 A - K(W/S) \frac{C_{h_\delta}}{C_{m_\delta}} \left(\frac{dC_m}{dC_L}\right)_{free} \qquad (5)$$

where

$$K = -G S_e c_e \eta_t$$

$$A = C_{h_\alpha} (\alpha_o - i_w + i_t) + C_{h_\delta} \delta_{e_o}$$

The gradient of stick force with normal load factor was obtained from

$$\frac{dF_s}{d_n} = \frac{K (W/S) C_{h_\delta}}{C_{m_\delta}} \left(\frac{dC_m}{dC_L}\right)_{free} - 57.3 K g l_t \rho/2 \left(C_{h_\alpha} - \frac{1.1 C_{h_\delta}}{\tau}\right) \qquad (6)$$

In order to determine the c.g. limits for normal airplane flight the following conditions were considered:

A. Limits on forward c.g.

1. maximum stick force per g gradient
2. maximum up elevator deflection in landing configuration

B. Limits on aft c.g.

1. power on stick-free neutral point
2. minimum stick force per g gradient

The most forward permissable c.g. position for maximum up elevator deflection for the landing condition was found from:

$$\frac{x_{c.g.}}{\bar{c}} = \frac{x_{a.c.}}{\bar{c}} - \frac{C_{m_\delta}}{C_{L_{max}}}\left[\epsilon_{e_{max}} + \left(\frac{\alpha_w - \epsilon - i_w + i_t}{\tau}\right) + \frac{C_{m_{a.c.}}}{C_{m_\delta}} + \frac{C_{m_{fus}}}{C_{m_\delta}} + \frac{C_{m_{nac}}}{C_{m_\delta}} + \frac{C_{m_{power}}}{C_{m_\delta}}\right] \quad (7)$$

where the wing and tail angles of attack were modified due to the ground effect.

For the purposes of this report, the c.g. positions as given in per cent mean aerodynamic chord are projected normal to the thrust axis which is the basic airplane reference.

3.4.1.2 Static Directional Stability and Control. The static directional stability level of the airplane is given by the following expression from Reference 3 :

$$\left(C_{n_\beta}\right)_{airplane} = \left(C_{n_\beta}\right)_{\substack{fus.\\nac.}} + \left(C_{n_\beta}\right)_{prop} + \Delta_1 C_{n_\beta} + \Delta_2 C_{n_\beta} + \left(C_{L_\alpha}\right)_v \frac{S_v \ell_v \eta_v}{S_w b} \quad (8)$$

The contributions of the fuselage, nacelles, propellers and interference effects were obtained by the methods of Reference 3. The vertical tail size was determined which provides the airplane directional stability level given by the following expression:

$$\left(C_{n_\beta}\right)_{desirable} = .0005\left(\frac{W}{b^2}\right)^{\frac{1}{2}} \quad (9)$$

The directional static stability of the airplane with the rudder free is given by equation (8) with the tail term rewritten as follows:

$$\left(C_{n_\beta}\right)_v = \left(C_{L_\alpha}\right)_v \frac{S_v \ell_v \eta_v}{S_w b} \left(1 - \frac{C_{h_{\alpha_{V_T}}}}{C_{h_{\delta_r}}}\right) - \frac{dT_n}{d\delta_r} \frac{\ell_n}{qS_w b} \frac{C_{h_{\alpha_v}}}{C_{h_{\delta_r}}} \qquad (10)$$

The first term of the above expression represents the vertical tail contribution with the rudder free and the second term the contribution of the exhaust nozzle which "floats" with the rudder.

The rudder hinge moment coefficients were determined from the hinge moment parameters given in Reference 15. The pedal forces were then calculated from the following expression:

$$PF = G_r q S_r \bar{c}_r \left[\left(C_{h_\alpha}\right)_v \beta - C_{h_{\delta_r}} \frac{\left(C_{n_\beta}\right)_{fix}}{C_{n_{\delta_r}}} \beta \right] \qquad (11)$$

3.4.1.3 Lateral Control

The rolling moment and yawing moment coefficients due to slot-lip aileron deflection were interpolated from the data of Figures 15 and 16 of Reference 16 for a .42 c_w aileron location for zero flap deflection.

The hinge moment coefficients due to a slot-lip aileron deflection were interpolated from the data of Figures 15 and 17 of Reference 17 for a .42 c_w aileron location and aileron hinge location of .25 c_a.

The lateral stick forces were calculated from the following expression:

$$F_s = \frac{\rho}{2} V^2 S_a \bar{c}_a \left[G_R C_{h_R} - G_L C_{h_L} \right] \qquad (12)$$

The aileron-stick gearing ratios for the right and left aileron were determined by assuming a variation of aileron deflection with stick position.

The rolling velocity parameter, $pb/_{2V}$, was calculated for a maximum lateral control stick force of 30 pounds by setting equation (12) equal to 30 pounds and determining the allowable aileron deflection and aileron hinge moment for various speeds. The rolling moment coefficients corresponding to these allowable deflections were then used to calculate the resulting values of $pb/_{2V}$.

$$\frac{pb}{2V} = - \frac{C_l}{C_{l_p}} \tag{13}$$

where $C_{l_p} = \frac{d C_l}{d \frac{pb}{2V}}$, the damping in roll parameter, was obtained by method 1 of Reference 18.

3.4.1.4 Dynamic Stability. The dynamic stability of the Model 92 in the conventional airplane flight regime was investigated for zero flap deflection. The three-degree-of-freedom investigations of the longitudinal and lateral stability were conducted by solution of the equations of motion on an IBM 650 digital computer and an analog computer. These results were subsequently supplemented by a five-degree-of-freedom normal flight simulation by using two PACE analog computers and a cockpit equipped with control stick and rudder pedals and a CRT oscilloscope display of pitch, roll and yaw motions.

The equations of motion used to determine the characteristic longitudinal three-degree-of-freedom solution are given as follows:

$$\dot{u} + g\theta \cos \gamma_o - X_u u - X_w w = 0 \tag{14}$$

$$\dot{w} - V q + g \theta \sin \gamma_o - Z_u u - Z_w w - Z_{\dot{w}} \dot{w} - Z_q q = 0 \tag{15}$$

$$\dot{q} = M_u u - M_w w - M_{\dot{w}} \dot{w} - M_q q = 0 \tag{16}$$

These equations represent the longitudinal motions of the airplane about a system of stability axes for small perturbations. The stability axes system is shown in Figure 7.1.

The dimensional stability derivative parameters in the equations of motion are derived in Reference 19. The non-dimensional static stability derivatives were developed from the static stability analysis in Section 3.4.1.1 and the non-dimensional damping derivatives were calculated using the expressions given in Reference 19.

The equations of motion used to determine the characteristic lateral-directional three-degree-of-freedom solution are given as follows:

$$\dot{\beta} + r - \frac{g}{V}\varphi\cos\gamma_o - \frac{g}{V}\Psi\sin\gamma_o - Y_v\beta = 0 \qquad (17)$$

$$\dot{p} - \dot{r}\frac{I_{xz}}{I_x} - L'_\beta\beta - L'_p p - L'_r r = 0 \qquad (18)$$

$$\dot{r} - \dot{p}\frac{I_{xz}}{I_z} - N_\beta\beta - N_p p - N_r r = 0 \qquad (19)$$

These equations represent the lateral-directional motions of the airplane about a system of stability axes for small perturbations.

The dihedral effect of the airplane was assumed to consist of contributions of the wing position on the fuselage, the wing-tip end plates and the vertical tail. In equation form,

$$C_{l_\beta} = \left[\left(\Delta C_{l_\beta}\right)_1 + \left(\Delta C_{l_\beta}\right)_2\right]_{\text{wing}} + \left(\Delta C_{l_\beta}\right)_{\substack{\text{end}\\\text{plates}}} - \left(C_{L_\alpha}\right)_v \frac{S_v z_v \eta_v}{S_w b} \qquad (20)$$

The increments due to the wing were determined from Reference 3 and the end plate effect was estimated from the wind tunnel data of References 20 and 21. The tail term is the sideforce on the vertical tail times the distance from the tail center of pressure to the X axis.

The sideforce derivative is broken down as follows:

$$C_{Y_\beta} = \left(C_{Y_\beta}\right)_{fuse} + \left(C_{Y_\beta}\right)_{props} + \left(C_{Y_\beta}\right)_{V} + \left(C_{Y_\beta}\right)_{\substack{end \\ plates}} \qquad (21)$$

The propeller and vertical tail contributions were determined from the static directional stability derivatives developed in Section 3.4.1.2. The fuselage contribution was obtained from Table 10 of Reference 15 and the end plate effect was estimated from the data of Reference 20.

The cross or rotary derivatives are given by:

$$C_{n_p} = \left(C_{n_p}\right)_{W} + \left(C_{n_p}\right)_{V} \qquad (22)$$

$$C_{l_r} = \left(C_{l_r}\right)_{W} + \left(C_{l_r}\right)_{V} \qquad (23)$$

The wing derivatives were estimated from Figures 10 and 13 of Reference 22 and the tail terms were calculated from equations (21) and (30) of the same reference.

The damping derivatives are given by:

$$C_{n_r} = \left(C_{n_r}\right)_{W} + \left(C_{n_r}\right)_{V} \qquad (24)$$

$$C_{l_p} = \left(C_{l_p}\right)_{W} + \left(C_{l_p}\right)_{V} \qquad (25)$$

The wing damping in yaw was estimated from Figure 13 of Reference 23 and the wing damping in roll was estimated from Method 1 of Reference 18. The vertical tail contributions to yaw and roll damping were calculated from equations (29a) and (24) of Reference 22.

A conventional flight simulation was set up on analog computers to facilitate studying the effects of changes in aircraft geometry on the stability and control characteristics of the airplane and to investigate the effectiveness of the various controls. The stability derivatives used were for the controls-fixed condition.

The degrees of freedom used in the study were reduced to five by assuming no change in forward velocity from a given trim speed, thus eliminating the equation representing motion along the flight path. The equations of motion used in the 5 degree of freedom study for a system of stability axes are given as follows:

$$\dot{v} = pw - rV + g\Psi \sin \gamma_o + g\varphi \cos \gamma_o + Y_\beta \beta + Y_{\delta_r} \delta_r \qquad (26)$$

$$\dot{w} = qV - pv + g \cos \gamma_o + Z_\alpha \alpha + Z_{\delta_e} \delta_e \qquad (27)$$

$$\dot{p} = (\dot{r} + pq) \frac{I_{xz}}{I_x} - \left(\frac{I_z - I_y}{I_x}\right) qr + L'_\beta \beta + L'_{\delta_a} \delta_a + L'_{\delta_r} \delta_r + L'_p p + L'_r r \qquad (28)$$

$$\dot{q} = (r^2 - p^2) \frac{I_{xz}}{I_y} + \left(\frac{I_z - I_x}{I_y}\right) pr + M_\alpha \alpha + M_{\delta_e} \delta_e + M_{\dot{\alpha}} \dot{\alpha} + M_q q \qquad (29)$$

$$\dot{r} = (\dot{p} - qr) \frac{I_{xz}}{I_z} - \left(\frac{I_y - I_x}{I_z}\right) pq + N_\beta \beta + N_{\delta_r} \delta_r + N_{\delta_a} \delta_a + N_p p + N_r r \qquad (30)$$

The aerodynamic derivatives used in both the 3 degree and 5 degree of freedom studies are presented in Table 3.2.

3.4.2 Hovering Control

3.4.2.1 Pitch and Yaw Control. Control in pitch and yaw is obtained by directing the engine exhaust gases through a swiveling nozzle at the tail of the airplane. The thrust forces expected from the nozzling action were determined from tests of a 1/3 scale model of the nozzle conducted by the Contractor.

The magnitude of the maximum nozzle thrust is such as to provide a minimum angular acceleration of the airplane about the pitch axis of approximately one rad/sec^2 and a minimum of 0.6 rad/sec^2 about the yaw axis.

The nozzle is controlled by moving the pilot's rudder pedals for yaw control and the control stick longitudinally for pitch control.

The forces available for pitch and yaw control were obtained from the following expressions:

$$T_{pitch} = \frac{\delta_{pn}}{\delta_n} T_n \qquad (31)$$

and

$$T_{yaw} = \frac{\delta_{yn}}{\delta_n} T_n \qquad (32)$$

where δ_n is the absolute nozzle deflection from the neutral position.

3.4.2.2 Roll Control. Hovering roll control is obtained by differentially varying the blade pitch of the two propellers by moving the control stick laterally.

The rolling moments and yawing moments due to differential pitch were estimated from test data of Reference 7 by the following procedure:

1. The measured rolling and yawing moments were plotted versus propeller r.p.m. for blade angles of 6.9 and 8.9 degrees. (Runs 28 and 29). The rolling and yawing moments at 2000 r.p.m. were then selected as being representative of actual operating conditions.
2. As the propeller torque reaction opposed the aerodynamic rolling moment of the Model 88, an estimated torque was calculated from

$$Q = \frac{-BHP \times 550}{2\pi n} \qquad (33)$$

The torque was algebraically subtracted from the measured rolling moment to obtain the net rolling moment

3. The estimated hovering control rolling moment per degree of differential pitch and the associated yawing moment, about axes parallel and perpendicular respectively to the thrust axis were calculated from:

$$\frac{dL'}{d(\Delta\beta)} = \left[\left(\frac{\Delta L'}{\Delta\beta}\right)_{\text{Model 88}} \times \frac{y}{(y)_{88}} + \frac{dQ}{d(\Delta\beta)}\right] 2 \qquad (34)$$

and

$$\frac{dN}{d(\Delta\beta)} = \left[\left(\frac{\Delta N}{\Delta\beta}\right)_{\text{Model 88}} \times \frac{y}{(y)_{88}} \times 2 \qquad (35)$$

where $\frac{dQ}{d(\Delta\beta)}$ is the torque reaction due to blade pitch change and which is favorable in the case of the Model 92 with counter-rotating propellers.

The amount of differential pitch required for roll control was such as to provide a minimum angular acceleration of one rad/sec^2 about an axis parallel to the thrust axis.

3.4.3 Hovering Stability

It is beyond the scope of this report to present the analytical methods used for estimating the hovering stability derivatives. In general, the derivatives were based upon estimated effects of the propeller slipstream (Reference 7 and NACA literature) due to small motions of the airplane and upon the direct forces and moments on the propellers themselves.

Inasmuch as the test data of Reference 7 was obtained in ground effect and the NACA propeller data was obtained out of ground effect, no attempt was made to define the hovering stability analysis as applying strictly either in or out of ground effect.

During the course of the hovering simulation a time constant of .25 seconds was used to simulate the time lag in the propeller hydraulic pitch-change mechaniam.

The simulator consisted of two PACE analog computers and the cockpit described in Section 3.4 1.4. In addition to the pitch, roll, and yaw display, side velocity, forward velocity and altitude were presented to the pilot on instruments in the cockpit. Propeller thrust was controlled by simulating the collective pitch control lever of the airplane.

3.4.3.1 Basic Equations. A system of body axes, as shown in Figure 7.2, was used for the hovering flight analysis. The values of the aerodynamic and control derivatives are tabulated in Table 3.3.

The equations of motion representing six degrees of freedom about the body axes system are given as follows:

$$\dot{u} = vr - wq - g \cos \Theta_o \theta + X_u u + X_w w + X_{\delta_{pn}} \delta_{pn} + X_T T \qquad (36)$$

$$\dot{w} = uq - vp + Z_u u + Z_w w + Z_{\delta_{pn}} \delta_{pn} + Z_T T \qquad (37)$$

$$\dot{q} = - \frac{rp\,(I_x - I_z)}{I_y} + \frac{(r^2 - p^2)}{I_y} I_{xz} + M_u u + M_w w + M_{\dot{\theta}} \dot{\theta} + M_{\delta_{pn}} \delta_{pn} + M_T T \qquad (38)$$

$$\dot{v} = wp - ur + g \cos \Theta_o \Phi + g \sin \Theta_o \Psi + Y_v v + Y_{\delta_{yn}} \delta_{yn} \qquad (39)$$

$$\dot{p} = \frac{I_{xz}}{I_x} (\dot{r} + pq) - qr \left(\frac{I_z - I_y}{I_x} \right) + L'_v v + L'_{\dot{\varphi}} \dot{\varphi} + L'_{\dot{\Psi}} \dot{\Psi} + L'_{\Delta\beta} \Delta\beta + L'_{\delta_{y_n}} \delta_{y_n} \qquad (40)$$

$$\dot{r} = \frac{I_{xz}}{I_z} (\dot{p} - qr) - pq \left(\frac{I_y - I_x}{I_z} \right) + N_v v + N_{\dot{\varphi}} \dot{\varphi} + N_{\dot{\Psi}} \dot{\Psi} + N_{\delta_{y_n}} \delta_{y_n} + N_{\Delta\beta} \Delta\beta \qquad (41)$$

3.4.3.2 Assumption and Limitations. The assumptions and limitations used in the hovering stability and control analysis are listed as follows:

1. The X axis was assumed parallel to the thrust axis and to act through the center of gravity.
2. The aerodynamic derivatives were assumed to be linear and to hold for small motions about a trimmed condition.
3. The aerodynamic derivatives were not assumed to hold for steady-state translational velocities other than zero.
4. The effect of free stream velocity was assumed to be small and was neglected.
5. The engine angular momentum is small and engine gyroscopic forces were neglected.

3.4.4 Transition Flight

3.4.4.1 Longitudinal Trim in Low-Speed Flight. In order to obtain representative data on the trim problem in transition, use was made of model test data reported in Reference 10. Although these test results are not directly appliable to the Model 92 due to differences in geometry, c.g. location, number of propellers, etc., the data are representative of a flapped wing-propellar combination and are used herein to indicate general magnitudes of the trim forces required.

The method of Reference 11 was used in applying the data of Reference 10 to obtain relationships between propeller thrust, airspeed, and lift at zero longitudinal force for a wing loading of 20 lbs/ft^2. The pitching moment coefficients corresponding to the available lift coefficients were then used to calculate the required trim forces. The nozzle thrust required was calculated from

$$T_n = \left[C_m \text{ "q" } S\bar{c} - C_{L_t} q_t S_t \ell_t \right] \frac{1}{\ell_n} \qquad (42)$$

For the hovering case, the untrimmed pitching moment was obtained from Figure 8 of Reference 24.

3.4.4.2 Directional Trim in Low-Speed Flight. Due to the lack of lateral-directional aerodynamic data of deflected slipstream aircraft in low speed flight, the directional trim problem was considered to arise solely from yawing moments induced by use of the hovering roll control.

The thrust required, obtained by the method of Section 3.4.4.1, was converted to propeller thrust coefficient form in order to find the propeller blade angles required for the speed range investigated. The blade angle and the rate of change of thrust coefficient with blade angle change were found from the curves of Reference 25.

The nozzle thrust required to trim the yawing moments due to the differential propeller thrust was calculated from

$$T_n = \left[2y \rho n^2 D^4 \left(dC_{T/d\beta}\right) \Delta\beta - C_{n_{\delta_r}} q Sb \delta_r \right] \frac{1}{\ell_n} \qquad (43)$$

3.4.5 Moments of Inertia

The airplane moments of inertia were obtained from the detailed weight and balance statements. The moments of inertia used in the conventional flight dynamic stability analysis were based upon a gross weight of 2308 pounds and are shown in Figure 3.1 as a function of angle of attack.

The moments of inertia used in the hovering stability analysis were based upon a revised gross weight of 2352 pounds and the body axes values are given in Table 3.3.

TABLE 3.1

AERODYNAMIC AND PHYSICAL CHARACTERISTICS USED FOR STATIC STABILITY AND CONTROL ANALYSIS

	δ_f = (0/0)°	δ_f = (10/11.6)°
General:		
BHP	100	120
W/S	19	19
Wing:		
AR (effective)	5.0	5.0
$(C_{L_\alpha})_W$ per deg.	.0655	.0784
$(C_{L_\alpha})_{Total}$ per deg.	.0866	.100
$C_{m_{a.c.}}$	-.0967	-.280
$\frac{x_{a.c.}}{\bar{c}}$	.250	.270
i_w (measured from thrust line)degs.	9.0	9.0
Horizontal Tail:		
C_{L_α} per deg.	.052	.052
C_{h_α} per deg.	-.0020	-.0020
C_{h_δ} per deg.	-.0070	-.0070
C_{m_δ} per deg.	-.0234	-.0234
τ	.47	.47
η	1.0	1.0
ℓ_t ft.	12.25	12.25
$d\epsilon/d\alpha$	.15	.20
G rad/ft	.63	.63

TABLE 3.1 (Cont'd)

	$\delta_f = (0/0)^o$
Vertical Tail:	
AR (effective)	1.66
C_{L_α} per deg.	.042
C_{h_α} per deg.	- .00322
C_{h_δ} per deg.	- .0114
$C_{n_{\delta_r}}$ per deg.	- .001275
τ	.40
η	1.0
ℓ_v ft.	11.8
G rad/ft.	1.48
Control Nozzle:	
ℓ_n ft.	16.0
$dT_n/d\delta_e$ lbs/deg.	12.0
$dT_n/d\delta_r$ lbs/deg.	7.0

TABLE 3.2

CONVENTIONAL FLIGHT STABILITY AXES

AERODYNAMIC DERIVATIVES

Quantity	Dimension	Case I	Case II	Case III	Case IV	Case V
V_T	ft/sec	115	150	200	250	300
α	degrees	12	6	2.2	0.6	- 0.3
I_x	slug-ft.^{2}	1292	1368	1425	1445	1475
I_y	slug-ft.^{2}	1824	1824	1824	1824	1824
I_z	slug-ft.^{2}	2405	2330	2275	2255	2223
I_{xz}	slug-ft.^{2}	309	415	472	485	511
C_L	dimensionless	1.2	.70	.38	.25	.18
C_{y_β}	per rad.	- .815	- .815	- .815	- .815	- .815
C_{n_β}	per rad.	.06	.06	.06	.06	.06
C_{n_p}	per rad.	.03	.07	.0926	.103	.108
C_{n_r}	per rad.	- .218	- .189	- .176	- .175	- .173
C_{l_β}	per rad.	- .0722	- .0912	- .1007	- .1047	- .1072
C_{l_p}	per rad.	- .360	- .397	- .411	- .417	- .420
C_{l_r}	per rad.	.353	.2685	.2185	.195	.1825
C_{L_α}	per rad.	4.92	4.92	4.92	4.92	4.92
$C_{L_{\dot\alpha}}$	per rad.	.855	.855	.855	.855	.855
C_{L_q}	per rad.	5.7	5.7	5.7	5.7	5.7
γ_o	rad.	0	0	0	0	0
C_{D_α}	per rad.	.94	.55	.298	.196	.141

TABLE 3.2 (Cont'd)

Quantity	Dimension	Case I	Case II	Case III	Case IV	Case V
$C_{y\delta_r}$	per rad.	.144	.144	.144	.144	.144
$C_{l\delta_r}$	per rad.	.0372	.0448	.049	.051	.052
$C_{l\delta_a}$	per rad.	.051	.043	.038	.035	.0335
$C_{n\delta_r}$	per rad.	-.0728	- .0728	- .0728	- .0728	- .0728
$C_{n\delta_a}$	per rad.	.0065	.0085	.0098	.010	.0105
$C_{L\delta_e}$	per rad.	.583	.583	.583	.583	.583
C_{m_α}	per rad.	- .561	- .561	- .561	- .561	- .561
$C_{m_{\dot{\alpha}}}$	per rad.	-1.97	-1.97	-1.97	-1.97	-1.97
C_{m_q}	per rad.	-13.1	-13.1	-13.1	-13.1	-13.1
$C_{m\delta_e}$	per rad.	-1.34	-1.34	-1.34	-1.34	-1.34
ρ	slugs per $ft.^3$	.002378	.002378	.002378	.002378	.002378
m	slugs	71.5	71.5	71.5	71.5	71.5

TABLE 3.3

DIMENSIONAL DERIVATIVES USED IN HOVERING STABILITY AND CONTROL ANALYSIS

Derivative	Dimension	
X_u	1/sec.	- .0409
X_w	1/sec.	- .33
$X_{\delta_{pn}}$	ft/deg-sec.^{2}	$f(T_n)$
X_T	ft/lb-sec.^{2}	.00595
Z_u	1/sec.	.0659
Z_w	1/sec.	- .795
$Z_{\delta_{pn}}$	ft/deg-sec.^{2}	$f(T_n)$
Z_T	ft/lb-sec.^{2}	.00919
M_u	1/ft-sec.	- .0266 $C_m"$
M_w	1/ft-sec.	.0709
M_θ^*	1/sec.	.42
$M_{\delta_{pn}}$	1/deg-sec.^{2}	$f(T_n)$
M_T	1/lb-sec.^{2}	.00253 $C_m"$
Y_v	1/sec.	- .0464
$Y_{\delta_{yn}}$	ft/deg-sec.^{2}	$f(T_n)$
L'_v	1/ft-sec.	.0452
L'^*_ϕ	1/sec.	- 1.74
L'^*_γ	1/sec.	- .1965
$L'_{\Delta\beta}$	1/deg-sec.^{2}	.675

Constants	Dimension	
m	slugs	73
I_x	slug-ft^2	1524
I_y	slug-ft^2	1998
I_z	slug-ft^2	2735
I_{xz}	slug-ft^2	457
Θ_o	degs.	33°
R/T	dimensionless	.78
n	rev/sec.	28.3

Control Deflections:

$\delta_{pn} = \pm 30°$

$\delta_{yn} = \pm 30°$

$\Delta\beta = \pm 2.0°$

TABLE 3.3 (Cont'd)

Derivative	Dimension	
$L'_{\delta_{yn}}$	1/deg-sec.^{2}	$f(T_n)$
N_v	1/ft-sec.	- .01156
$N_{\dot{\varphi}}$	1/sec.	.375
$N_{\dot{\psi}}$	1/sec.	- .134
$N_{\delta_{yn}}$	1/deg-sec.^{2}	$f(T_n)$
$N_{\Delta\beta}$	1/deg-sec.^{2}	.263

Figure 3.1

[illegible] MODEL 58

[illegible]

[illegible]

V = [illegible] KNS

I_y = [illegible]

REFERENCE - STABILITY AXES

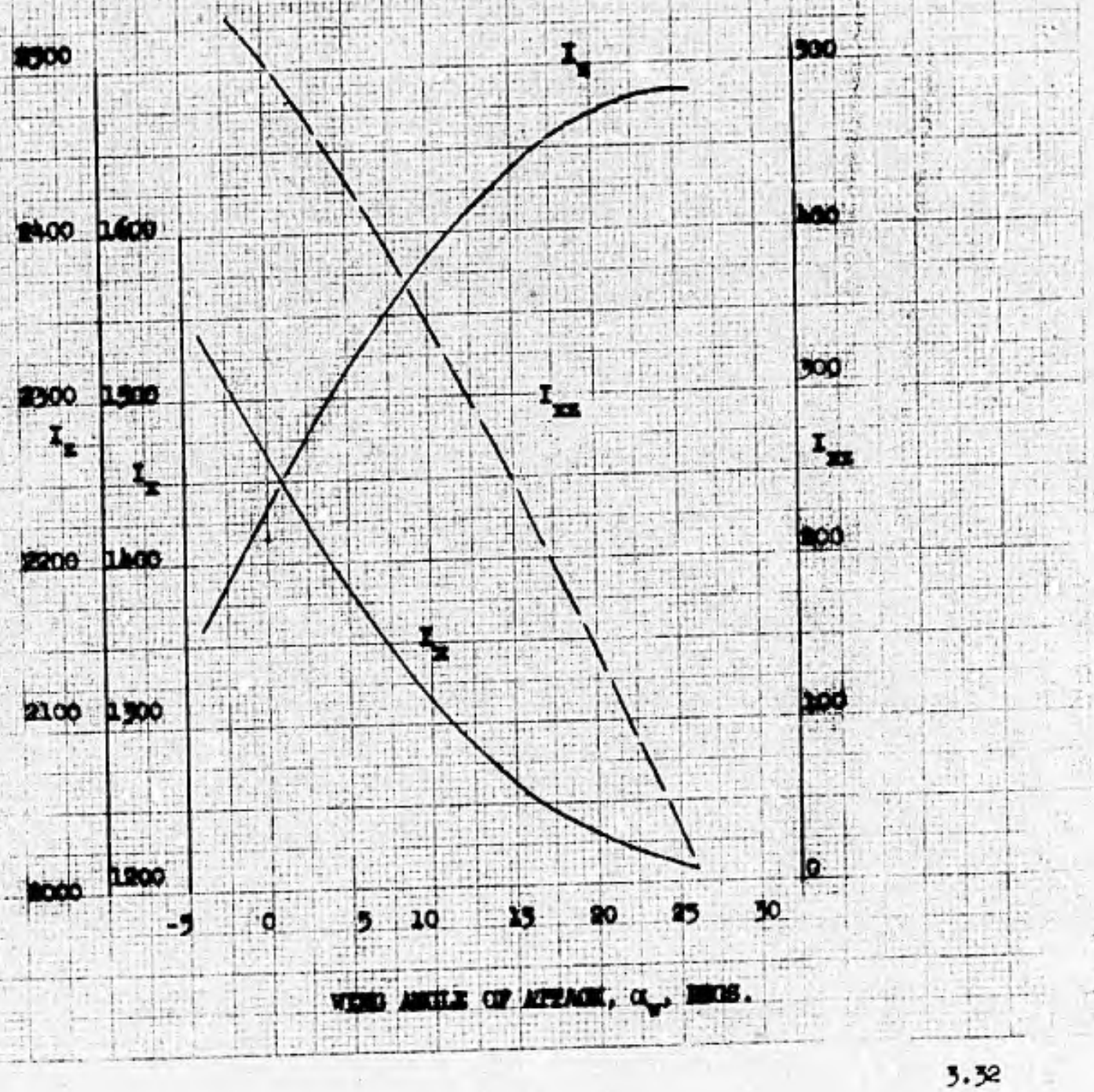

4.0 DISCUSSION

Determining the performance characteristics of the Model 92 required (1) determining the physical characteristics of the several configurations, (2) calculating and analyzing the performance characteristics, and (3) defining the mission.

4.1 Physical Characteristics

The Model 92 is a high wing, single engine, twin propeller, two place, vertical rising or short take-off airplane. The physical characteristics of weight, power plant, aerodynamic characteristics and thrust are discussed in the following sections.

4.1.1 Weights

The last weight statement available for the Model 92 shows the following information:

	WEIGHT	c.g. LOCATION FUSELAGE STATION	c.g. LOCATION FUSELAGE WATER LINE
Weight Empty	1926.9	151.6	78.75
Gross Weight	2351.9	143.5	77.58

Fore and aft accelerations are limited to $\pm$ 2.4 g's, due to engine mount structural limitations, and vertical accelerations are limited to +3 5 and -1.5 g's because of airframe structural limitations.

4.1.2 Power Plant Characteristics

The power plant characteristics of the Model 92 had to be analyzed from the standpoint of (1) the engine and (2) the propellers.

4.1.2.1 Engine. The airframe contains a single Lycoming YT-53-L-1 turboprop engine described in Reference 1. The engine specification data were corrected for installation losses by the methods of the above reference and the resulting SHP was considered to be acting on the drive shaft emanating from the engine. The power train is shown in Figure 4.1. The RPM's are maximum allowable.

FIGURE 4.1

SCHEMATIC DIAGRAM OF THE POWER TRANSMISSION SYSTEM

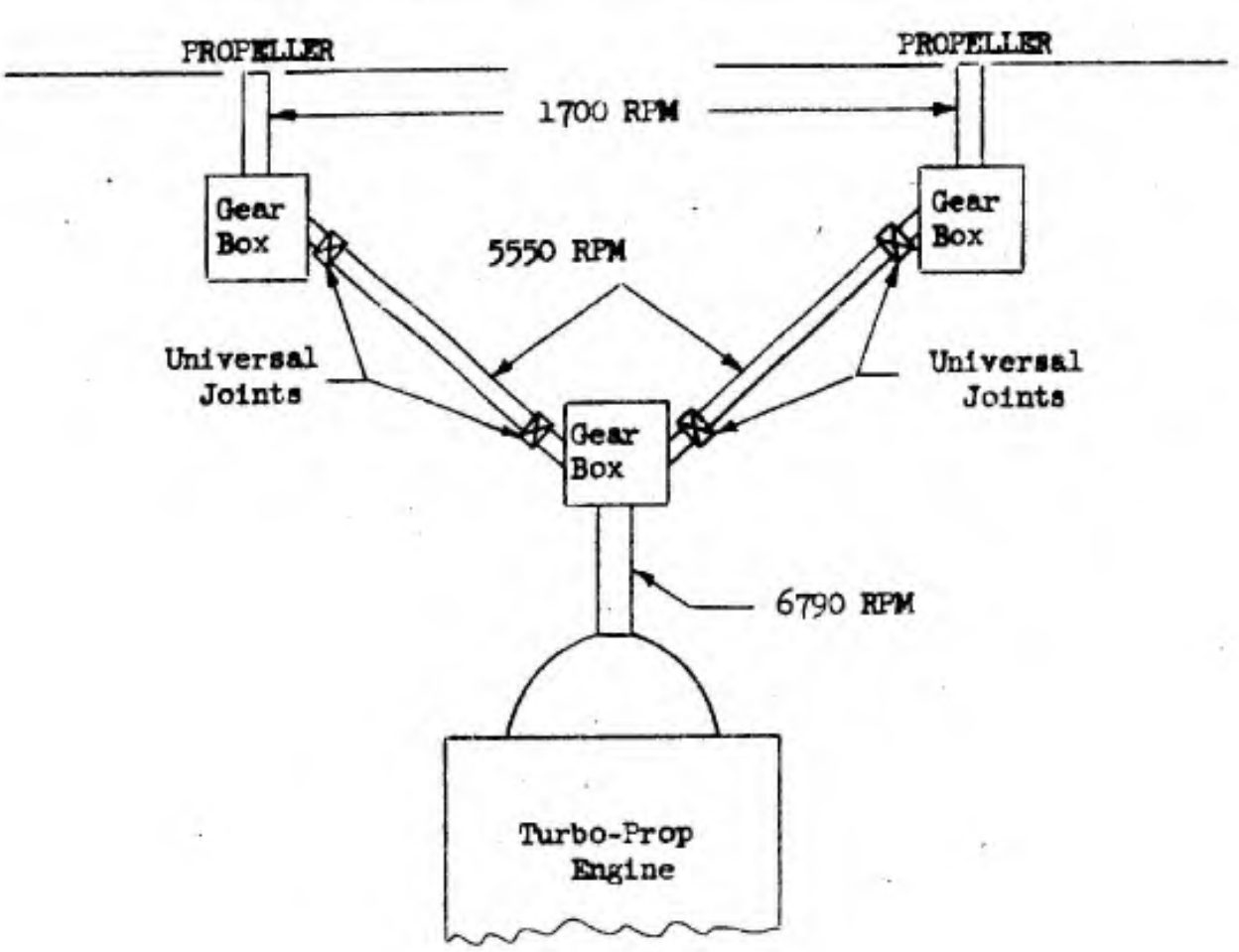

A 6 percent loss in SHP due to the exhaust nozzle restriction and 3 percent loss in SHP due to the inlet duct configuration have been estimated. Both of the above losses were based on static conditions; however, the available information indicates that these percentages will not change significantly with forward speeds.

The losses from the engine output shaft to the propeller shaft are due to the gear boxes and universal joints between the engine and propeller. These estimated losses are relatively small, being only 1/2 of 1 percent for each gear box and 1/2 of 1 percent for the four universal joints.

The specification fuel flows have been adjusted for the installation losses and a 5 percent service tolerance factor included in the computations to account for engine and airframe deviation from the blueprint installation.

4.1.2.1 Propeller. The method by which the propeller data were analyzed gives good agreement with the value calculated by the propeller manufacturer, i.e., 1843 pounds of thrust per propeller at 1700 RPM for static conditions. Since propeller efficiency must be calculated for each specific case, a curve of propeller efficiency has not been presented in this report.

4.1.3 Aerodynamic Characteristics

Lift and drag coefficient calculations were based on a wing plan-form area of 125 square feet for normal flight and take-off calculations. The wing plan-form area becomes a variable when the flaps are extended;

however, all the lift and drag coefficients have been based on the plan-form area of 125 square feet. Figure 8.2 (in Section 8.0) presents the power-off lift versus drag coefficients for the operating range of flaps; however, the maximum flap deflections permitted at this time are 35 degrees forward flap and 35 degrees aft flap deflections due to structural, air loads, and lift-drag considerations. Figure 8.3 presents the lift coefficient versus angle of attack for power-off and flap deflections.

4.1.4 Thrust

The Lycoming YT-53-L-1 engine specifications are shown in Reference 1 and give the manufacturers engine performance curves of SHP and fuel flow. All fuel flows have been increased by 5 percent when used in the performance calculations to account for manufacturing tolerances.

4.1.4.1 Thrust Required. Thrust required was determined from the drag characteristics of the configuration being investigated. Figures 8.4 through 8.9 present the thrust required at various altitudes and airspeeds for three weights.

4.1.4.2 Thrust Available. Thrust available was determined by subtracting the installation losses (including gear boxes, tailpipe area reduction, and incidental losses) from the engine specification shaft horsepower and transforming the remaining horsepower into net thrust of the engine-propeller combination. The installed thrust curves are superimposed on the thrust required curves of figures 8.4 through 8.9. MRT and NRT refer to the net thrust obtained from the engine-propeller combination for Military Rated Power and Normal Rated Power settings, respectively. Thrust available on an ANA standard hot day is presented for two power settings in Figure 8.10. Fuel flows for the various power settings are presented in Figures 8.11 through 8.15.

4.2 Performance

The results of the calculations for maximum speed, stall speed, rate of climb, service ceiling, climb to altitude, endurance, range and wing angle of attack in climb are discussed in the following sections.

4.2.1 Flight Envelope

4.2.1.1 Maximum Speed. Maximum speed was determined by the intersection of the thrust required - - thrust available curves of Figures 8.4 through 8.9. The results of these intersections are shown plotted in Figure 8.16 and indicate that a speed of 195 knots, true airspeed, occurs at 25,000 feet altitude. This may or may not be the maximum speed since engine data is available only up to 25,000 feet. The limit speed from a structural standpoint is 185 knots true airspeed sea level; consequently, operation at full throttle will be restricted to that setting which will not exceed the 185 knots limit speed. Weight appears to have little effect on maximum speed up to the 25,000 feet altitude for a given power setting.

Figure 8.16 also presents the maximum airspeeds for MRT, 90 percent MRT, 75 percent MRT and 50 percent MRT, in addition to the MRT curve. Three climb schedules also appear on Figure 8.16, and it will be noted that there is very little difference in speed between the climb schedules for the several power settings. In the ultimate analysis, one climb schedule appears to be feasible for all the power settings with very little sacrifice in climb performance.

Figure 8.17 presents the limit speed at all the various flap deflections and shows the maximum speed from the structural limitations criteria with the

flaps undeflected (185 knots true airspeed).

4.2.1.2 Stall Speeds. Power-on stall speeds for various weights, altitudes, power settings, and flaps undeflected are shown in Figure 8.18 through 8.22. These data show that a minimum stall speed of 55.5 knots occurs at sea level and 2,000 pounds gross weight. This airspeed increases with either an increase in weight and/or altitude. The data presented above are for the no flap deflection configuration and MRT. Power-off stall speeds are presented in Figure 8.23 for flaps undeflected and three weights. Again, the minimum stall speed (56 knots true airspeed at a gross weight of 2,000 pounds) occurs at sea level.

4.2.2 Rate of Climb

Rate of climb was determined by the difference in thrust available and required as seen in Figures 8.4 through 8.9. The results of these calculations for rate of climb are presented in Figures 8.24 through 8.53 for 5 power settings (MRT, NRT, 90 percent NRT, 75 percent NRT, and 50 percent NRT) and weights of 2,000, 2,200, and 2,400 pounds. An inspection of these curves reveals that a climb schedule which is constant for all weights is possible with little if any deleterious effects on rate of climb. Consequently, an average climb schedule is the recommended schedule in the interest of simple pilot operating techniques.

4.2.3 Service Ceiling

Service ceilings were not determined for the Model 92 due to a lack of engine data above 25,000 feet.

4.2.3 Climb to Altitude

4.2.4.1 Time to Climb. Time to climb to altitude was based on the climb schedules of Figure 8.16, and the results of the calculations are presented in Figures 8.54 through 8.58. Since 5 power settings are under consideration, the time to climb curves are presented as a function of the power parameter.

4.2.4.2 Fuel Used in Climb. Fuel used in climbing from one altitude to another was based on the climb schedules of Figure 8.16, and the results of the calculations are presented in Figures 8.54 through 8.58 and again in Figures 8.59 through 8.63. 5 power settings were used, and the results are shown plotted for each of the power settings.

4.2.4.3 Horizontal Distance Gained in Climb. The "on course" distance gained in climb was based on the climb schedules of Figure 8.16 and the results of the calculations are presented in Figures 8.59 through 8.63. 5 power settings were used, and the results are shown plotted for each of the power settings.

4.2.5 Endurance

Endurance, as presented in Figures 8.64 through 8.68, was based on the amount of fuel required to climb in a Military power setting, and then on the rate of fuel consumption at each of the 5 power settings under consideration until the basic fuel load of 30 gallons was expended. The cruise endurance was based on cruising at the airspeeds of Figure 8.16 for each power setting and altitude.

4.2.6 Range

The range was also based on climbing at a military power setting and then cruising out at each of the five power settings until the fuel was expended. Figures 8.69 through 8.73 present the range based on the speeds shown in Figure 8.16 for each of the power settings.

4.2.7 Wing Angle of Attack in Climb

The wing angle of attack in a climb was also obtained from the rate of climb calculations performed by the IBM 650 digital computer. The actual angles as presented in Figures 8.74 through 8.78 were those obtained at the climb schedule airspeeds of Figure 8.16 for specific power settings. To obtain fuselage angle of incidence, subtract 22 degrees from the wing angle of attack.

4.3 Take-Off Characteristics

The analysis of the take-off characteristics required analysis of three basic flight regimes: (a) short take-off; (b) vertical take-off; (c) transition characteristics.

4.3.1 Short Take-Off

The STO calculations for an ICAO standard day indicate that it would require 90 feet ground distance from brake release to wheels off in the Military Power setting. The flaps were considered to be deflected 30.9 percent of their total deflection (forward flap down 10° and the aft down 11.6°) which gives a C_L of 2.37 and C_D of 0.640 at a wing angle of attack of 20°.

The hot day STO calculations were based on a sea level temperature of 103° F as shown in ANA Bulletin 421. The configuration was the same as for the standard day, and the results of these calculations indicate that it would require 176 feet from brake release to wheels off on a hot day.

Figure 8.79 presents short take-off distances for the several power settings (ICAO standard day).

4.3.2 Vertical Take-Off

Vertical take-off is possible by virtue of the fact that 80 percent of the thrust is converted to lift by deflecting the slipstream downward as shown in the experimental data of Reference 7. Figure 8.80 presents the results of the VTO calculations for thrust to weight ratios of 1.0, 1.05 and 1.10 at power settings of Military, Normal and 90 percent Normal on an ICAO standard day. The forward and aft flaps were assumed to be deflected 35 degrees for these calculations. The results of this figure show that it would be possible to rise off the ground at a gross weight of approximately 2940 pounds. Since the Model 92 weighs only 2350 pounds, with one person aboard, there remains ample thrust for vertical take-off and acceleration upwards.

Data in Reference 7 show that when the airplane is operating within ground effects it is possible to convert 95 percent of the propeller thrust into lift. After leaving ground effects the same reference shows that only 80 percent of the propeller thrust is converted to lift; consequently, the latter number was used in all VTO calculations.

Vertical take-off on a hot day would be lowered in terms of weight lifted due to a reduction in thrust. On a hot day of 103° F the thrust is reduced from a Military setting of 3606 pounds to a Military setting of 2580 pounds or a reduction of 29.9 percent in thrust due to the temperature increase. This reduction in thrust allows only 2060 pounds to be lifted vertically which leaves a deficiency of approximately 290 pounds excess weight.

The figures upon which the VTO calculations were based are slightly conservative; consequently, the airplane should be able to better the estimated performance by some small margin.

4.3.3 Transition Characteristics

The transition characteristics of the Model 92 were not known at the time of this writing. Consequently, no attempt has been made to analyze this flight regime.

4.4 Missions

4.4.1 Test Mission

1. Allow 2 minutes for start, warm-up and checks.

   Power Setting = 50 percent Normal Rated Thrust

   Fuel Flow = 386 lbs/hr

   Fuel Used = 12.9 lbs

2. Allow 30 seconds for STO and clean-up.

   Power Setting = Military Rated Thrust

   Fuel Flow = 615 lbs/hr

   Fuel Used = 5.1 lbs

3. Climb to test altitude of 5,000 feet.

   Power Setting = Military Rated Thrust

   Fuel Flow = 580 lbs/hr

   Fuel Used = 9.0 lbs

   Time = 0.9 minutes

4. Hover at 5,000 feet until 10 percent of the fuel remains (20 lbs.).

   Power Setting = Approximately 95 percent Normal Rated Thrust at start of hovering, reducing to approximately 90 percent Normal Rated Thrust as fuel is burned out.

   Fuel Flow = 497 lbs/hr (average)

   Fuel Used = 148 lbs

   Time = 17.9 minutes

5. Assume no fuel used in letdown and fuel expended after taxi back to parking area.

6. Summary

   Initial Fuel = 195 lbs

   Fuel Used to End of Hovering = 175 lbs

   Time elapsed to End of Hovering = 21.3 minutes

4.4.2 Ferry Mission

1. Allow 2 minutes for start, warm-up and checks

   Power Setting = 50 percent Normal Rated Thrust

   Fuel Flow = 386 lbs/hr

Fuel Used = 12.9 lbs

Distance = 0 nautical miles

2. Allow 30 seconds for VTO and transition.

Power Setting = Military Rated Thrust

Fuel Flow = 615 lbs/hr

Fuel Used = 5.1 lbs

Distance = 0 nautical miles

3. Climb to cruising altitude of 25,000 feet.

Power Setting = Military Rated Thrust

Fuel Flow = 440 lbs/hr (average)

Fuel Used = 44 lbs

Time = 6 minutes

Distance = 8.5 nautical miles

4. Cruise at 25,000 feet until 10 percent of total fuel remains (20 lbs).

Power Setting = 50 percent Normal Rated Thrust

Fuel Flow = 171 lbs/hr

Fuel Used = 113 lbs.

Time = 39.6 minutes

Distance = 88.4 nautical miles

5. Assume no distance gained or fuel used in letdown and fuel expended after taxi back to parking area.

6. Summary

Initial Fuel	=	195 lbs
Fuel Used to End of Cruise	=	175 lbs
Time Elapsed to End of Cruise	=	48.1 minutes
Distance to End of Cruise	=	96.9 nautical miles

4.5 Stability and Control

The estimated stability and control characteristics of the Ryan Model 92 airplane for the conventional, hovering, and transition flight regimes are discussed in this section.

4.5.1 Conventional Flight

The conventional flight characteristics were analyzed for zero flap deflection and for the front flap deflected 10° and rear flap 11.6° which represents a landing configuration. The speed range of the conventional flight regime is from approximately 50 knots to the maximum design speed of the airplane. The major aerodynamic and physical characteristics used in the static stability and control analysis were presented in Table 3.1 and 3.2.

4.5.1.1 Static Longitudinal Stability and Control

The estimated static longitudinal stability contributions of the fuselage and nacelles, wing, power effects, and horizontal tail are shown in Figure 8.81. The curve representing the total of the contributions has a stable slope of $dC_m/dC_L = -.11$ with the c.g. at .515 $\bar{c}$.

The elevator angles required for trim and the tail incidence angles required for trim with zero elevator deflection are shown in Figures 8.82 and 8.83, respectively. Larger trim deflection ranges are required with power-off than with power-on because of the destabilizing effects of power. As shown in Figure 8.83 the condition with flaps deflected and with power-off requires the largest change of tail incidence angle (8.5°) for trim over the range of lift coefficients.

The longitudinal stability with the controls free is shown in Figure 8.84 as a function of airspeed. Freeing the elevator reduces the stability margin from .11 to .052. The destabilizing effect of the free nozzle increases with decreasing airspeed and results in neutral stability at a speed of approximately 68 knots. With power-off, the airplane is stable stick-free over the entire conventional flight speed range.

Figure 8.85 shows the variation of longitudinal control stick force with airspeed. The stick force variation is stable and the forces can be trimmed to zero with less than 2 degrees change of stabilizer incidence angle. The control nozzle effect was neglected in the stick force calculations.

The various c.g. limits are shown in Figure 8.86. The most forward permissable c.g. position imposed by the landing condition with full up-elevator deflection is at .43 $\bar{c}$. The most aft c.g. position is determined by the minimum allowable gradient of stick force with normal load factor which was set at 6 lbs. per g. This criterion places the most aft c.g. position at .55 $\bar{c}$ and results in a useable c.g. range of .12 $\bar{c}$. Also shown in Figure 8.86, the c.g. position determined from weight and balance estimates is well within the established limits.

4.5.1.2 Static Directional Stability and Control.

The static directional rudder-fixed stability of the airplane, $(C_{n_\beta})_{fixed}$, is estimated to be .0011 per degree. With the rudder free, the stability is reduced to .0007. Figure 8.87 shows the effect of the free control nozzle, reducing the stability to zero at a speed of 63 knots. The effect of the

nozzle results in neutral directional and neutral longitudinal stability at approximately the same speed (see Figure 8.84).

The rudder is capable of producing one degree of sideslip per degree of rudder deflection. The gradient of rudder pedal force with sideslip angle, presented in Figure 8.88, shows that a rudder pedal force of 72 pounds is required to hold a sideslip angle of 10 degrees at 185 knots.

4.5.1.3 Lateral Control

Rolling moment and yawing moment coefficients due to deflection of the right-wing slot-lip aileron are plotted in Figure 8.89 for various values of wing angle of attack. The yawing moment coefficients are favorable except for intermediate aileron deflections at 20 degrees angle of attack. These data, taken from Reference 16 were obtained from a right hand semi-span wing model and are for an unflapped wing. Tests of a slot-lip aileron operating in the slot ahead of a trailing edge slotted flap, reported in Reference 26, show that the aileron effectiveness increases with increasing flap deflection. This increased effectiveness should prove to be beneficial in the transition flight region where the hovering roll control means is not utilized.

The hinge moment coefficients due to deflection of a single slot-lip aileron are shown in Figure 8.90 for wing angles of attack of 0 and 15 degrees. These data are for an aileron with its hinge axis at $.25c_a$.

The ailerons of the Ryan Model 92 airplane, though similar to spoilers in operation, are differentially geared together to insure positive aileron control and to eliminate unbalanced stick forces at the neutral stick position.

The assumed control stick-aileron linkage relationship presented in Figure 8.91 was used for stick force calculations.

Lateral control stick force versus control stick displacement is shown in Figure 8.92 for two airspeeds. The non-linearities result from the non-linear hinge moment variations in Figure 8.90.

The estimated rolling performance for a maximum control stick force of 30 pounds is presented in Figure 8.93. Full control deflection can be maintained to a speed of 115 knots at which point the value of pb/2V is .075. The non-linear variations in pb/2V and the roll rate at the lower speeds is due to the variation of the rolling moment coefficient with angle of attack. (Figure 8.89).

4.5.1.4 Dynamic Stability

The results of the solution of the three longitudinal equations of motion are summarized in the following table.

TABLE 4.1

LONGITUDINAL DYNAMIC STABILITY CHARACTERISTICS

V = 150 Knots

Roots	P	$T_{1/2}$	ω, cps
-.0652		10.60	
-.166		4.18	
$-3.71 \pm 3.54j$	1.23	.187	.815

The short period oscillation is well damped requiring only .152 cycles to damp to half amplitude. The normal phugoid mode is replaced by the two

negative real roots indicating two convergences. This is possibly due to the effective drag of the propeller thrust which varies inversely with speed. High drags are known to damp the phugoid mode.

The lateral-directional characteristics of the airplane, as determined by the 3 degree of freedom analog computer analysis, are shown in Figure 8.94 in terms of the damping criteria of Reference 27. The high-speed case is satisfactorily damped but the low speed case is marginal. The effect of speed on the period and damping of the short period oscillation is shown in Figure 8.95. The average period is about 3.5 seconds corresponding to a natural frequency of .286 cycles per second. The time required to damp to half amplitude increases rapidly with decreasing airspeed, resulting in the relatively poorer damping characteristics at low speeds.

Although the ratio of C_{ℓ_β} to C_{n_β} is large, the values of the ratio of roll to sideslip, φ/β, are in the normal range. As shown in Figure 8.96, φ/β increases linearly with increasing airspeed.

A five degree of freedom analysis was conducted to investigate possible cross-coupling of the lateral-directional motions with longitudinal motions and to facilitate studying the changes in aerodynamic derivatives required to improve the lateral-directional damping characteristics. Typical analog time histories are shown in Figures 8.97 and 8.98 of the response of the airplane to a sideslip disturbance.

A sideslip disturbance introduces a small disturbance in pitch through the inertia coupling terms. Since the longitudinal motions are well damped, however, primary emphasis during the simulation was placed upon studying the

lateral-directional characteristics, particularly at the lower speeds.

The principal factors believed to adversely affect the stability and handling characteristics were a large product of inertia, resulting from a downward inclination of the principal axis, and rolling moments due to the vertical tail.

Reductions in wing incidence angle to reduce the product of inertia and moderate increases in the static directional stability, while improving the damping characteristics, did not, from the viewpoint of pilot observation, appreciably improve the handling characteristics of the airplane.

The major results of the 5 degree of freedom simulation are shown in Figure 8.99. The effects of lower-surface end plates on the horizontal tail and of arbitrary reductions in the airplane's dihedral effect are shown. The end plates were 9.0 $ft.^2$ each in area and increased the static directional stability of the airplane by a factor of approximately 4.0. However, due to the height of the tail above the longitudinal axis, the end plates also served to increase the airplane's dihedral effect.

For the low speed case of 68 knots, considerable improvement in damping is noted by the addition of the end plates, and some additional improvement is gained by a reduction in dihedral effect. As noted in Figure 8.99 the dihedral is given in terms of wing geometric dihedral angle.

For the high-speed case of 178 knots, addition of the end plates results in only a small improvement in damping and introduces an extremely high value of φ/β. Reducing the effective dihedral, however, results in a highly damped configuration with a better value of φ/β.

For both speeds a wing dihedral angle of -2 degrees yields the best damping characteristics. Preliminary calculations have indicated that by extending the span of the lower surface wing-tip end plates, to increase the end plate area by 30 percent, a reduction in dihedral effect equivalent to the required wing dihedral angle of -2 degrees can be achieved.

Qualitative analysis in the form of pilot opinion indicated the above simulated modifications to the airplane resulted in improved handling characteristics. Flight testing the airplane will further serve to determine the degree of airplane configuration modification required to insure acceptable lateral-directional flight characteristics.

4.5.2 Hovering Flight

The following sections discuss the Ryan Model 92 airplane hovering flight characteristics. The hovering flight regime is considered generally to apply to a zero speed condition but may also apply to small translational velocities of the order of 10 knots.

4.5.2.1 Hovering Control. The estimated forces developed by the pitch and yaw control nozzle are presented in Figure 8.100. The normal force acts perpendicular to the centerline of the exhaust pipe and the forward component acts along the exhaust pipe centerline. A small additional airplane nose-up pitch angle will be required to balance out the forward component. However, no pitching moment is created since this component acts through the c.g..

Differential propeller pitch provides a powerful means for roll control in hovering flight. The major unknown is the time lag of blade angle change

due to the hydraulic mechanism in the propeller hub. The response characteristics of the roll control system can be determined during the ground test program.

The following table summarizes the estimated angular acceleration capability of the airplane with full control displacements for attitude control about the three body axes.

TABLE 4.2

ANGULAR ACCELERATION CAPABILITY IN HOVERING FLIGHT

W = 2350 Lbs.

Axis	Control Displacement	Control Moment, ft. lbs	Angular Acceleration, rad/sec^2
Roll	$\pm 2^{o}$	2060	1.35
Pitch	$\pm 30^{o}$	2210	1.10
Yaw	$\pm 30^{o}$	2210	.81

4.5.2.2 Hovering Trim. The center of gravity of the airplane was located to minimize any pitching moments due to the resultant lifting force of the wing-propeller combination. The approximate location of the resultant force was determined from analysis of test data of Reference 7. The location of the resultant force vector shows no tendency to shift with changes in propeller thrust, but there is a shift due to ground effect. Removal of the ground plane used for the tests of Reference 7 resulted in a forward shift of the resultant force of .075 $\bar{c}_w$. A shift of this magnitude in the case of the Model 92, coupled with a reduction in the turning angle of 6 degrees, requires a change in trim equivalent to 18 percent of the available control pitching moment.

4.5.2.3 Hovering Stability. Although the major effort in the hovering stability analysis was conducted on the analog computer simulator, the stability characteristics were also obtained from IBM digital computer solutions of the equations of motion and are summarized in Table 4.3.

TABLE 4.3

HOVERING STABILITY CHARACTERISTICS

Longitudinal			
ROOTS	P SECS.	$T_{1/2}$ SECS.	ω CPS
- .1456	———	4.75	———
-1.496	———	.463	———
.1929 ± .8855j	6.93	-3.60	.144

Lateral-Directional			
ROOTS	P SECS.	$T_{1/2}$ SECS.	ω CPS
- .159	———	4.36	———
.6529	———	-1.06	———
-1.214 ± .488j	4.80	.570	.207

The longitudinal motion is characterized by two negative real roots, indicating speed stability, and a pair of complex roots corresponding to an unstable oscillation. These results are in agreement with statements made in Reference 28 and with results of NACA free-flight model tests reported in References 29 and 30.

The lateral-directional motion is characterized by a stable oscillation, a convergence and a divergence. A divergent motion, involving translational side velocity and rolling, was noted in the tests of References 29 and 30.

The simulator studies indicated that the lateral-directional motions could be controlled provided the side velocity was maintained at low values. When the side velocity exceeded approximately 20 ft/sec. loss of roll control was experienced and the motion diverged.

The pitch oscillation, though of long period, was difficult to control, particularly when trying to maintain lateral control simultaneously. Analysis of the time histories obtained during the hovering simulation revealed that in 6 degrees of freedom, the motions could be controlled for approximately 25 seconds. Increases in the pitch damping readily stabilized the pitch oscillation and indicated the capability of a stabilization system to improve the hovering longitudinal handling characteristics of the airplane.

4.5.3 Transition Flight

The following sections discuss the longitudinal and directional trim characteristics in low speed flight. The transition flight regime includes speeds from zero forward flight to a flaps-up level flight speed of approximately 60 knots.

4.5.3.1 Longitudinal Trim in Low-Speed Flight. Figure 8.101 shows the forces required to trim the pitching moments to zero as a function of speed. Tail lift coefficient required for zero nozzle thrust and values of nozzle thrust required for various tail lift coefficients are presented.

In applying the data of the wind tunnel model of Reference 10, flap deflection was decreased with increasing speed at a constant angle of attack of 20 degrees up to a speed of 52 knots. At this speed the flap deflection was zero and the angle of attack was then progressively reduced to zero at 110 knots.

Constant tail lift coefficients as low as .10 require nozzle thrust forces that are within the capability of the pitch nozzle. As shown in Figure 8.101, the tail lift coefficient required increases rapidly with decreasing speed below 20 knots due to small values of free stream dynamic pressure. At speeds above 20 knots the lift coefficient required decreases with increasing speed. Also shown in Figure 8.101 is a curve of tail lift coefficient, calculated from the flaps-up static stability analysis of the present report, which shows generally good agreement with the NACA method over the applicable speed range.

4.5.3.2 Directional Trim in Low-Speed Flight. Figure 8.102 shows the nozzle thrust required to trim the yawing moment due to differential propeller pitch while using full rudder control. Since the method used for calculating the yawing moments did not take into account the drag force of the flaps due to propeller thrust change, the dashed portion of the curve is faired through the value of nozzle thrust at zero airspeed which corresponds to the yawing moment determined by the method of Section 3.4.2.2 of this report.

It is planned to phase out the differential pitch control in transition flight by a mechanical linkage operated by the flaps. The curve of Figure 8.102 indicates that the differential pitch control should be phased out while the flaps are still at large deflections, corresponding to low speeds, in order to minimize the induced yawing moments. The optimum transition from hovering roll control to normal flight roll control, however, will depend upon the aileron effectiveness at large flap deflections at low speeds.

5.0 CONCLUSIONS

The following conclusions are made based on the data and analysis in this report:

1. The Model 92 is limited to 185 knots, true airspeed, at sea level due to structural criteria.
2. The Model 92 is capable of lifting up to 2940 pounds gross weight in a vertical take-off on an ICAO standard day.
3. The basic airplane configuration is statically and dynamically stable with controls fixed in conventional flight.
4. The lateral-directional short-period oscillation damping characteristics for normal flight can be improved, by adding end plates to the horizontal tail and reducing the dihedral effect of the wing. Reducing the dihedral effect by two degrees requires that the added end plate area be equivalent to the existing vertical tail area.
5. Flight tests of the airplane will be required to determine the degree of modification to the airplane required to obtain satisfactory handling characteristics in conventional flight.
6. The characteristic motions of the airplane in hovering flight are an unstable oscillation in the longitudinal mode and a divergence in the lateral-directional mode.
7. Stabilization of the pitch oscillation by artificial means appears necessary in order for the pilot to control the airplane in sustained hovering flight.
8. The jet exhaust control system provides adequate control power for hovering flight and enables trimmed conditions to be maintained in low-speed transition flight.

6.0 REFERENCES

1. Model Specification, YT-53-L-1, Shaft Turbine Engine, Lycoming Model LTC 1B-1. Lycoming Division, Avco Manufacturing Corporation. Specification No. 104.9, 28 September 1956.

2. Hamilton Standard Generalized Propeller Performance Method. Aerodynamic Note No. 20, 13 July 1956.

3. Perkins, Courtland D. and Hage, Robert E.: Airplane Performance Stability and Control, John Wiley and Sons, Inc., 1949.

4. Diehl, Walter Stuart: Engineering Aerodynamics, The Ronald Press Company, 1928 and 1936.

5. Dommasch, Daniel O., Sherby, Sidney S., and Connolly, Thomas F.: Airplane Aerodynamics, Pitman Publishing Corporation, 1951.

6. Jacobs, Eastman N., Ward, Kenneth E., and Pinkerton, Robert M.: The Characteristics of 78 Related Airfoil Sections from Tests in the Variable-Density Wind Tunnel, NACA TR 460, 1933.

7. Price, H.S.: Static Characteristics of the Ryan Model 88 Monoplane and Biplane-Type Apparatus for Deflecting a Propeller Slipstream through Large Angles, Ryan Aeronautical Co., Report No. 8820-3, 4-27-56.

8. Kuhn, Richard E., and Draper, John W.: Investigation of Effectiveness of Large-Chord Slotted Flaps in Deflecting Propeller Slipstreams Downward for Vertical Take-Off and Low-Speed Flight, NACA TN 3364, January 1955.

9. Kuhn, Richard E., and Draper, John W.: Some Effects of Propeller Operation and Location on Ability of a Wing With Plain Flaps to Deflect Propeller Slipstreams Downward for Vertical Take Off, NACA TN 3360, January 1955.

10. Kuhn, Richard E., and Hayes, William C., Jr.: Wind Tunnel Investigation of Effect of Propeller Slipstreams on Aerodynamic Characteristics of a Wing Equipped With a 50-Percent-Chord Sliding Flap and a 30-Percent-Chord Slotted Flap, NACA TN 3918.

11. Kuhn, Richard E., and Draper, John W.: An Investigation of a Wing-Propeller Configuration Employing Large-Chord Plain Flaps and Large Diameter Propeller for Low-Speed Flight and Vertical Take-Off, NACA TN 3307, December 1954.

12. Ribner, Herbert S.: Notes on the Propeller and Slipstream in Relation to Stability, NACA ARR L4I12a, October 1944.

13. Silverstein, Abe and Ratzoff, H.: Design Charts for Predicting Downwash Angles and Wake Characteristics Behind Plain and Flapped Wings, NACA TR 648, 1939.

14. Sears, Richard I.: Wind Tunnel Data on the Aerodynamic Characteristics of Airplane Control Surfaces, NACA ACR 3L0 8, December 1943.

15. Pass, H.R.: Analysis of Wind Tunnel Data on Directional Stability and Control, NACA TN 775, September 1940.

16. Shortal, Joseph A.. Wind Tunnel and Flight Tests of Slot-Lip Ailerons, NACA TR 602, 1937.

17. Weick, Fred E., and Shortal, Joseph A.. Development of the NACA Slot-Lip Aileron, NACA TN 547, November 1935.

18. Goodman, Alex, and Adair, Glenn H.. Estimation of the Damping in Roll of Wings Through the Normal Flight Range of Lift Coefficient, NACA TN 1924, July 1949.

19. Fundamentals of Design of Piloted Aircraft Flight Control Systems, Volume II: Dynamics of the Airframe, Bureau of Aeronautics Report AE-61-4, February 1953.

20. Riebe, John M., and Watson, James M.. The Effect of End Plates on Swept Wings at Low Speed, NACA TN 2229, November 1950.

21. Goodman, Alex, and Wolhart, Walter D.. Experimental Investigation of the Low Speed Static and Yawing Stability Characteristics of a 45° Sweptback High-Wing Configuration with Various Twin Vertical Wing Fins, NACA 2534, November 1951.

22. Campbell, John P., and McKinney, Marion O.. Summary of Methods for Calculating Dynamic Lateral Stability and Response and for Estimating Lateral Stability Derivatives, NACA TN 2409, July 1951.

23. Pearson, Henry A., and Jones, Robert T.. Theoretical Stability and Control Characteristics of Wings with Various Amounts of Taper and Twist, NACA TR 635, 1938.

24. Kuhn, Richard E.: Investigation of Effectiveness of a Wing Equipped with a 50-Percent-Chord Sliding Flap, a 30-Percent-Chord Slotted Flap, and a 30-Percent-Chord Slat in Deflecting Propeller Slipstreams Downward for Vertical Take-Off, NACA TN 3919, January 1957.

25. Hartman, Edwin P., and Biermann, David.: The Aerodynamic Characteristics of Full-Scale Propellers Having 2, 3 and 4 Blades of Clark Y and RAF 6 Airfoil Section, NACA TR 640, 1938.

26. Rogallo, Francis M., and Spano, Bartholomew S.: Wind Tunnel Investigation of a Plain and a Slot-Lip Aileron on a Wing with a Full Span Slotted Flap, NACA ACR 284, April 1941.

27. Anonymous: Flying Qualities of Piloted Airplanes, Requirements For Military Specification MIC-F-8785 (ASG), Addendum 2, October 17, 1955.

28. Zimmerman, Charles H.: Some Stability Problems of Vertically Rising Aircraft; Proceedings of the Second Annual Western Forum of the American Helicopter Society, September 1955.

29. McKinney, Marion O., Tosti, Louis P., and Davenport, Edwin E.: Dynamic Stability and Control Characteristics of a Cascade-Wing Vertically Rising Airplane Model in Take-Offs, Landings, and Hovering Flight, NACA TN 3198, June 1954.

30. Tosti, Louis P., and Davenport, Edwin E.: Hovering Flight Tests of a Four-Engine-Transport Vertical Take-Off Airplane Model Utilizing a Large Flap and Extensible Vanes for Redirecting the Propeller Slipstream, NACA TN 3440, May 1955.

7.0 SYMBOLS, NOMENCLATURE AND AXES SYSTEMS

AR	Aspect ratio, b^2/S
BHP	Brake horsepower
C_D	Drag coefficient, D/qS
C_h	Control surface hinge moment coefficient, $\frac{\text{Hinge Moment}}{q\,S\bar{c}}$
C_L	Lift coefficient, L/qS
$C_{L_{max}}$	Maximum trimmed lift coefficient
C_ℓ	Rolling moment coefficient, $L'/q\,Sb$
C_m	Pitching moment coefficient, $M/q\,S\bar{c}$
C_m''	Pitching moment coefficient, $M/q''S\bar{c}$
C_n	Yawing moment coefficient, N/qSb
C_T	Propeller thrust coefficient, $T/\rho n^2 D^4$
$C_{1/2}$	Number of cycles to damp to half amplitude, $\frac{T_{1/2}}{P}$
D	Drag, lbs.
D	Propeller diameter, ft.
E	Flap chord/wing chord
F_n	Net thrust, pounds
F_{na}	Thrust available, lbs.
F_{nr}	Thrust required, lbs.
F_s	Control stick force, lbs.
G	Control gearing ratio, $\delta/\ell_s\ \delta_s$, per ft.
I_x	Moment of inertia about x axis, slug - ft.^{2}

I_y	Moment of inertia about ŷ axis, Slug - ft.^{2}
I_z	Moment of inertia about z axis, Slug - ft.^{2}
I_{xz}	Product of inertia, Slug - ft.^{2}
L	Lift, lbs.
L'	Rolling moment, ft.-lbs.
MRT	Net thrust available from the propellers when the engine is operated at a Military Rated Power Setting.
M	Pitching moment, ft.-lbs.
NRT	Net thrust available from the propellers when the engine is operated at Normal Rated Power Setting.
N	Yawing moment, ft.-lbs.
N_o'	Static stick-free neutral point
P	Period of oscillation, sec.
PF	Pedal force, lbs.
Q	Propeller shaft torque, ft.-lbs.
R	Resultant wing - propeller force, lbs.
R_d	μ_d(W-L), rolling friction, lbs.
S	Aerodynamic surface area, sq. ft.
S_G	Linear distance on ground, ft.
SHP	Shaft horsepower
S_{NM}	Horizontal distance gained, nautical miles
STOL	Short take-off and landing
T	Thrust, lbs.
$T_{1/2}$	Time to damp to half amplitude, secs.
V	True airspeed, F.P.S.
V_T	True airspeed, knots
V_o	Initial true airspeed, knots
V_1	Minimum control true airspeed, knots

V_2	1.1 minimum control true airspeed, knots
$\bar{V}$	Horizontal tail volume coefficient, $\frac{S_t \ \ell_t}{S_w \ \bar{c}}$
VTOL	Vertical take-off and landing
V_3	True airspeed at altitude h_1, knots
V_4	True airspeed at altitude h_2, knots
W	Gross weight, lbs.
W_{fG}	Fuel used, lbs.
$(W_f)_1$	Fuel flow rate at altitude h_1, lbs/min.
$(W_f)_2$	Fuel flow rate at altitude h_2, lbs/min.
X	Weighting factor dependent upon the ratio of the rates of climb at altitude h_1 and h_2 (Section 8.0)
Y	Sideforce, lbs.
Z	Weighting factor dependent upon the ratio of the rates of climb at altitudes h_1 and h_2 (Section 8.0)
a	$\frac{F_n - D - R_d}{W/g}$, airplane acceleration, ft/sec.^{2}
b	Wing span, ft.
c	Chord, ft.
$\bar{c}$	Mean aerodynamic chord, ft.
c.g.	Center of gravity
g	Gravitational constant, 32.19 ft/sec.^{2}
h_1	Initial altitude, ft.
h_2	Final altitude, ft.

i	Incidence angle, degs.
i_{F_n}	Thrust axis angle of inclination, degs.
ℓ	Distance measured from airplane c.g., ft.
ℓ_s	Length of control stick, ft.
m	Mass of airplane, (W/g), slugs
n	Propeller rotational speed, rev/sec.
n	Airplane normal load factor
p	Rolling velocity about the x axis, rad/sec.
q	Pitching velocity about the y axis, rad/sec.
q	Free stream dynamic pressure, $1/2\rho V^2$, lbs/ft.^{2}
q"	Propeller slipstream dynamic pressure, $q + T/\frac{\pi}{4} D^2$, lbs/ft.^{2}
r	Yawing velocity about the z axis, rad/sec.
r_d	Coefficient of rolling friction
r/c	Rate of climb, ft/min.
t	Time
u	Velocity component along x axis, ft/sec.
v	Sideslip velocity along y axis, ft/sec.
w	Velocity component along z axis, ft/sec.
x	Distance from wing leading edge measured parallel to thrust axis, ft.
y	Distance from plane of symmetry to propeller thrust axis, ft.
z	Vertical distance from center of pressure of vertical tail to x axis, ft.
α	Angle of attack, degs.
β	Angle of sideslip, degs.
$\Delta\beta$	Differential propeller blade pitch angle, per propeller, degs.

Γ	Wing dihedral angle, degs.
γ	Climb angle, degs.
γ_1	Climb angle at altitude h_1, degs.
γ_2	Climb angle at altitude h_2, degs.
δ	Control surface, nozzle, or wing flap deflection, deg. (where wing flap deflections are given, the first number refers to the forward flap).
ϵ	Downwash angle, deg.
η	Dynamic pressure efficiency at the tail
θ	Pitch angle, radians
ρ	Mass density of air, $lb_m\text{-}sec^2/ft.^4$
τ	Control surface effectiveness parameter, $d\alpha/d\delta$
φ	Roll angle, radians
φ/V_e	Roll to sideslip parameter, $\varphi/\beta \times \frac{57.3}{V}$
ψ	Yaw angle, radians
ω	Frequency of oscillation, cycles per sec.

Subscripts:

R	Right aileron	s	control stick
L	Left Aileron	t	horizontal tail
a	aileron	v	vertical tail
a.c.	wing aerodynamic center	w	wing
c.g.	center of gravity	yn	yaw nozzle
e	elevator		
f	flaps		
n	nozzle		
pn	pitch nozzle		
r	rudder		

Figure 7.1

STABILITY AXES SYSTEM

DIRECTION OF ARROWS INDICATES POSITIVE SENSE OF FORCES, MOMENTS AND DEFLECTIONS. POSITIVE HINGE MOMENTS TEND TO DEFLECT CONTROL SURFACES IN POSITIVE DIRECTION.

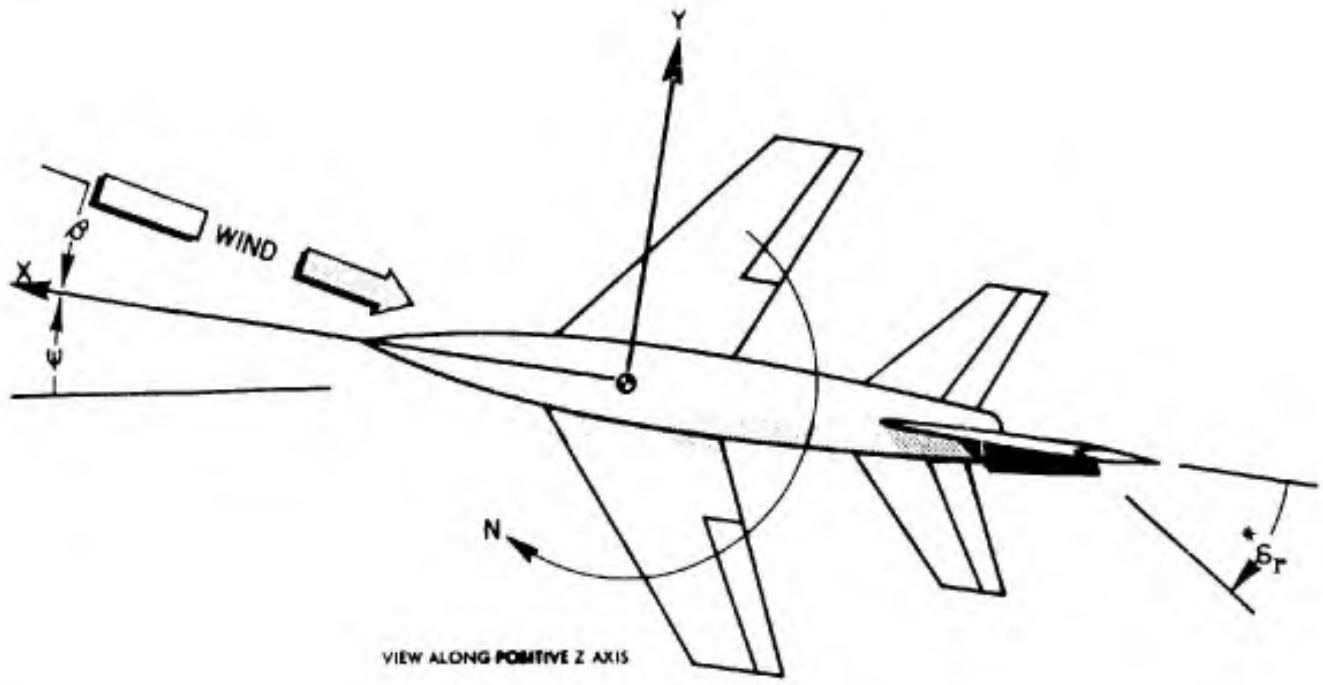

VIEW ALONG POSITIVE Z AXIS

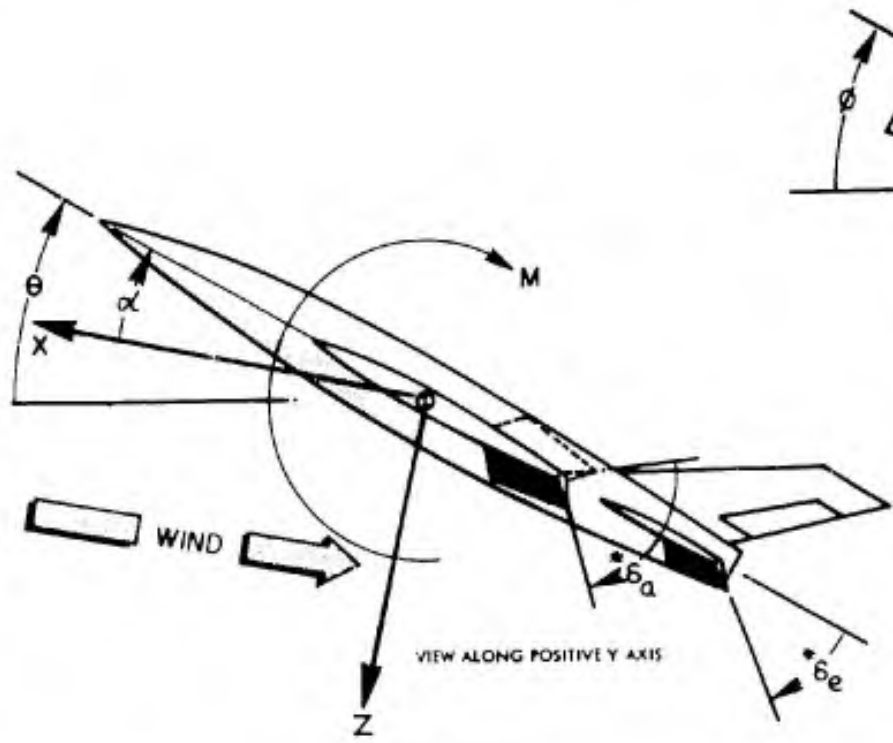

VIEW ALONG POSITIVE Y AXIS

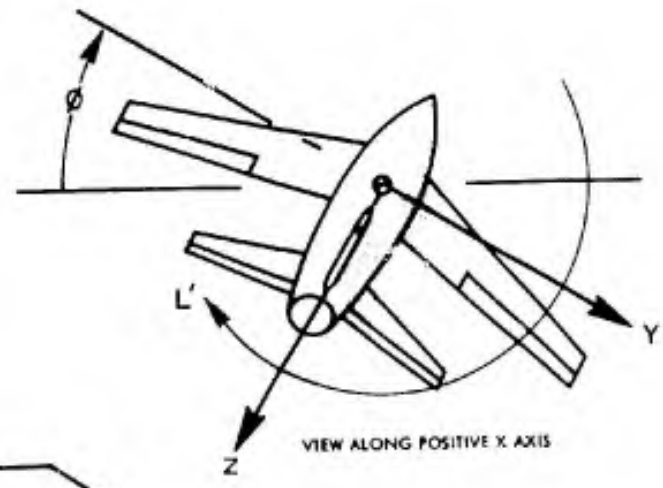

VIEW ALONG POSITIVE X AXIS

* NOTE: DEFLECTIONS MEASURED NORMAL TO HINGE LINE.

Figure 7.2

RYAN MODEL 92

BODY AXES SYSTEM

DIRECTION OF ARROWS INDICATES POSITIVE SIGNS OF FORCES AND MOMENTS. NOZZLE THRUST ACTS IN THE SAME DIRECTION AS NOZZLE DEFLECTION.

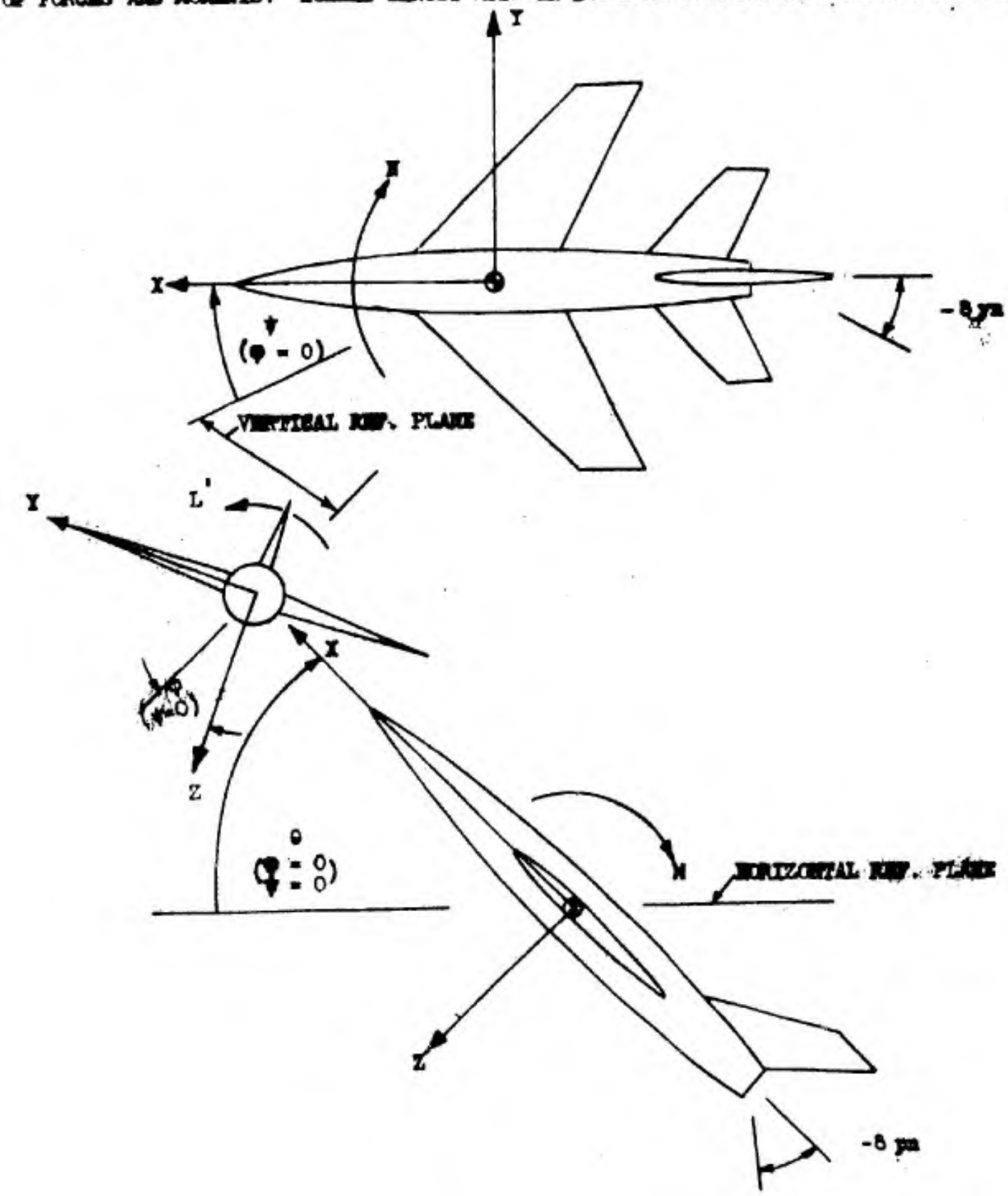

Figure 8.1

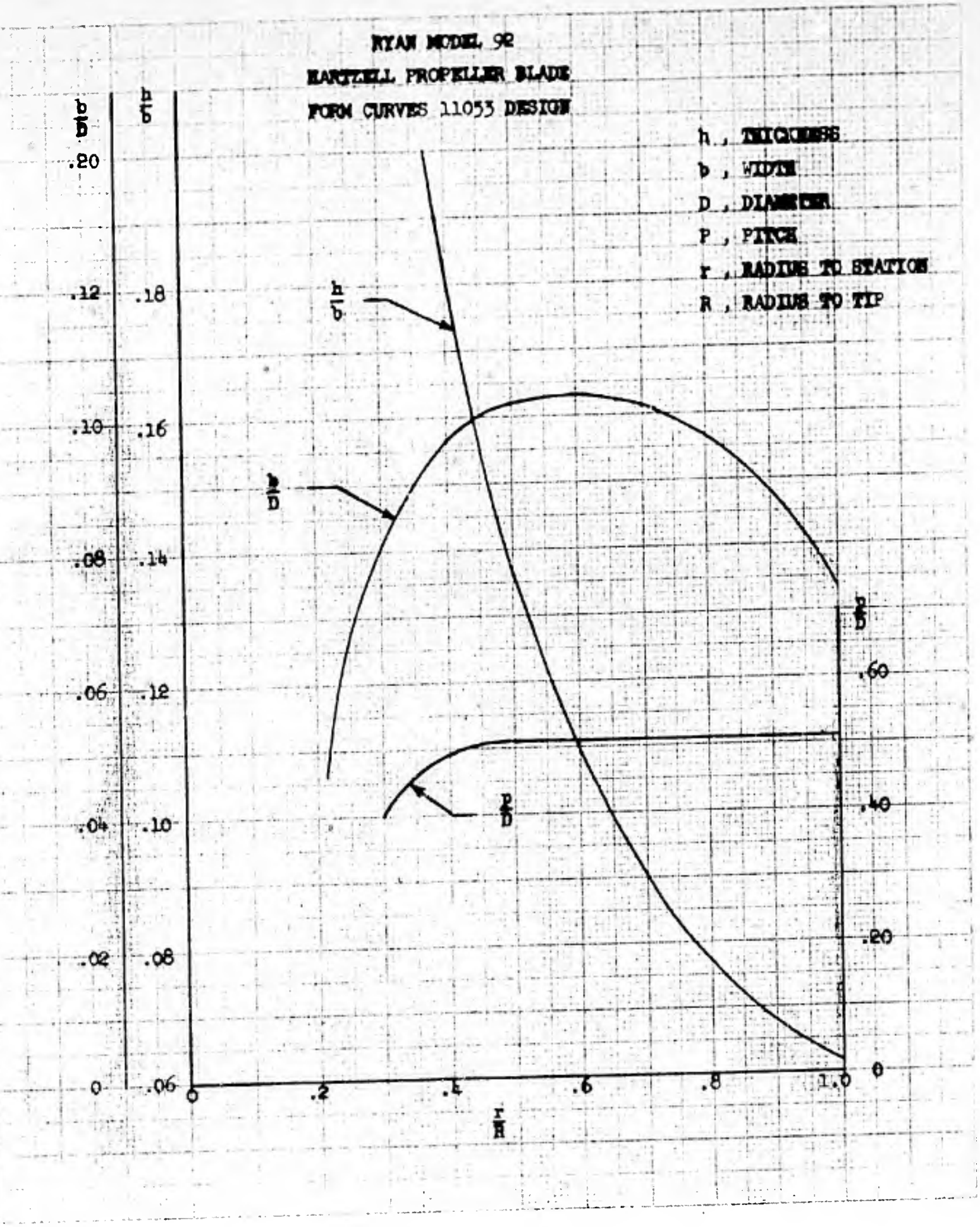
RYAN MODEL 92
HARTZELL PROPELLER BLADE
FORM CURVES 11053 DESIGN
h , THICKNESS
b , WIDTH
D , DIAMETER
P , PITCH
r , RADIUS TO STATION
R , RADIUS TO TIP
h/b
b/D
p/D
r/R
.20
.12
.10
.08
.06
.04
.02
0
.18
.16
.14
.12
.10
.08
.06
.60
.40
.20
0
.2
.4
.6
.8
1.0

Figure 8.2

RYAN MODEL 92

LIFT COEFFICIENT VERSUS

DRAG COEFFICIENT WITH AND WITHOUT FLAP DEFLECTIONS

POWER OFF

ICAO STANDARD ATMOSPHERE

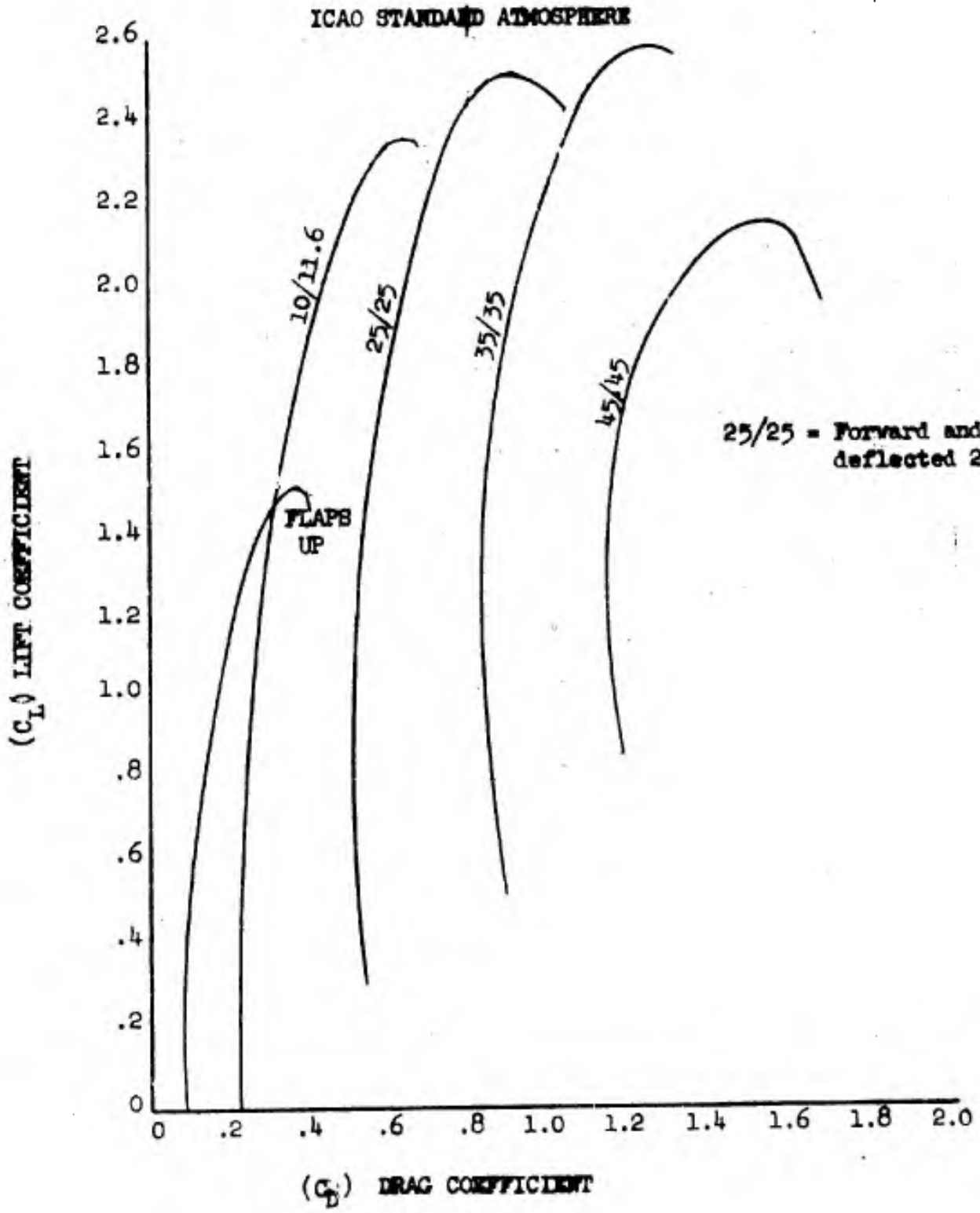

Figure 8.3

RYAN MODEL 92

LIFT COEFFICIENT VERSUS

ANGLE OF ATTACK WITH AND WITHOUT FLAP DEFLECTIONS

POWER OFF

ICAO STANDARD ATMOSPHERE

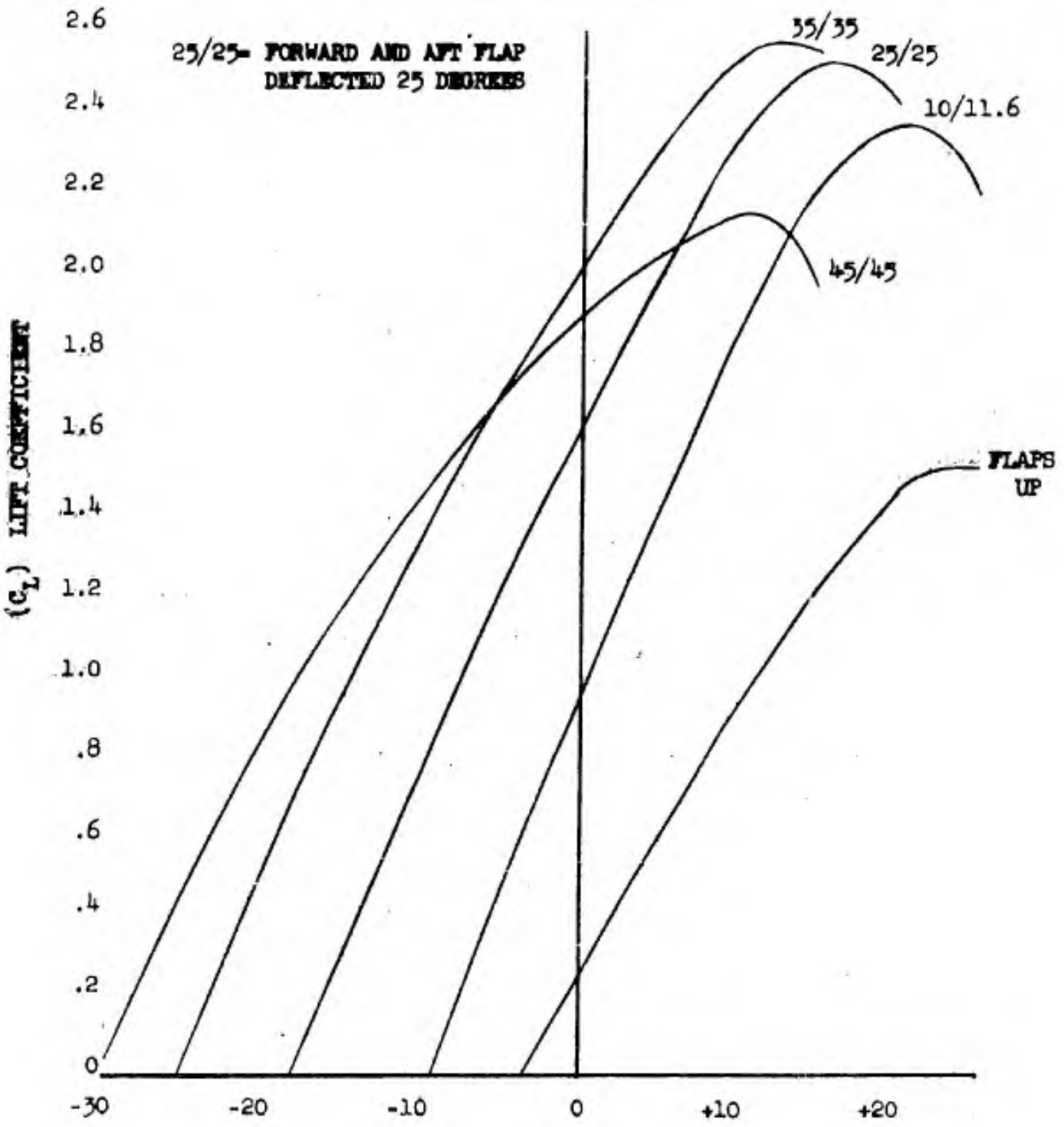

Figure 8.4

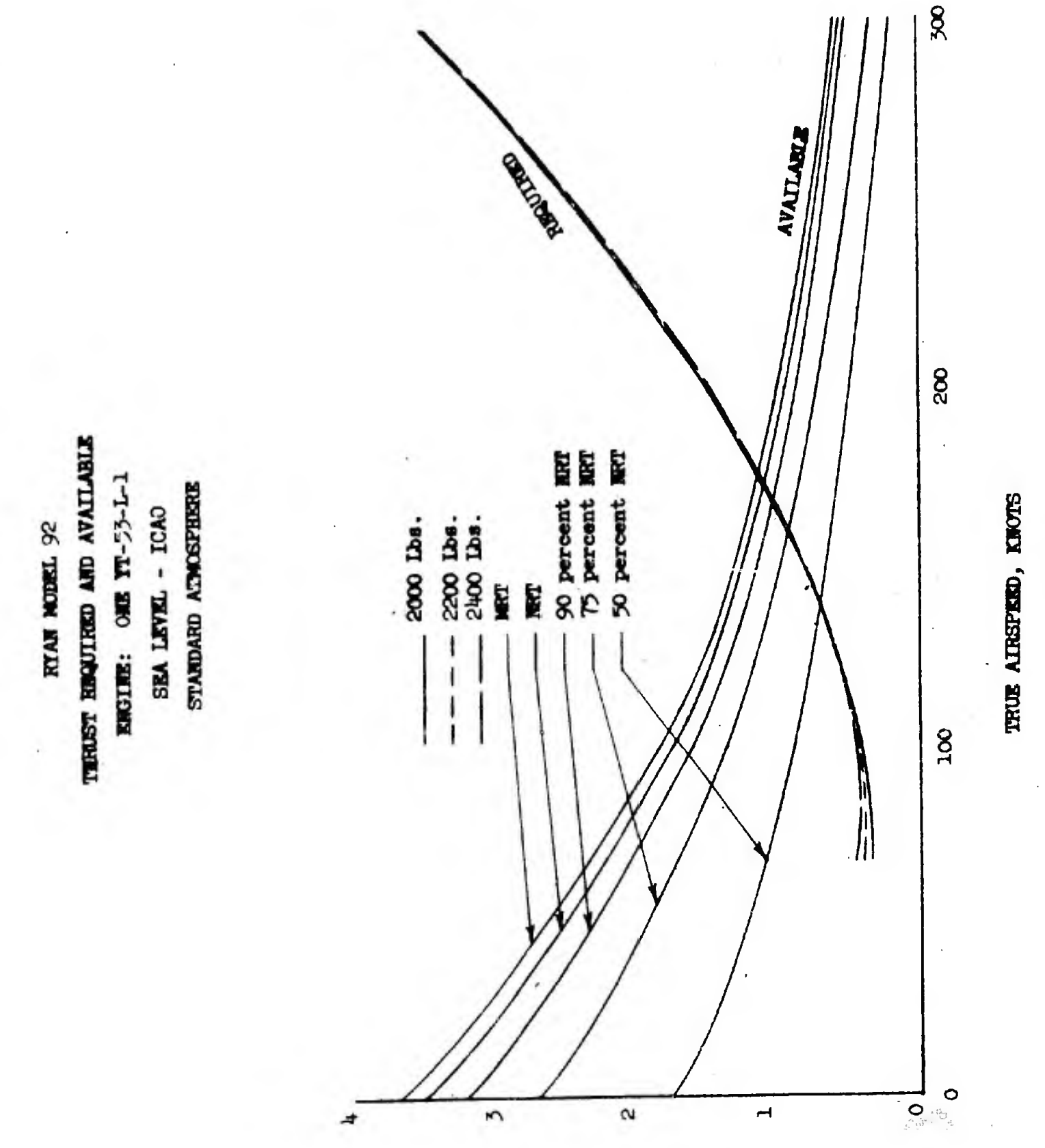
RYAN MODEL 92
THRUST REQUIRED AND AVAILABLE
ENGINE: ONE YT-53-L-1
SEA LEVEL - ICAO
STANDARD ATMOSPHERE
REQUIRED
AVAILABLE
2000 Lbs.
2200 Lbs.
2400 Lbs.
MRT
MRT
90 percent MRT
75 percent MRT
50 percent MRT
THRUST, LBS. x 10⁻³
TRUE AIRSPEED, KNOTS
0
1
2
3
4
100
200
300

Figure 8.5

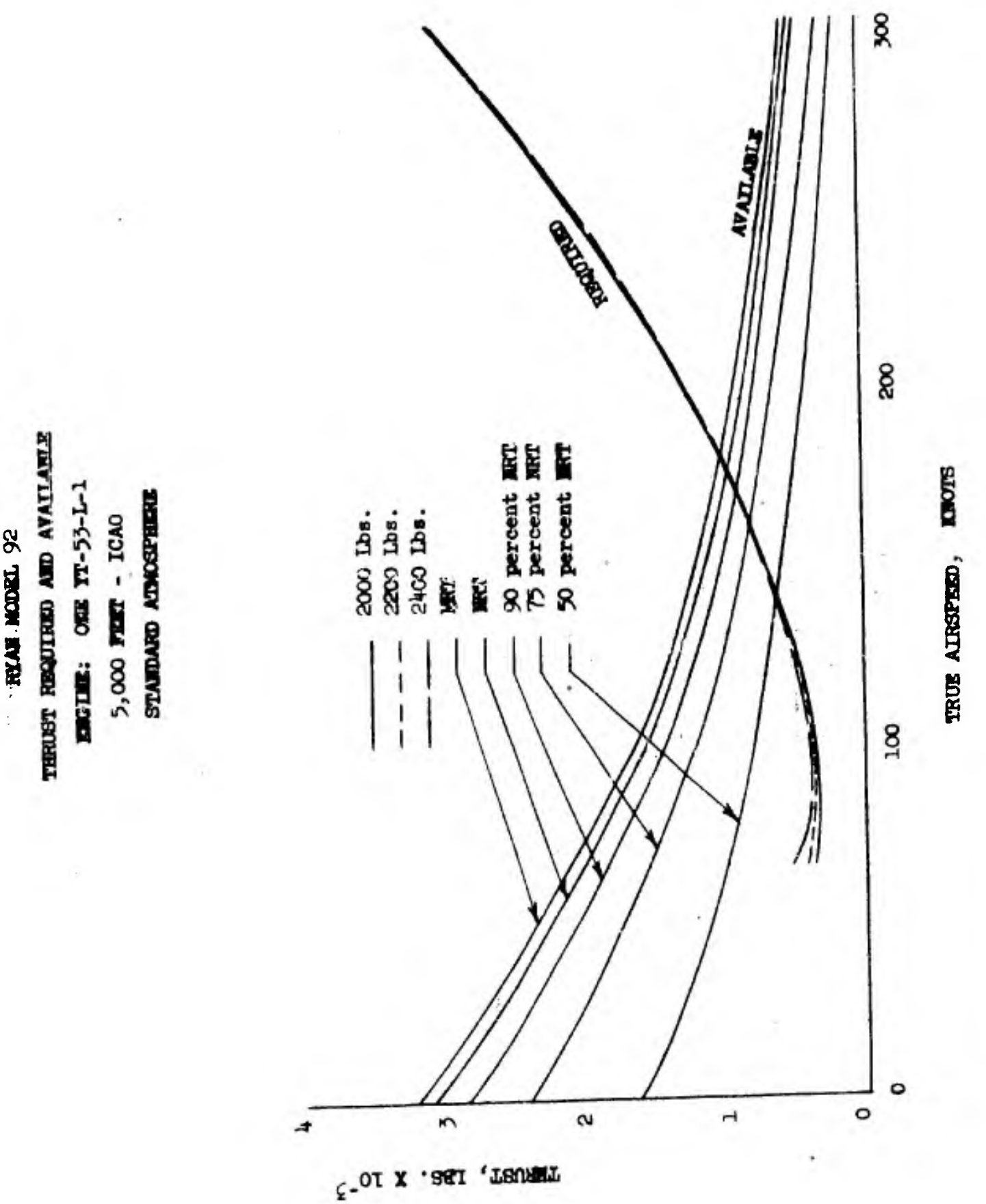
RYAN MODEL 92
THRUST REQUIRED AND AVAILABLE
ENGINE: ONE YT-53-L-1
5,000 FEET - ICAO
STANDARD ATMOSPHERE
2000 Lbs.
2200 Lbs.
2400 Lbs.
MRT
MRT
90 percent MRT
75 percent MRT
50 percent MRT
REQUIRED
AVAILABLE
300
200
100
0
TRUE AIRSPEED, KNOTS
4
3
2
1
0
THRUST, LBS. X 10⁻³

Figure 8.6

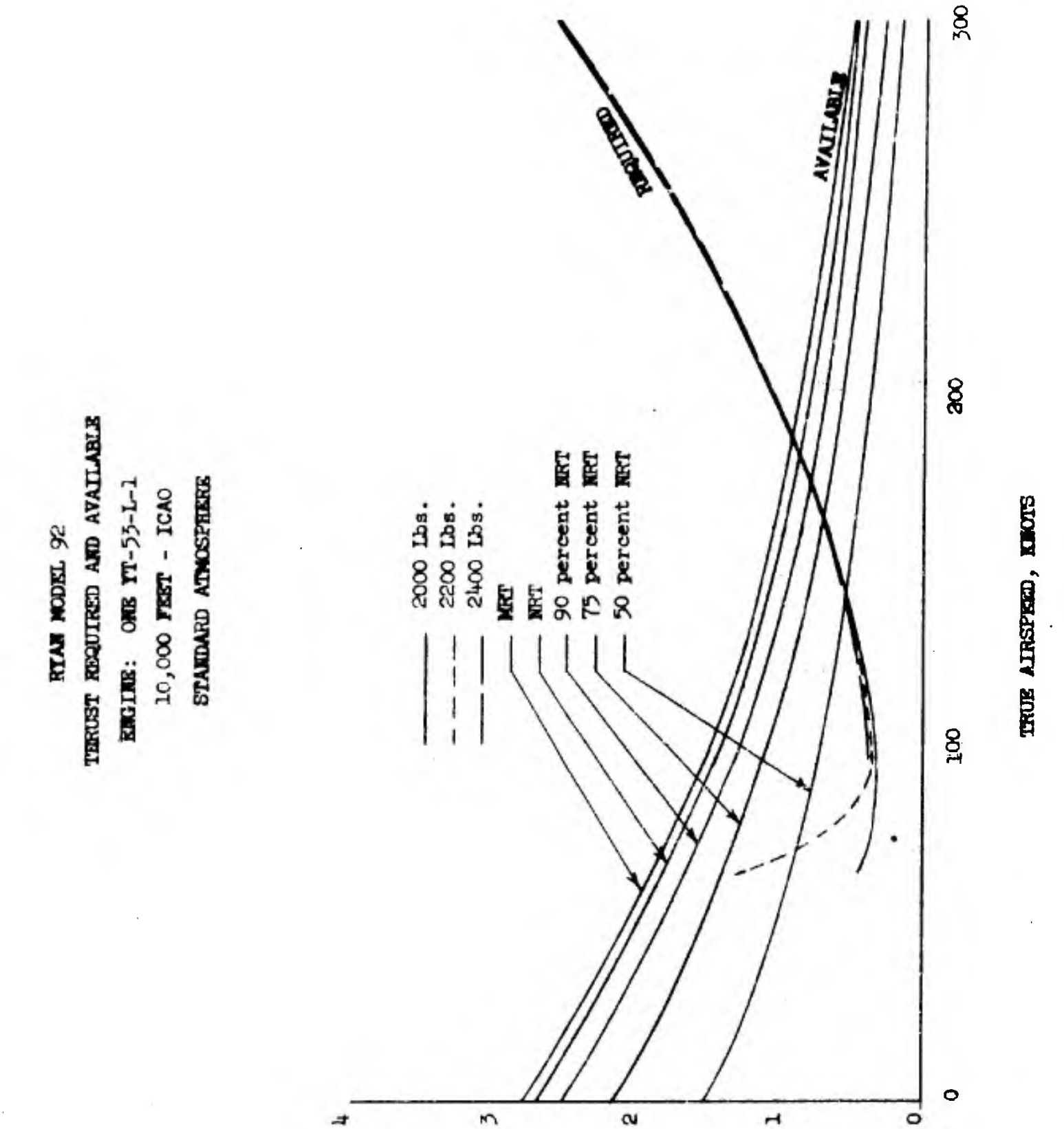
RYAN MODEL 92
TRUST REQUIRED AND AVAILABLE
ENGINE: ONE YT-53-L-1
10,000 FEET - ICAO
STANDARD ATMOSPHERE
2000 Lbs.
2200 Lbs.
2400 Lbs.
MRT
NRT
90 percent MRT
75 percent MRT
50 percent MRT
REQUIRED
AVAILABLE
TRUE AIRSPEED, KNOTS
THRUST, LBS. X 10^{-3}
0
100
200
300
0
1
2
3
4

Figure 8.7

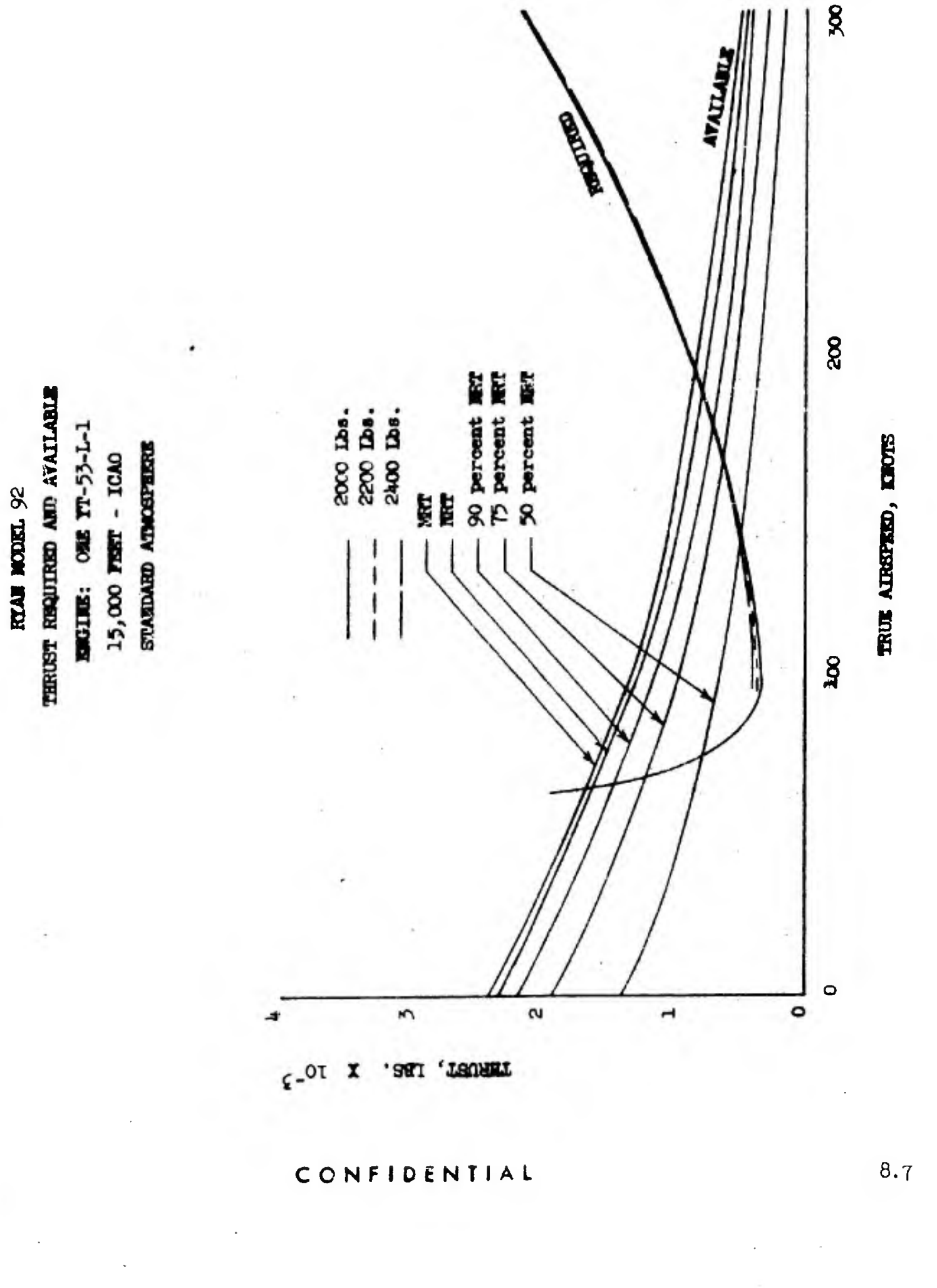
RYAN MODEL 92
THRUST REQUIRED AND AVAILABLE
ENGINE: ONE YT-53-L-1
15,000 FEET - ICAO
STANDARD ATMOSPHERE
2000 Lbs.
2200 Lbs.
2400 Lbs.
MRT
MRT
90 percent MRT
75 percent MRT
50 percent MRT
REQUIRED
AVAILABLE
THRUST, LBS. X 10⁻³
TRUE AIRSPEED, KNOTS
0
1
2
3
4
0
100
200
300

Figure 8.8

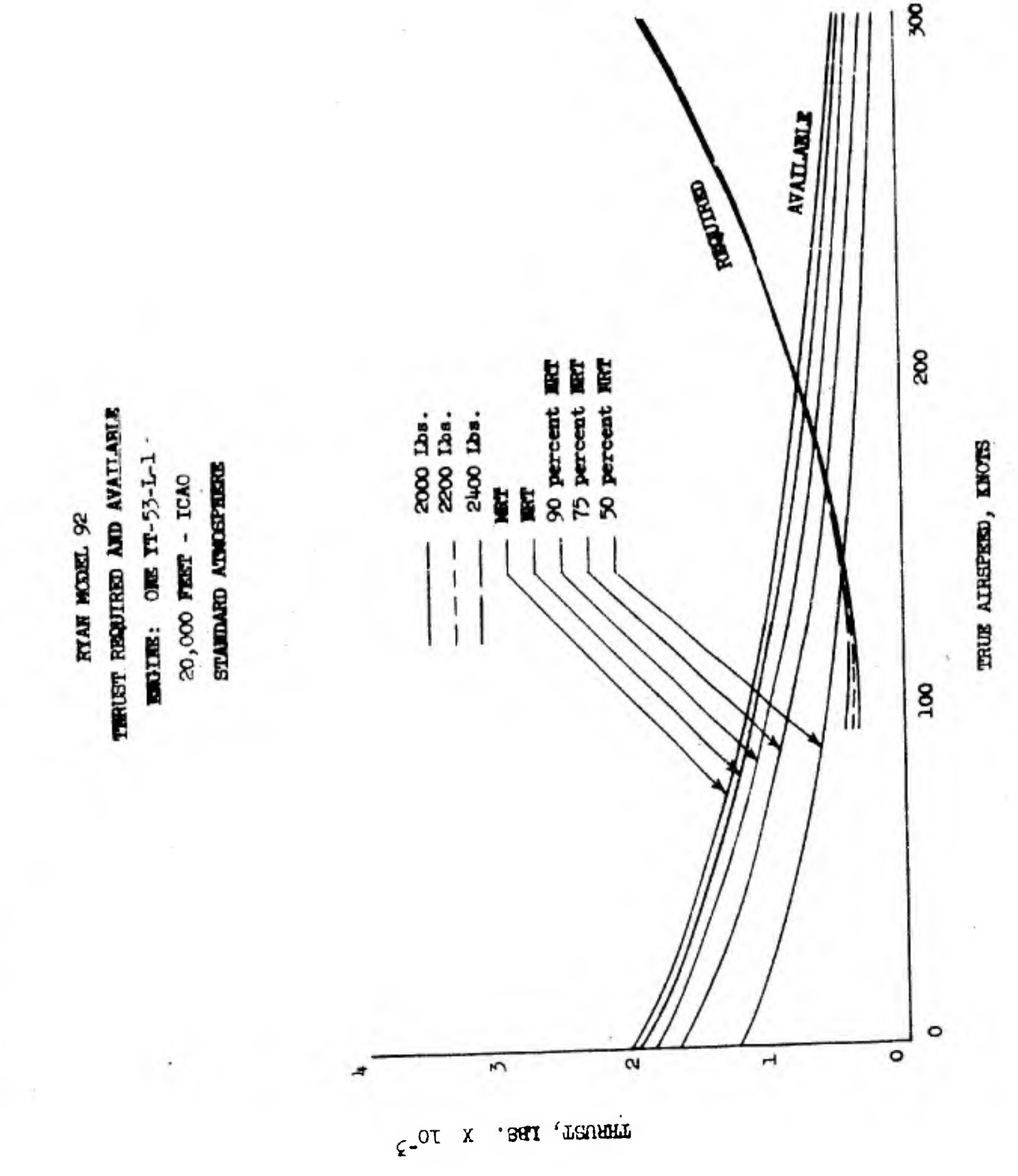
RYAN MODEL 92
THRUST REQUIRED AND AVAILABLE
ENGINE: ONE YT-53-L-1 - ICAO
20,000 FEET - 100 KNOTS
STANDARD ATMOSPHERE
2000 Lbs.
2200 Lbs.
2400 Lbs.
MRT
MRT
90 percent MRT
75 percent MRT
50 percent MRT
REQUIRED
AVAILABLE
THRUST, LBS. X 10^{-3}
TRUE AIRSPEED, KNOTS
0
1
2
3
4
100
200
300

Figure 8.9

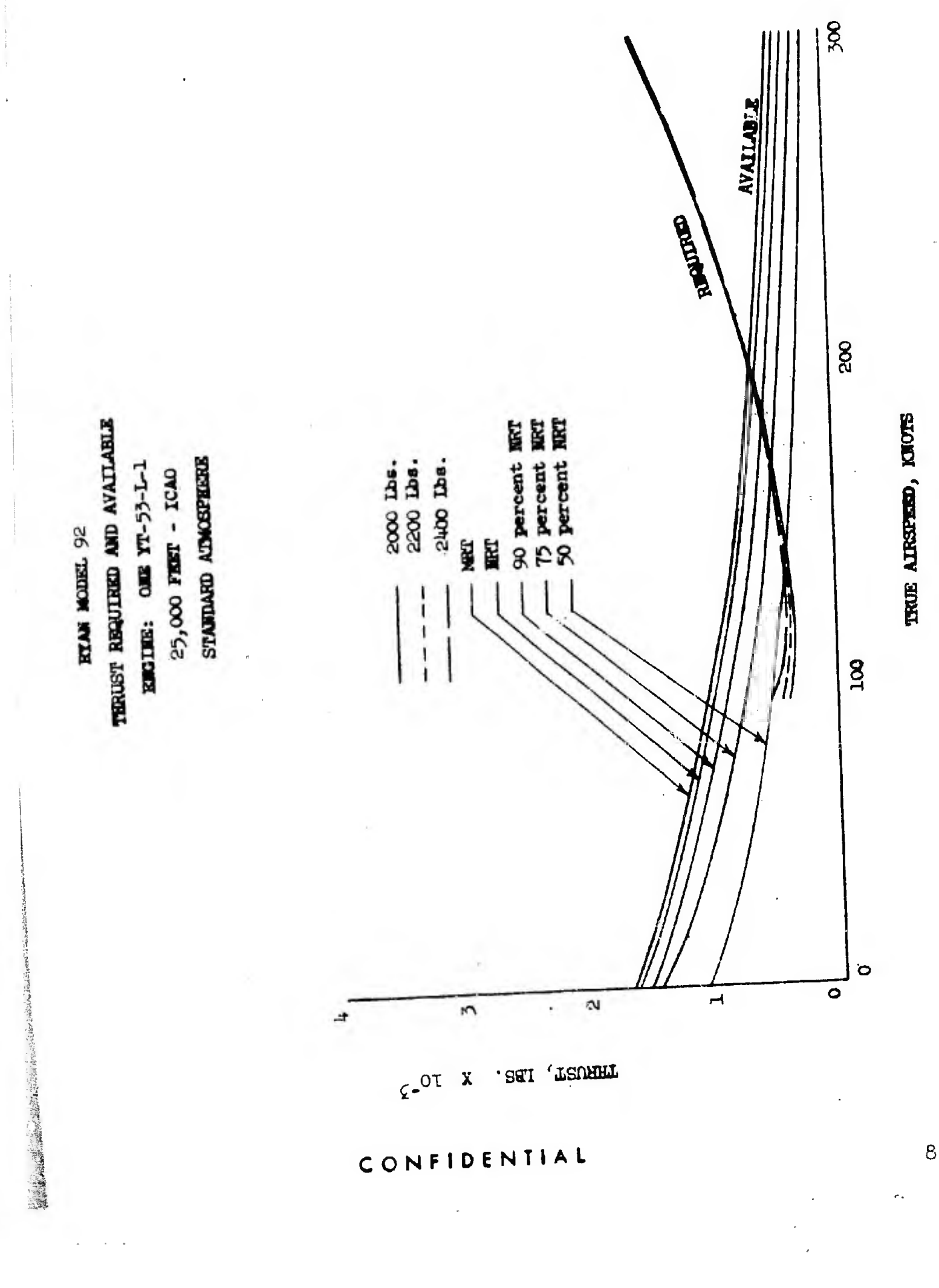
RYAN MODEL 92
THRUST REQUIRED AND AVAILABLE
ENGINE: ONE YT-53-L-1
25,000 FEET - ICAO
STANDARD ATMOSPHERE
2000 Lbs.
2200 Lbs.
2400 Lbs.
MRT
MRT
90 percent MRT
75 percent MRT
50 percent MRT
REQUIRED
AVAILABLE
300
200
100
0
TRUE AIRSPEED, KNOTS
THRUST, LBS. X 10^{-3}
4
3
2
1
0

Figure 8.10

RYAN MODEL 92
HOT DAY (103 °F) THRUST
ENGINE: ONE YT-53-L-1
ICAO STANDARD ATMOSPHERE
STATIC OPERATION

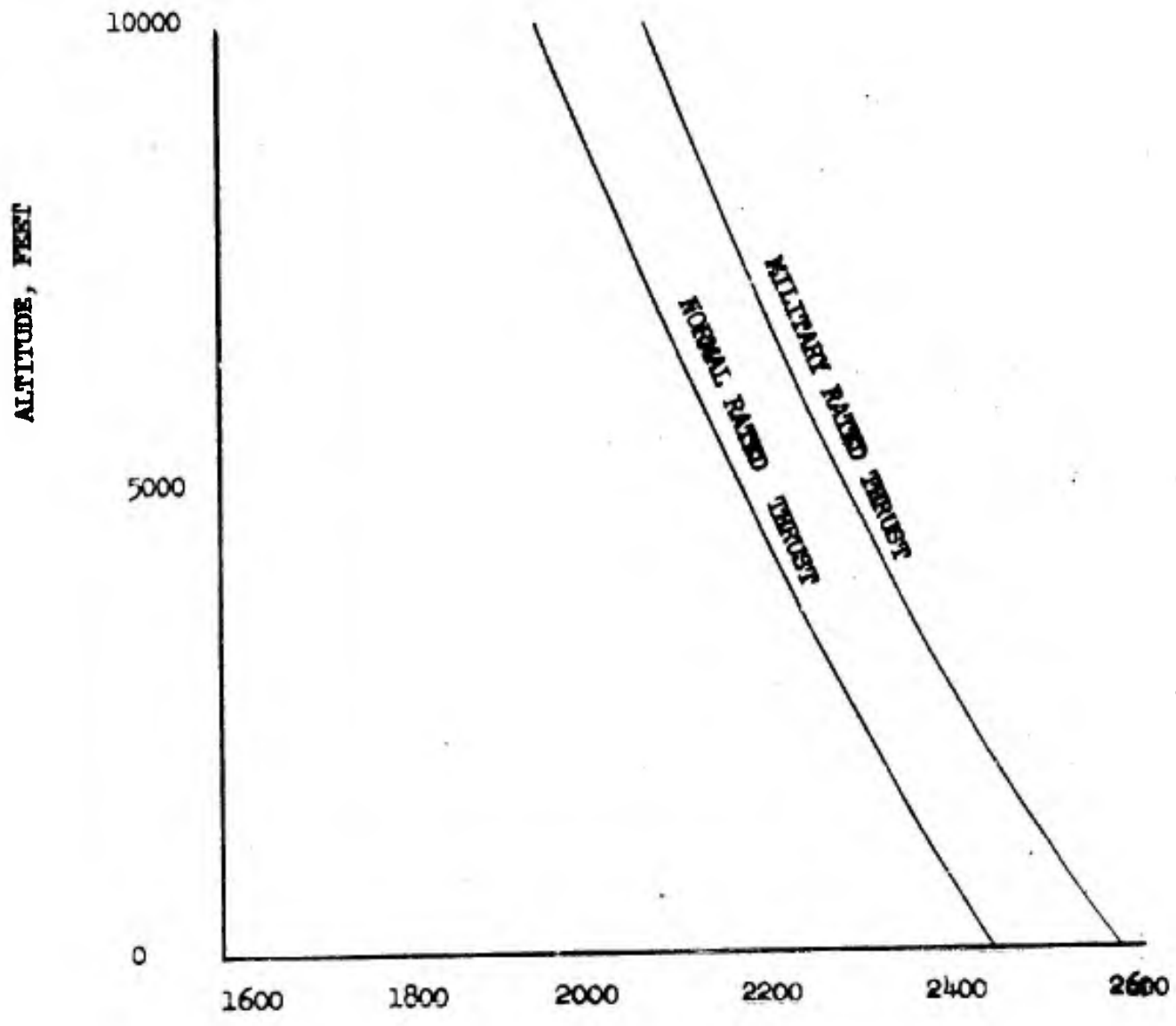

Figure 8.11

RYAN MODEL 92
FUEL FLOW VERSUS AIR SPEED
(INCLUDES 5 PERCENT TOLERANCE)

ENGINE: ONE YT-53-L-1
MILITARY RATED THRUST
ICAC STANDARD ATMOSPHERE

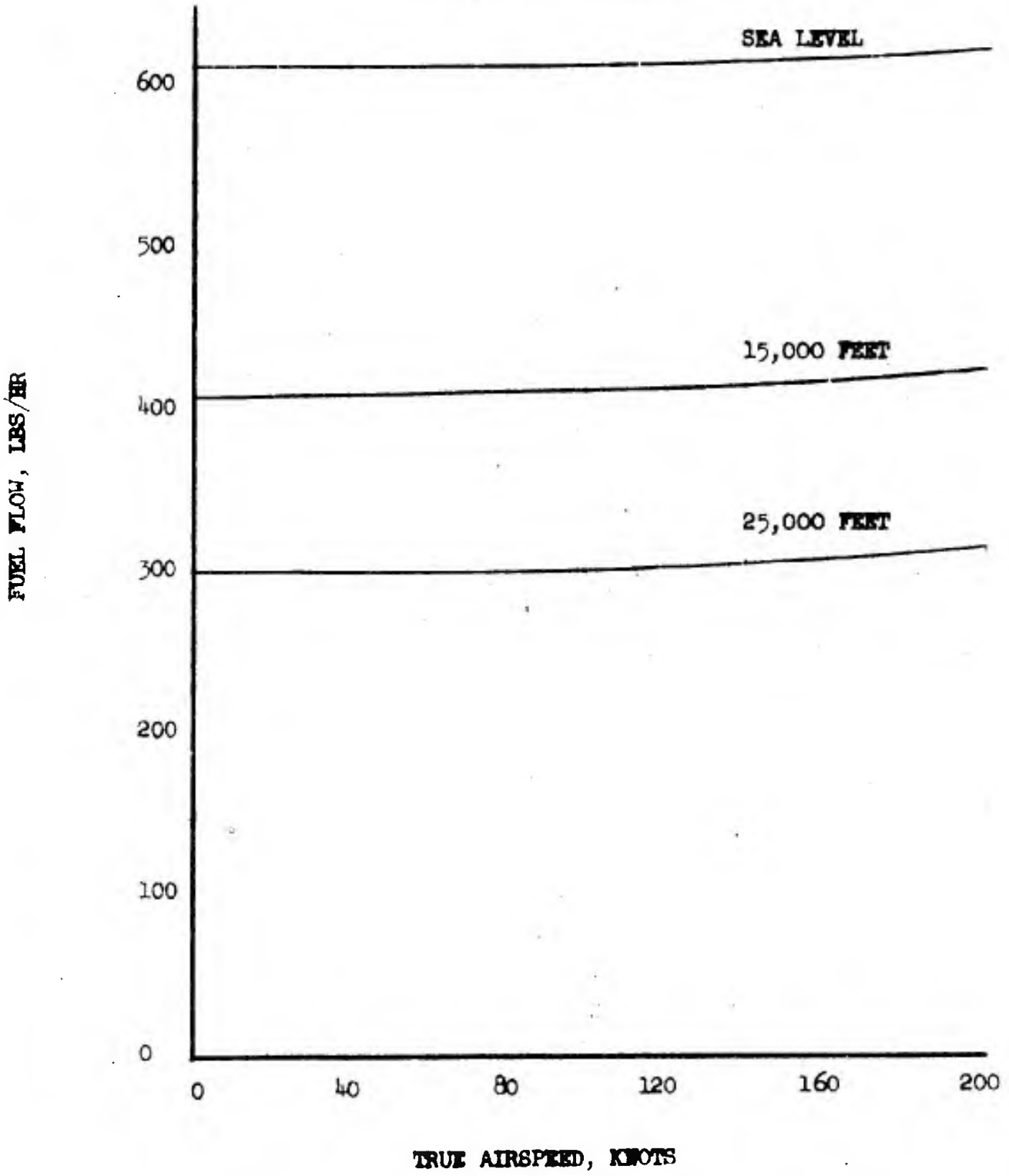

Figure 8.12

RYAN MODEL 92
FUEL FLOW VERSUS AIRSPEED
(INCLUDES 5 PERCENT TOLERANCE)

ENGINE: ONE YT-55-L-1
NORMAL RATED THRUST
ICAO STANDARD ATMOSPHERE

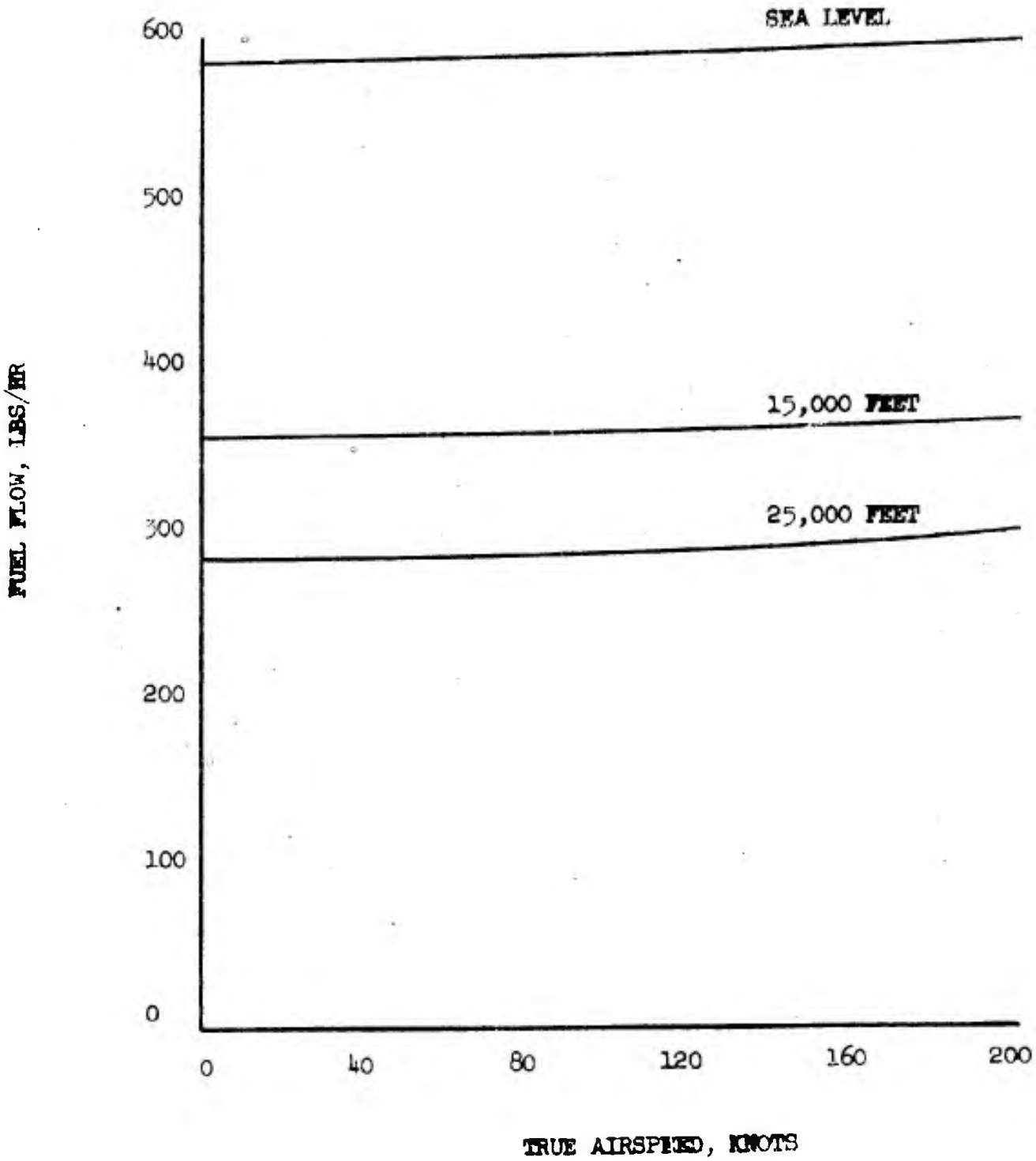

Figure 8.13

RYAN MODEL 9e

FUEL FLOW VERSUS AIRSPEED
(INCLUDES 5 PERCENT TOLERANCE)

ENGINE: ONE YT-53-L-1
90 PERCENT NORMAL RATED THRUST
ICAO STANDARD ATMOSPHERE

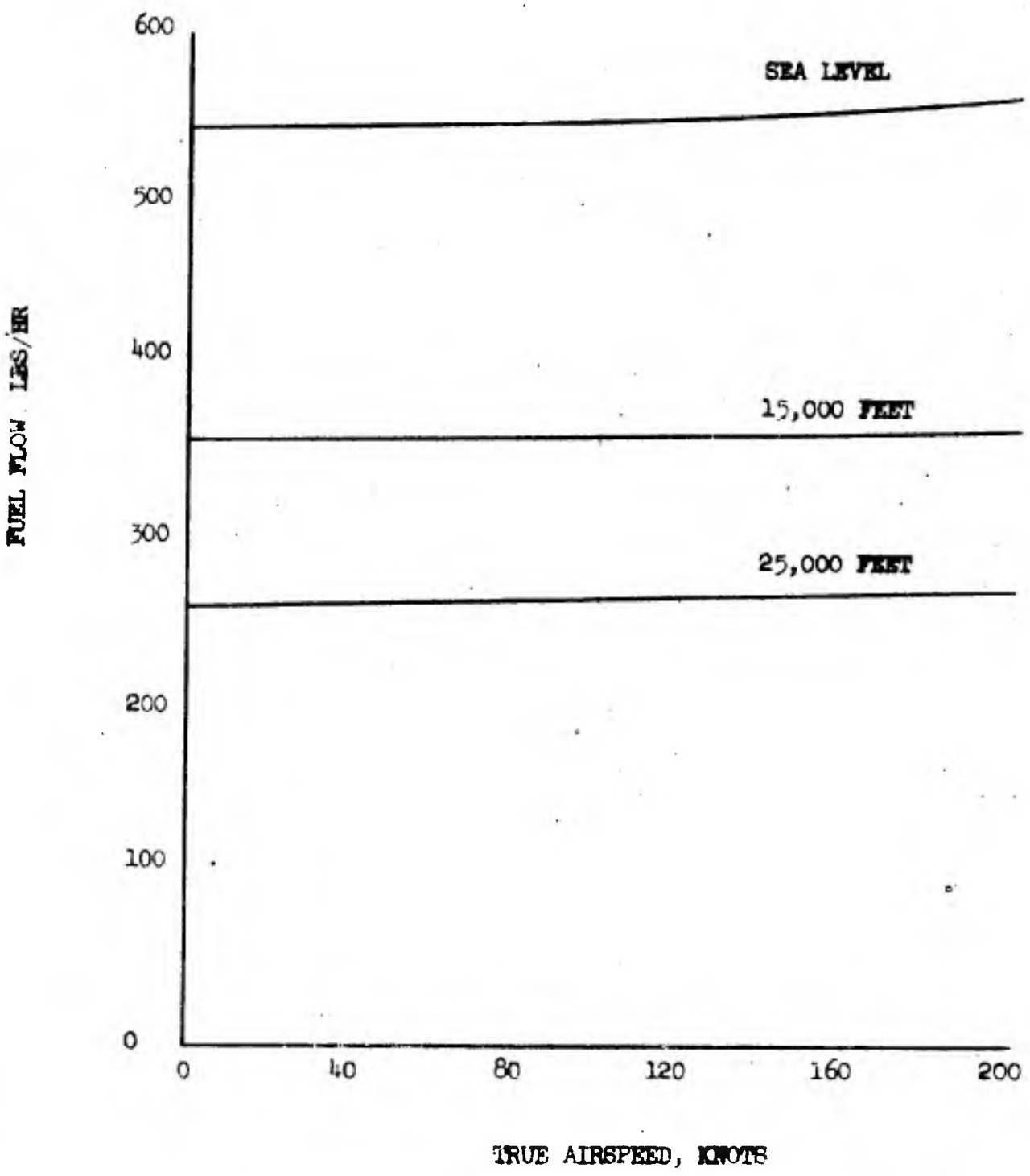

Figure 8.14

RYAN MODEL 92

FUEL FLOW VERSUS AIRSPEED
(INCLUDES 5 PERCENT TOLERANCE)

ENGINE: ONE YT-53-L-1
75 PERCENT NORMAL RATED THRUST
ICAO STANDARD ATMOSPHERE

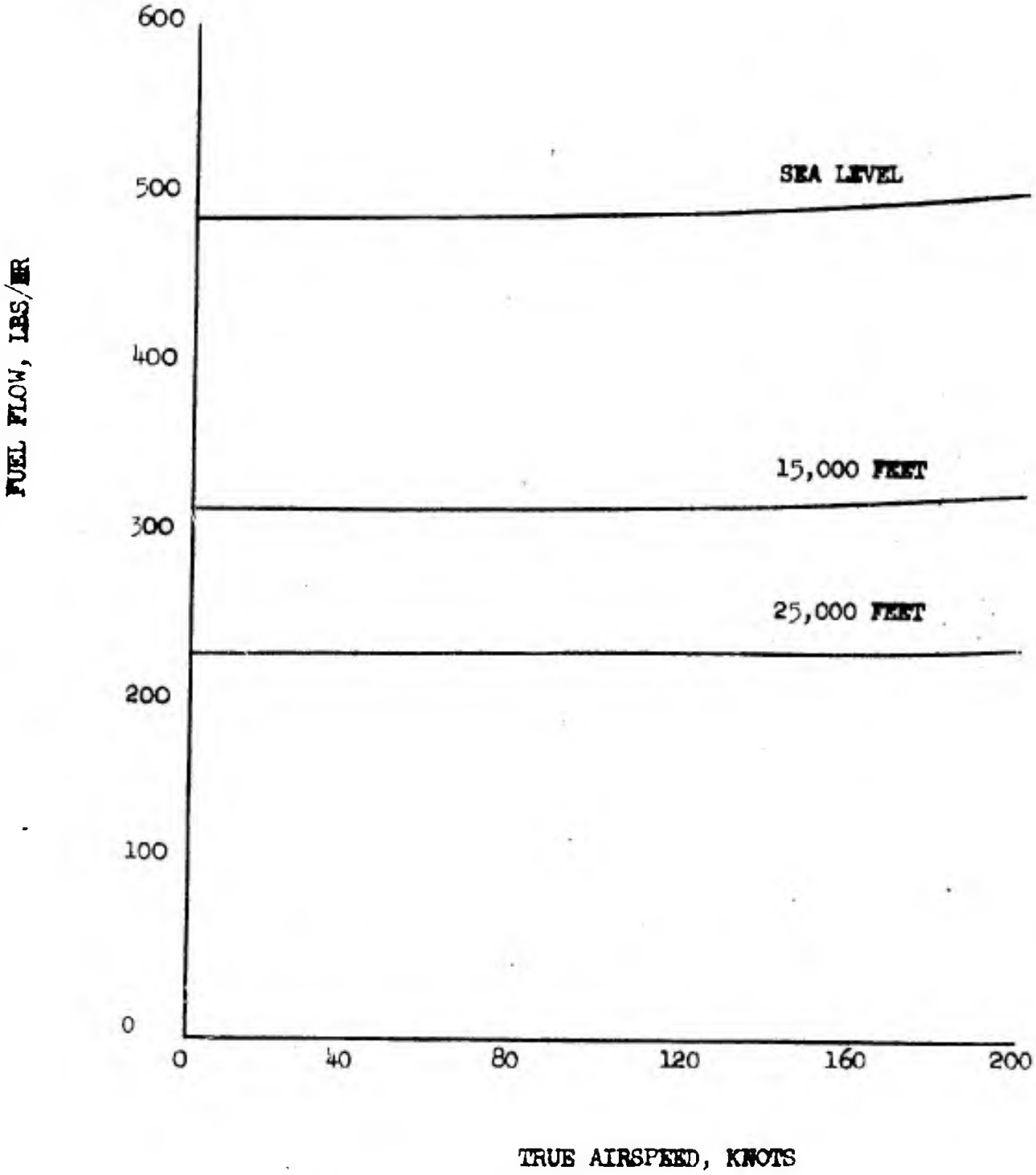

Figure 8.15

RYAN MODEL 92

FUEL FLOW VERSUS AIRSPEED
(INCLUDES 5 PERCENT TOLERANCE)

ENGINE: ONE YT-53-L-1
50 PERCENT NORMAL RATED THRUST
ICAO STANDARD ATMOSPHERE

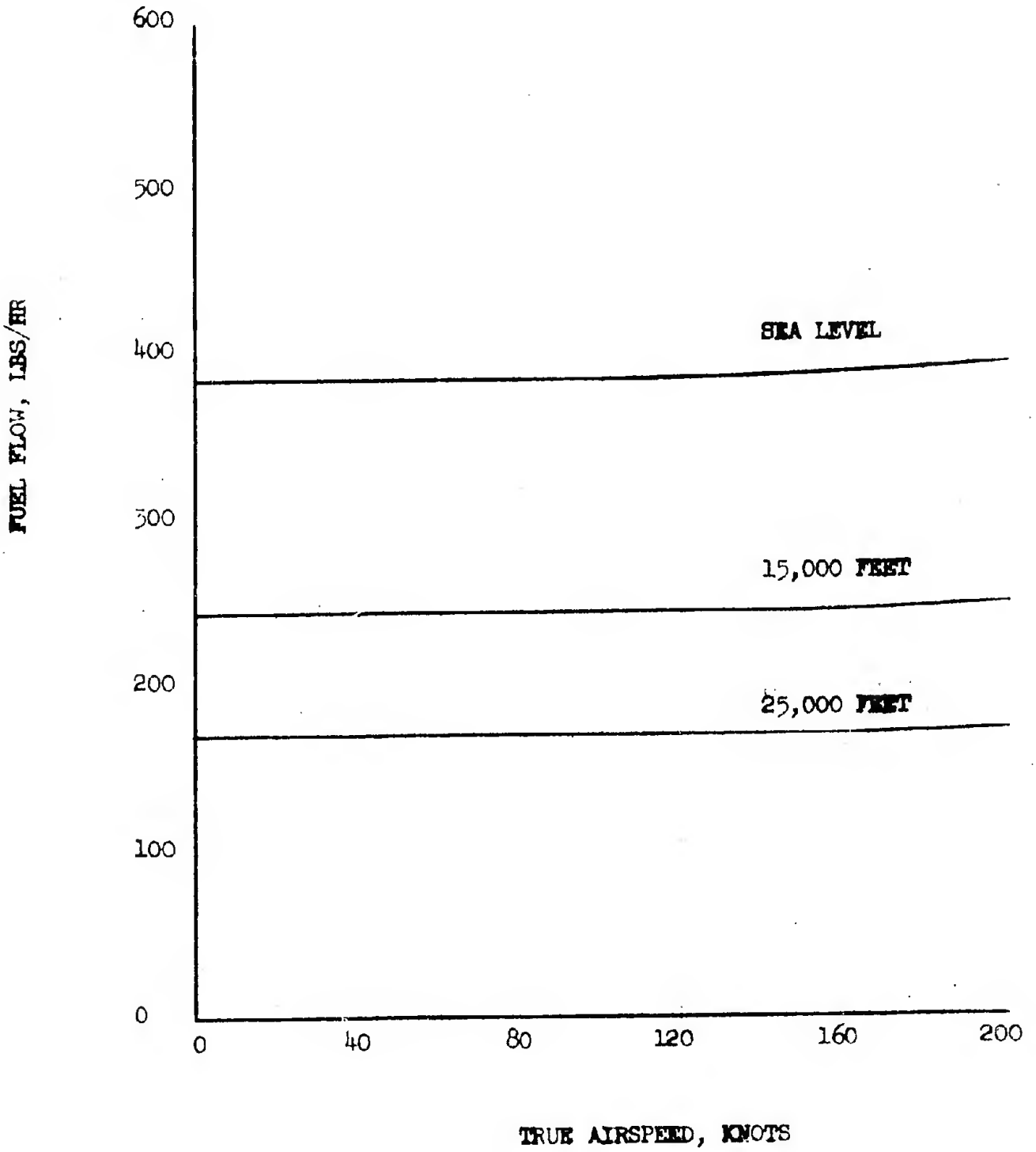

Figure 8.16

RYAN MODEL 92

MAXIMUM SPEED AND
CLIMB SCHEDULES VERSUS TRUE AIRSPEED

ENGINE: ONE YT-53-L-1
ICAO STANDARD ATMOSPHERE

185 Knots Constant Calibrated Airspeed

_ _ _ _ _ LIMIT OF ENGINE DATA

____ ____ AIRPLANE LIMIT SPEED

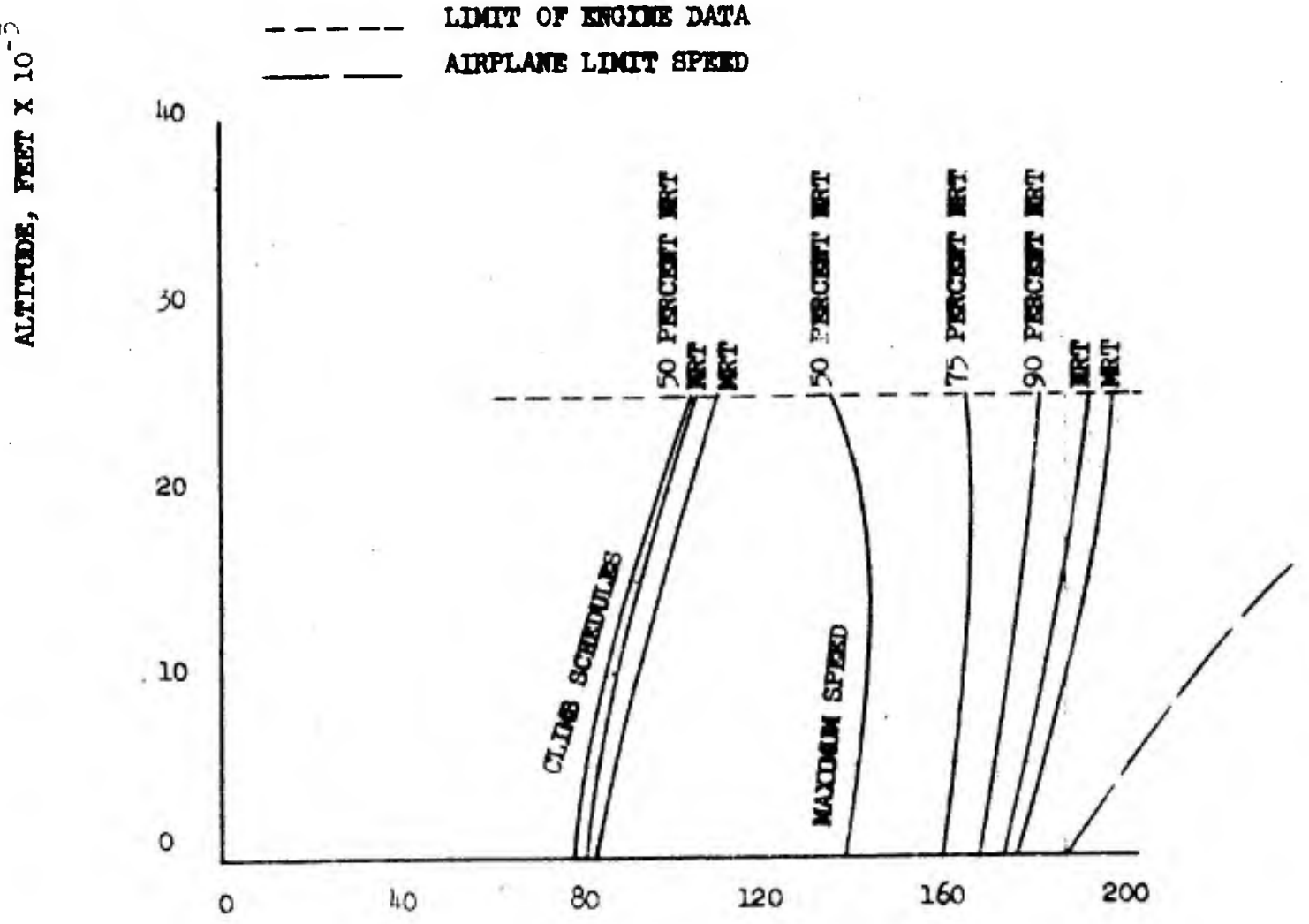

Figure 8.17

RYAN MODEL 92

LIMIT SPEEDS AT
VARIOUS FLAP DEFLECTIONS

ENGINE: ONE YT-53-L-1
ICAO STANDARD ATMOSPHERE
SEA LEVEL

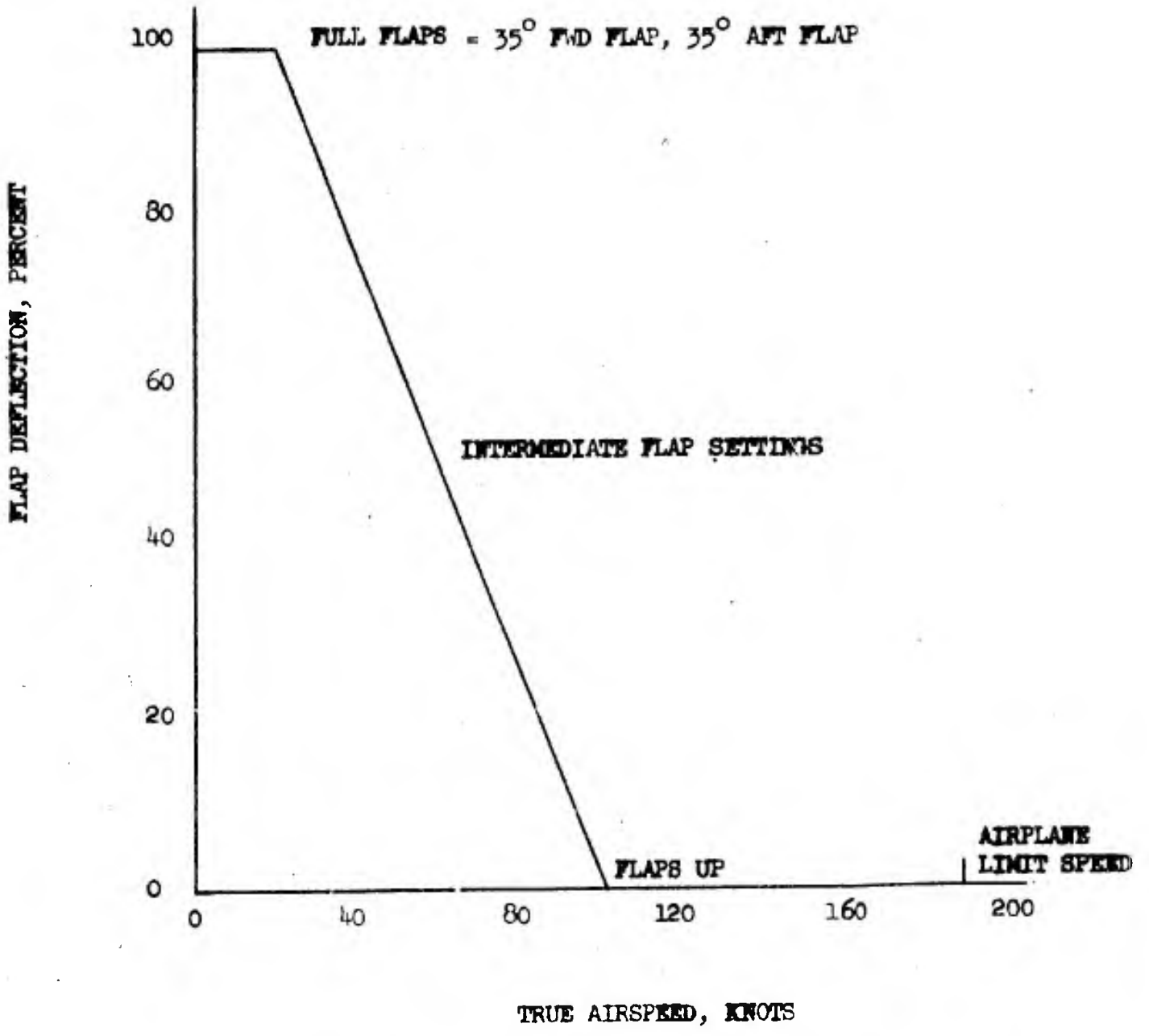

Figure 8.18

RYAN MODEL 92

POWER-ON STALL SPEEDS
NO FLAP DEFLECTION

ENGINE: ONE YT-53-L-1
MILITARY RATED THRUST
ICAO STANDARD ATMOSPHERE

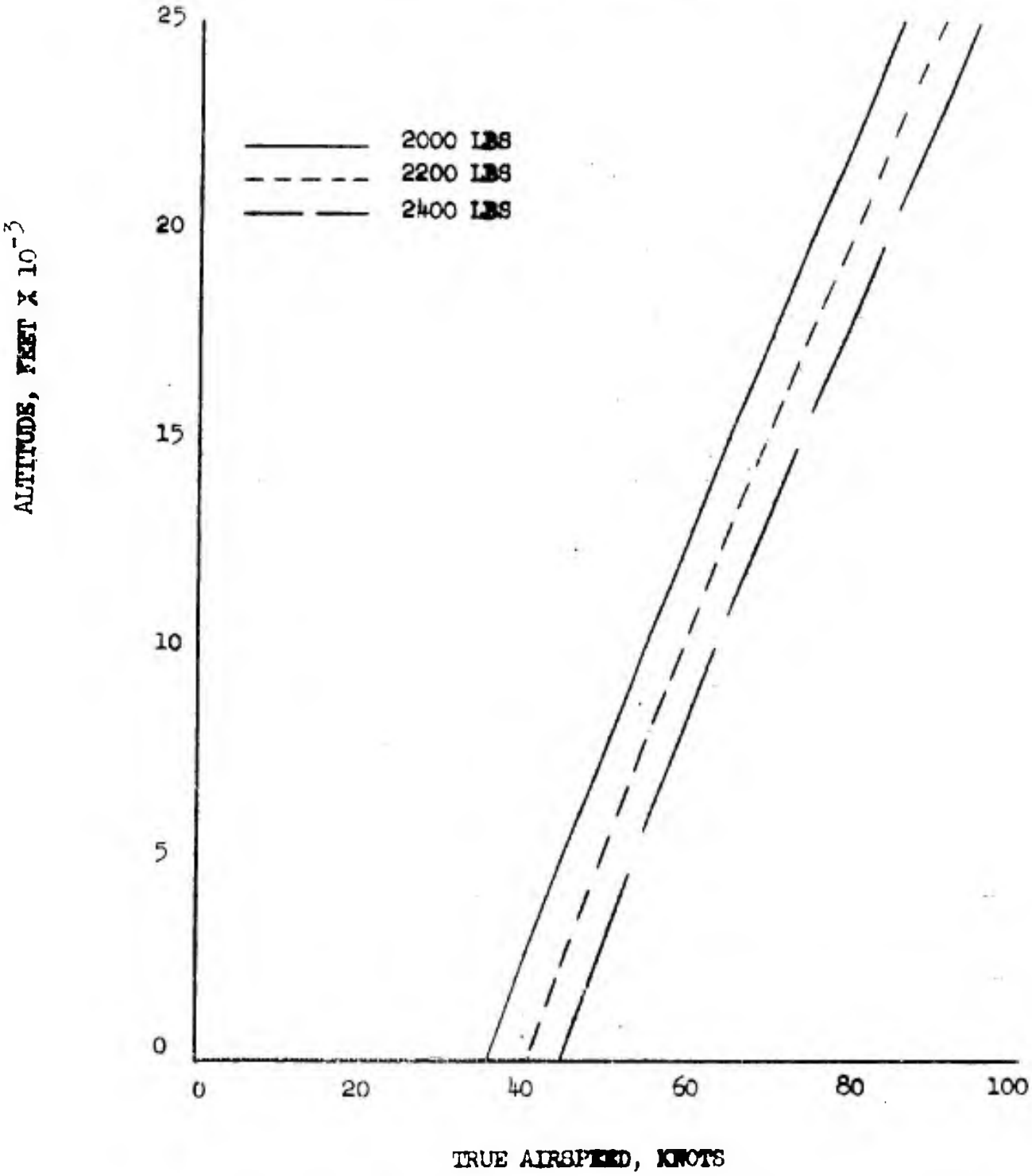

Figure 8.19

RYAN MODEL 92

POWER-ON STALL SPEEDS
NO FLAP DEFLECTION

ENGINE: ONE YT-53-L-1
NORMAL RATED THRUST
ICAO STANDARD ATMOSPHERE

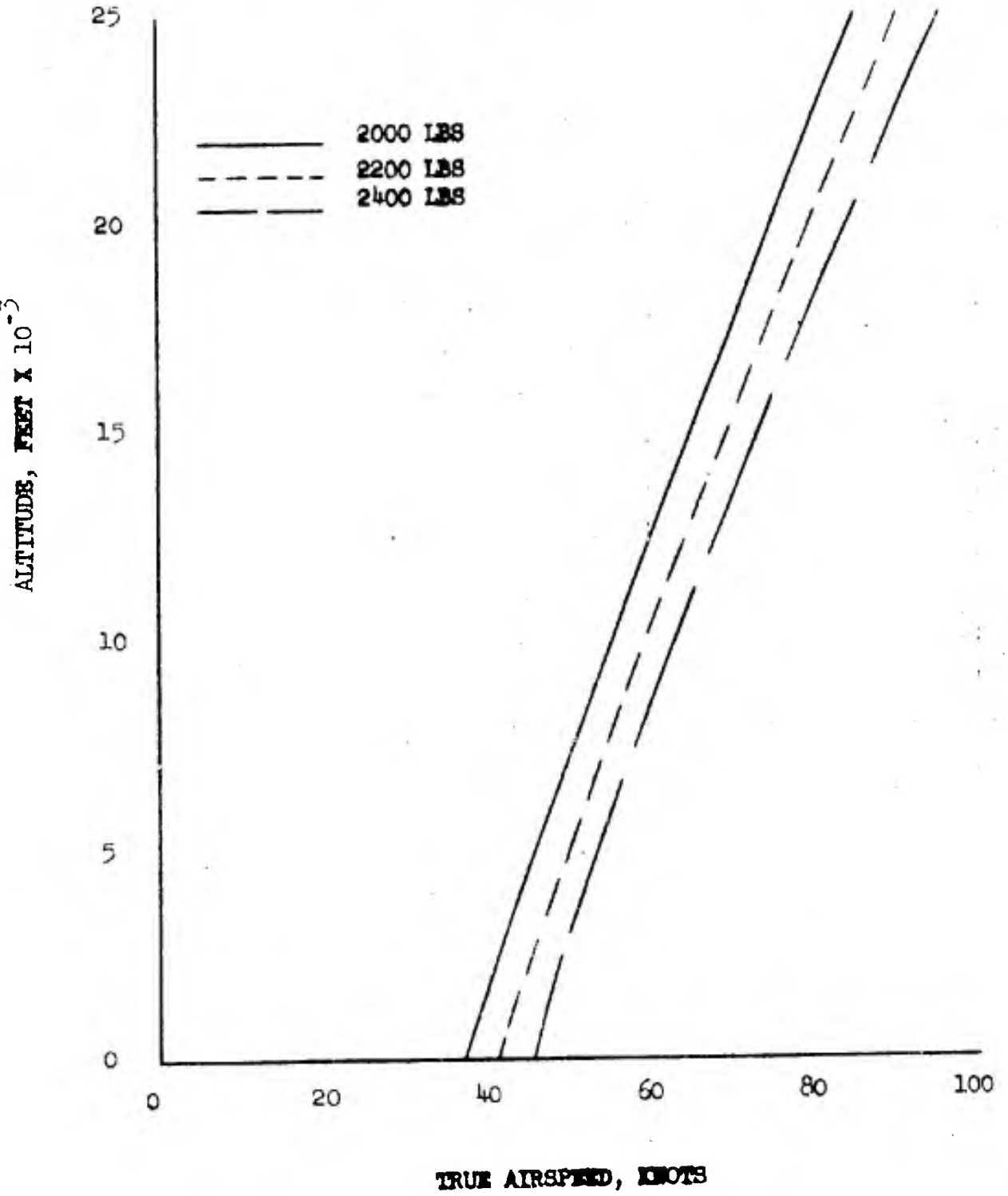

Figure 8.20

RYAN MODEL 92

POWER-ON STALL SPEEDS
NO FLAP DEFLECTION

ENGINE: ONE YT-53-L-1
90 PERCENT NORMAL RATED THRUST
ICAO STANDARD ATMOSPHERE

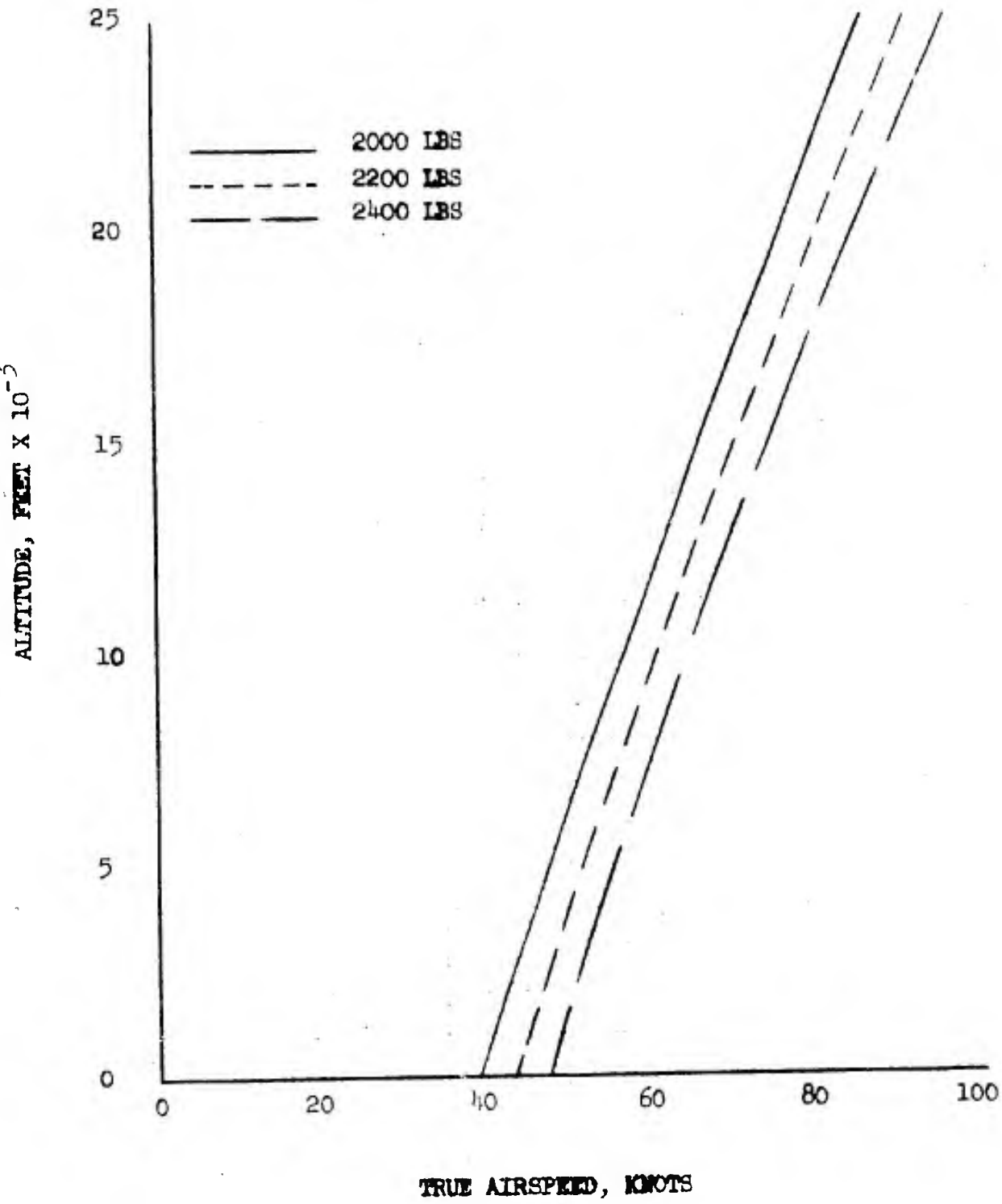

Figure 8.21

RYAN MODEL 92

POWER-ON STALL SPEED
NO FLAP DEFLECTION

ENGINE: ONE YT-53-L-1
75 PERCENT NORMAL RATED THRUST
ICAO STANDARD ATMOSPHERE

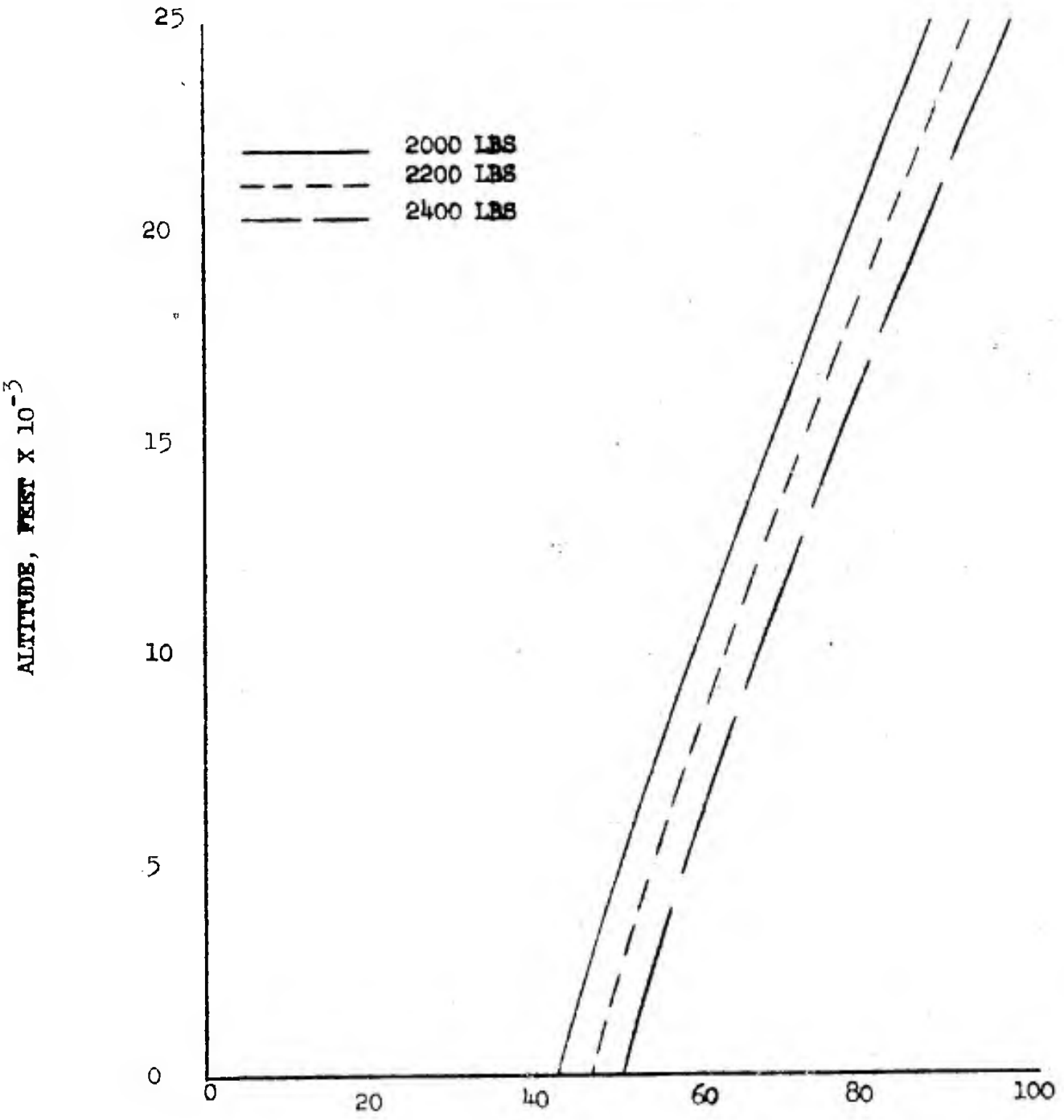

Figure 8.22

RYAN MODEL 92

POWER-ON STALL SPEEDS
NO FLAP DEFLECTION

ENGINE: ONE YT-53-L-1
50 PERCENT NORMAL RATED THRUST
ICAO STANDARD ATMOSPHERE

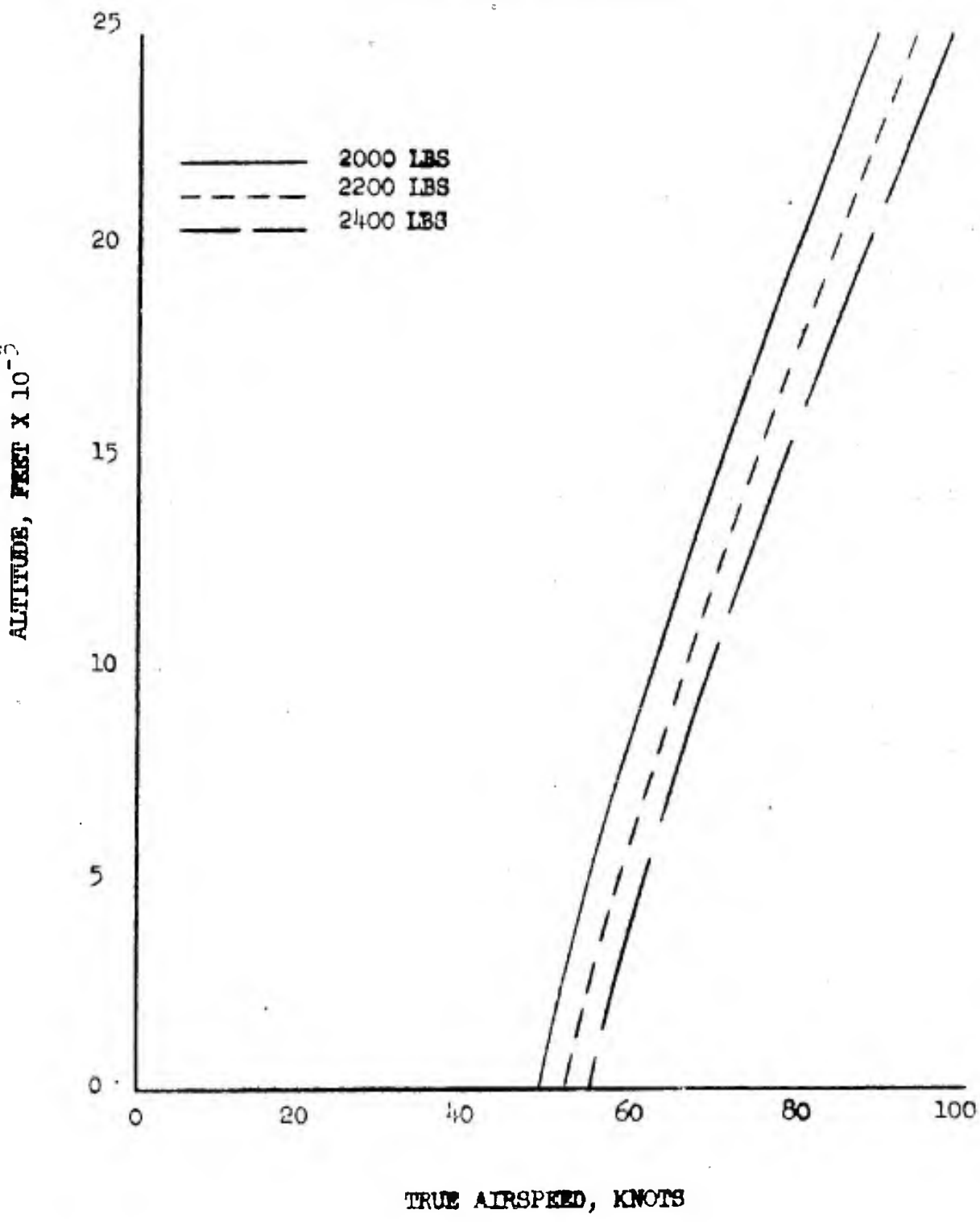

Figure 8.23

RYAN MODEL 92

POWER-OFF STALL SPEEDS
NO FLAP DEFLECTION

ENGINE: ONE YT-53-L-1

ICAO STANDARD ATMOSPHERE

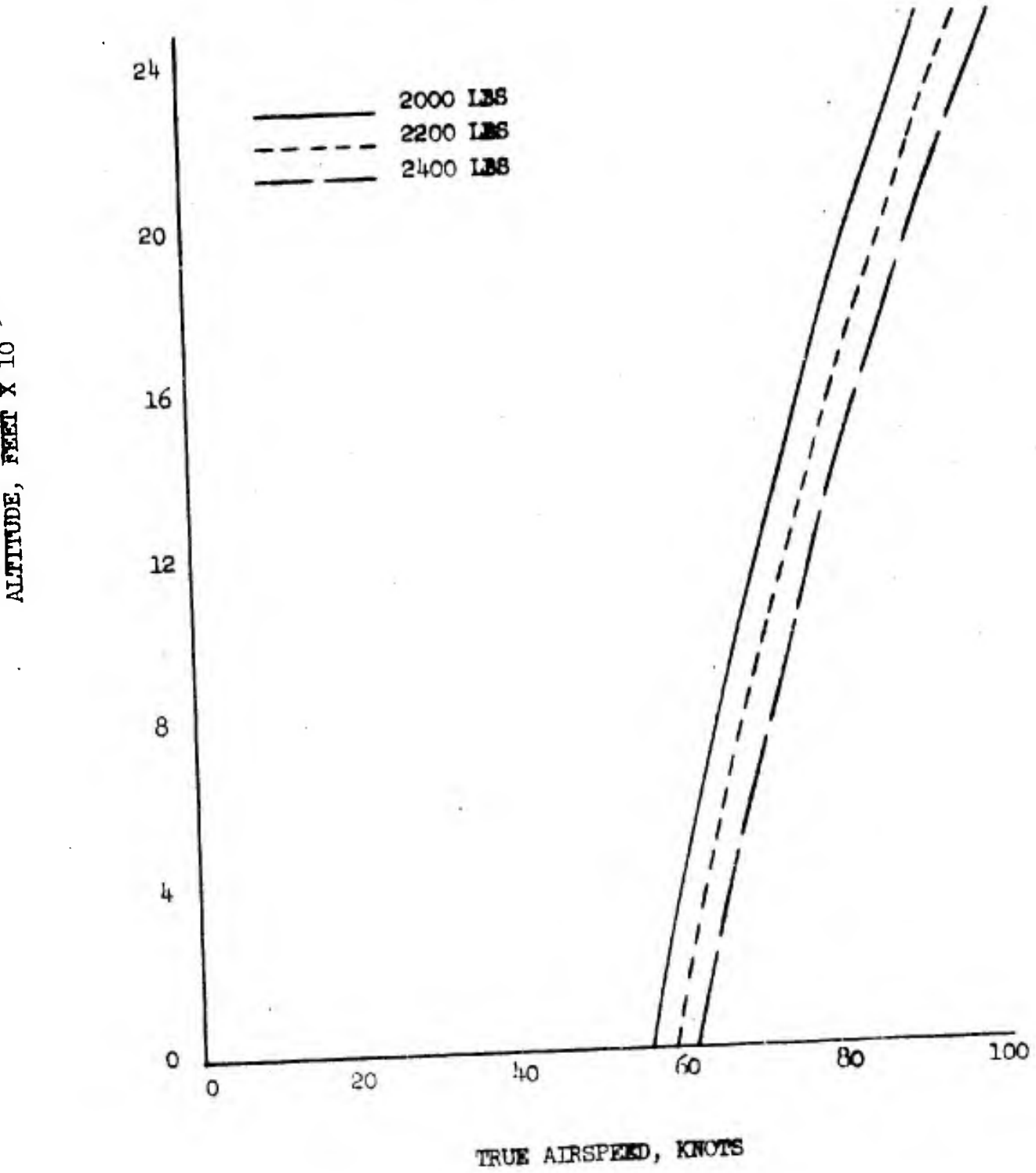

Figure 8.24

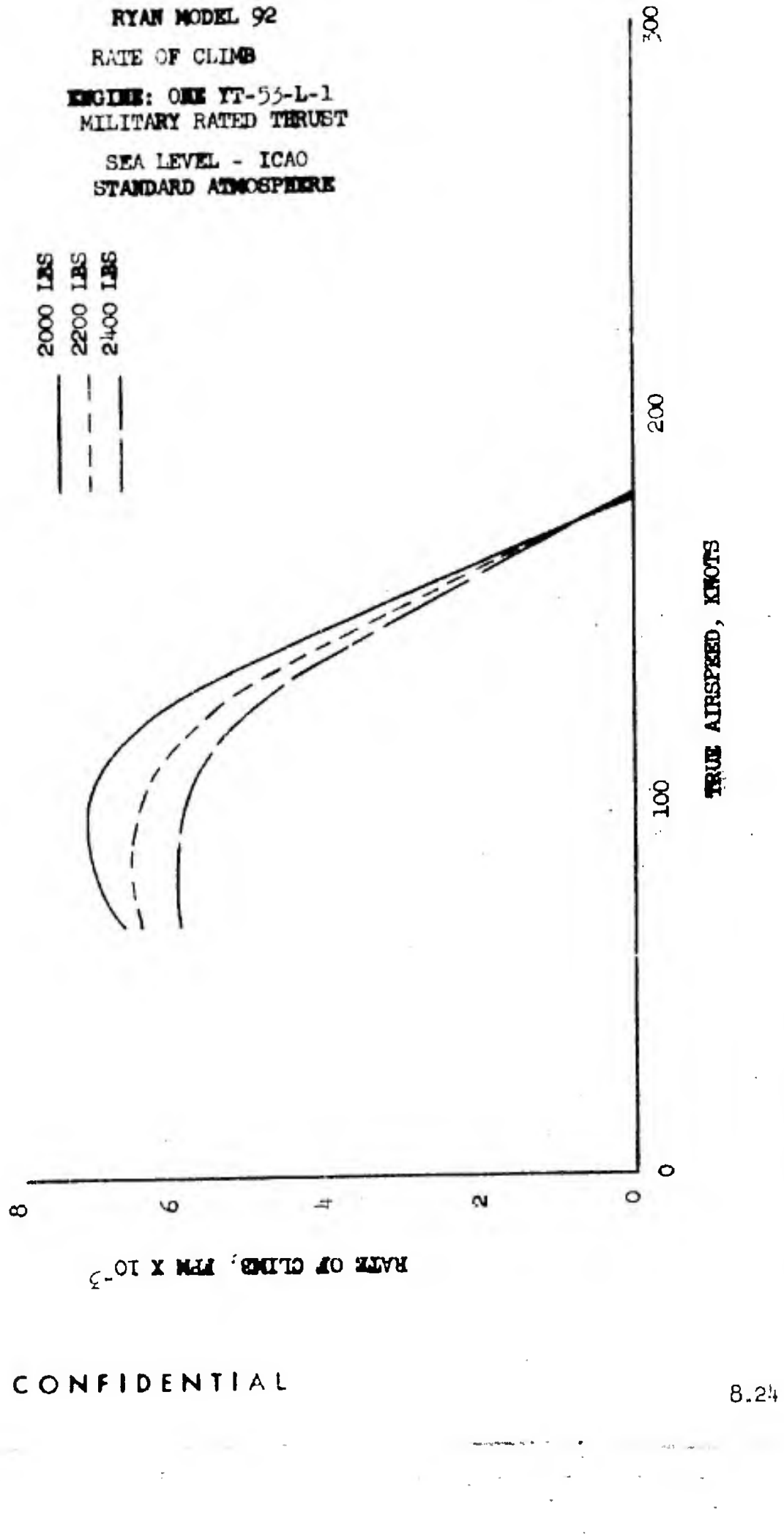
RYAN MODEL 92
RATE OF CLIMB
ENGINE: ONE YT-53-L-1
MILITARY RATED THRUST
SEA LEVEL - ICAO
STANDARD ATMOSPHERE
2000 LBS
2200 LBS
2400 LBS
300
200
100
0
TRUE AIRSPEED, KNOTS
RATE OF CLIMB, FPM X 10⁻³
8
6
4
2
0

Figure 8.25

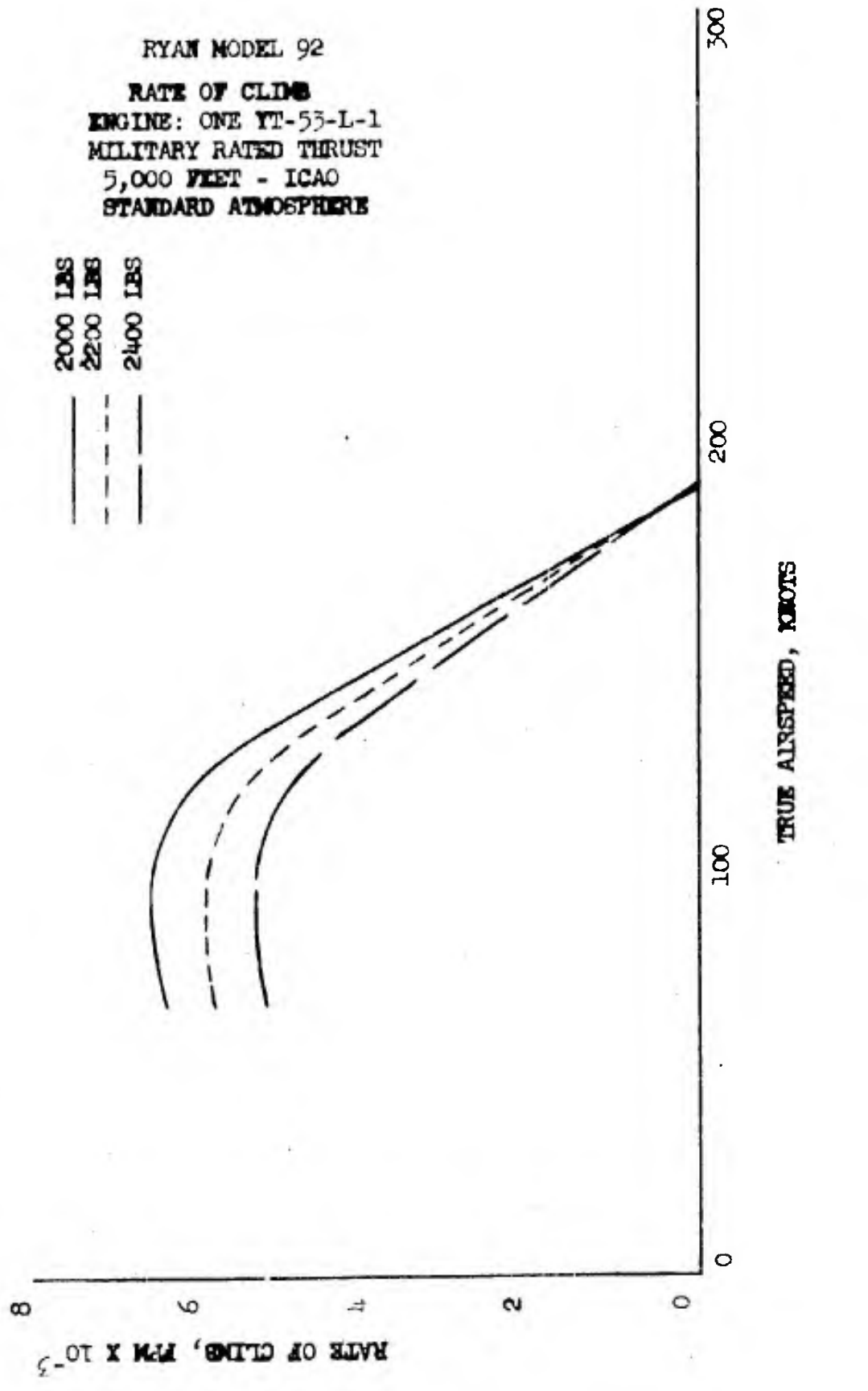
RYAN MODEL 92
RATE OF CLIMB
ENGINE: ONE YT-53-L-1
MILITARY RATED THRUST
5,000 FEET - ICAO
STANDARD ATMOSPHERE
2000 LBS
2200 LBS
2400 LBS
TRUE AIRSPEED, KNOTS
0
100
200
300
RATE OF CLIMB, FPM X 10^-3
0
2
4
6
8

Figure 8.26

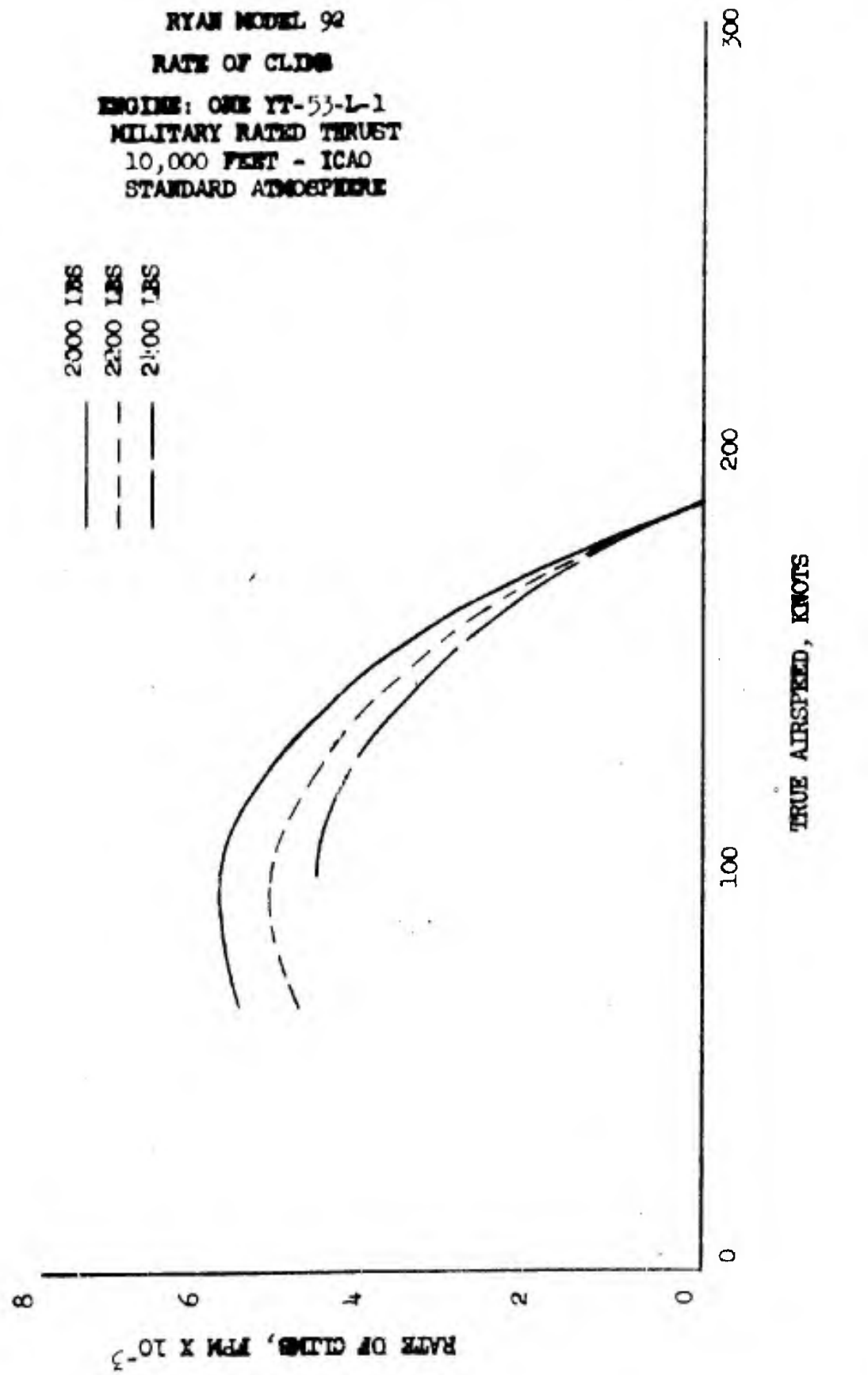
RYAN MODEL 92
RATE OF CLIMB
ENGINE: ONE YT-53-L-1
MILITARY RATED THRUST
10,000 FEET - ICAO
STANDARD ATMOSPHERE
2000 LBS
2200 LBS
2400 LBS
RATE OF CLIMB, FPM X 10⁻³
0
2
4
6
8
0
100
200
300
TRUE AIRSPEED, KNOTS

Figure 8.27

RYAN MODEL 92
RATE OF CLIMB

ENGINE: ONE YT-53-L-1
MILITARY RATED THRUST
15,000 FEET - ICAO
STANDARD ATMOSPHERE

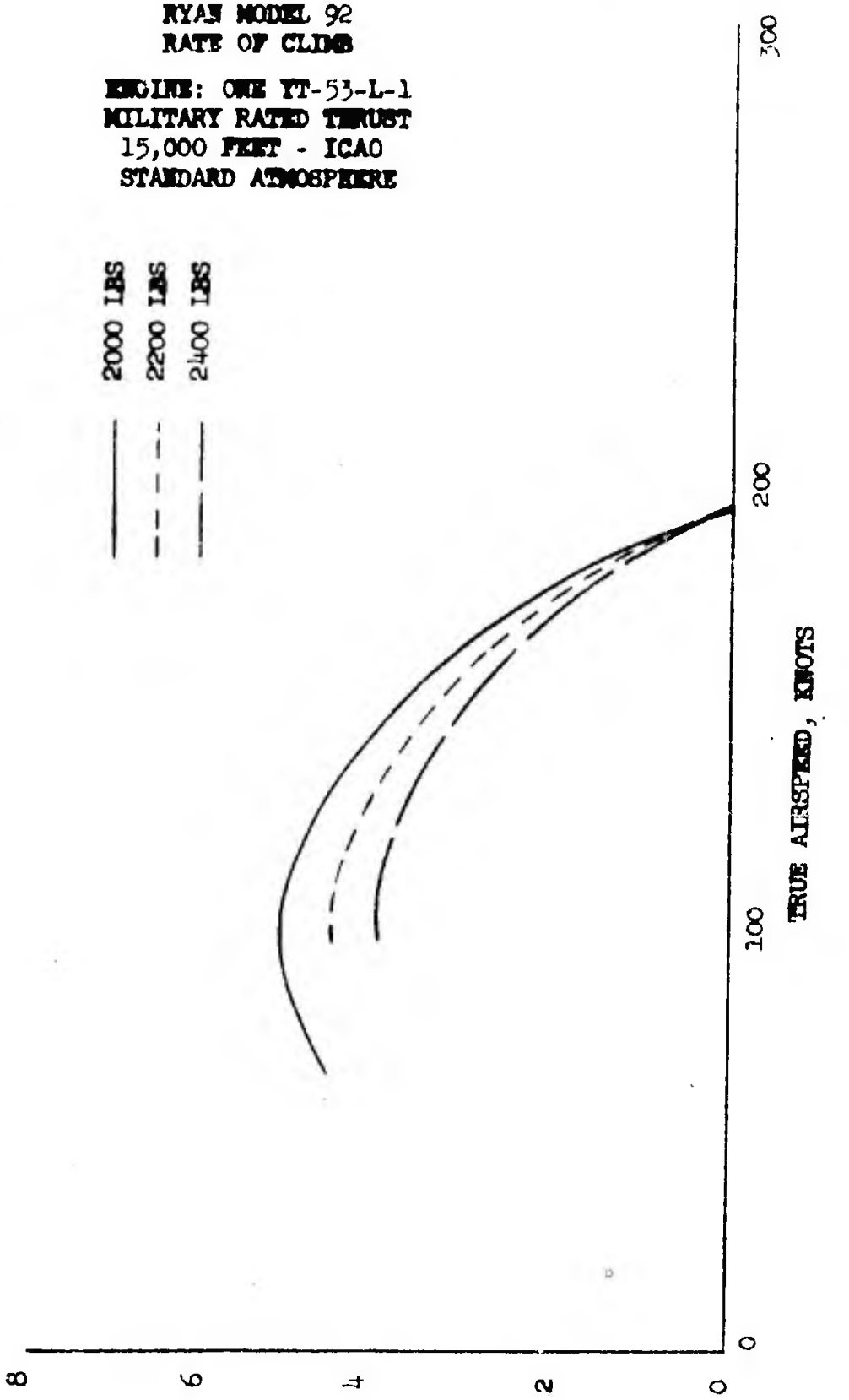

Figure 8.28

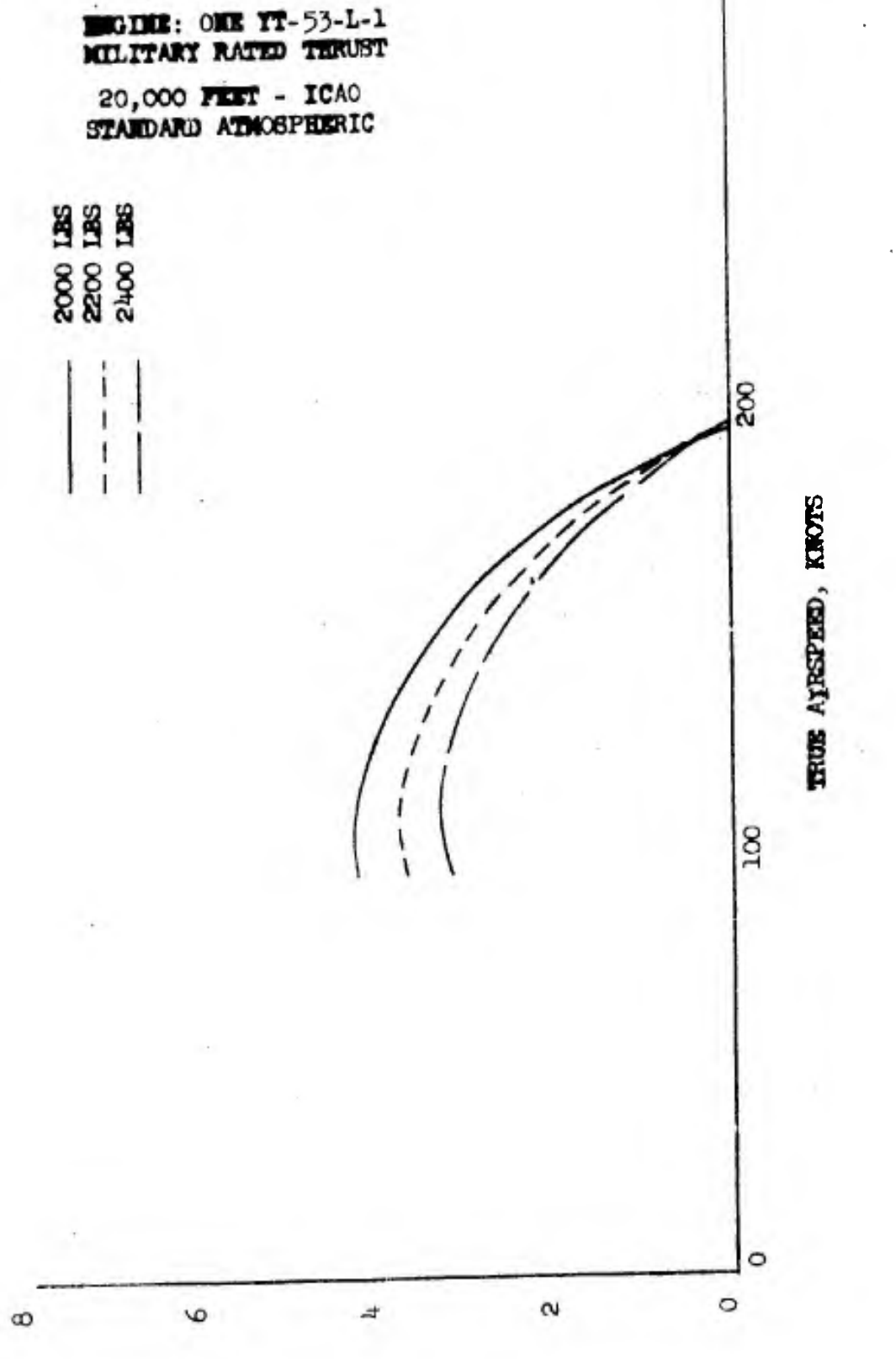
RYAN MODEL 92
RATE OF CLIMB
ENGINE: ONE YT-53-L-1
MILITARY RATED THRUST
20,000 FEET - ICAO
STANDARD ATMOSPHERIC
2000 LBS
2200 LBS
2400 LBS
TRUE AIRSPEED, KNOTS
RATE OF CLIMB, FPM X 10⁻³
0
100
200
300
0
2
4
6
8

Figure 8.29

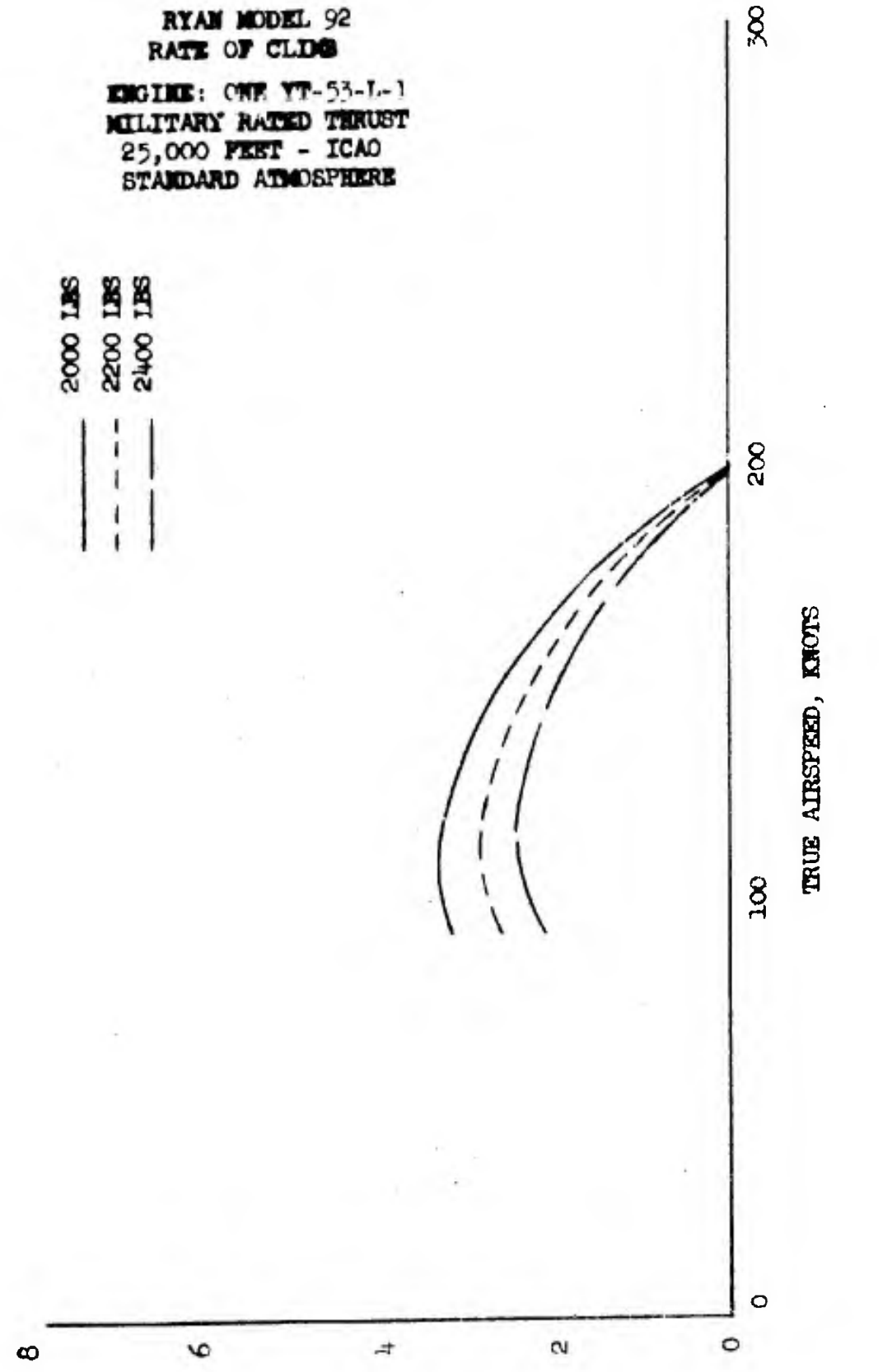
RYAN MODEL 92
RATE OF CLIMB
ENGINE: ONE YT-53-L-1
MILITARY RATED THRUST
25,000 FEET - ICAO
STANDARD ATMOSPHERE
2000 LBS
2200 LBS
2400 LBS
300
200
100
0
TRUE AIRSPEED, KNOTS
0
2
4
6
8
RATE OF CLIMB, FPM X 10^{-3}

Figure 8.30

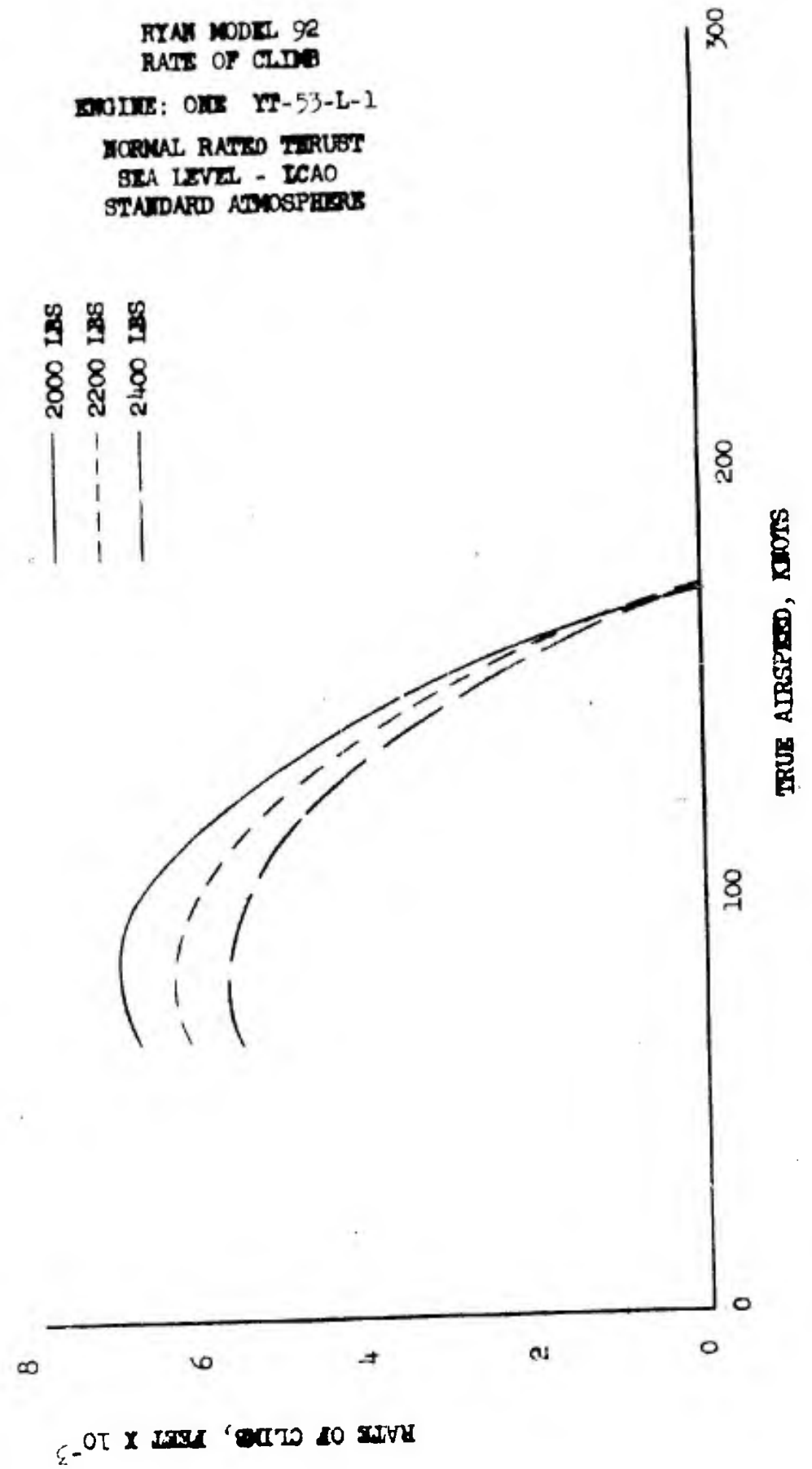
RYAN MODEL 92
RATE OF CLIMB
ENGINE: ONE YT-53-L-1
NORMAL RATED THRUST
SEA LEVEL - ICAO
STANDARD ATMOSPHERE
2000 LBS
2200 LBS
2400 LBS
TRUE AIRSPEED, KNOTS
0
100
200
300
RATE OF CLIMB, FEET X 10⁻³
0
2
4
6
8

Figure 8.31

RYAN MODEL 92
RATE OF CLIMB

ENGINE: ONE YT-53-L-1
NORMAL RATED THRUST
5000 FEET - ICAO
STANDARD ATMOSPHERE

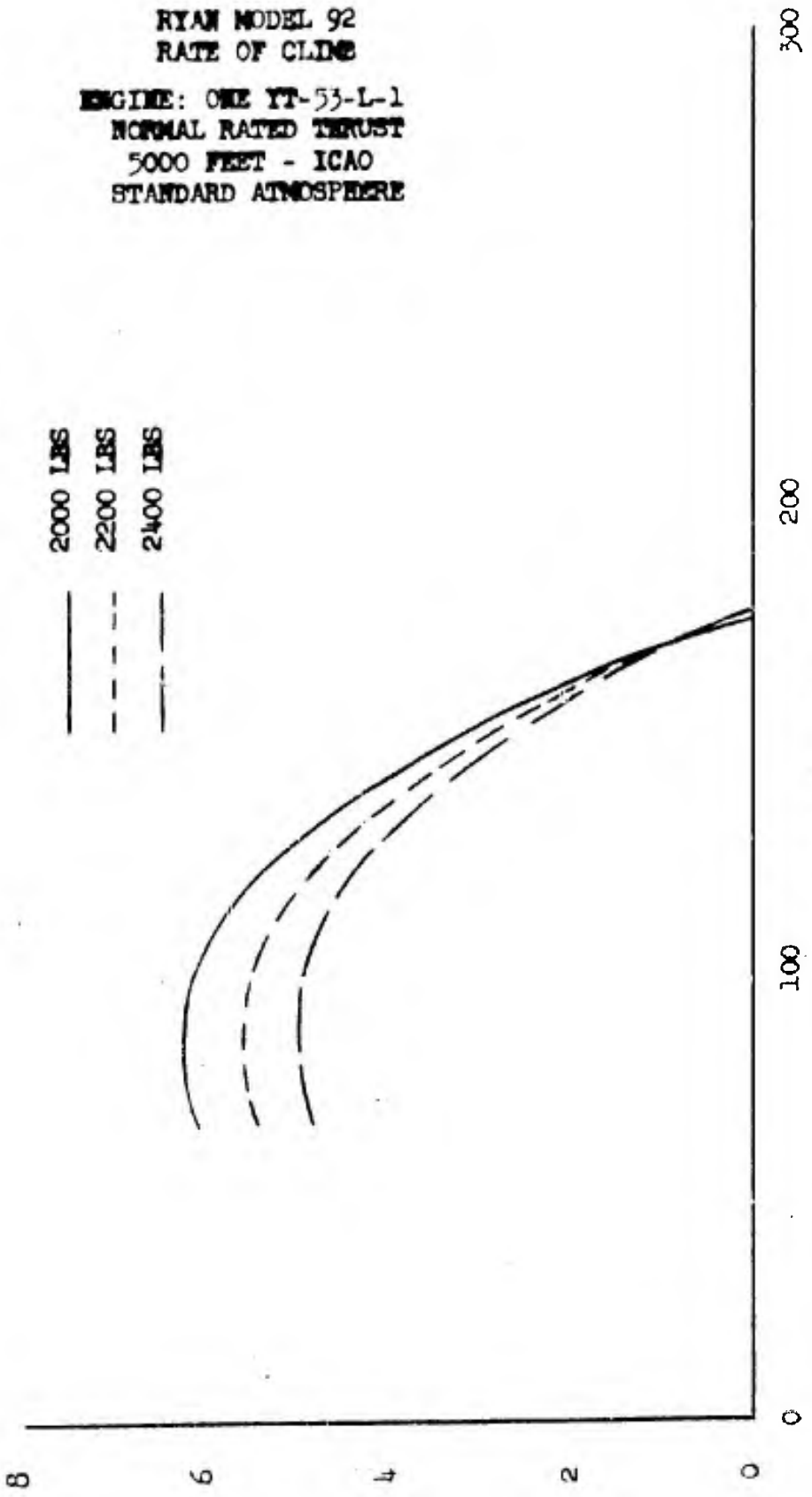

Figure 8.32

RYAN MODEL 92
RATE OF CLIMB

ENGINE: ONE YT-55-L-1
NORMAL RATED THRUST
10,000 FEET - ICAO
STANDARD ATMOSPHERE

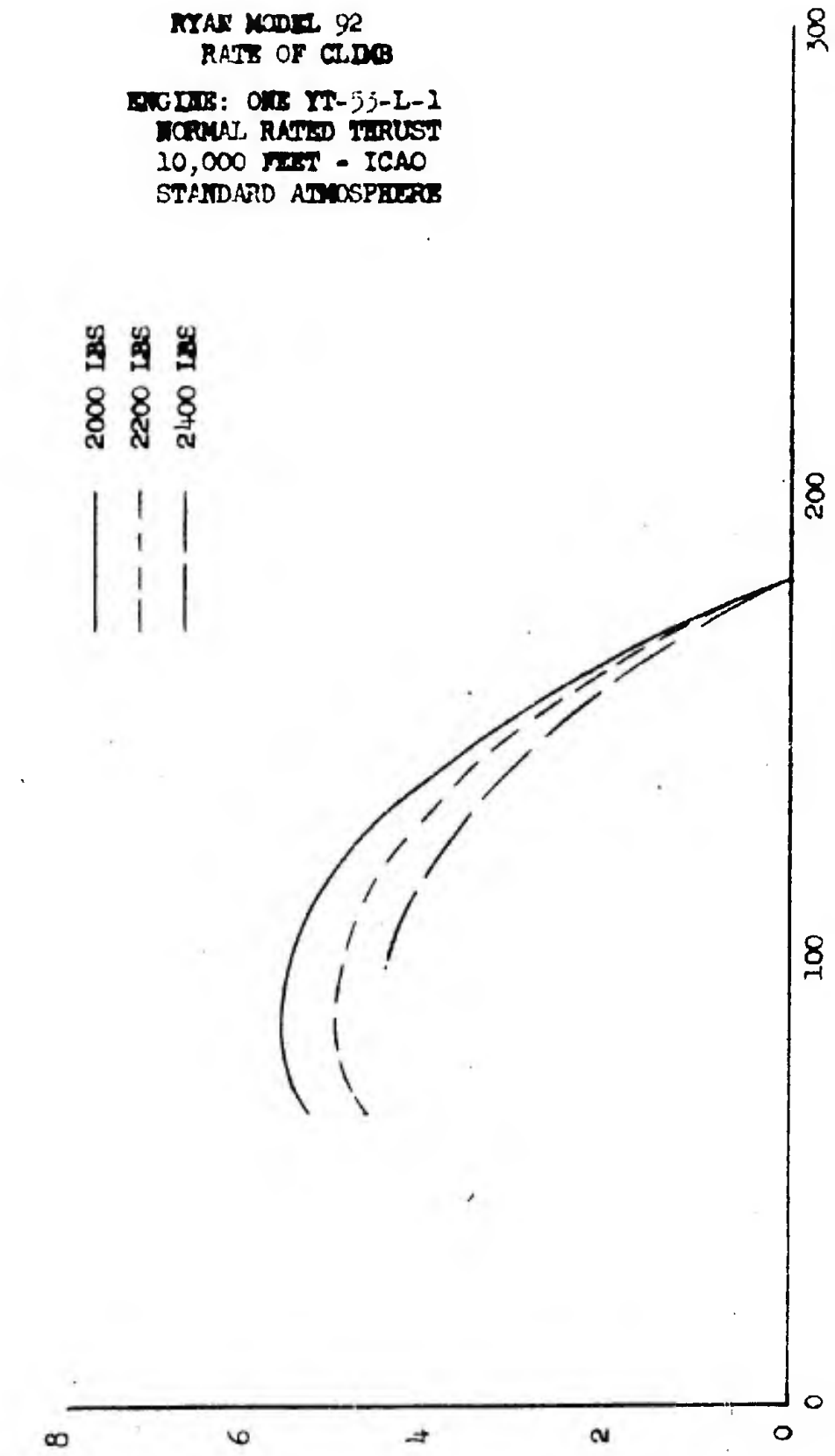

Figure 8.33

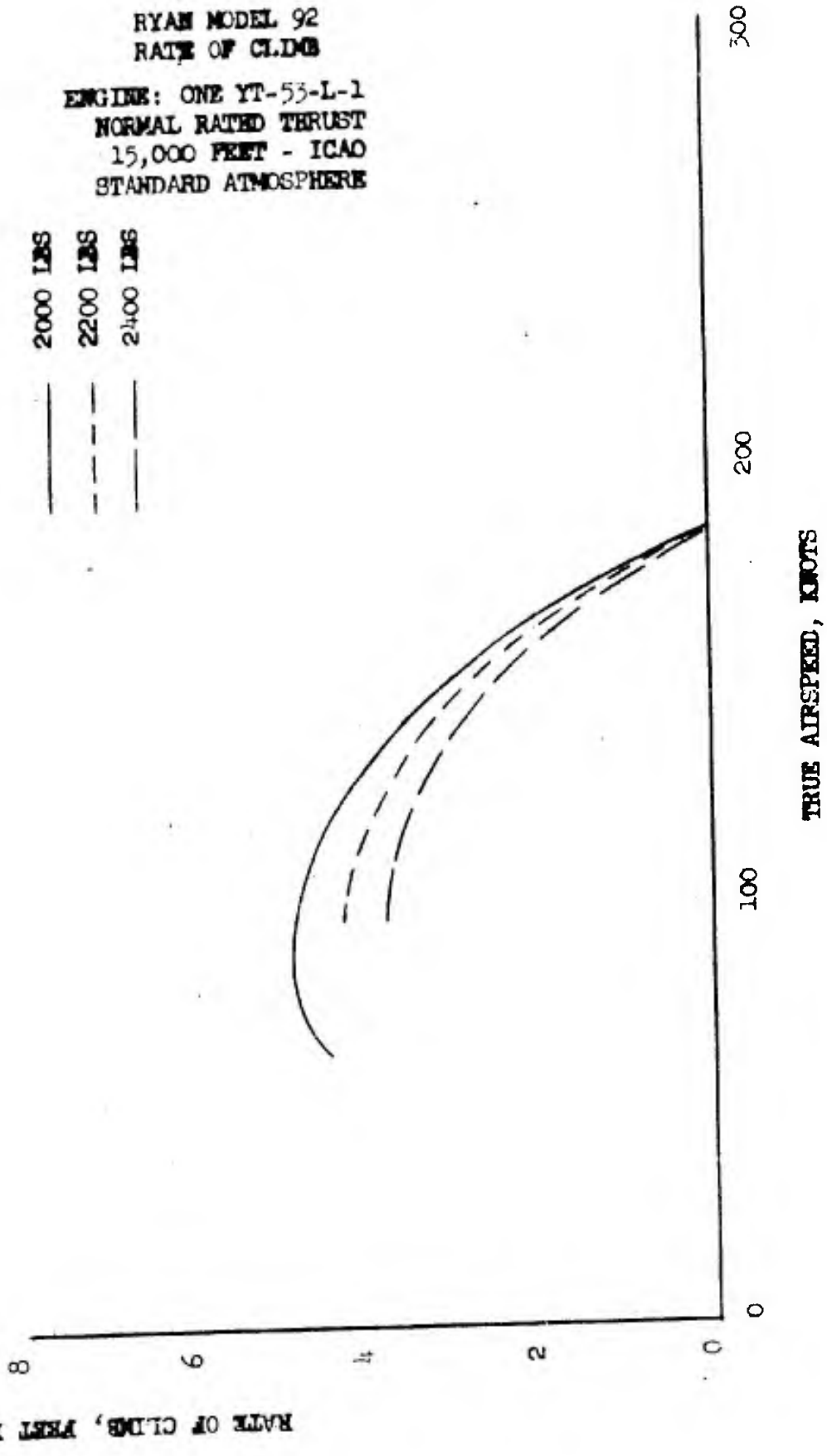
RYAN MODEL 92
RATE OF CLIMB
ENGINE: ONE YT-53-L-1
NORMAL RATED THRUST
15,000 FEET - ICAO
STANDARD ATMOSPHERE
2000 LBS
2200 LBS
2400 LBS
TRUE AIRSPEED, KNOTS
0
100
200
300
0
2
4
6
8
RATE OF CLIMB, FEET X 10⁻³

Figure 8.34

RYAN MODEL 92
RATE OF CLIMB

ENGINE: ONE YT-53-L-1
NORMAL RATED THRUST
20,000 FEET - ICAO
STANDARD ATMOSPHERE

2000 LBS
2200 LBS
2400 LBS

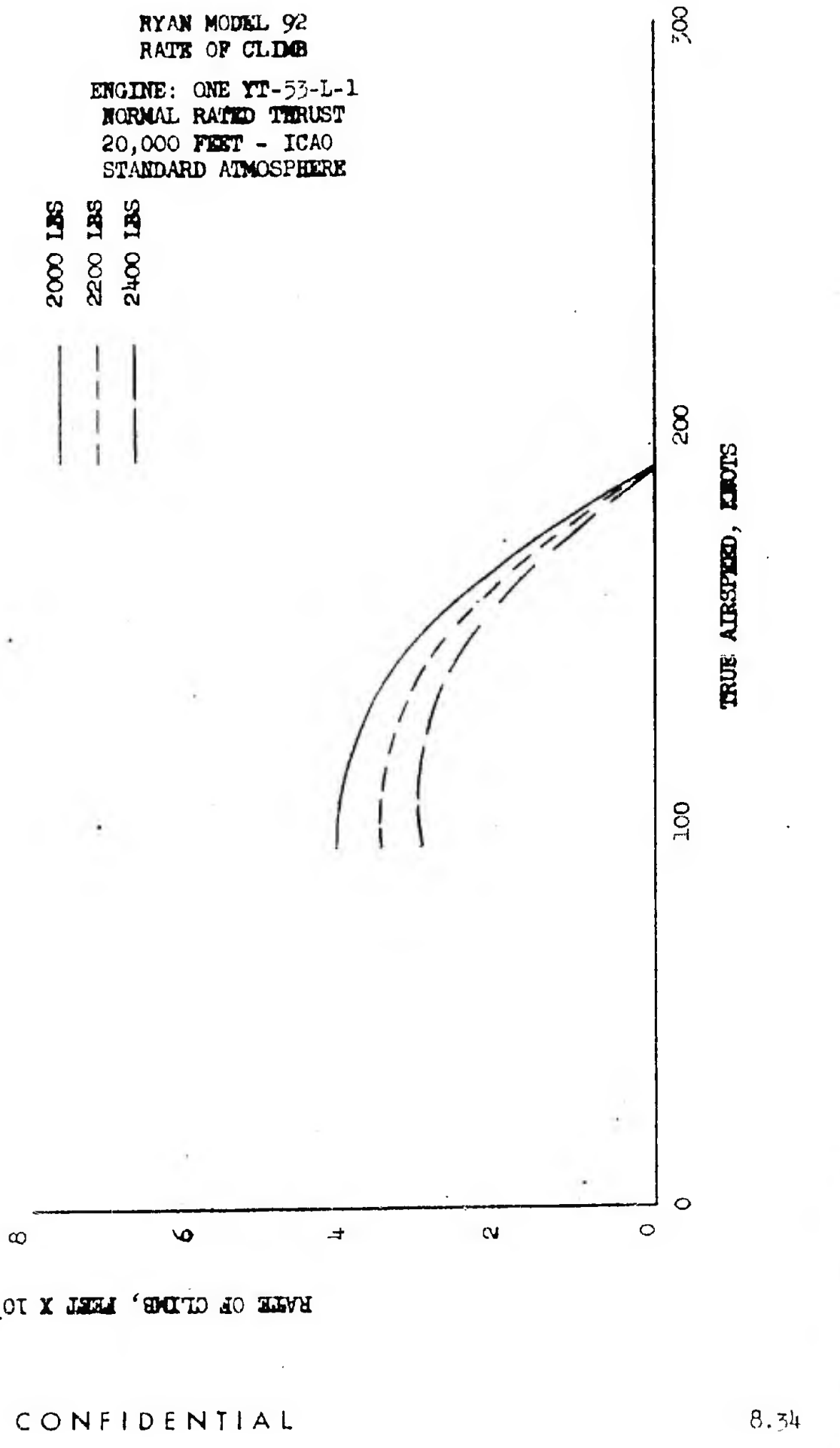

Figure 8.35

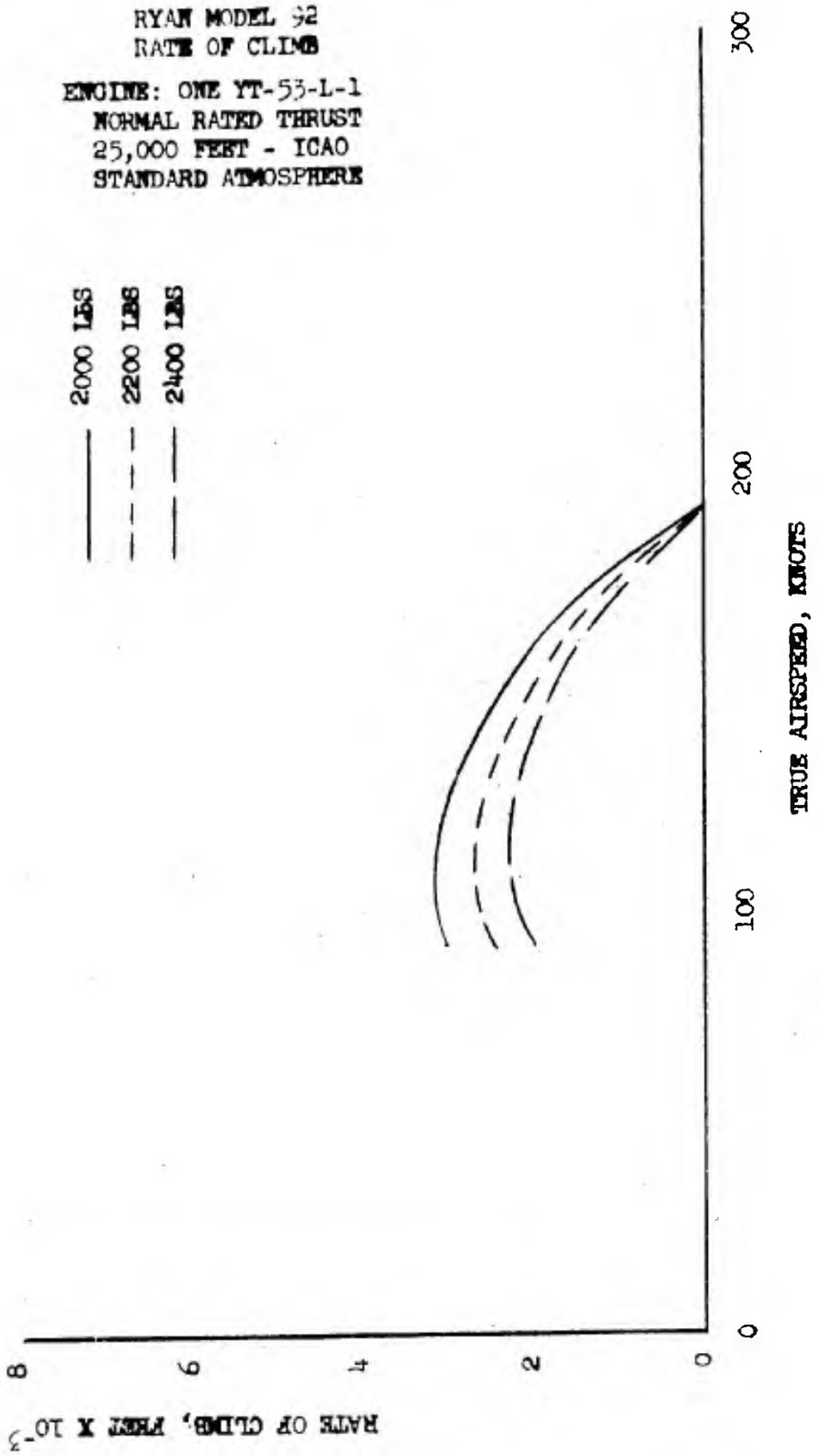
RYAN MODEL 92
RATE OF CLIMB
ENGINE: ONE YT-53-L-1
NORMAL RATED THRUST
25,000 FEET - ICAO
STANDARD ATMOSPHERE
2000 LBS
2200 LBS
2400 LBS
TRUE AIRSPEED, KNOTS
0
100
200
300
RATE OF CLIMB, FPSEC X 10⁻³
0
2
4
6
8

Figure 8.36

RYAN MODEL 92

RATE OF CLIMB

ENGINE: ONE YT-53-L-1
90 PERCENT NORMAL RATED THRUST

SEA LEVEL - ICAO
STANDARD ATMOSPHERE

2000 LBS
2200 LBS
2400 LBS

TRUE AIRSPEED, KNOTS

300
200
100
0

0
2
4
6
8

RATE OF CLIMB, FPM X 10^{-3}

Figure 8.37

RYAN MODEL 92
RATE OF CLIMB
ENGINE: ONE YT-53-L-1
90 PERCENT NORMAL RATED THRUST
5,000 FEET - ICAO
STANDARD ATMOSPHERE

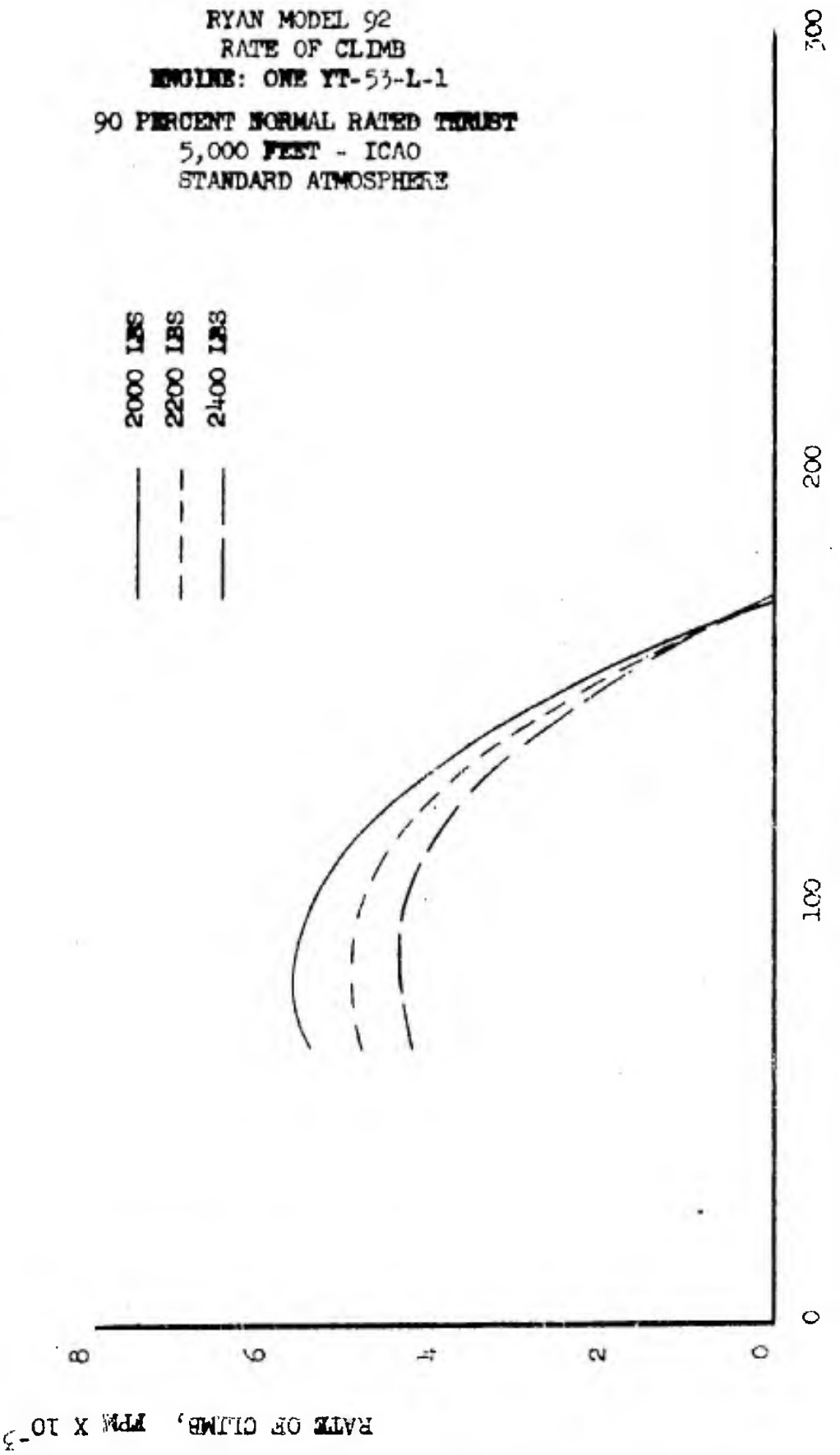

Figure 8.38

RYAN MODEL 92
RATE OF CLIMB

ENGINE: ONE YT-53-L-1
90 PERCENT NORMAL RATED THRUST
10,000 FEET - ICAO
STANDARD ATMOSPHERE

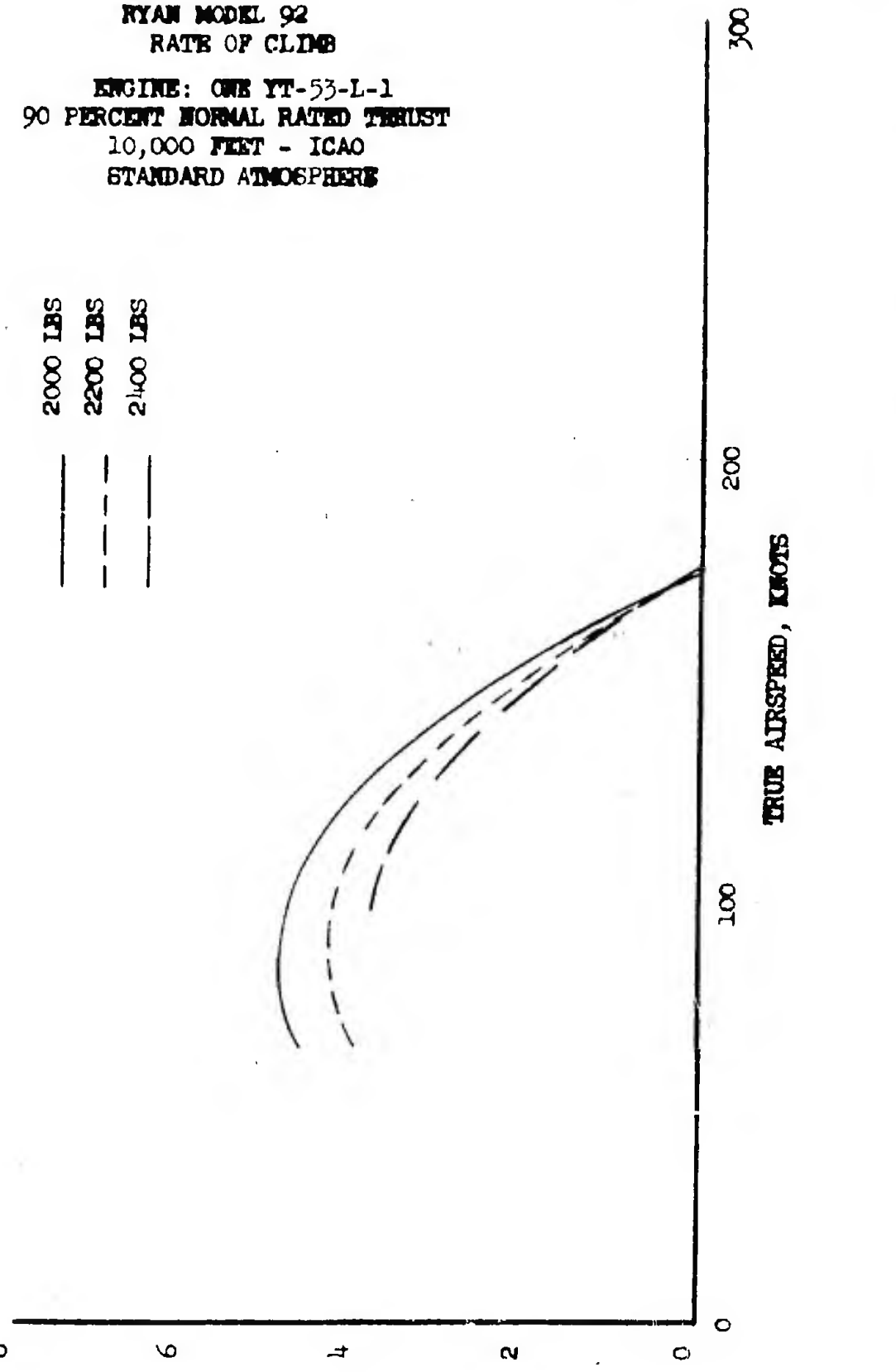

Figure 8.39

RYAN MODEL 92
RATE OF CLIMB

ENGINE: ONE YT-53-L-1
90 PERCENT NORMAL RATED THRUST
15,000 FEET - ICAO
STANDARD ATMOSPHERE

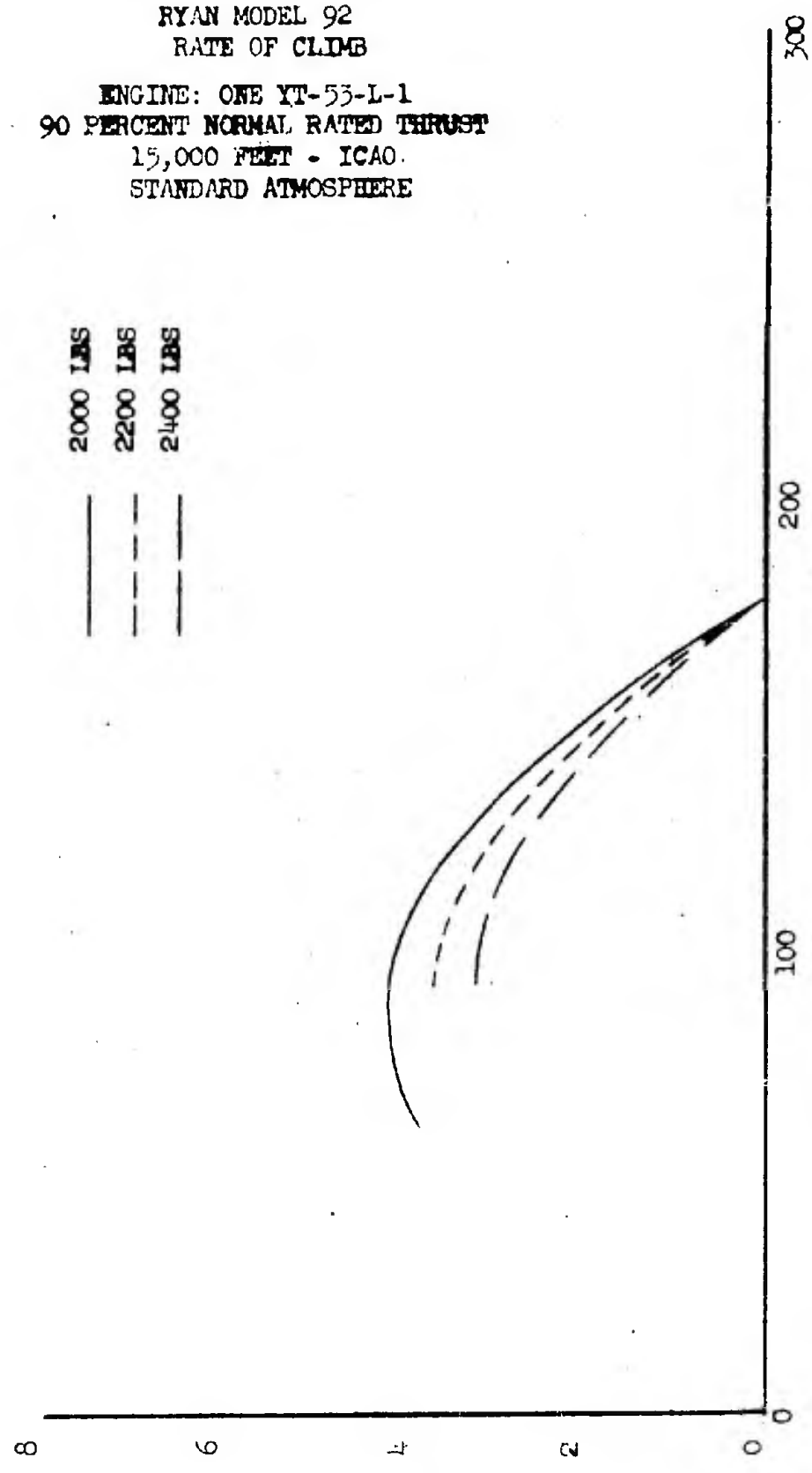

Figure 8.40

RYAN MODEL 92
RATE OF CLIMB

ENGINE: ONE YT-53-L-1
90 PERCENT NORMAL RATED THRUST
20,000 FEET - ICAO
STANDARD ATMOSPHERE

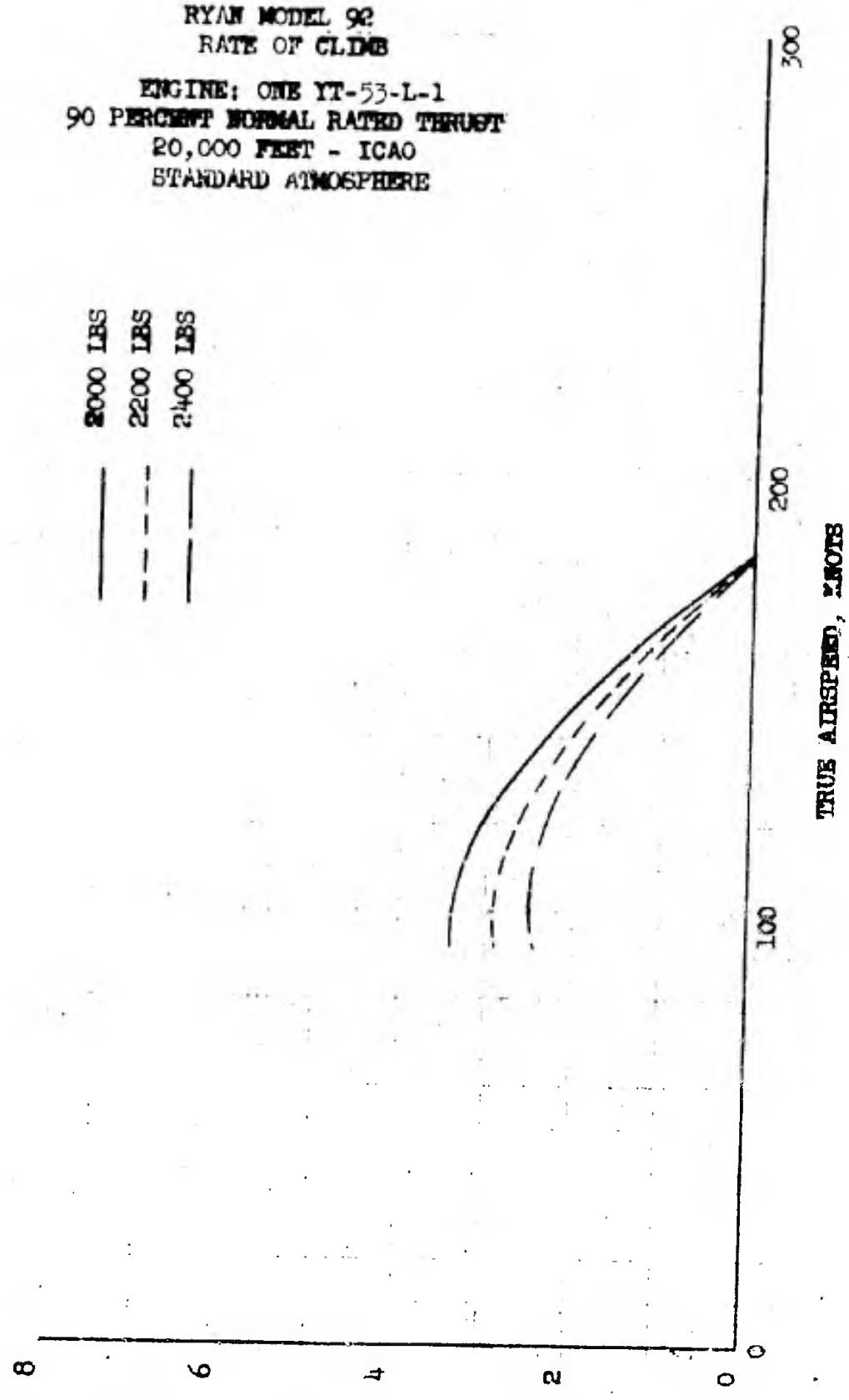

Figure 8.41

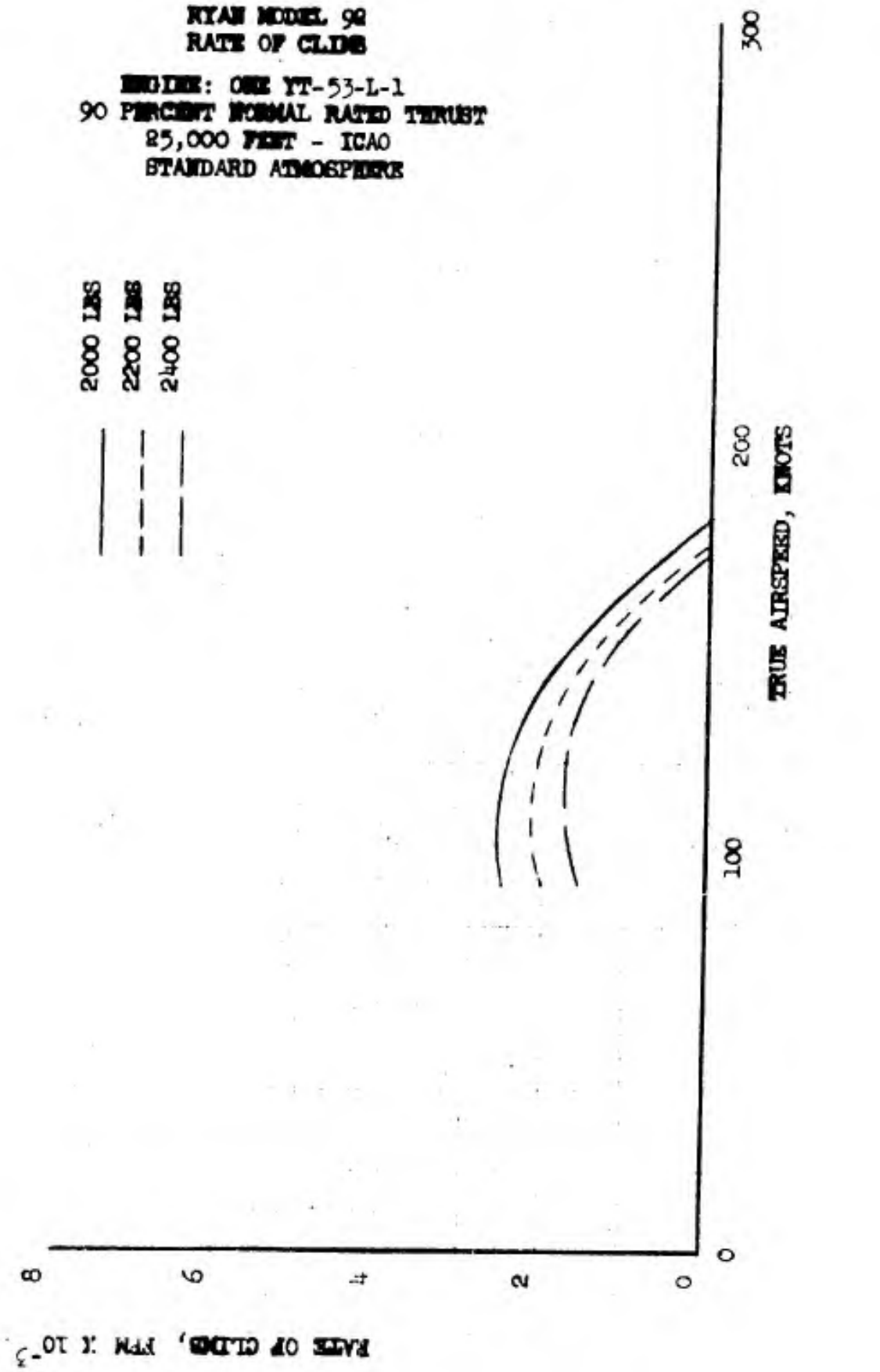
RYAN MODEL 92
RATE OF CLIMB
ENGINE: ONE YT-53-L-1
90 PERCENT NORMAL RATED THRUST
25,000 FEET - ICAO
STANDARD ATMOSPHERE
2000 LBS
2200 LBS
2400 LBS
TRUE AIRSPEED, KNOTS
300
200
100
0
RATE OF CLIMB, FPM X 10⁻³
8
6
4
2
0

Figure 8.42

RYAN MODEL 92
RATE OF CLIMB

ENGINE: ONE YT-53-L-1
75 PERCENT NORMAL RATED THRUST
SEA LEVEL - ICAO
STANDARD ATMOSPHERE

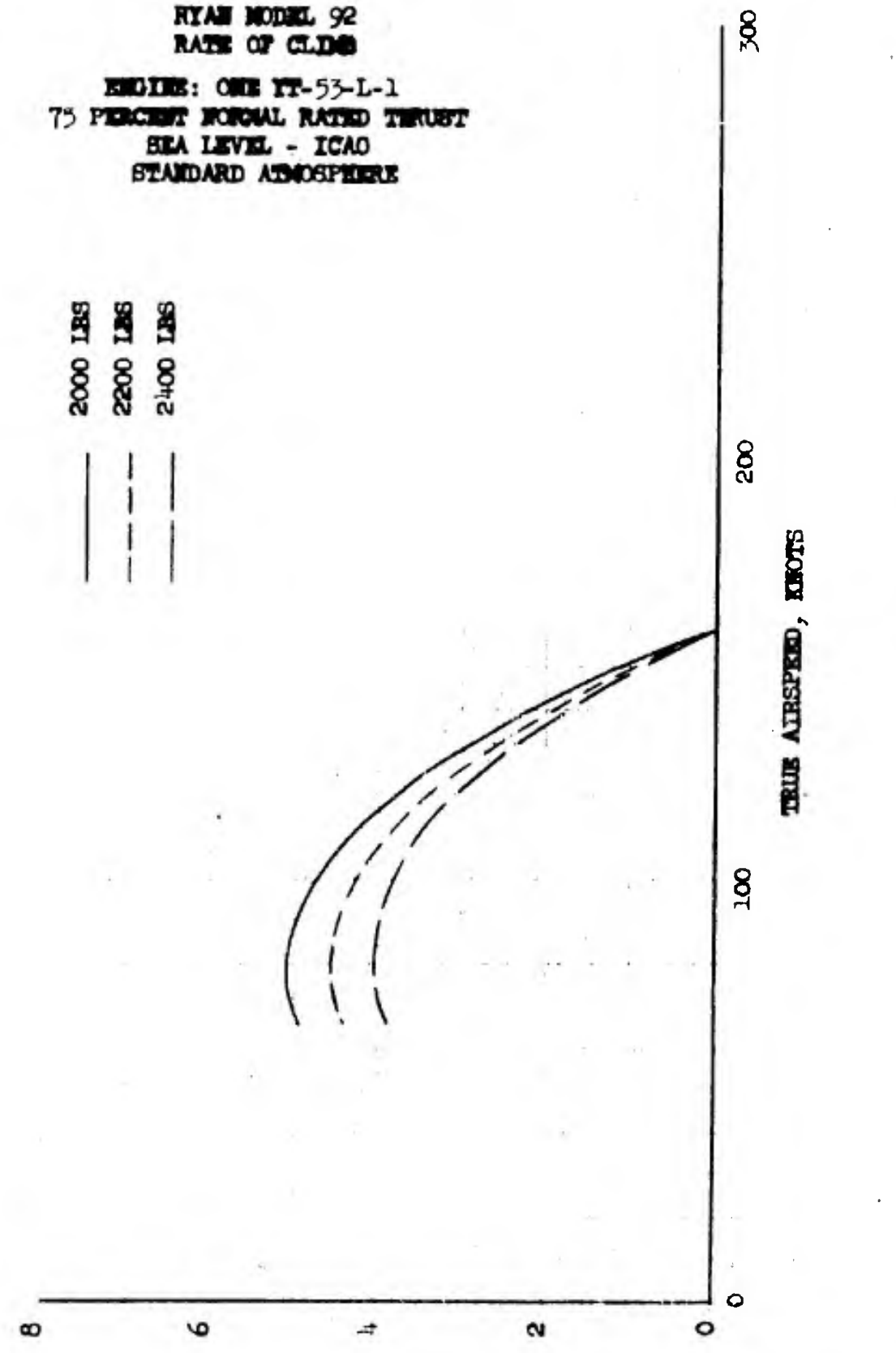

Figure 8.43

RYAN MODEL 92
RATE OF CLIMB

ENGINE: ONE YT-53-L-1
75 PERCENT NORMAL RATED THRUST
5,000 FEET - ICAO
STANDARD ATMOSPHERE

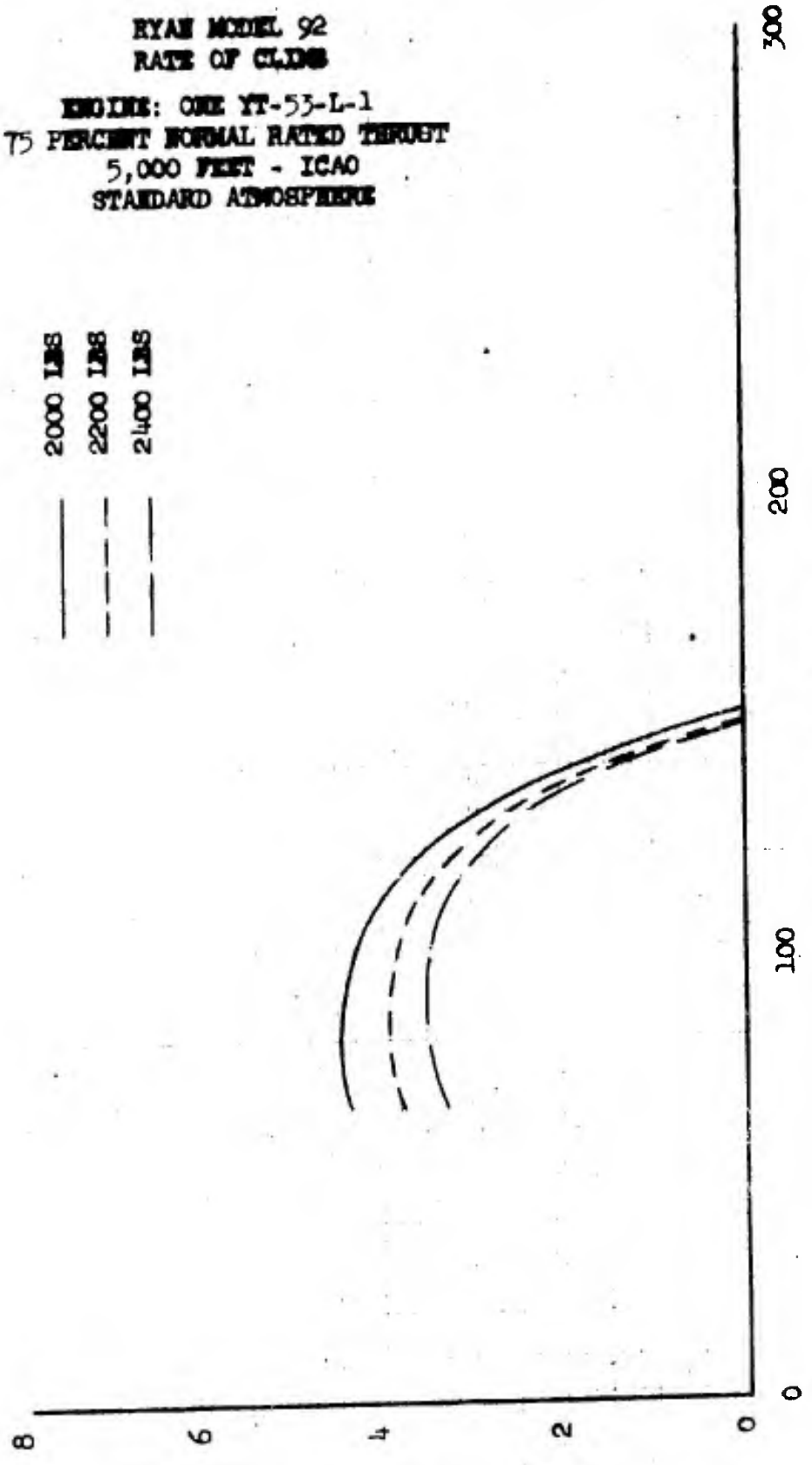

Figure 8.44

RYAN MODEL 92
RATE OF CLIMB

ENGINE: ONE YT-53-L-1
75 PERCENT NORMAL RATED THRUST
10,000 FEET - ICAO
STANDARD ATMOSPHERE

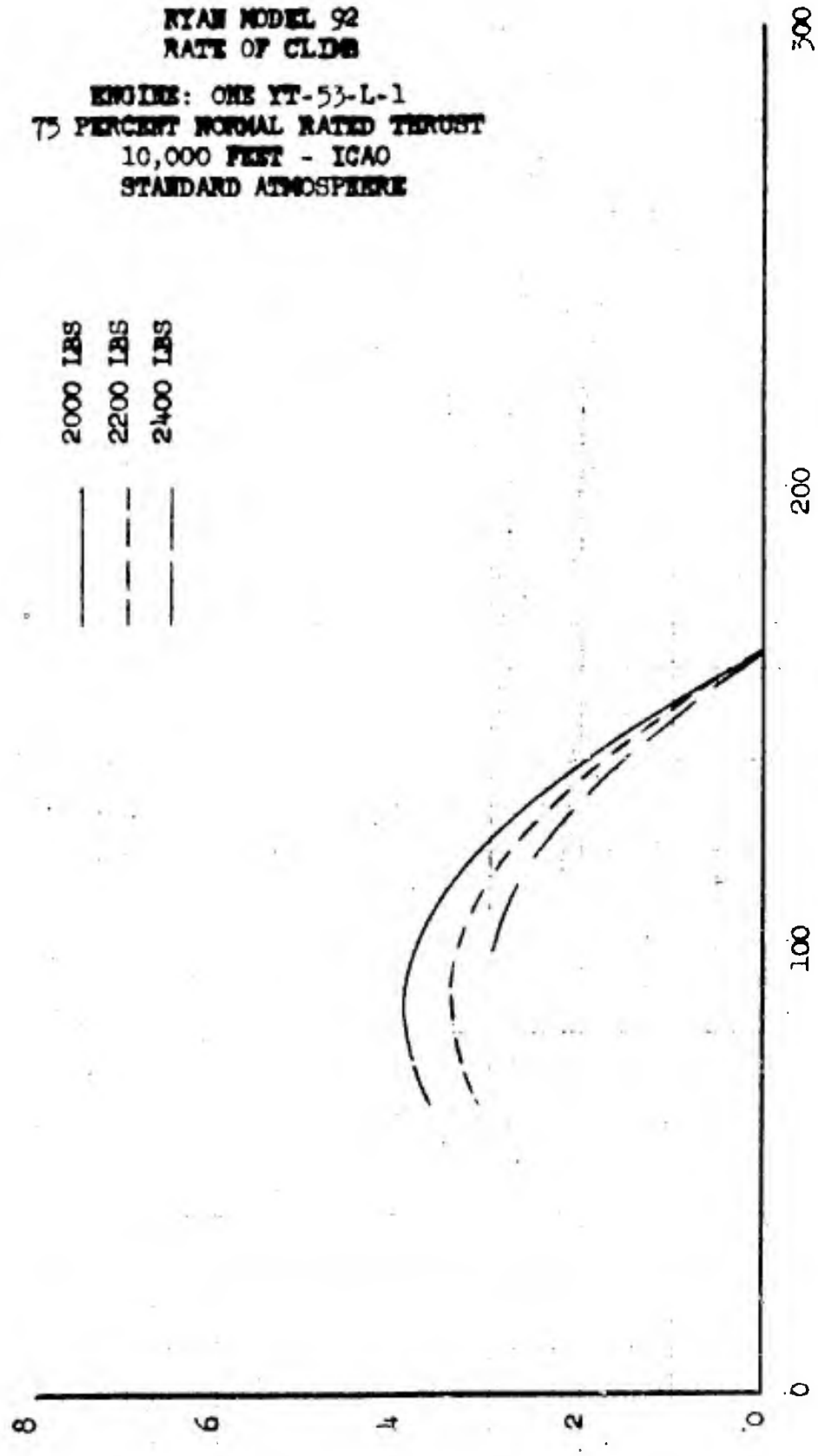

Figure 8.45

RYAN MODEL 92
RATE OF CLIMB

ENGINE: ONE YT-53-L-1
75 PERCENT NORMAL RATED THRUST
15,000 FEET - ICAO
STANDARD ATMOSPHERE

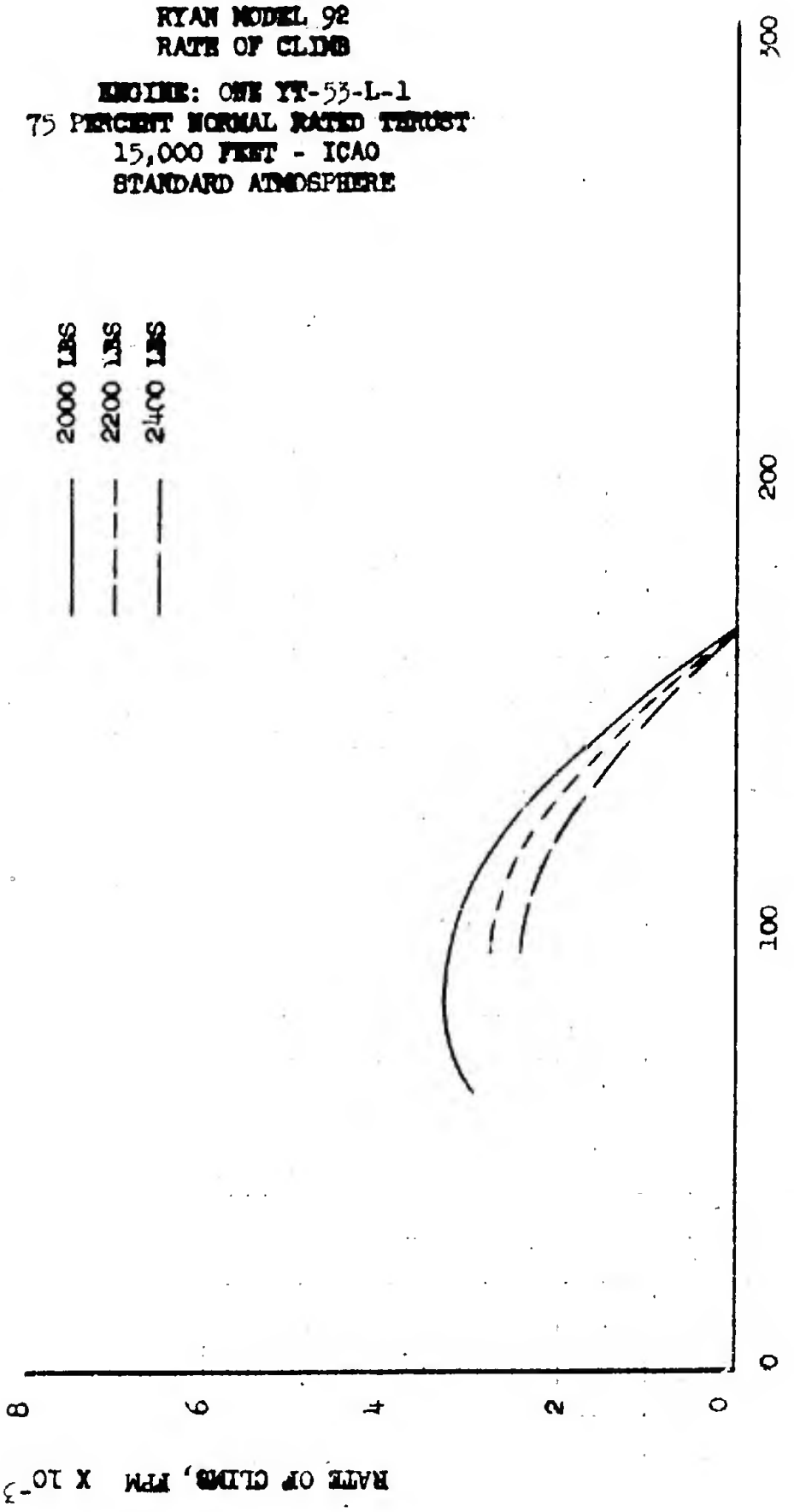

Figure 8.46

RYAN MODEL 92
RATE OF CLIMB

ENGINE: ONE YT-53-L-1
75 PERCENT NORMAL RATED THRUST
20,000 FEET - ICAO
STANDARD ATMOSPHERE

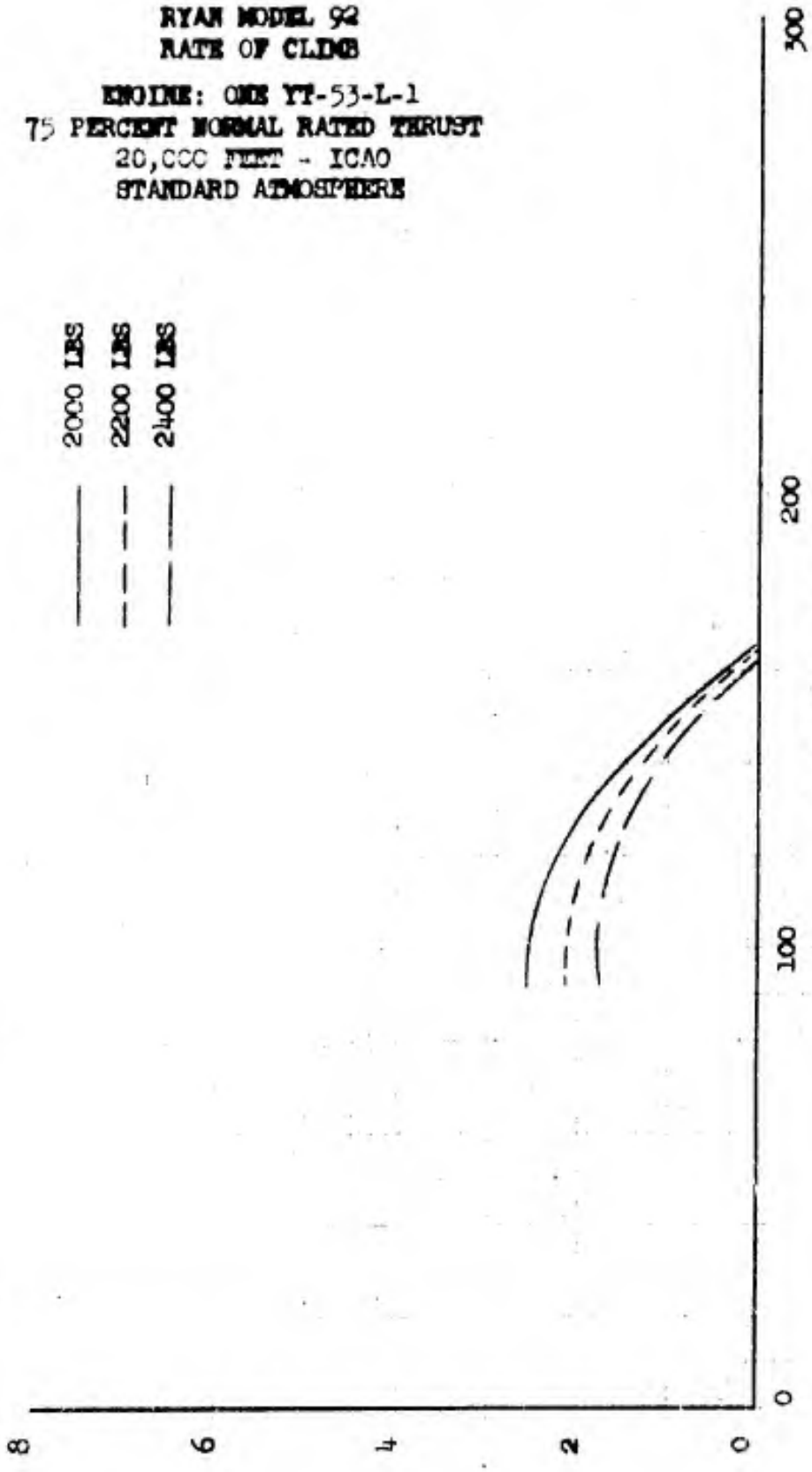

Figure 8.47

RYAN MODEL 92
RATE OF CLIMB

ENGINE: ONE YT-53-L-1
75 PERCENT NORMAL RATED THRUST
25,000 FEET - ICAO
STANDARD ATMOSPHERE

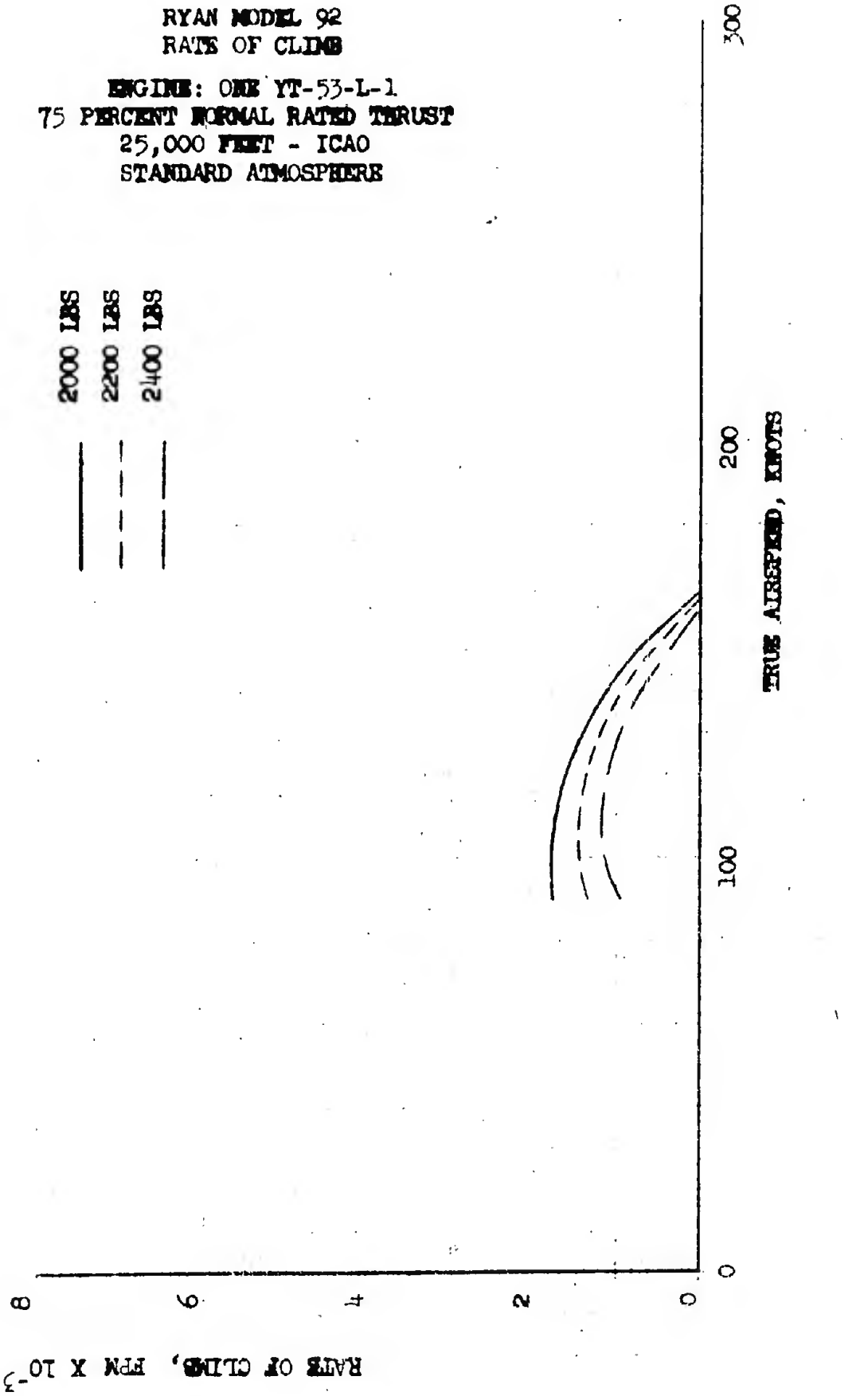

Figure 8.48

RYAN MODEL 92
RATE OF CLIMB

ENGINE: ONE YT-53-L-1
50 PERCENT NORMAL RATED THRUST
SEA LEVEL - ICAO
STANDARD ATMOSPHERE

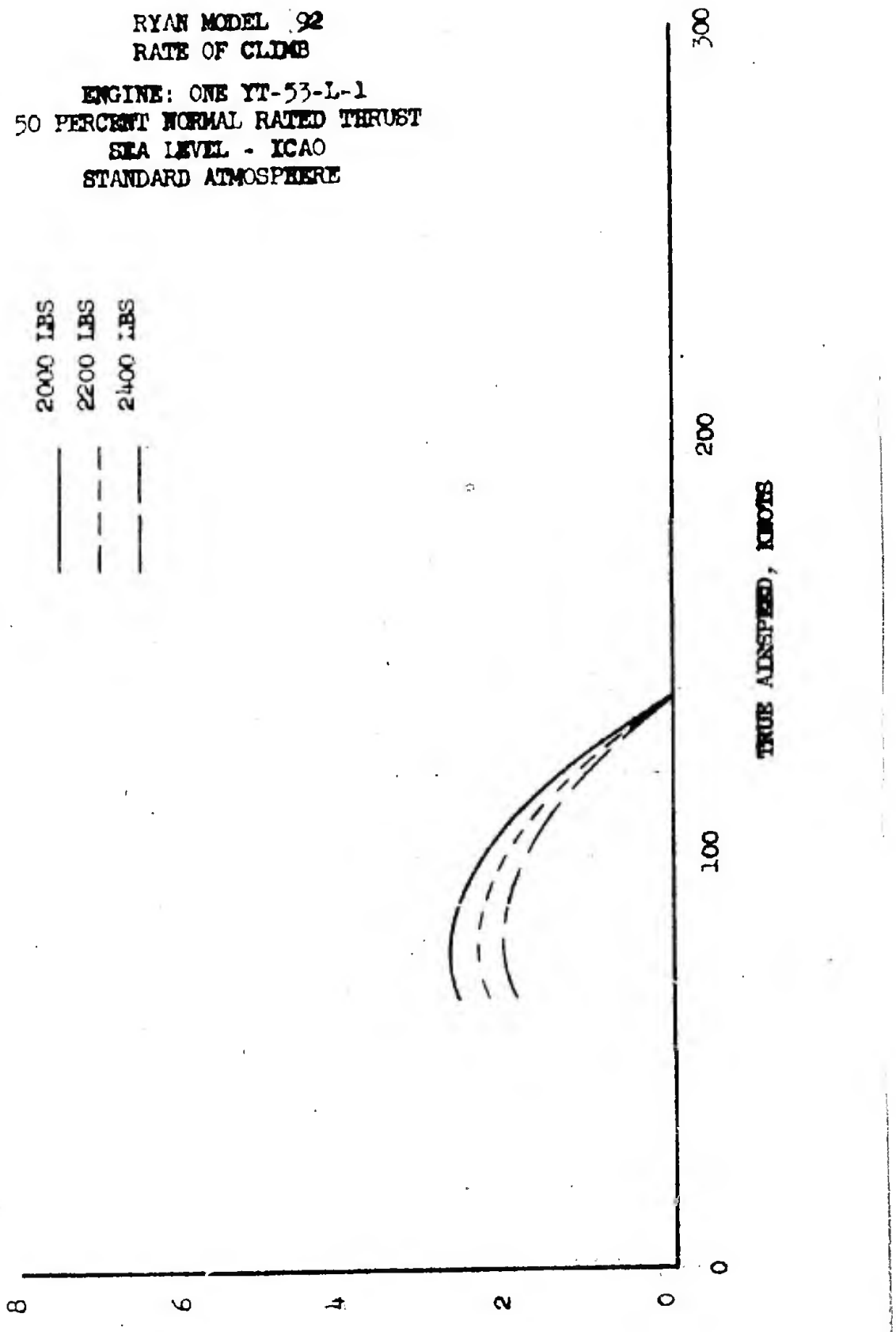

Figure 8.49

RYAN MODEL 92
RATE OF CLIMB

ENGINE: ONE YT-53-L-1
50 PERCENT NORMAL RATED THRUST
5,000 FEET - ICAO
STANDARD ATMOSPHERE

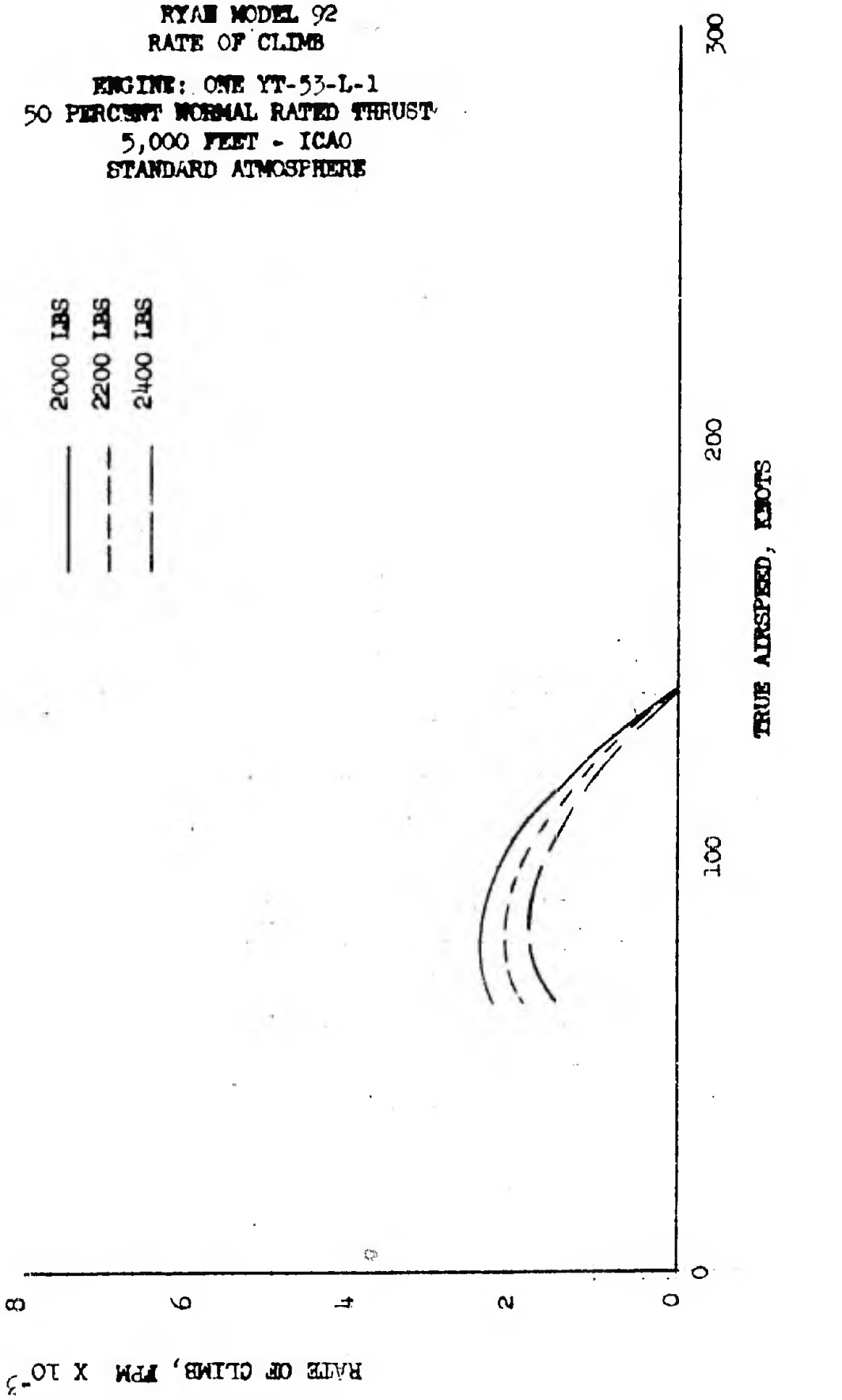

Figure 8.50

RYAN MODEL 92
RATE OF CLIMB

ENGINE: ONE YT-53-L-1
50 PERCENT NORMAL RATED THRUST
10,000 FEET - ICAO
STANDARD ATMOSPHERE

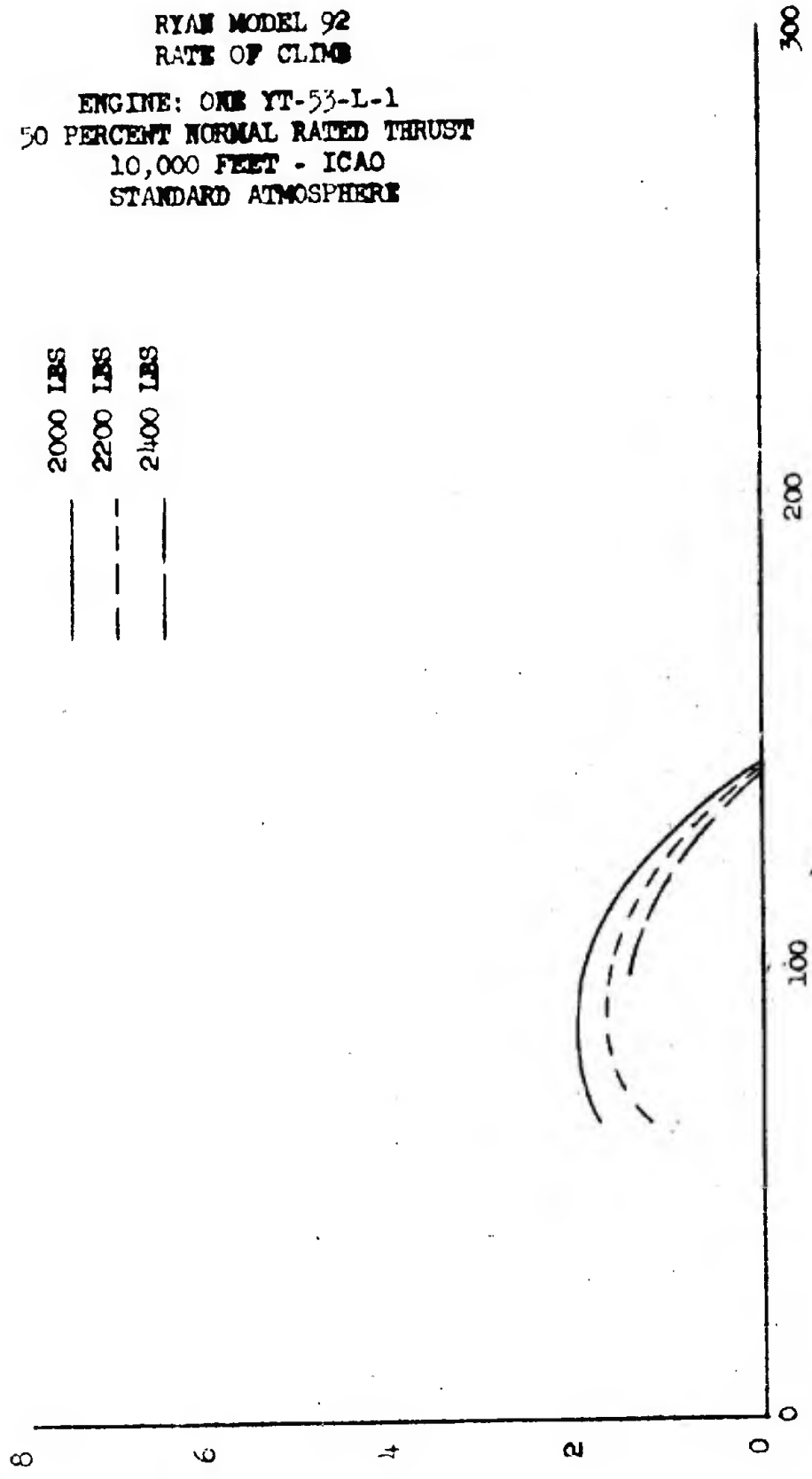

Figure 8.51

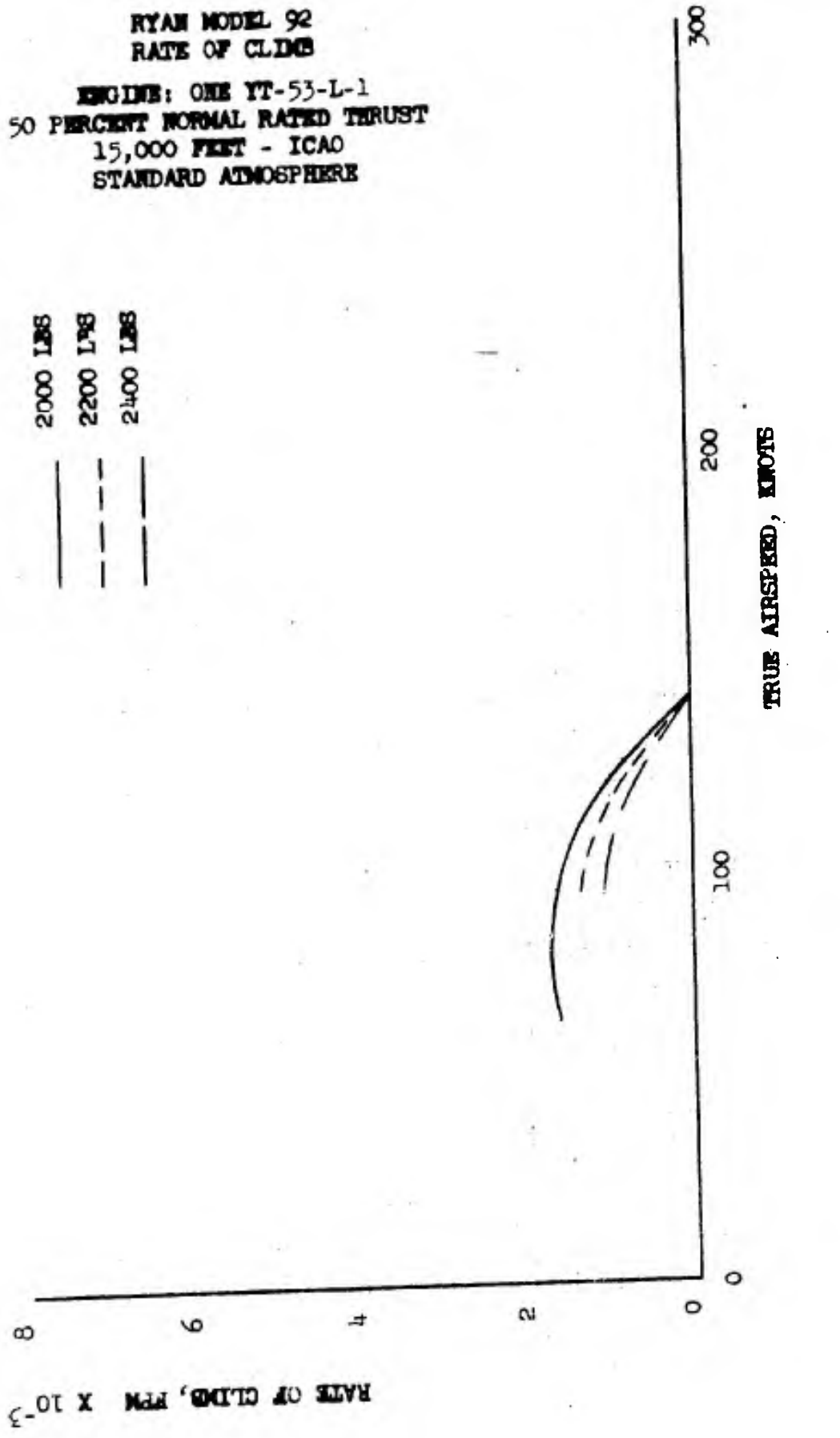
RYAN MODEL 92
RATE OF CLIMB
ENGINE: ONE YT-53-L-1
50 PERCENT NORMAL RATED THRUST
15,000 FEET - ICAO
STANDARD ATMOSPHERE
2000 LBS
2200 LBS
2400 LBS
TRUE AIRSPEED, KNOTS
0
100
200
300
0
2
4
6
8
RATE OF CLIMB, FPM X 10⁻³

Figure 8.52

RYAN MODEL 92
RATE OF CLIMB

ENGINE: ONE YT-53-L-1
50 PERCENT NORMAL RATED THRUST
20,000 FEET - ICAO
STANDARD ATMOSPHERE

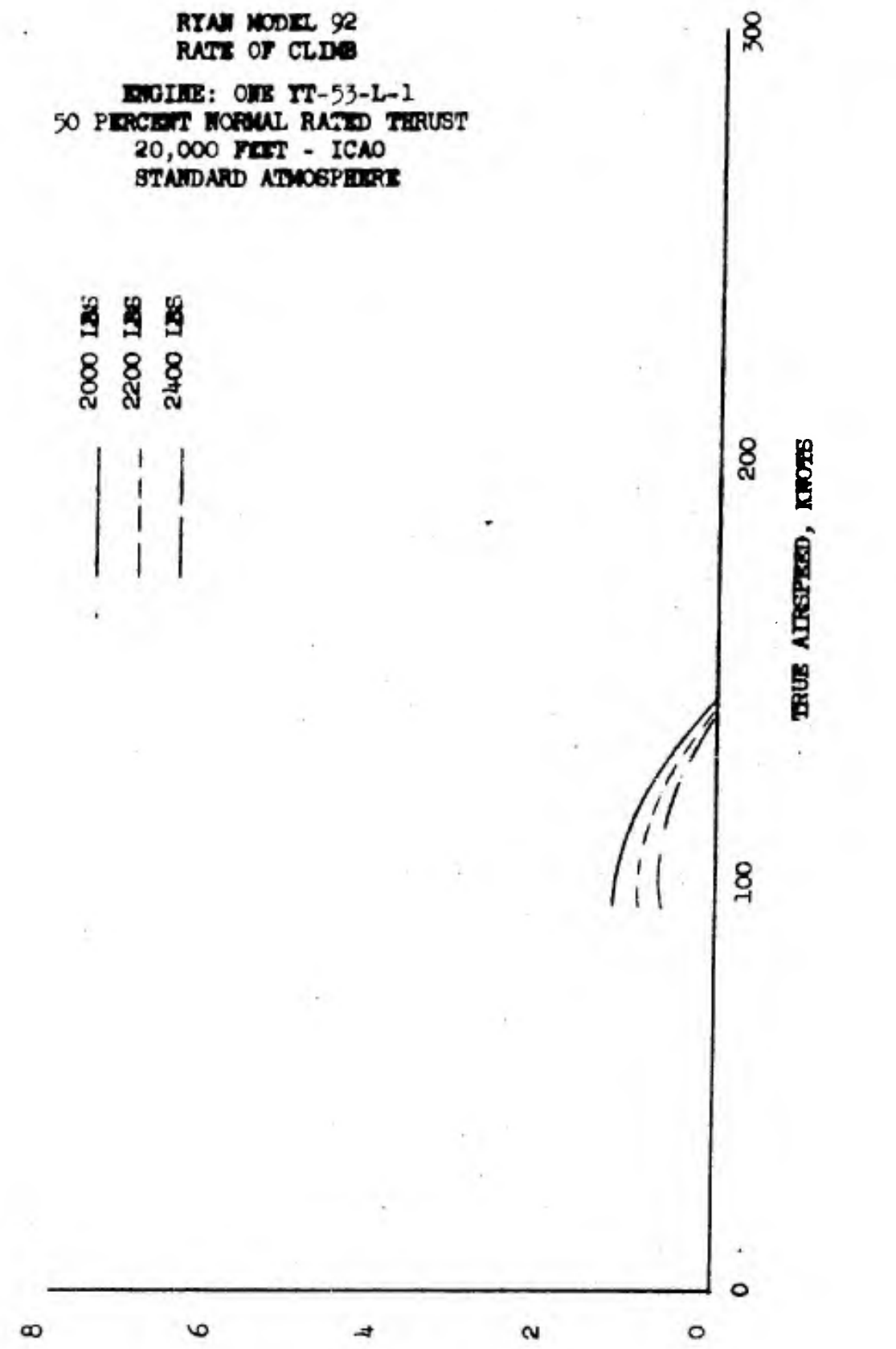

Figure 8.53

RYAN MODEL 92
RATE OF CLIMB

ENGINE: ONE YT-53-L-1
50 PERCENT NORMAL RATED THRUST
25,000 FEET - ICAO
STANDARD ATMOSPHERE

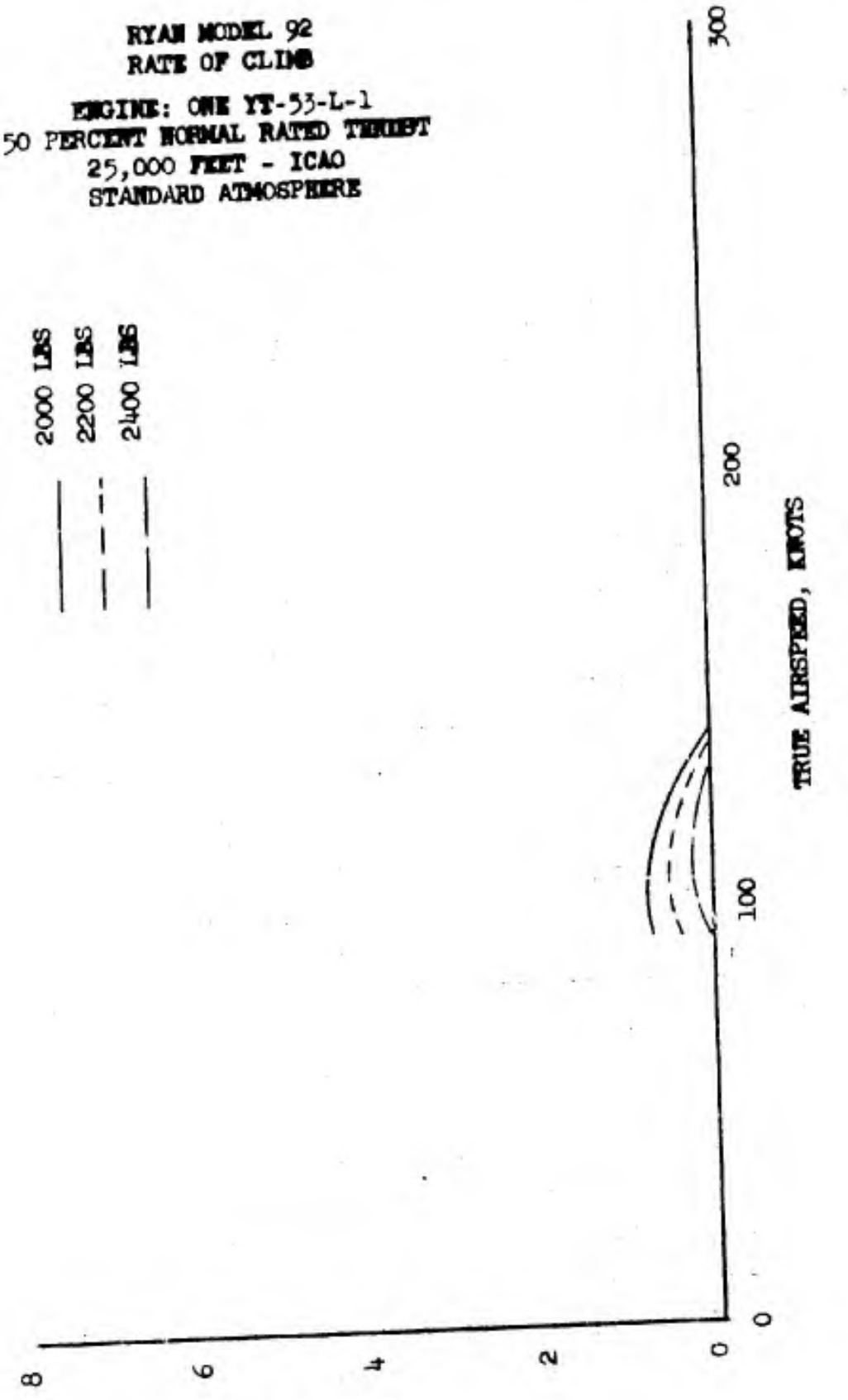

Figure 8.54

RYAN MODEL 92

TIME TO CLIMB

ENGINE: ONE YT-53-L-1
MILITARY RATED THRUST
ICAO STANDARD ATMOSPHERE

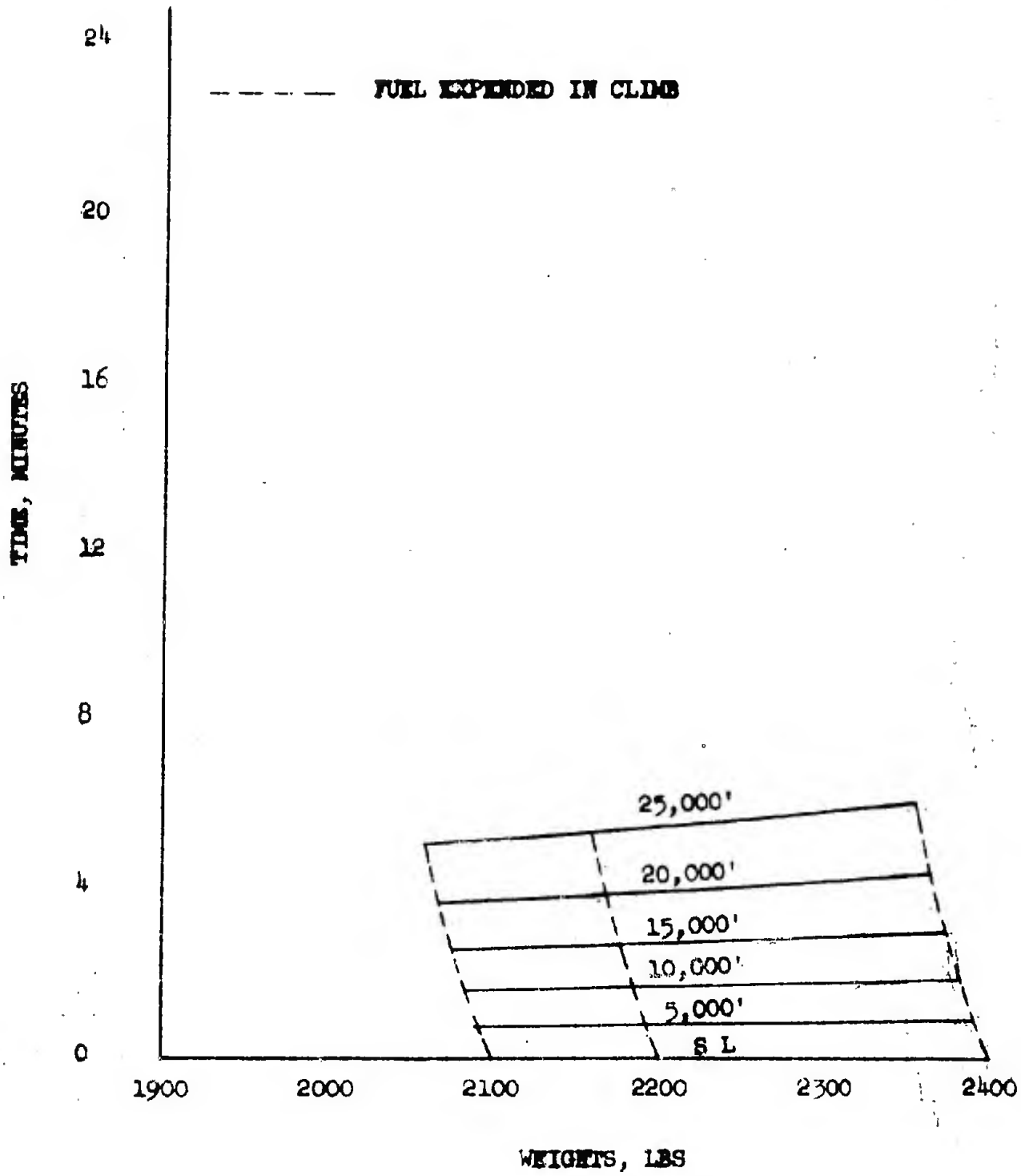

Figure 8.55

RYAN MODEL 92

TIME TO CLIMB

ENGINE: ONE YT-53-L-1
NORMAL RATED THRUST
ICAO STANDARD ATMOSPHERE

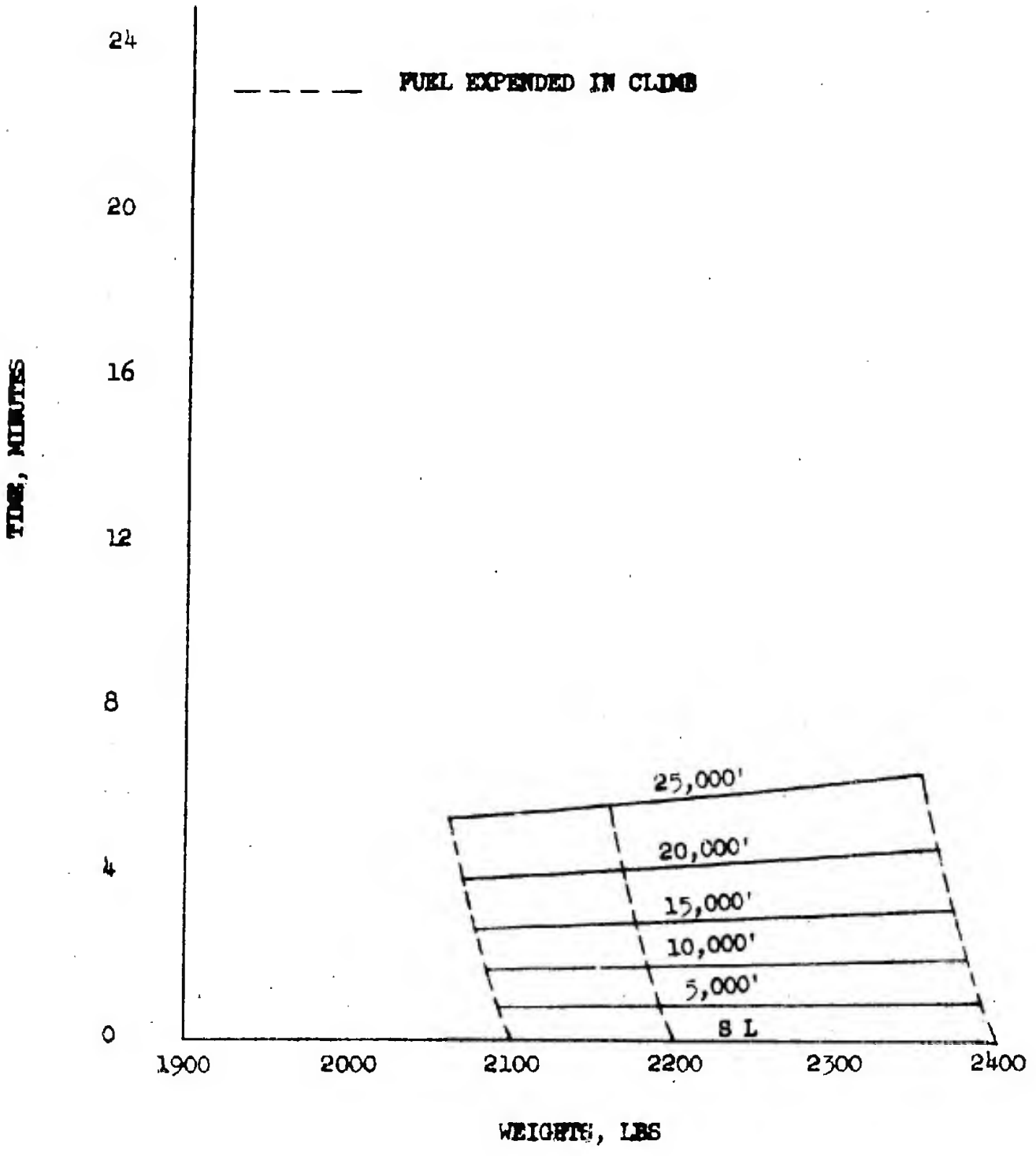

Figure 8.56

RYAN MODEL 92

TIME TO CLIMB

ENGINE: ONE YT-53-L-1
90 PERCENT NORMAL RATED THRUST
ICAO STANDARD ATMOSPHERE

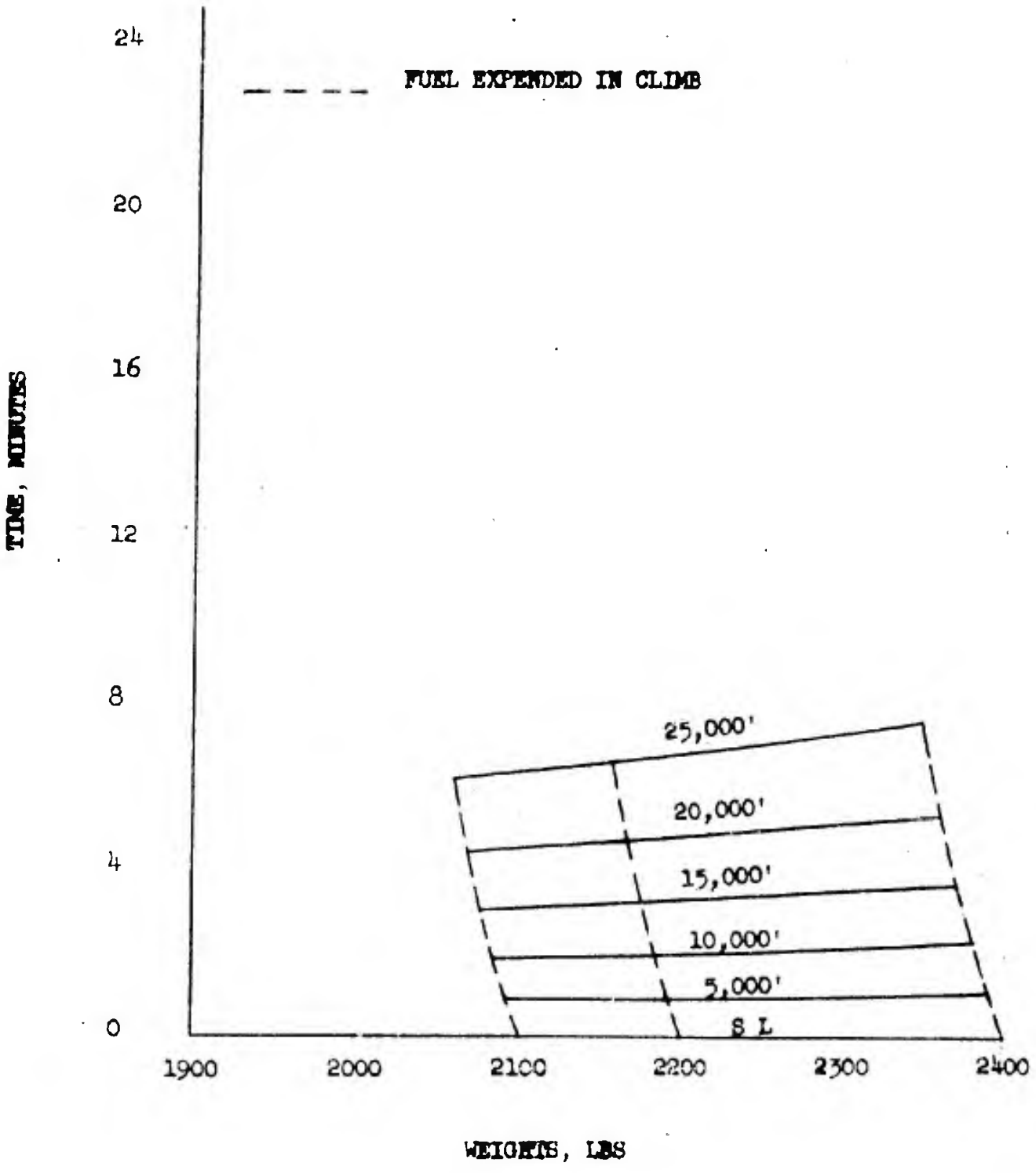

Figure 8.57

RYAN MODEL 92

TIME TO CLIMB

ENGINE: ONE YT-33-L-1
75 PERCENT NORMAL RATED THRUST
ICAC STANDARD ATMOSPHERE

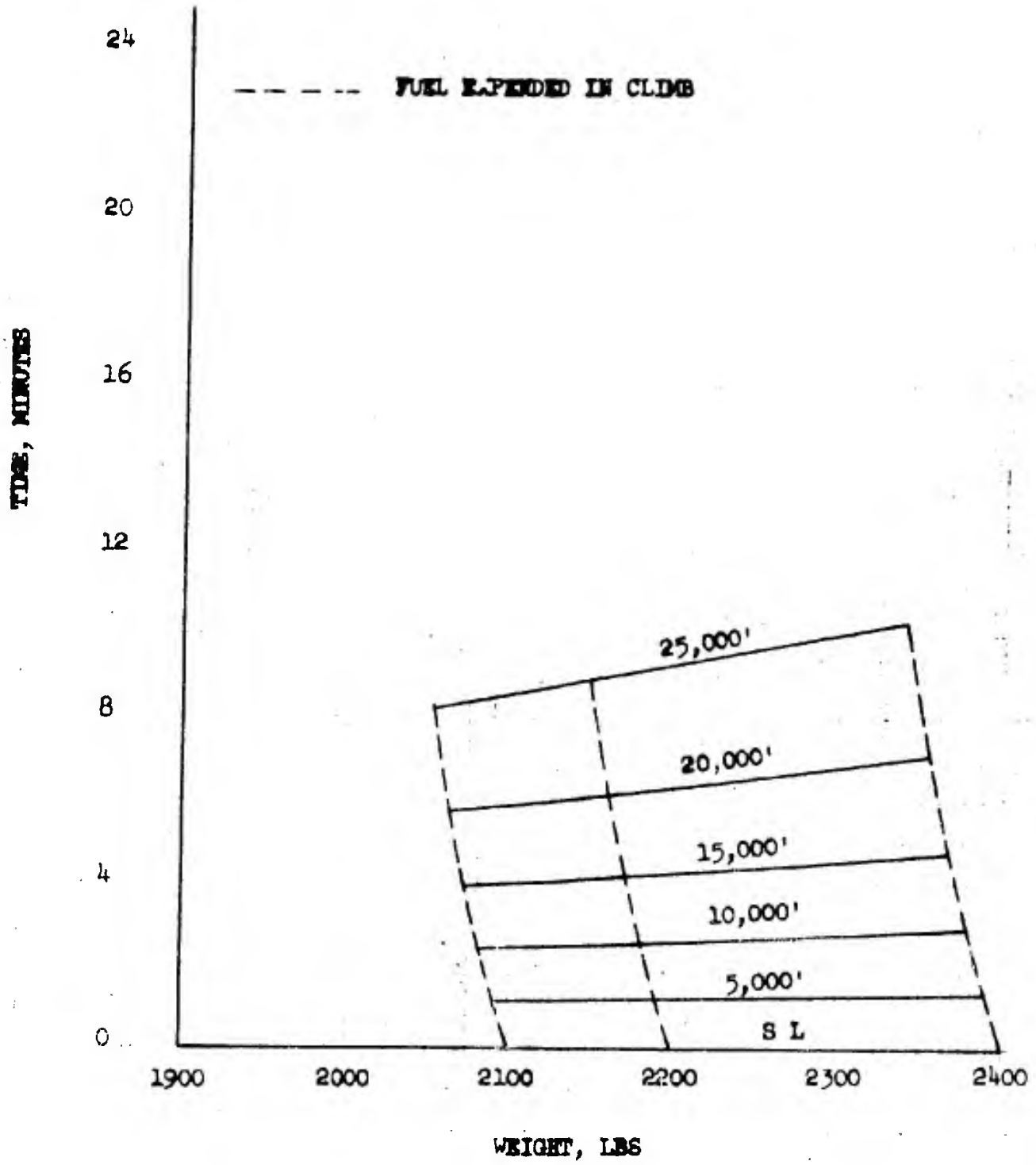

Figure 8.58

RYAN MODEL 92

TIME TO CLIMB

ENGINE: ONE YT-53-L-1
50 PERCENT NORMAL RATED THRUST
ICAO STANDARD ATMOSPHERE

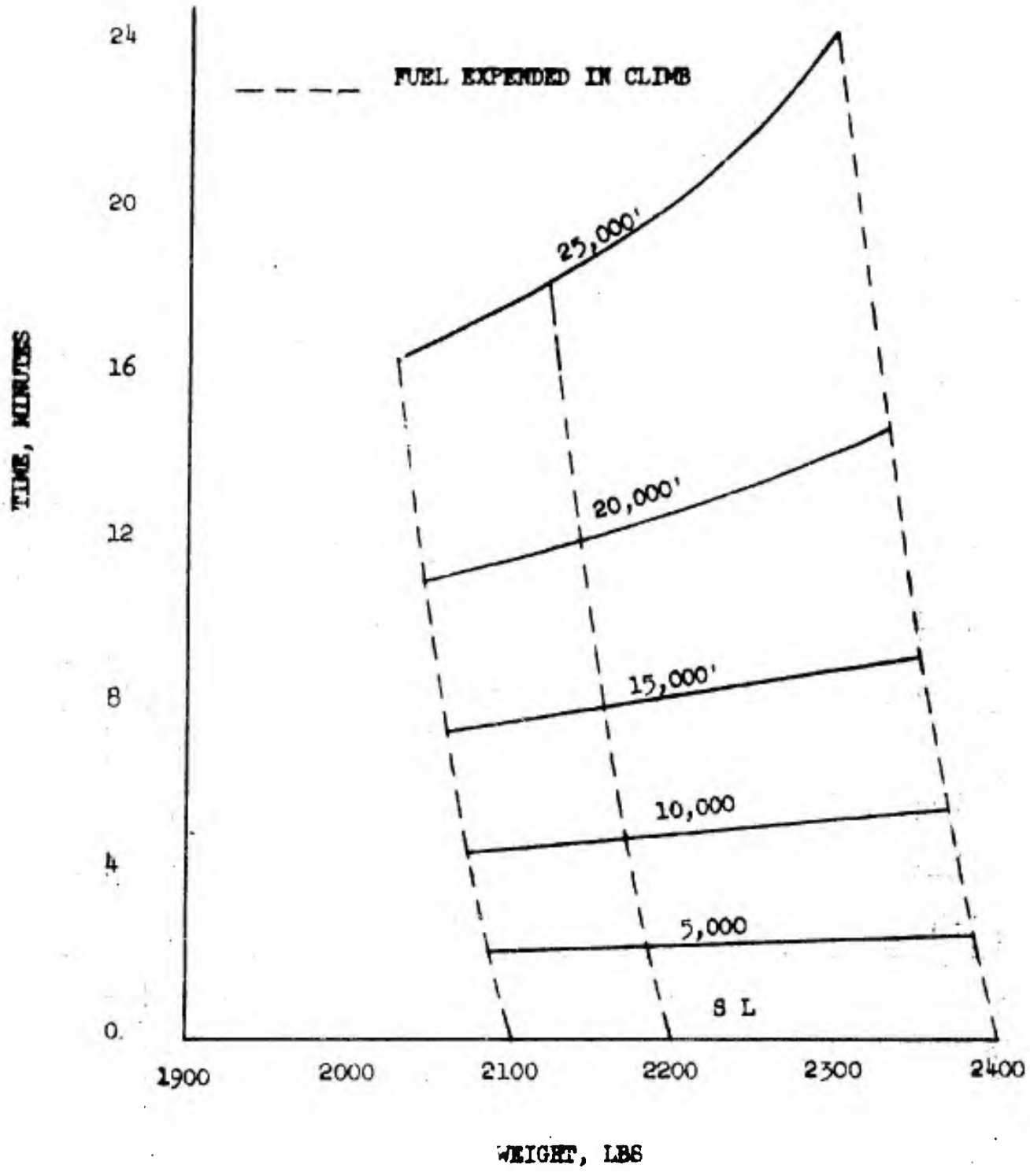

Figure 8.59

RYAN MODEL 92

HORIZONTAL DISTANCE
GAINED IN CLIMB

ENGINE: ONE YT-53-L-1
MILITARY RATED THRUST
ICAO STANDARD ATMOSPHERE

_ _ _ _ _ FUEL EXPENDED IN CLIMB

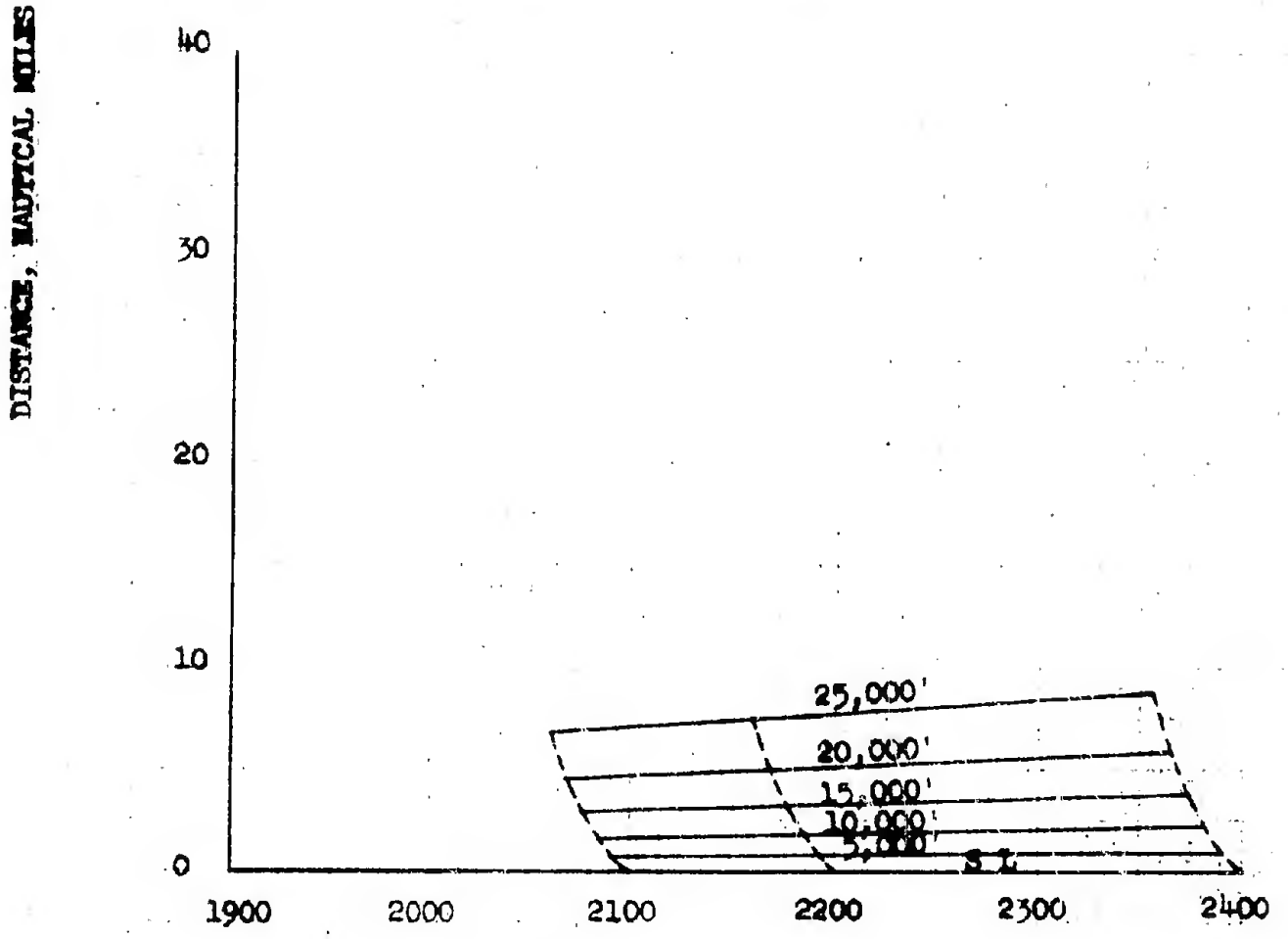

Figure 8.60

RYAN MODEL 92

HORIZONTAL DISTANCE
GAINED IN CLIMB

ENGINE: ONE YT-53-L-1
NORMAL RATED THRUST
ICAO STANDARD ATMOSPHERE

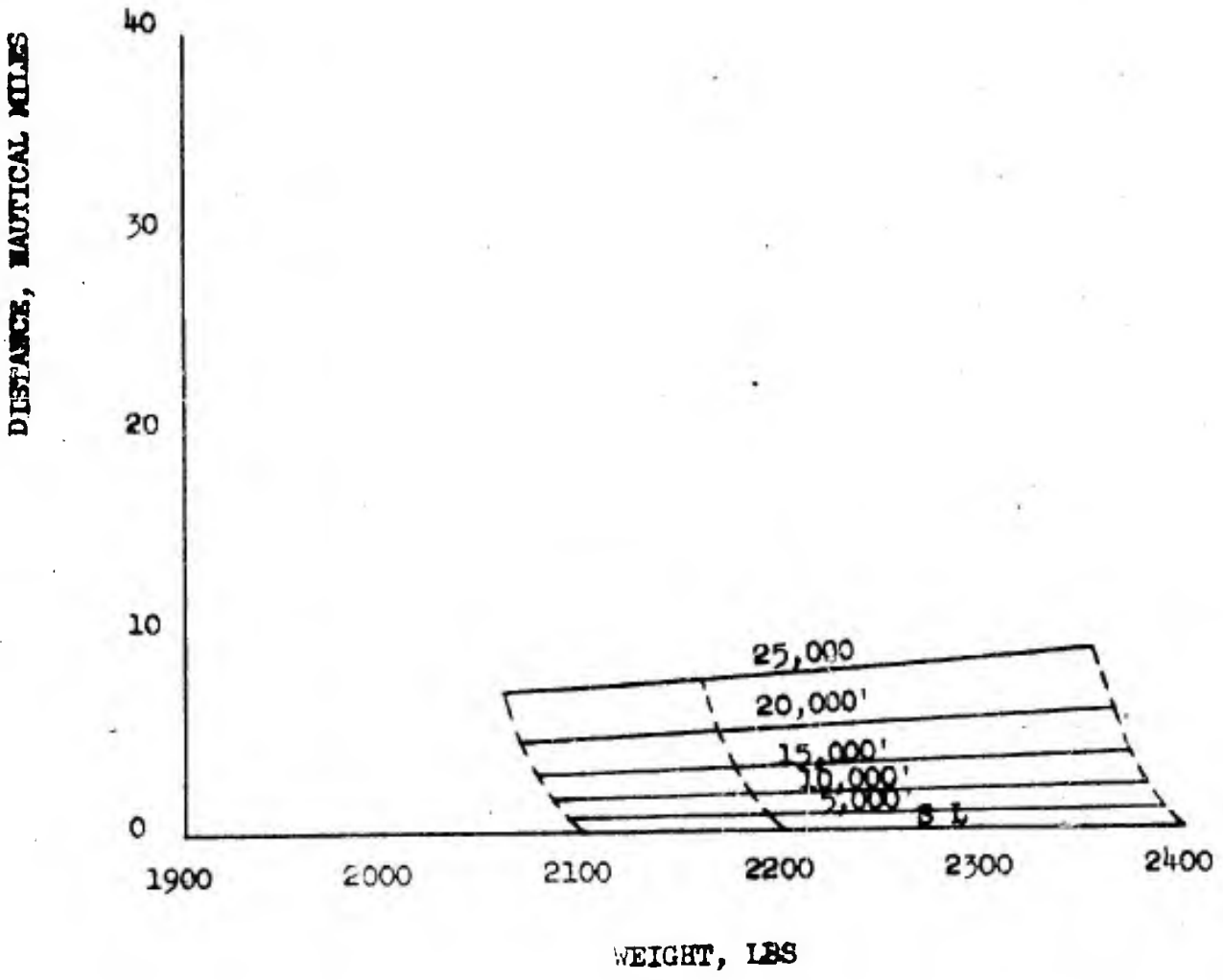

Figure 8.62

RYAN MODEL 92

HORIZONTAL DISTANCE
GAINED IN CLIMB

ENGINE: ONE YT-53-L-1
90 PERCENT NORMAL RATED THRUST
ICAO STANDARD ATMOSPHERE

_ _ _ _ FUEL EXPENDED IN CLIMB

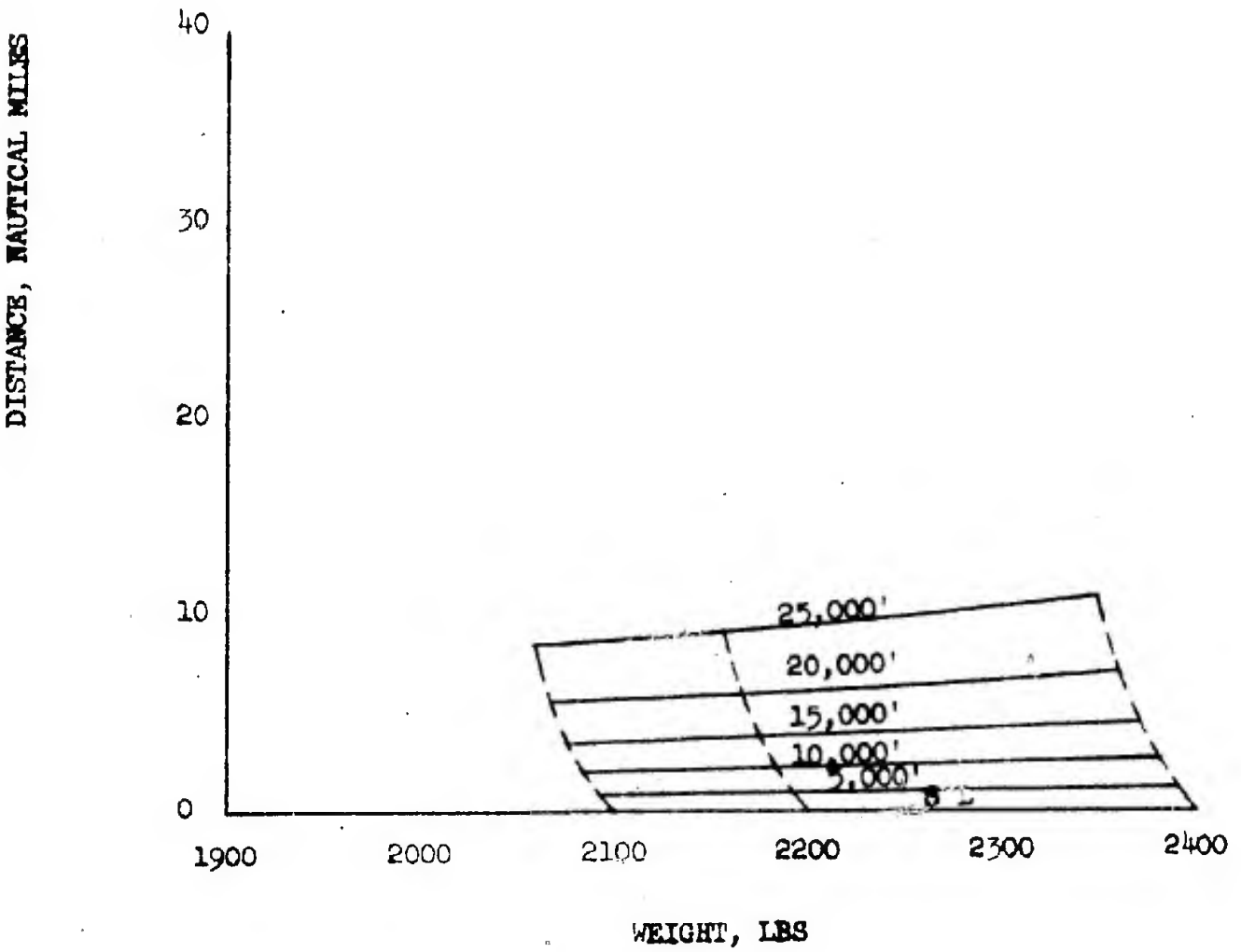

Figure 8.62

RYAN MODEL 92

HORIZONTAL DISTANCE
GAINED IN CLIMB

ENGINE: ONE YT-55-L-1
75 PERCENT NORMAL RATED THRUST
ICAO STANDARD ATMOSPHERE

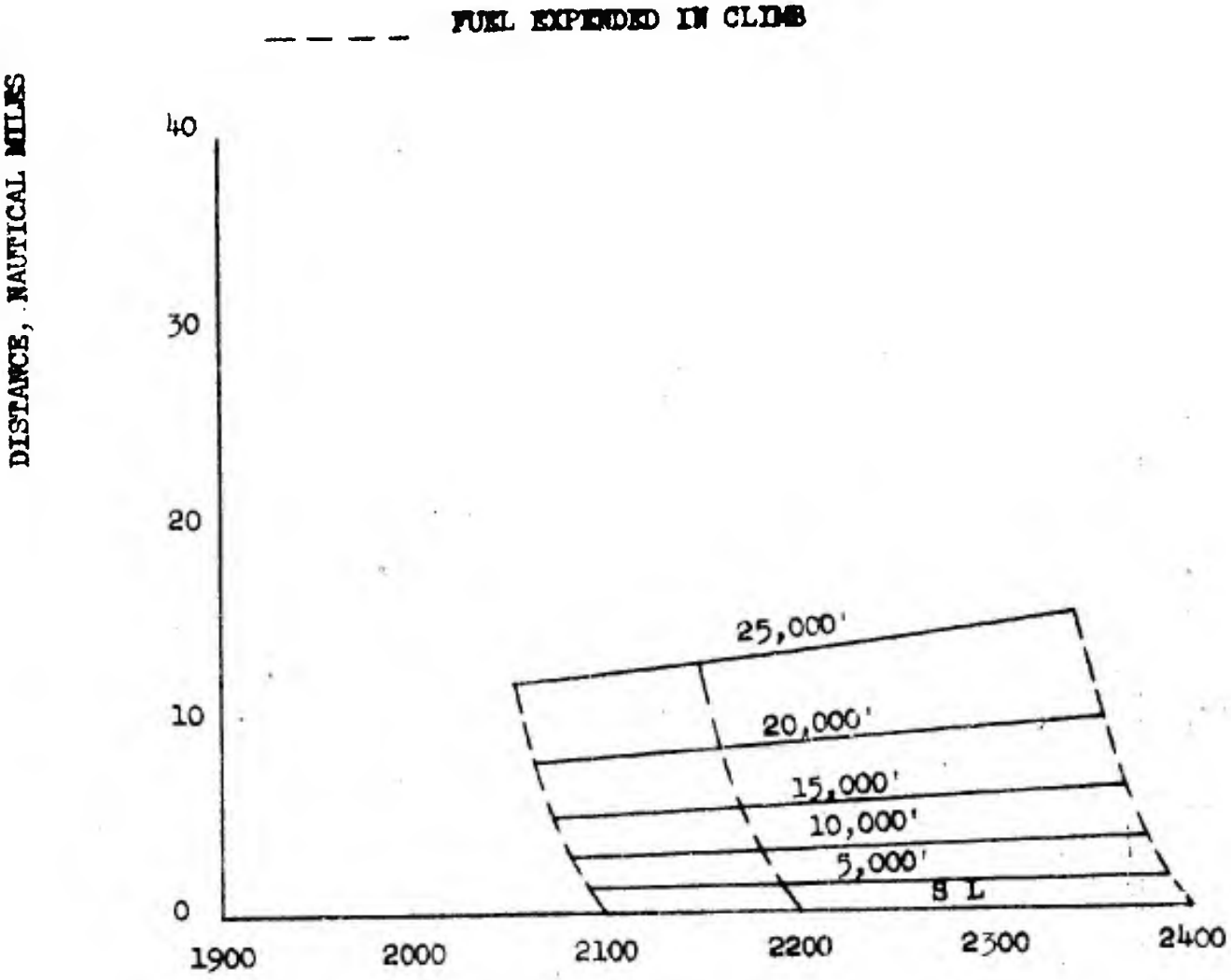

Figure 8.63

RYAN MODEL 92

HORIZONTAL DISTANCE
GAINED IN CLIMB

ENGINE: ONE YT-53-L-1
50 PERCENT NORMAL RATED THRUST
ICAO STANDARD ATMOSPHERE

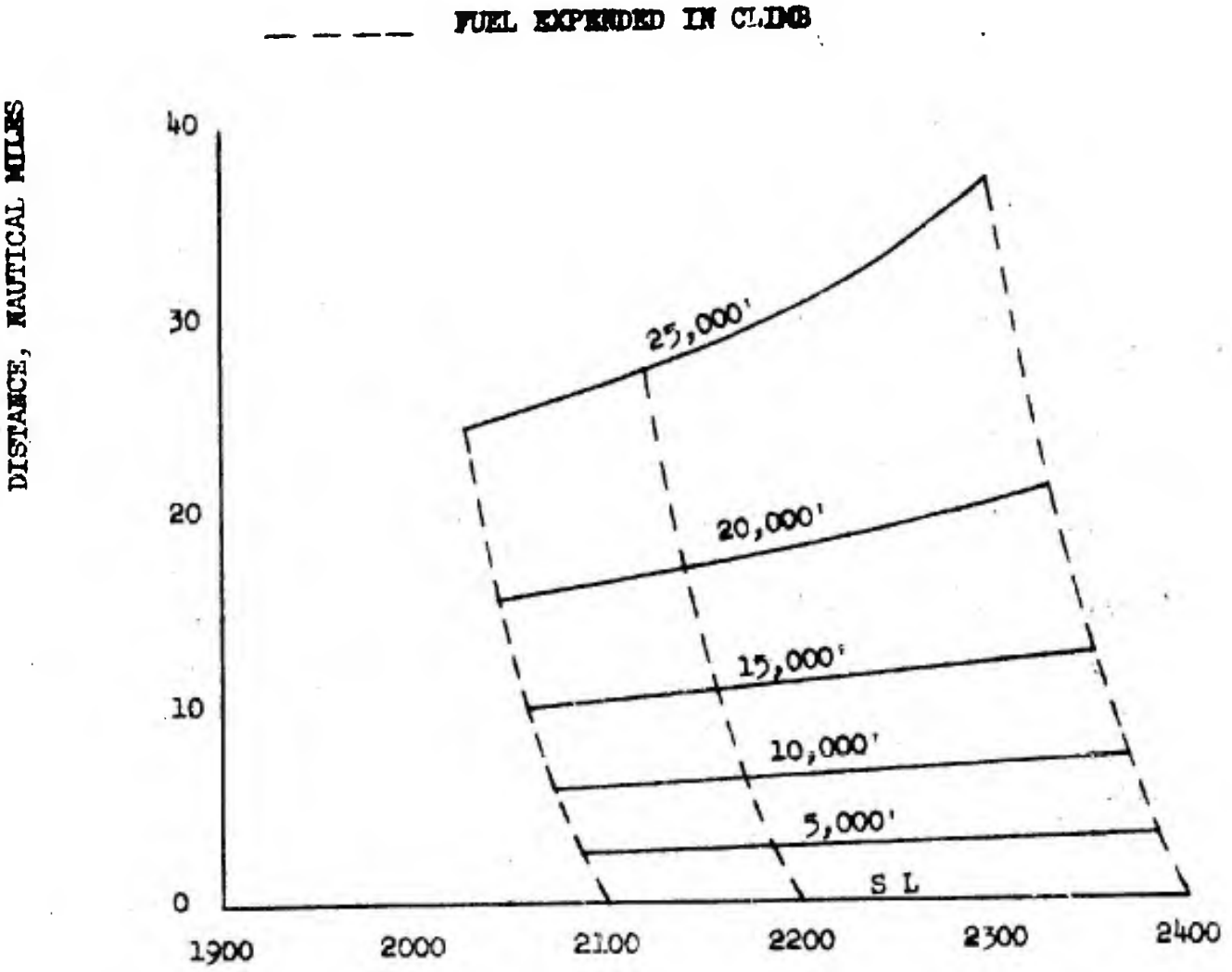

Figure 8.64

RYAN MODEL 92

ENDURANCE

ENGINE: ONE YT-53-L-1
MILITARY RATED THRUST
ICAO STANDARD ATMOSPHERE

NOTE: BASED ON 2352 LBS STARTING GROSS WEIGHT (30 GALS JP-4 AT 6.5 LBS/GAL)

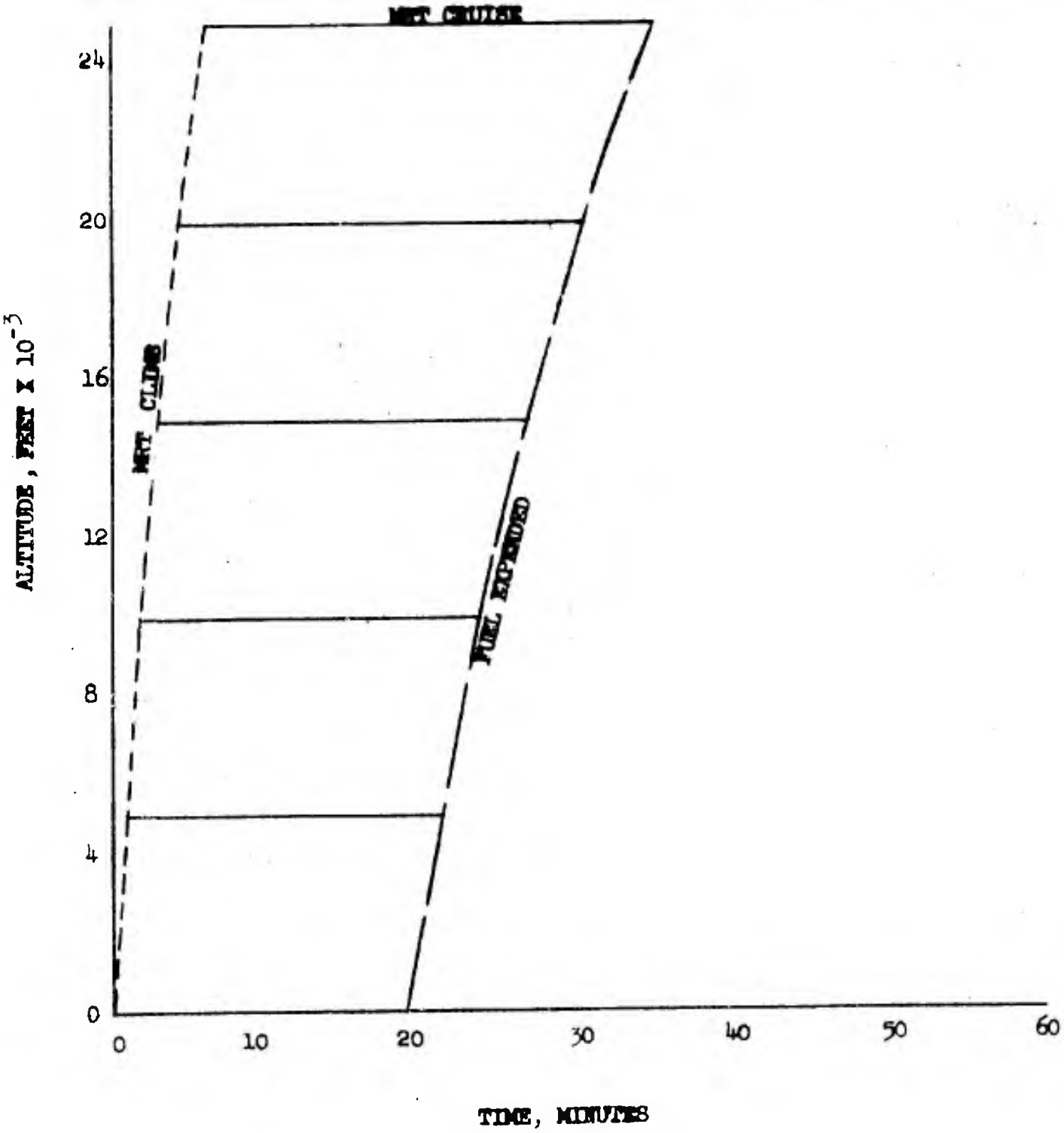

Figure 8.65

RYAN MODEL 92

ENDURANCE
ENGINE: ONE YT-53-L-1
NORMAL RATED THRUST
ICAO STANDARD ATMOSPHERE

NOTE: BASED ON 2352 LBS STARTING GROSS WEIGHT (30 GALS JF-4 AT 6.5 LBS/GAL)

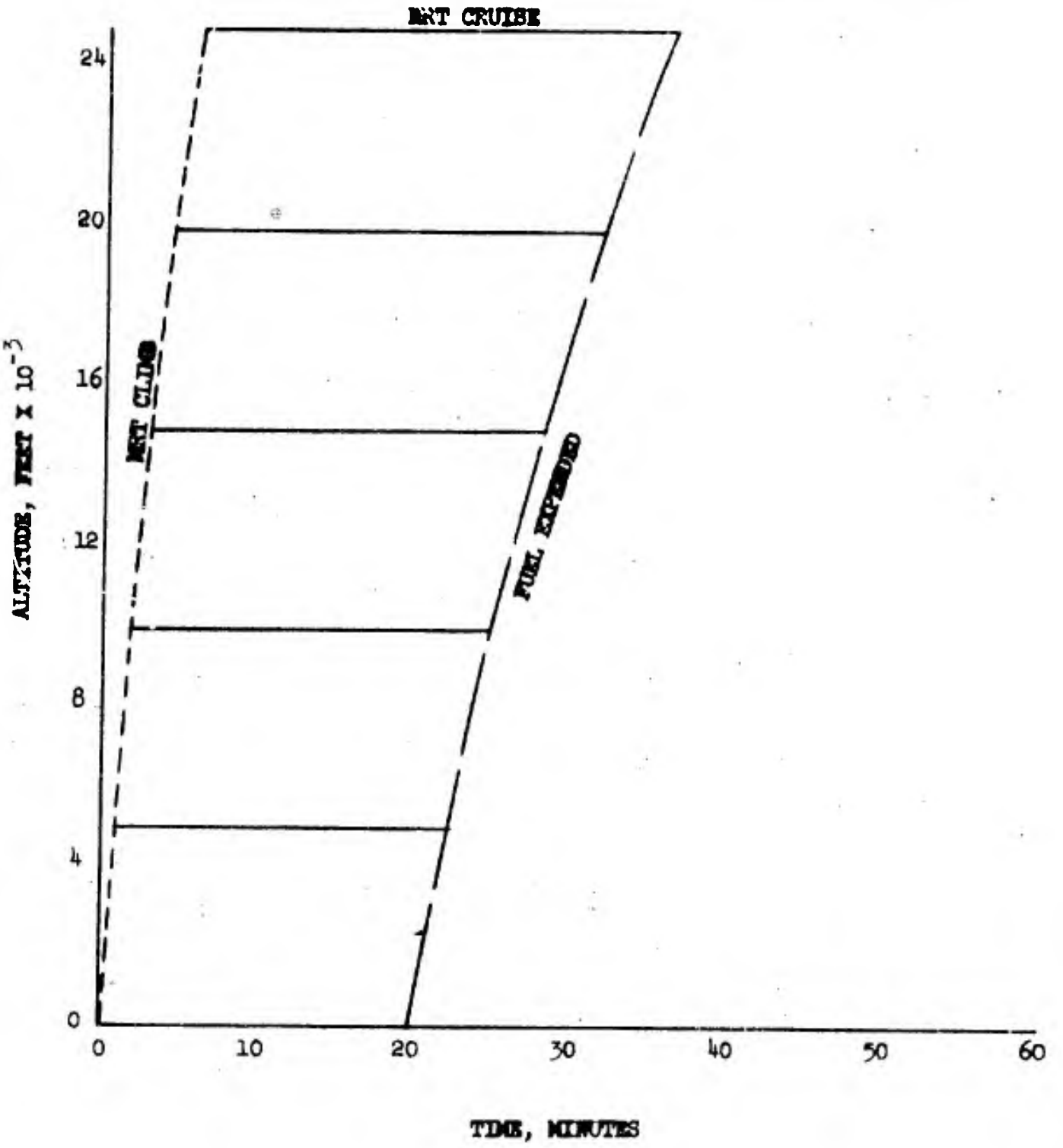

Figure 8.66

RYAN MODEL 92

ENDURANCE

ENGINE: ONE YT-53-L-1
90 PERCENT NORMAL RATED THRUST
ICAO STANDARD ATMOSPHERE

NOTE: BASED ON 2352 LBS STARTING GROSS WEIGHT (30 GALS JP-4 AT 6.5 LBS/GAL)

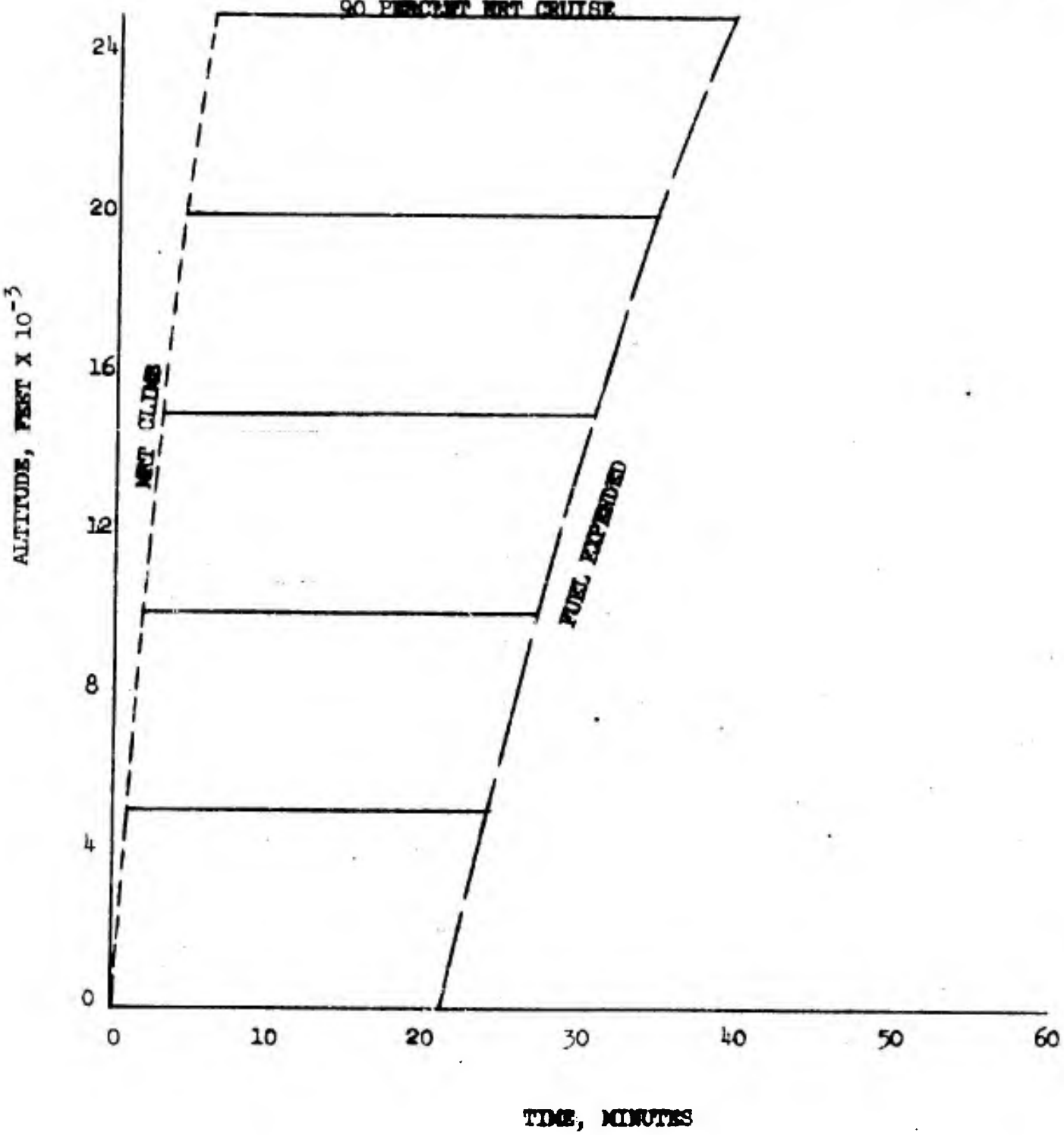

Figure 8.67

RYAN MODEL 92

ENDURANCE

ENGINE: ONE YT-53-L-1
75 PERCENT NORMAL RATED THRUST
ICAO STANDARD ATMOSPHERE
NOTE: BASED ON 2352 LBS STARTING GROSS WEIGHT (30 GALS JP-4 AT 6.5 LBS/GAL)

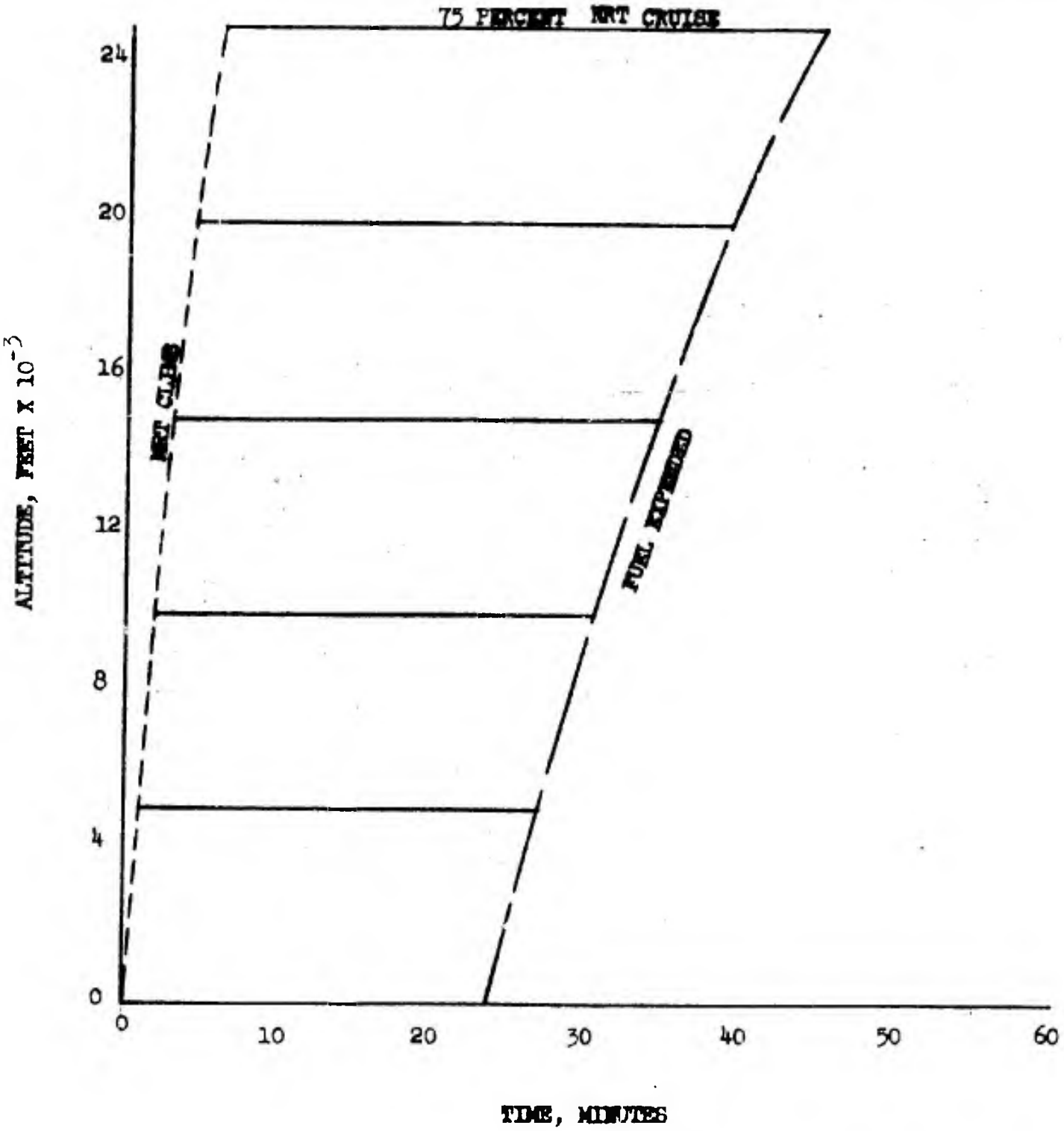

Figure 8.68

RYAN MODEL 92

ENDURANCE

ENGINE: ONE YT-53-L-1

50 PERCENT NORMAL RATED THRUST
ICAO STANDARD ATMOSPHERE

NOTE: BASED ON 2352 LBS STARTING GROSS WEIGHT (30 GALS JP-4 AT 6.5 LBS/GAL)

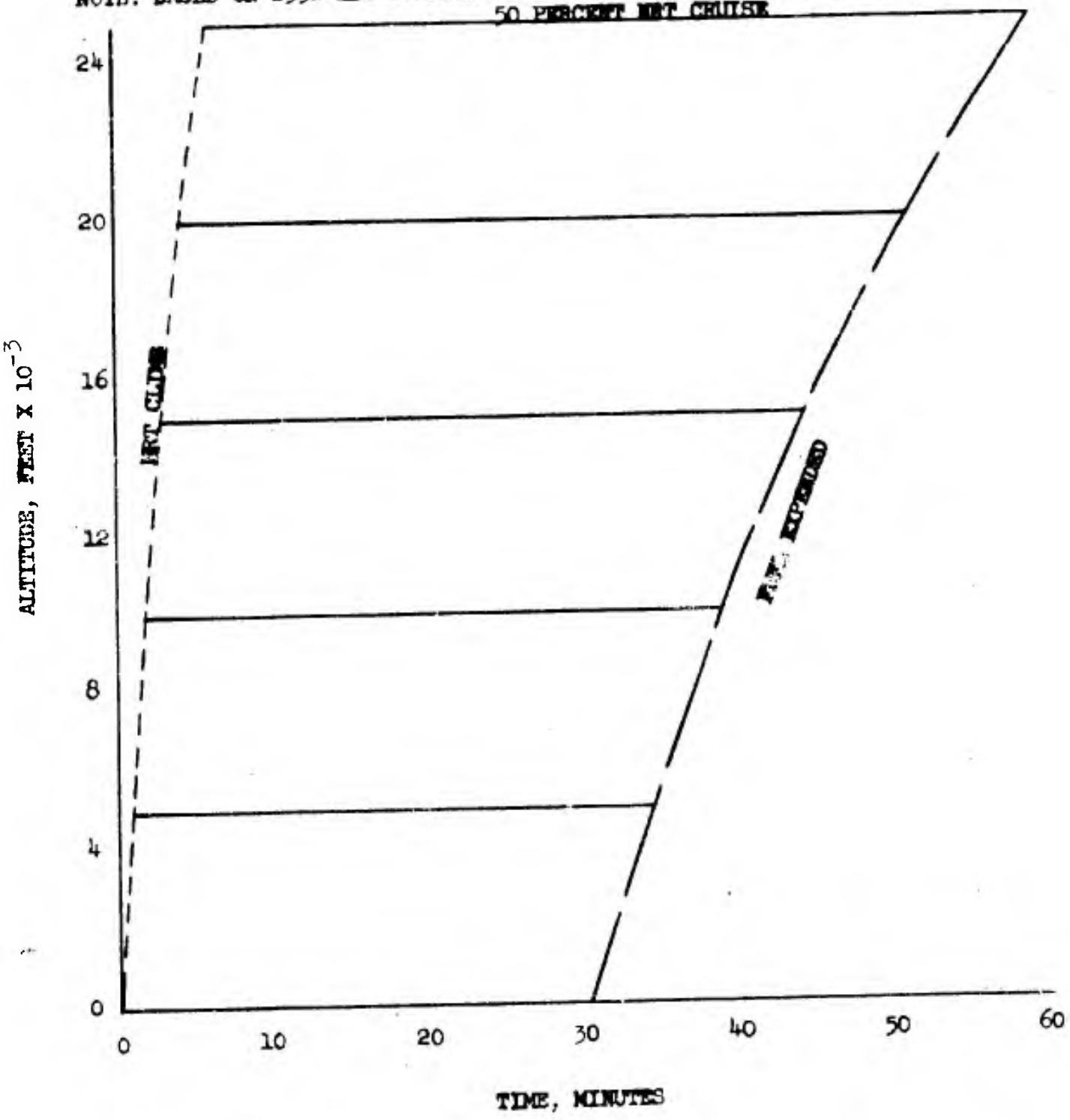

Figure 8.69

RYAN MODEL 92

RANGE
ENGINE: ONE YT-53-L-1
MILITARY RATED THRUST
ICAO STANDARD ATMOSPHERE

NOTE: BASED ON 3352 LBS STARTING GROSS WEIGHT (30 GALS JP-4 AT 6.5 LBS/GAL)

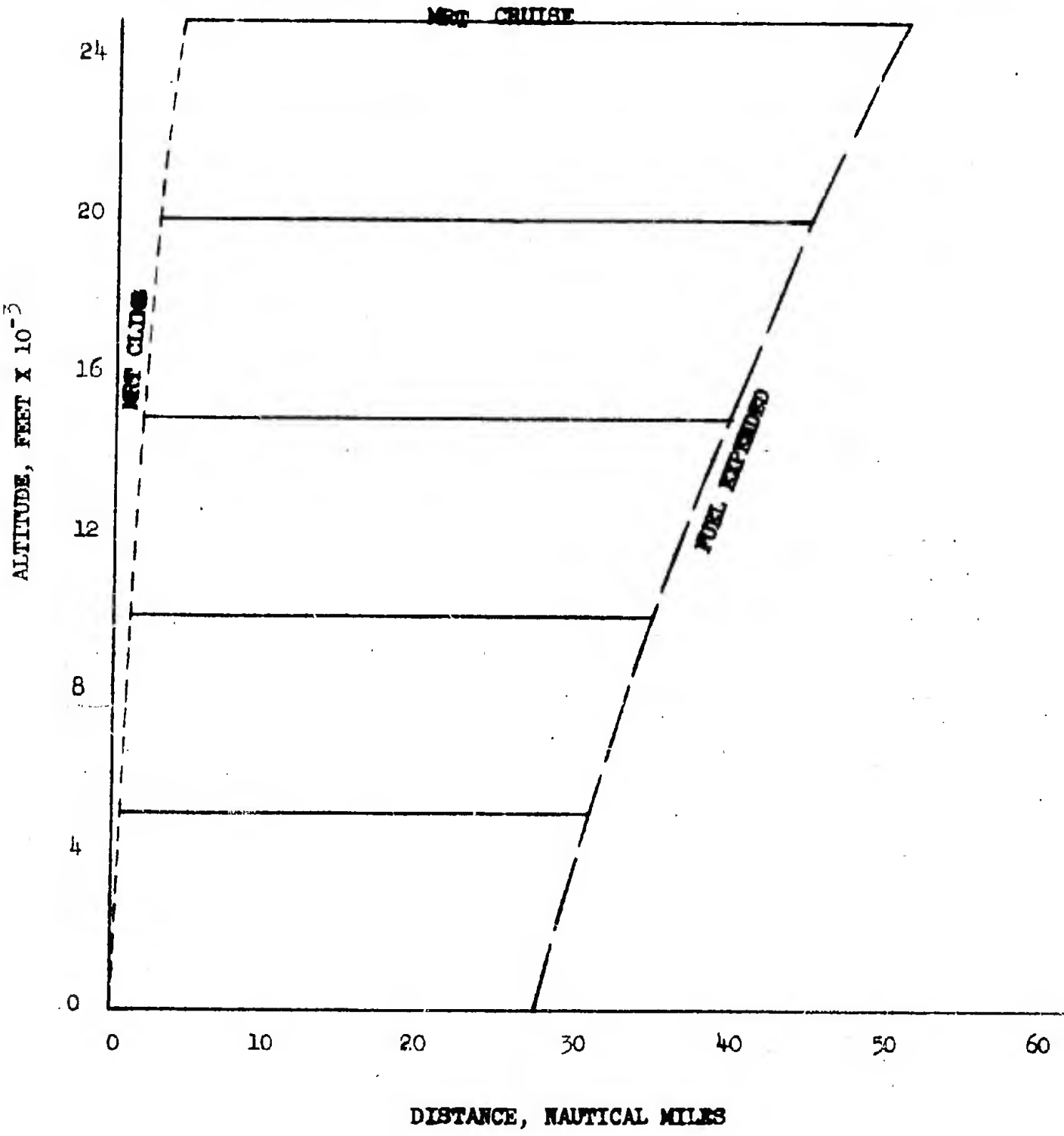

Figure 8.70

RYAN MODEL 92

RANGE
ENGINE: ONE YT-53-L-1
NORMAL RATED THRUST
ICAO STANDARD ATMOSPHERE

NOTE: BASED ON 2352 LBS STARTING GROSS WEIGHT (30 GALS JP-4 AT 6.5 LBS/GAL)

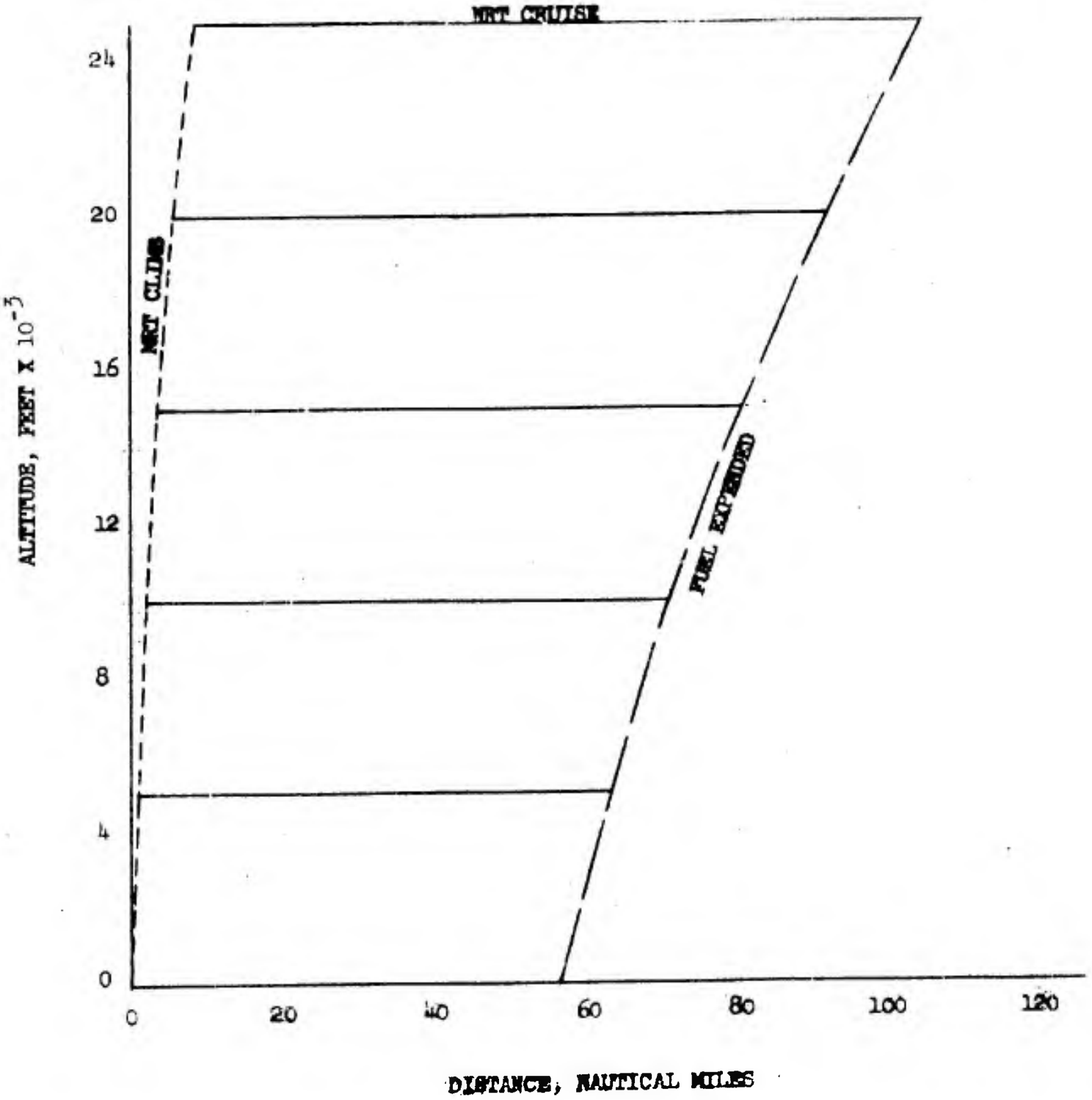

Figure 8.71

RYAN MODEL 92

RANGE
ENGINE: ONE YT-53-L-1
90 PERCENT NORMAL RATED THRUST
ICAO STANDARD ATMOSPHERE

NOTE: BASED ON 2352 LBS STARTING GROSS WEIGHT (30 GALS JP-4 AT 6.5 LBS/GAL)

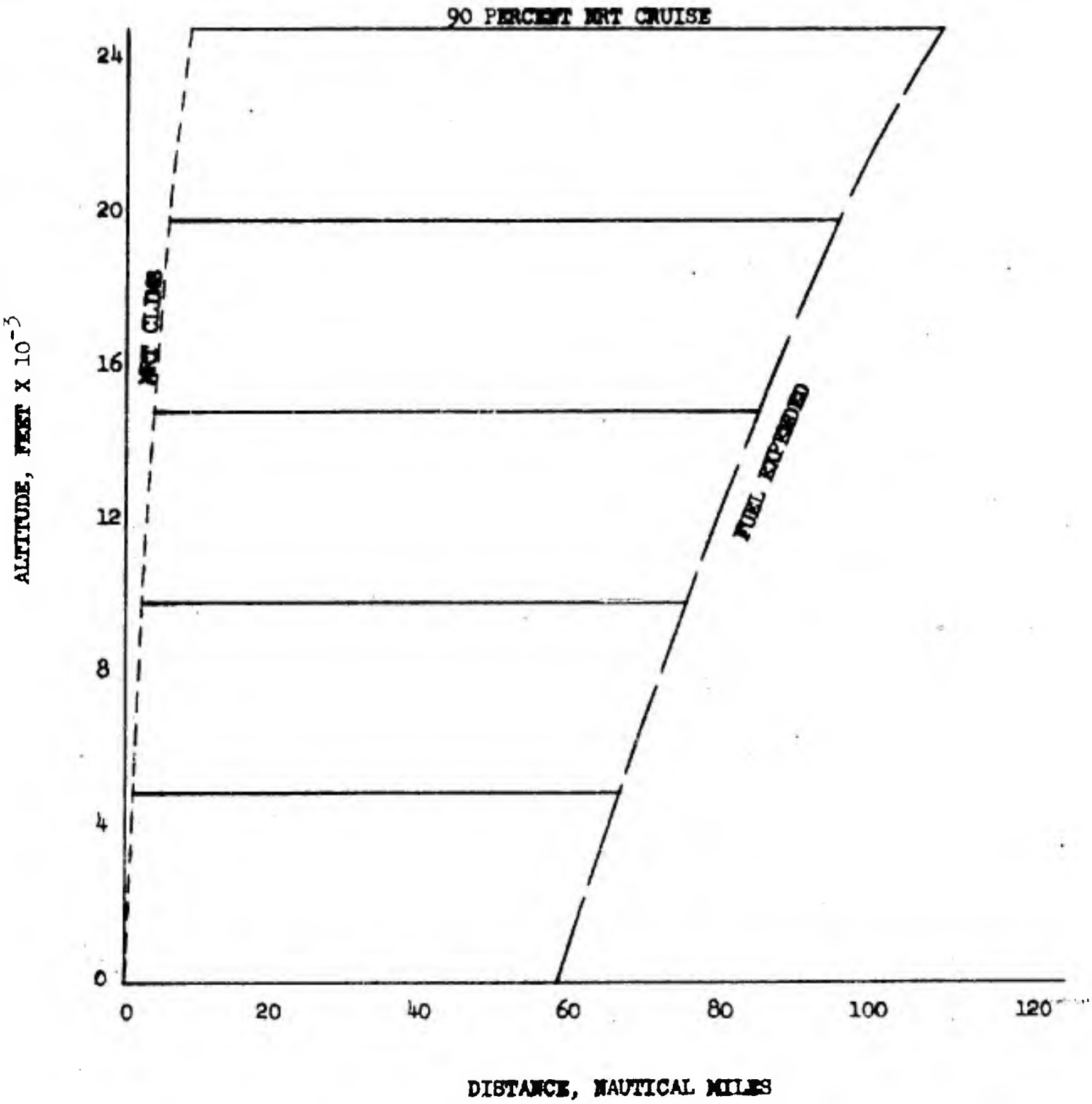

Figure 8.72

RYAN MODEL 92

RANGE

ENGINE: ONE YT-53-L-1

75 PERCENT NORMAL RATED THRUST

ICAO STANDARD ATMOSPHERE

NOTE: BASED ON 2352 LBS STARTING GROSS WEIGHT (30 GALS JP-4 AT 6.5 LBS/GAL)

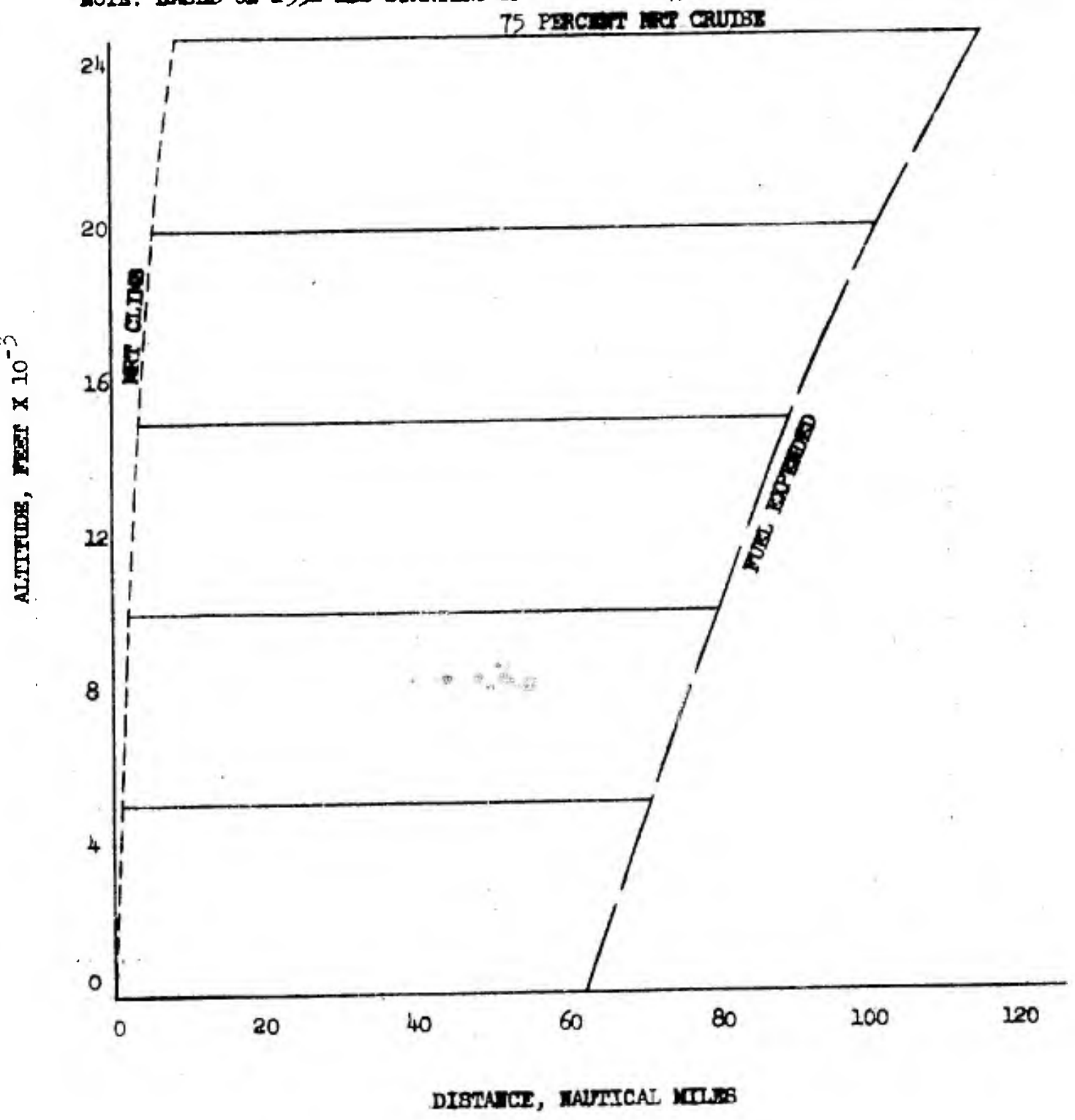

Figure 8.73

RYAN MODEL 92

RANGE

ENGINE: ONE YT-53-L-1

50 PERCENT NORMAL RATED THRUST

ICAO STANDARD ATMOSPHERE

NOTE: BASED ON 2352 LBS STARTING GROSS WEIGHT (30 GALS JP-4 AT 6.5 LBS/GAL)

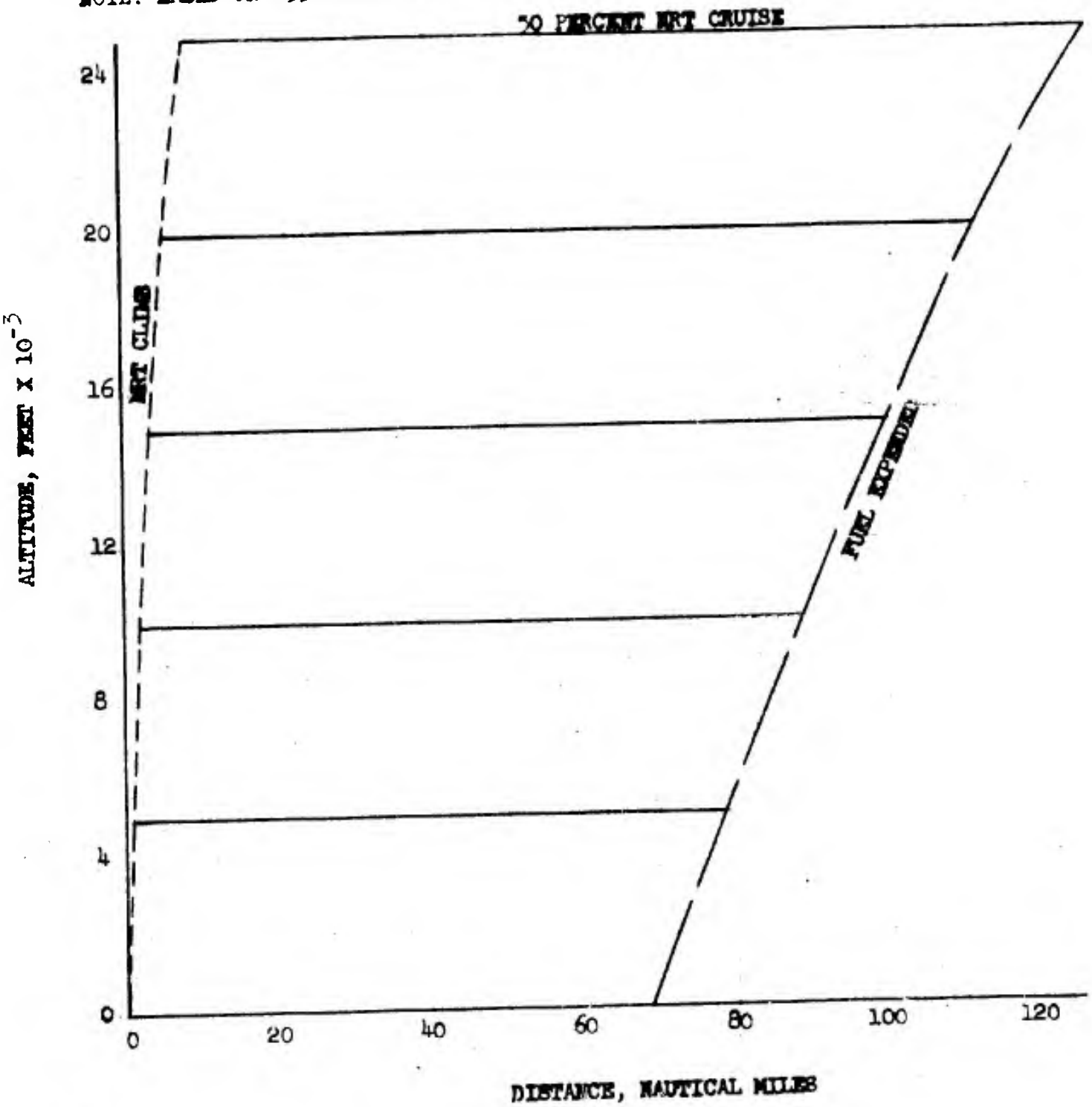

Figure 8.74

RYAN MODEL 92

WING ANGLE OF ATTACK IN CLIMB
AT VARIOUS TRUE AIRSPEEDS

ENGINE: ONE YT-53-L-1
MILITARY RATED THRUST
ICAO STANDARD ATMOSPHERE

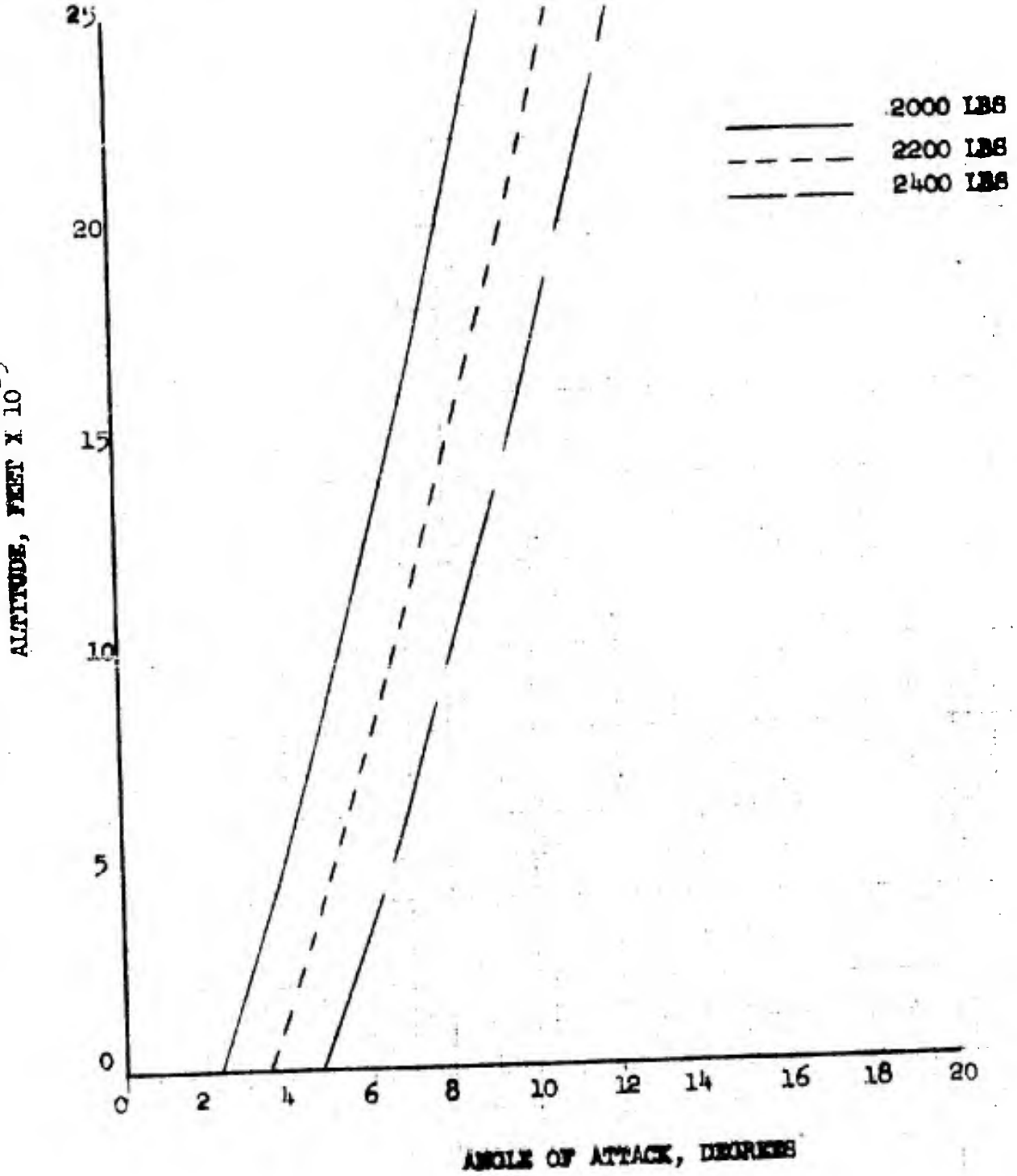

Figure 8.75

RYAN MODEL 92

WING ANGLE OF ATTACK IN CLIMB
AT VARIOUS TRUE AIRSPEEDS

ENGINE: ONE YT-53-L-1
NORMAL RATED THRUST
ICAO STANDARD ATMOSPHERE

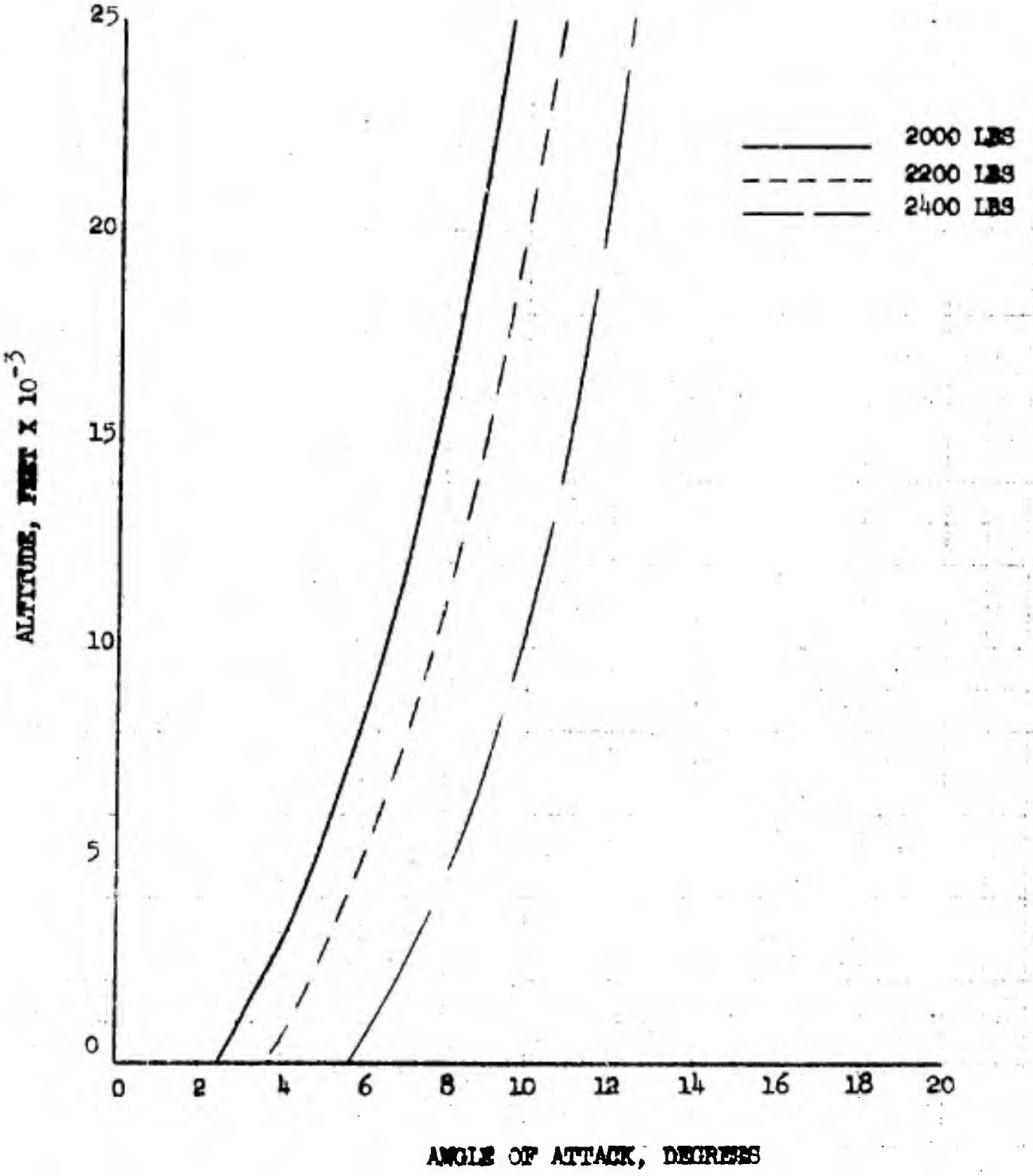

Figure 8.76

RYAN MODEL 92

WING ANGLE OF ATTACK IN CLIMB
AT VARIOUS TRUE AIRSPEEDS

ENGINE: ONE YT-53-L-1
90 PERCENT NORMAL RATED THRUST
ICAO STANDARD ATMOSPHERE

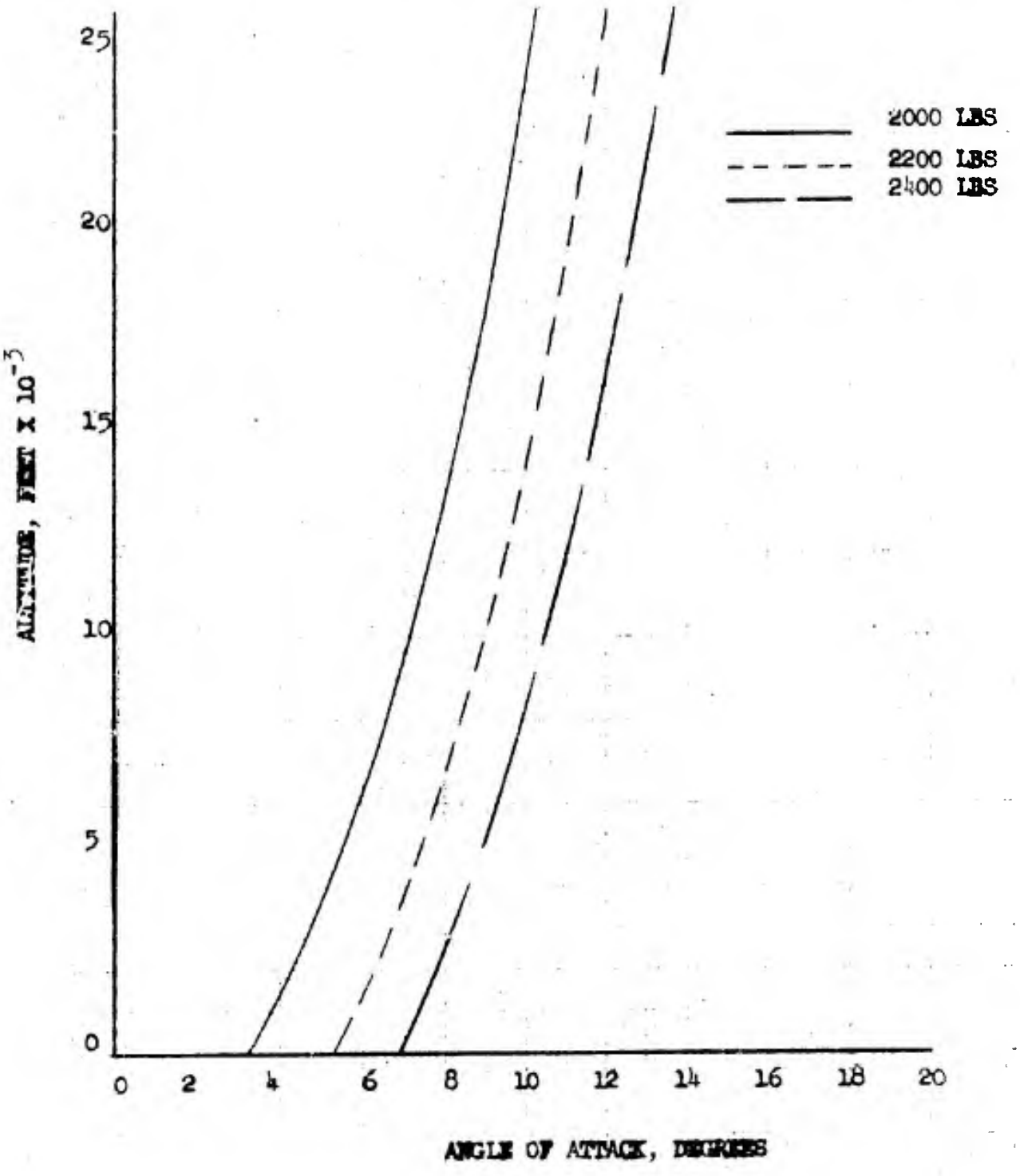

Figure 8.77

RYAN MODEL 92

WING ANGLE OF ATTACK IN CLIMB
AT VARIOUS TRUE AIRSPEEDS

ENGINE: ONE YT-33-L-1
75 PERCENT NORMAL RATED THRUST
ICAO STANDARD ATMOSPHERE

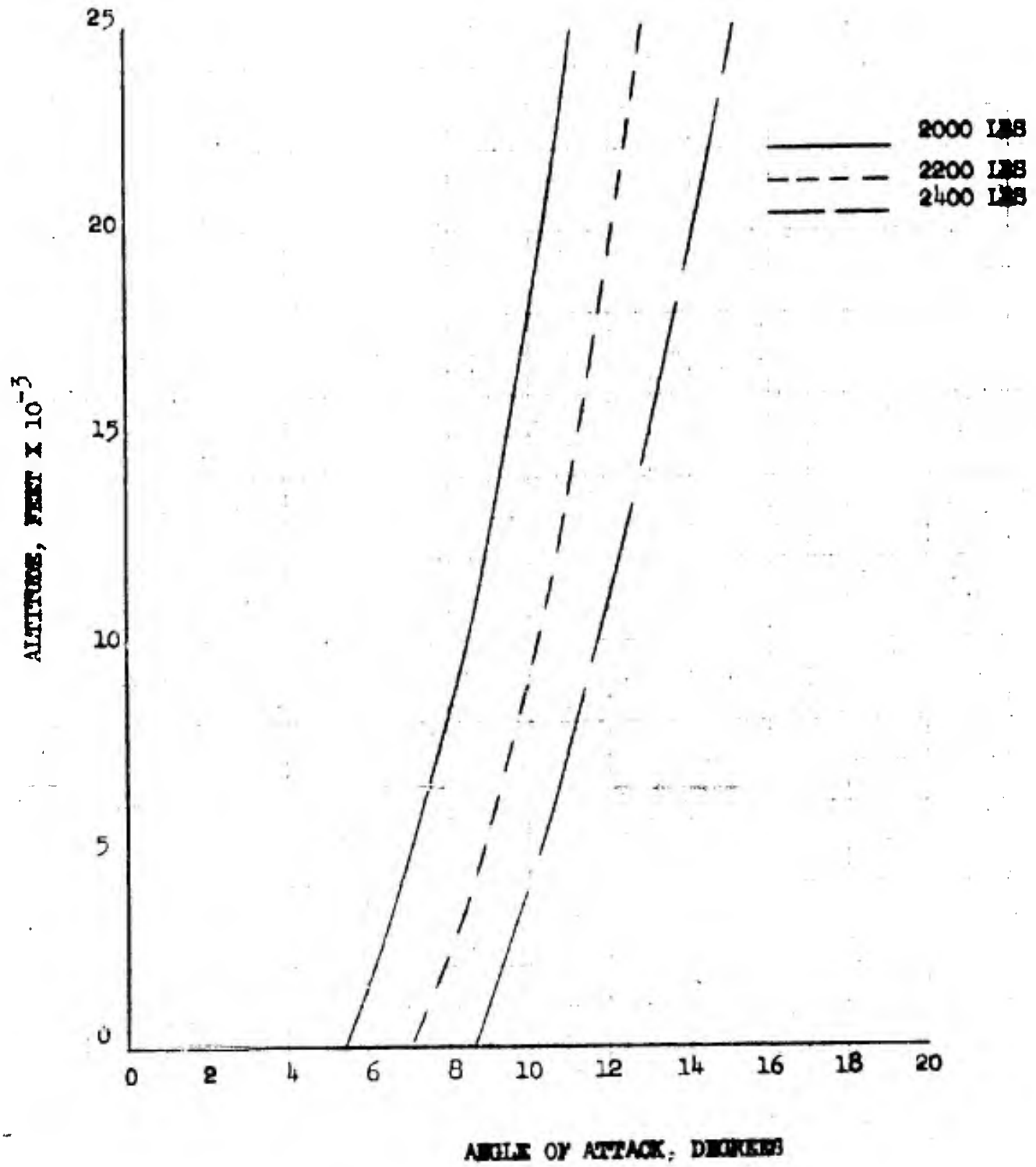

Figure 8.75

RYAN MODEL 92

ANGLE OF ATTACK IN CLIMB
AT VARIOUS TRUE AIRSPEEDS

ENGINE: ONE YT-53-L-1
50 PERCENT NORMAL RATED THRUST
ICAO STANDARD ATMOSPHERE

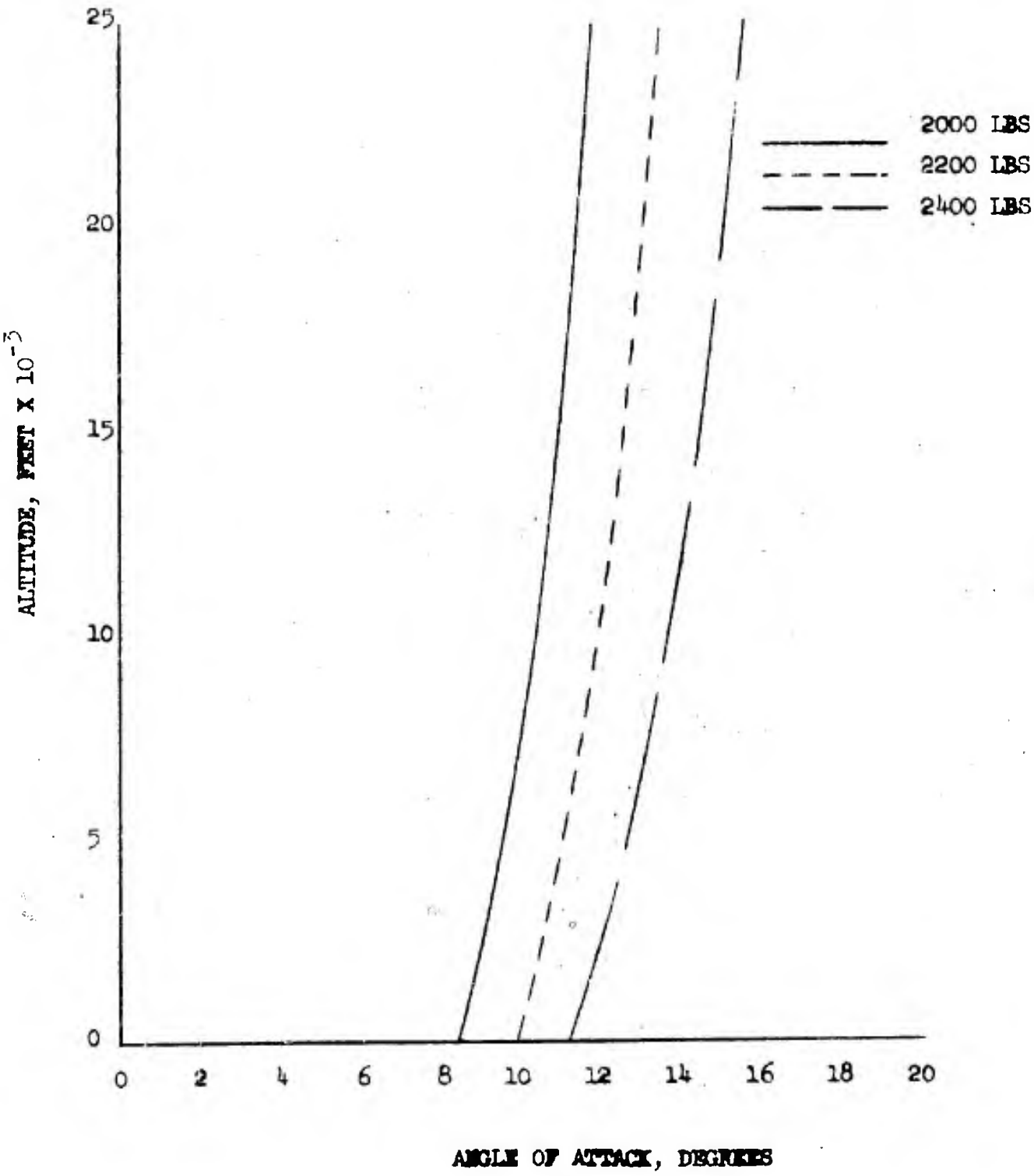

Figure 8.7

RYAN MODEL 92

CONVENTIONAL TAKE-OFF DISTANCE VERSUS

POWER SETTING

ENGINE: ONE YT-53-L-1

ICAO STANDARD ATMOSPHERE

AND ANA HOT DAY (103 °F)

WEIGHT: 2352 LBS

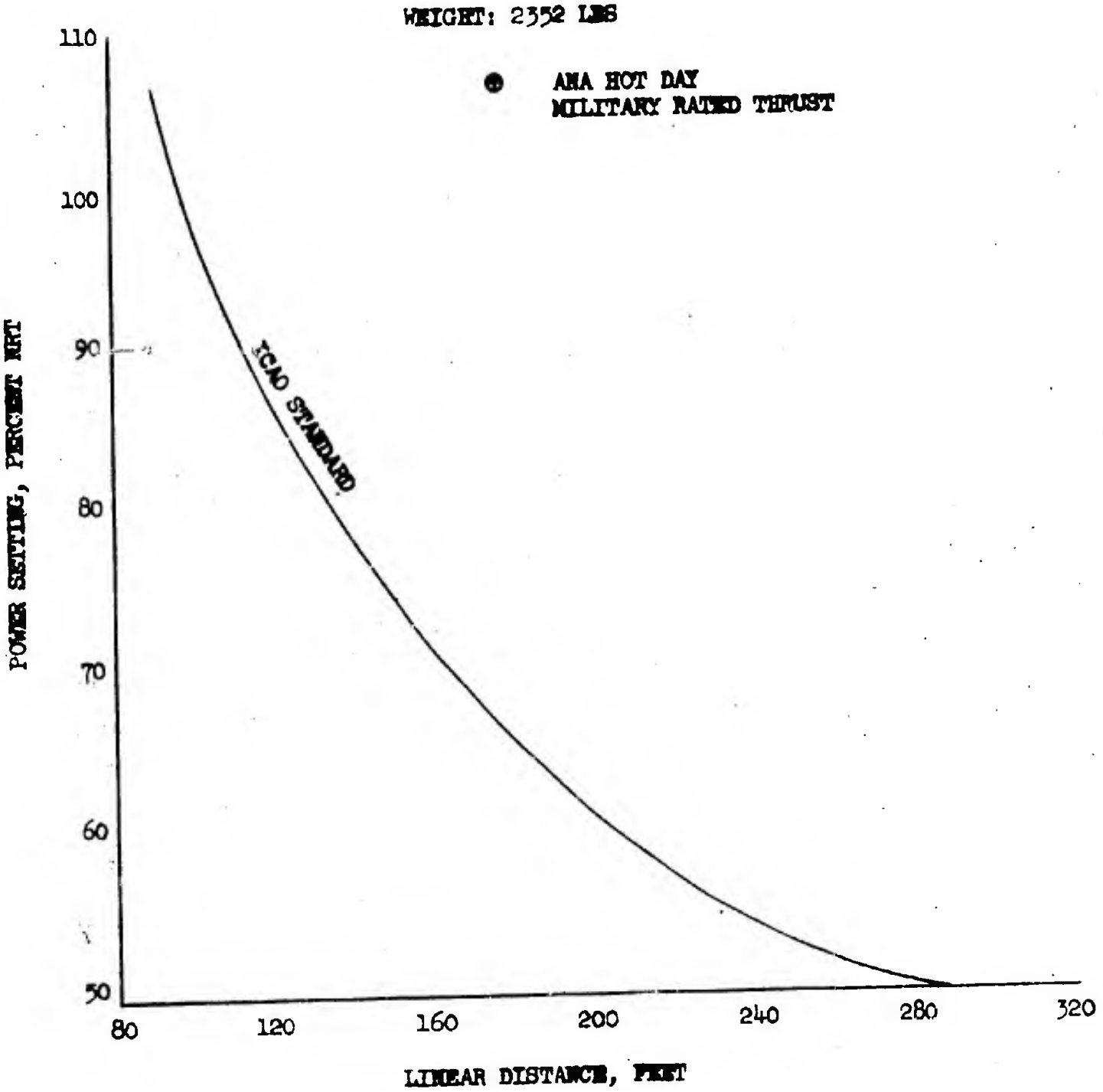

Figure 8.80

RYAN MODEL 92

HOVERING CHARACTERISTICS WITH FORWARD AND AFT FLAP DEFLECTED 55°

ENGINE: ONE YT-55-L-1

ICAO STANDARD ATMOSPHERE

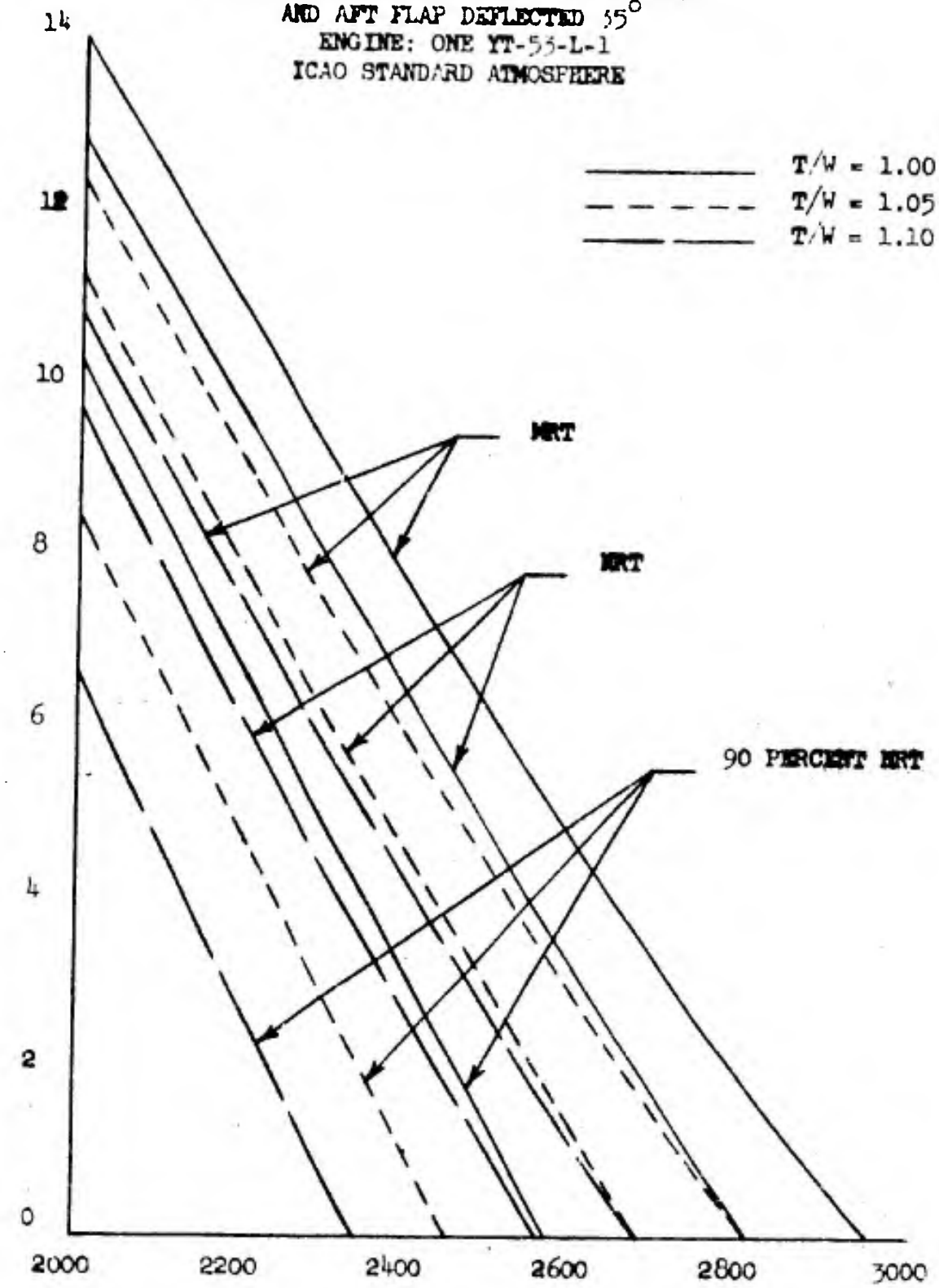

Figure 8.81

RYAN MODEL 92

STATIC LONGITUDINAL STABILITY BREAKDOWN

ZERO FLAP DEFLECTION

$\frac{X_{c.g.}}{\bar{c}} = .515$

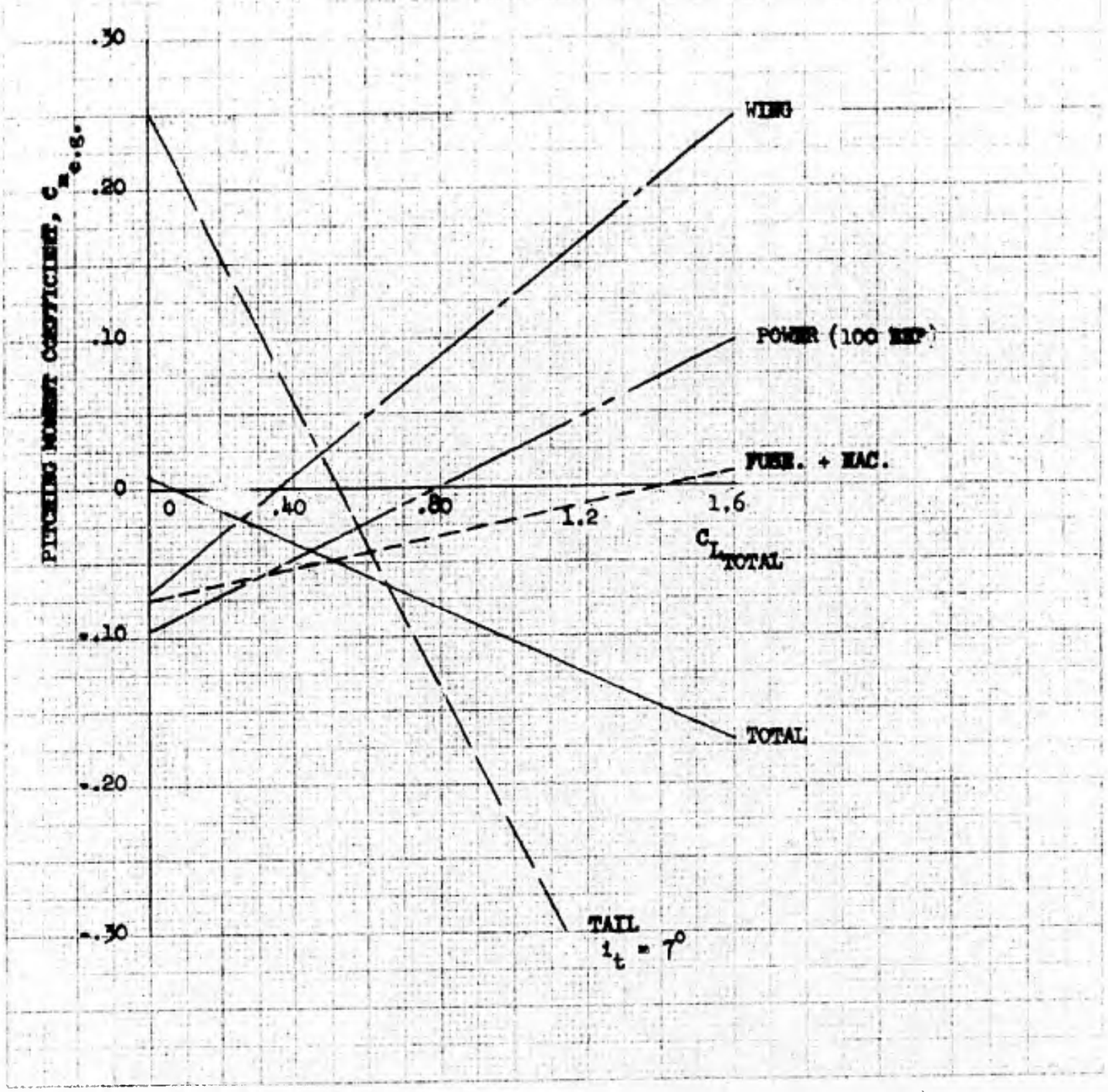

Figure 8.82

RYAN MODEL 92

ELEVATOR ANGLE REQUIRED FOR TRIM

ZERO FLAP DEFLECTION

$\frac{X_{c.g.}}{\bar{c}} = .515$

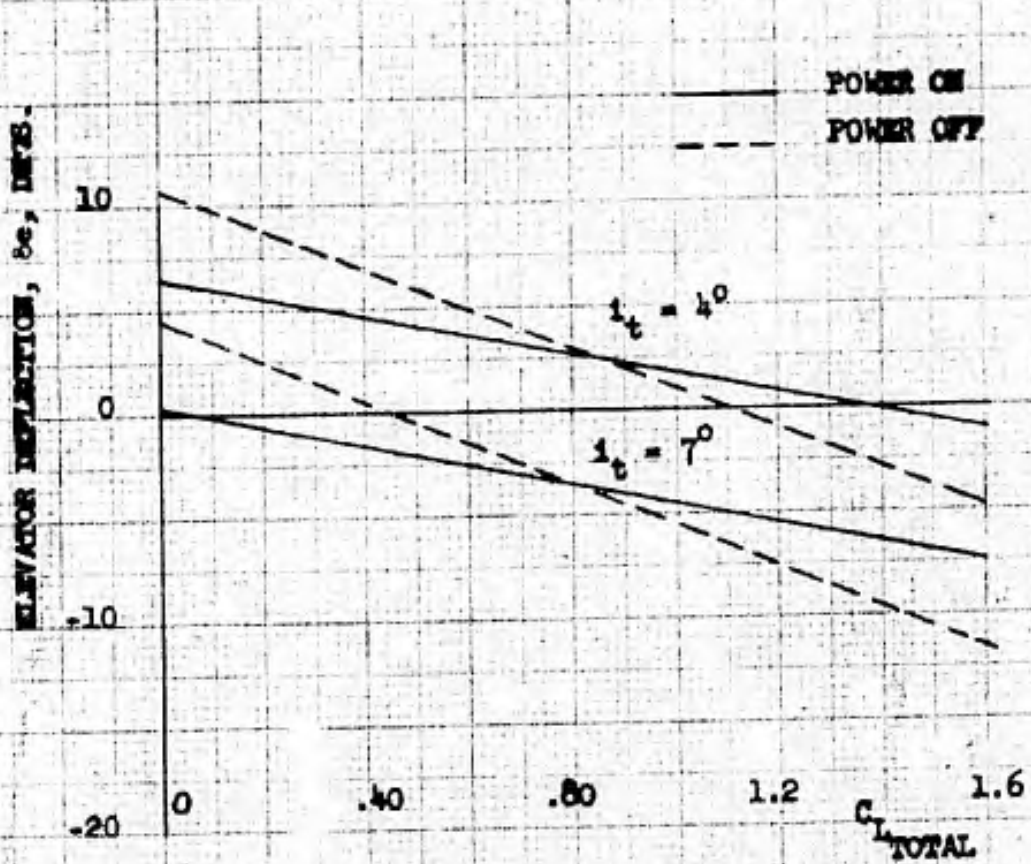

Figure 8.83

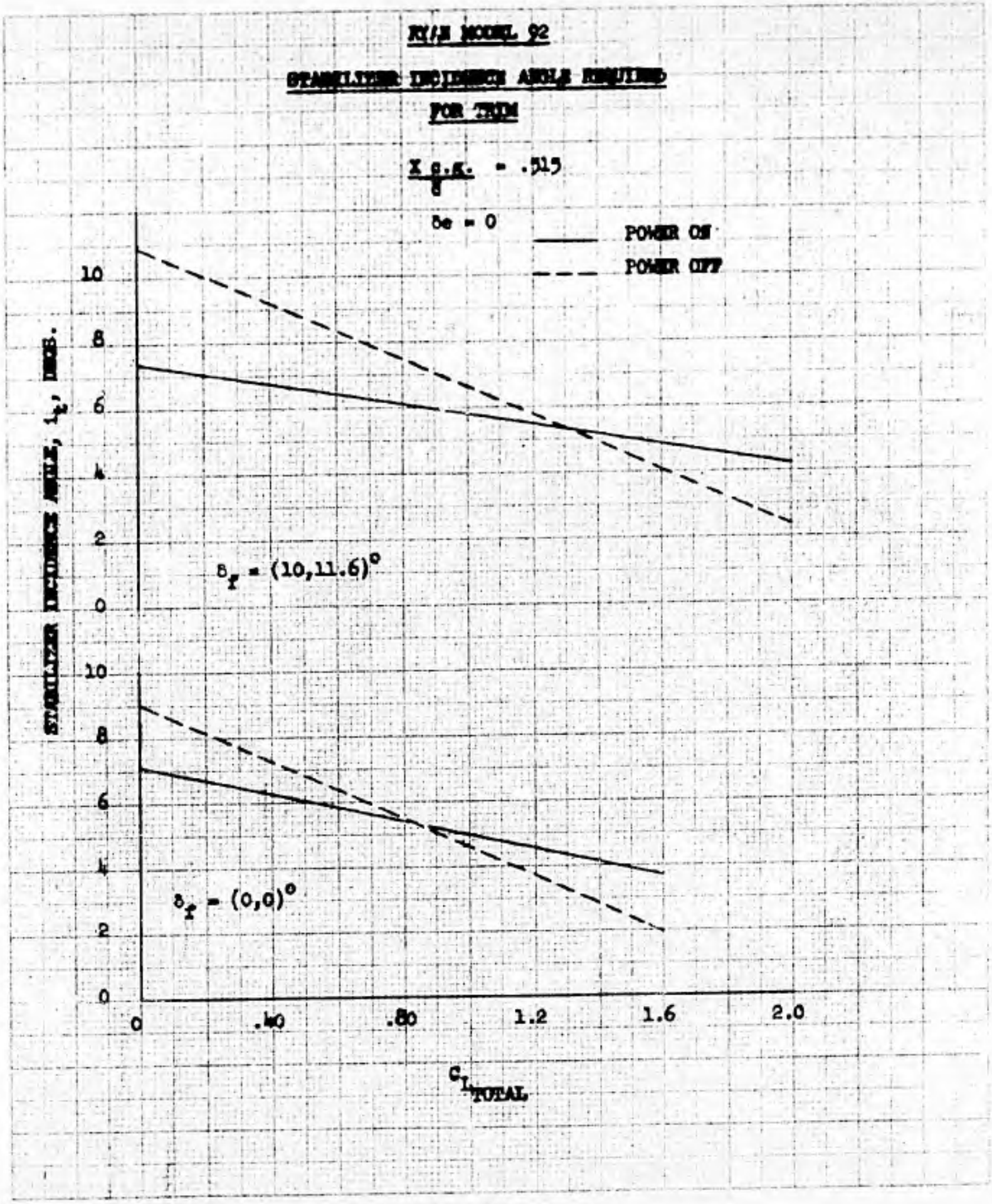
XF/A MODEL 92
STABILIZER INCIDENCE ANGLE REQUIRED FOR TRIM
X c.g. = .515
δe = 0
POWER ON
POWER OFF
δf = (10,11.6)°
δf = (0,0)°
STABILIZER INCIDENCE ANGLE, iT, DEGS.
10
8
6
4
2
0
0
.40
.80
1.2
1.6
2.0
CL TOTAL

Figure 8.84

RYAN MODEL 92

EFFECT OF TAIL NOZZLE THRUST
ON STICK FREE LONGITUDINAL STABILITY

$\bar{X}_{cg}$ = .515

NOTE: Nozzle thrust based on Military Rated Power.

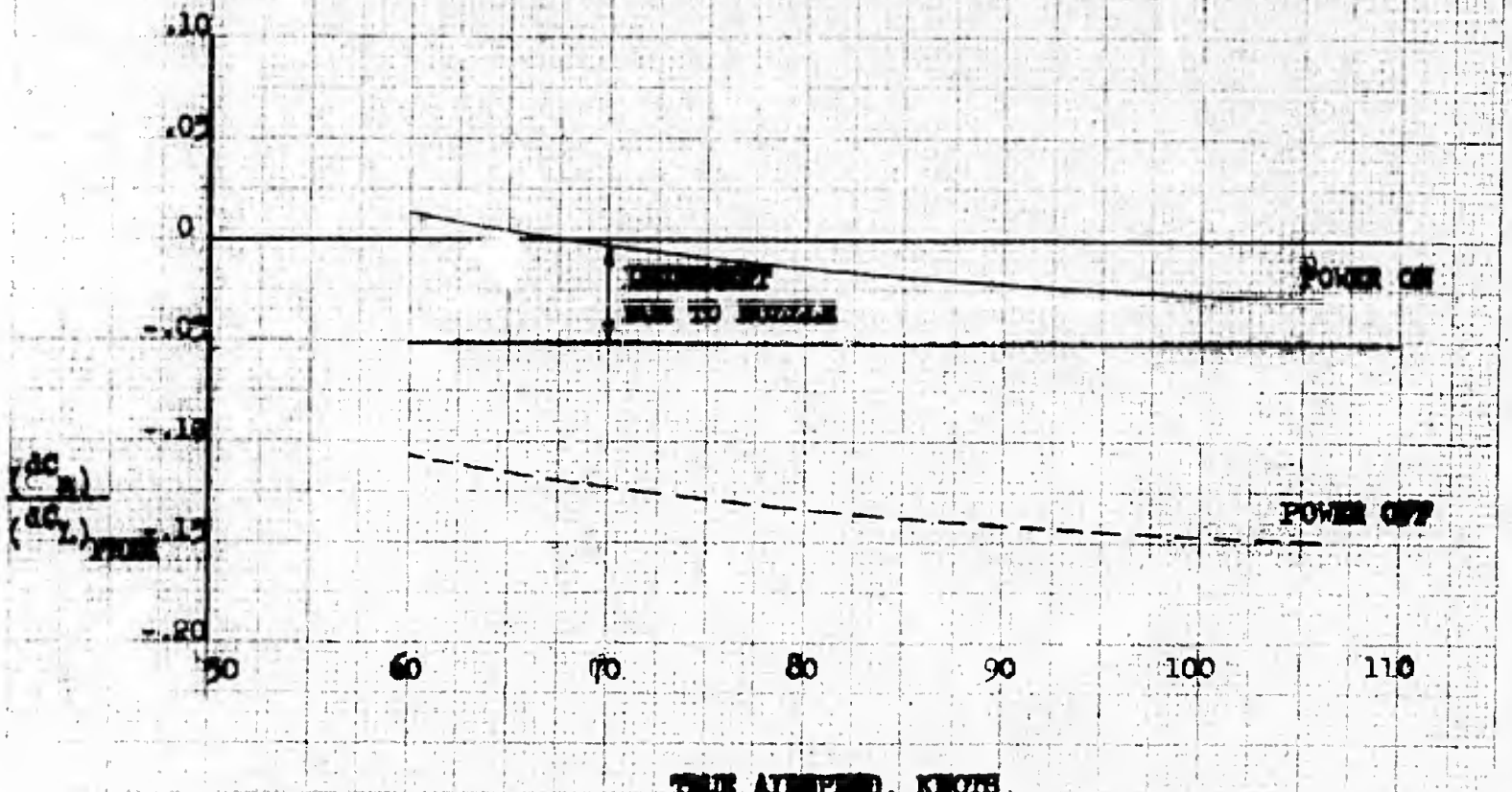

Figure 8.85

RYAN MODEL 92

LONGITUDINAL STICK FORCE VARIATION WITH SPEED

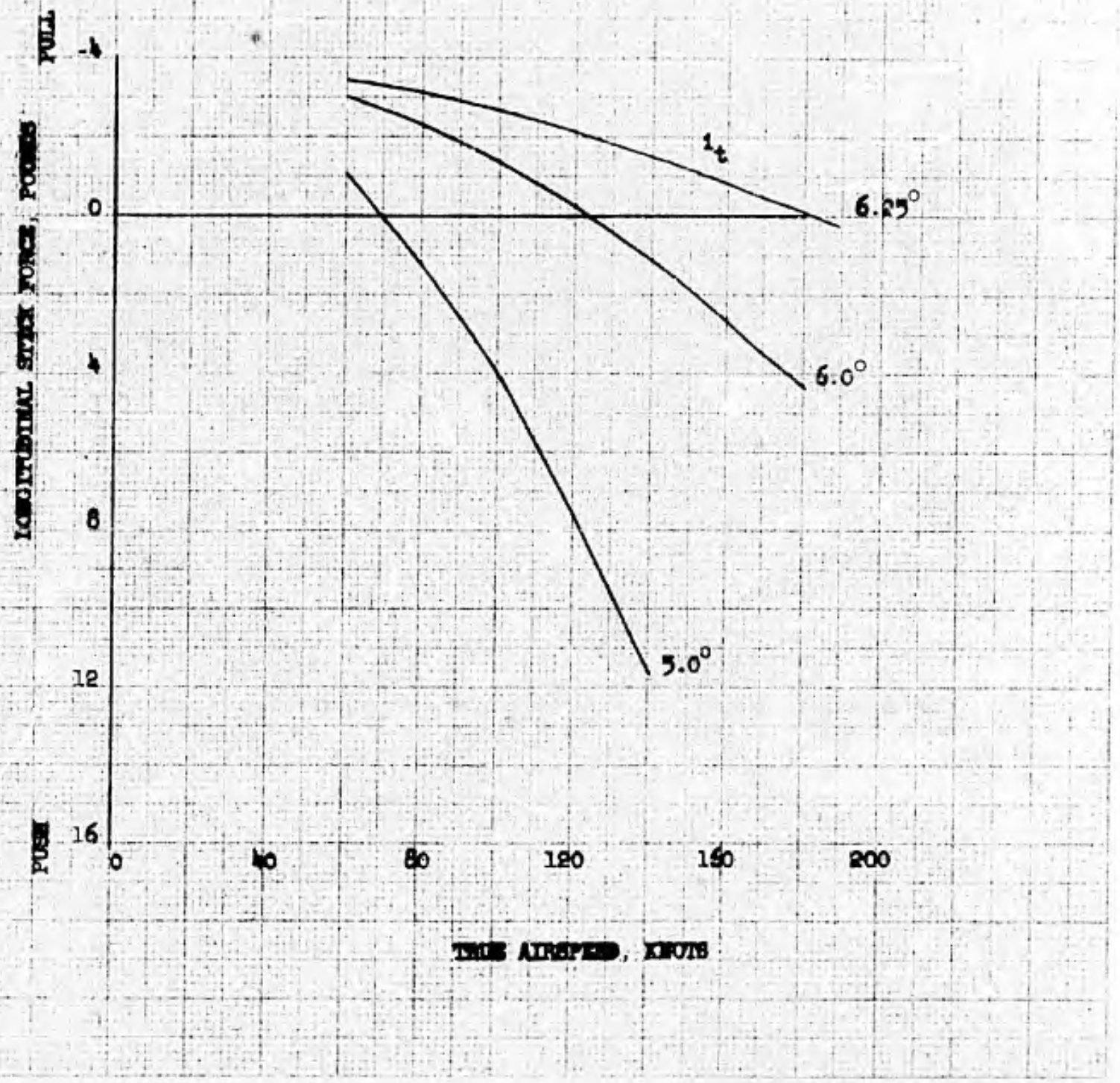

Figure 8.86

RYAN MODEL 92

SUMMARY OF C.G. LIMITS

SYMBOL SHOWN FOR c.g. FROM
WEIGHT AND BALANCE ESTIMATE
(W=2752 LBS.)

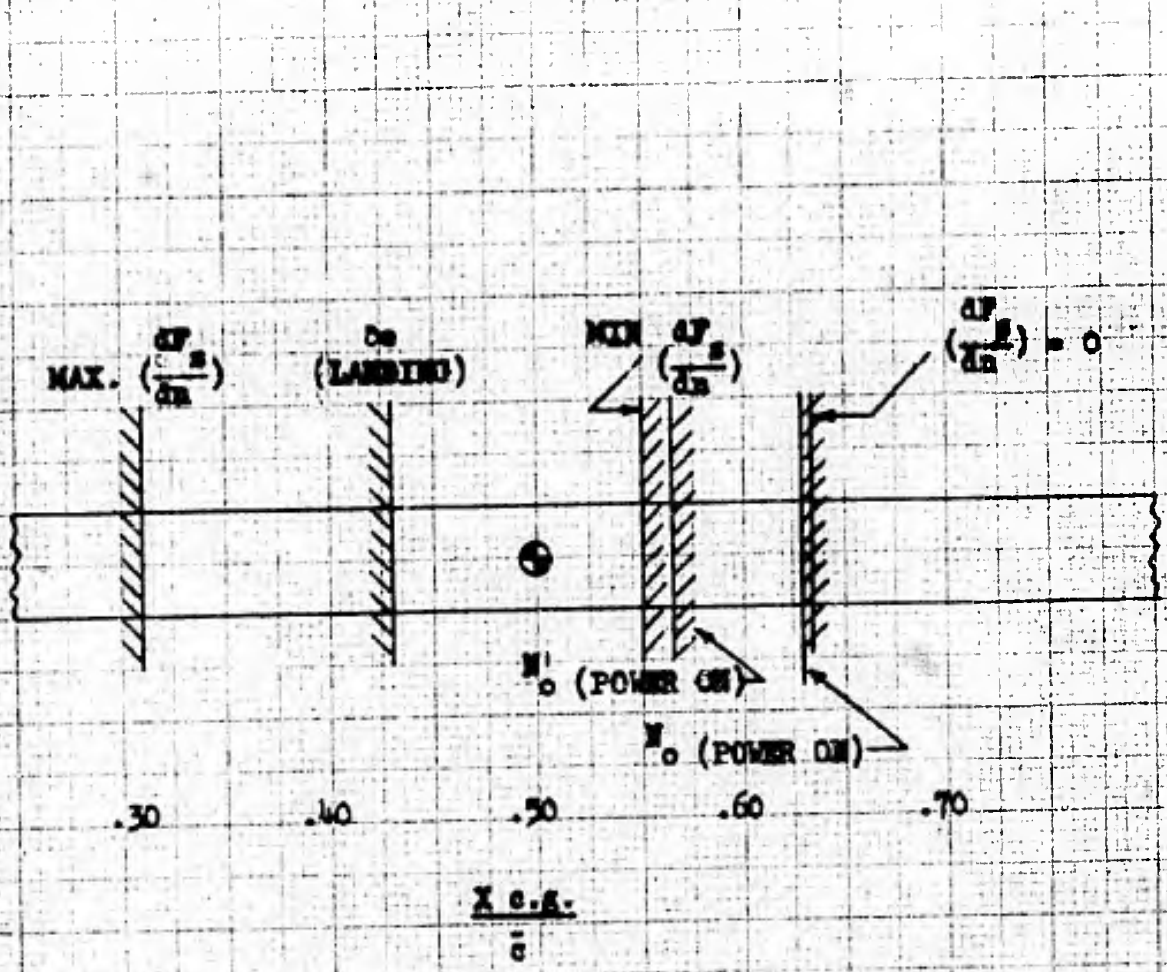

Figure 8.87

RYAN MODEL 92

EFFECT OF TAIL NOZZLE THRUST

ON RUDDER-FREE DIRECTIONAL STABILITY

NOTE: Nozzle thrust based on Military Rated Power

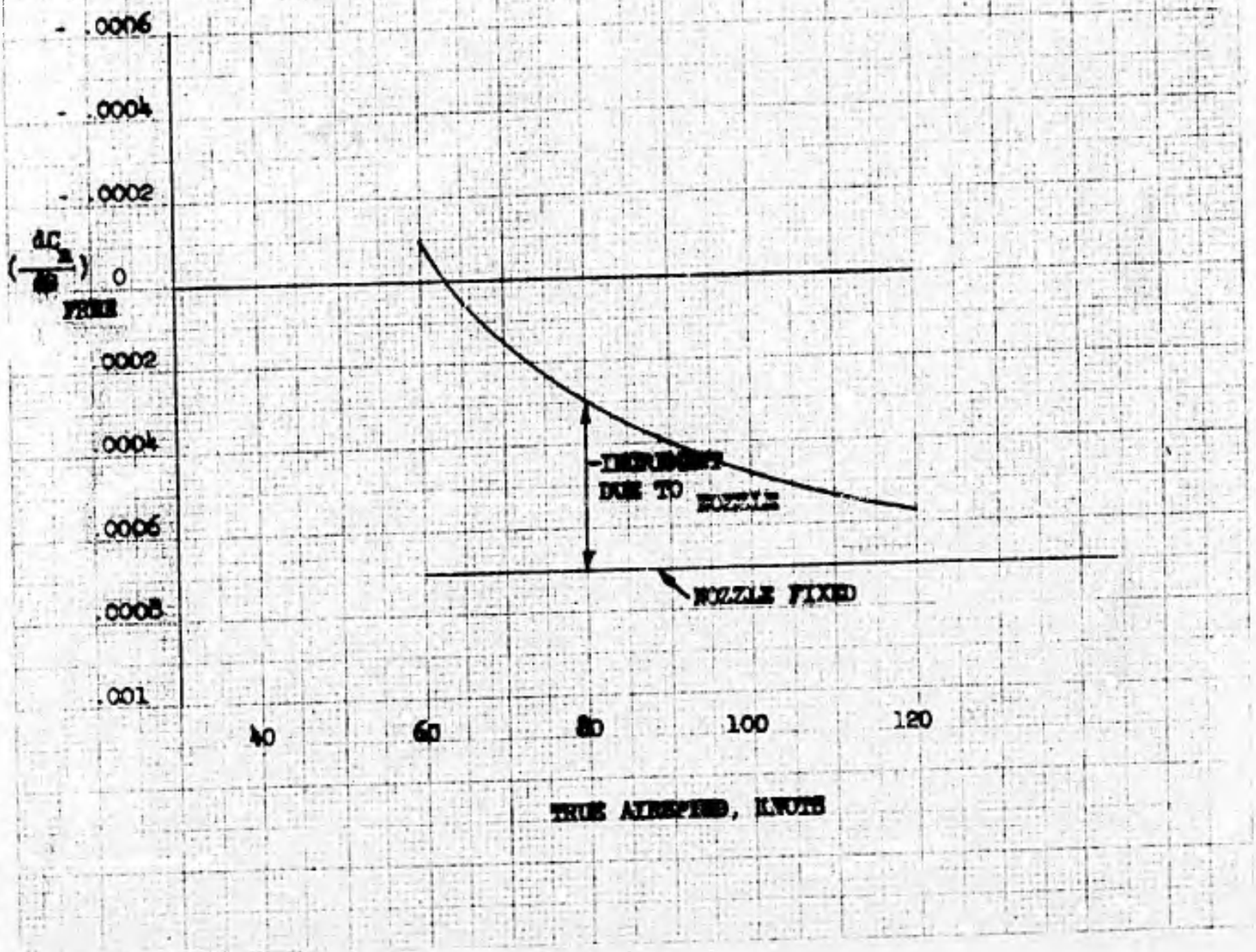

Figure 8.88

RYAN MODEL 92

VARIATION OF PEDAL FORCE GRADIENT WITH SPEED

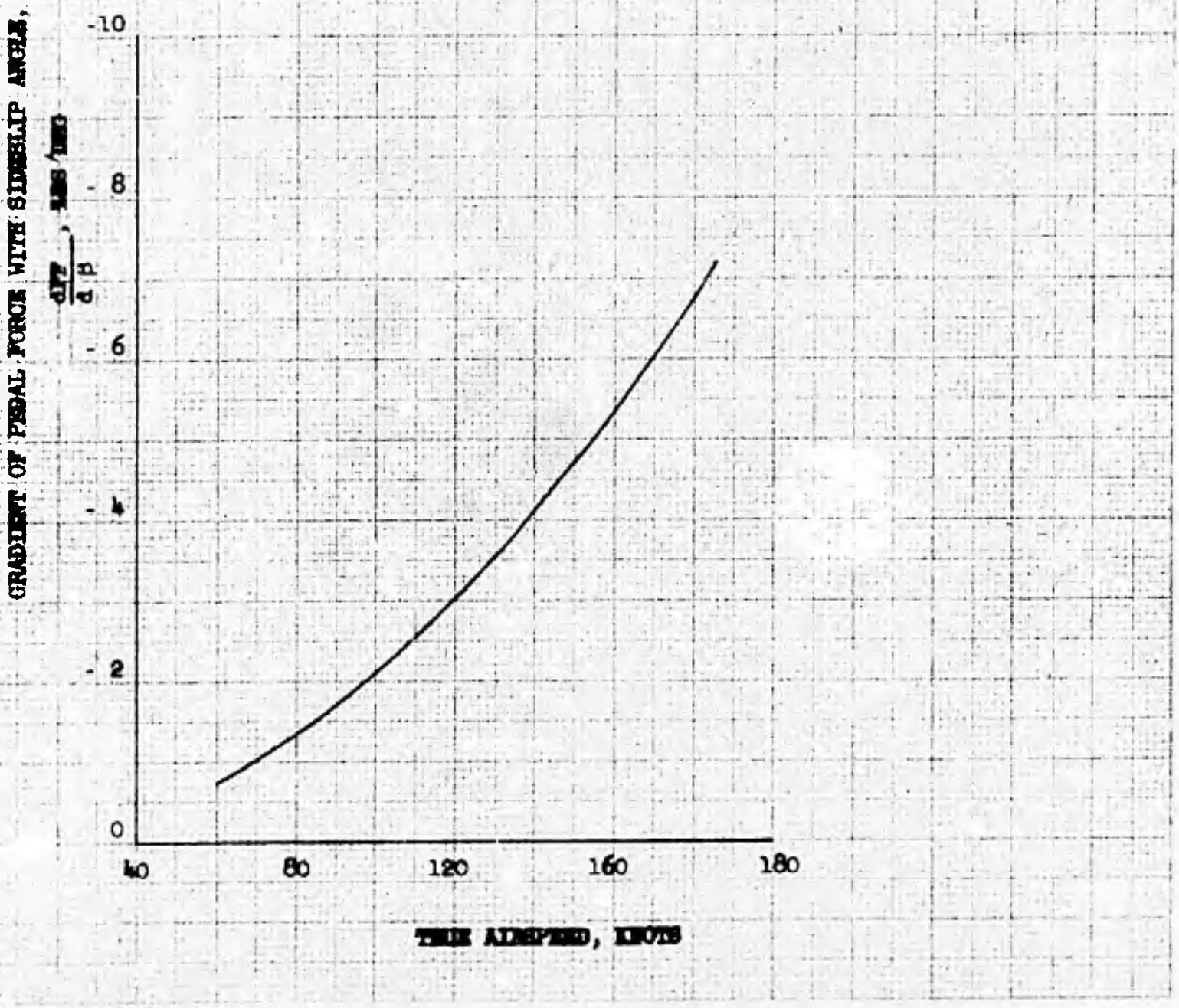

Figure 8.89

RYAN MODEL 98

ROLLING AND YAWING MOMENT COEFFICIENTS DUE TO SLOT-LIP AILERON DEFLECTION

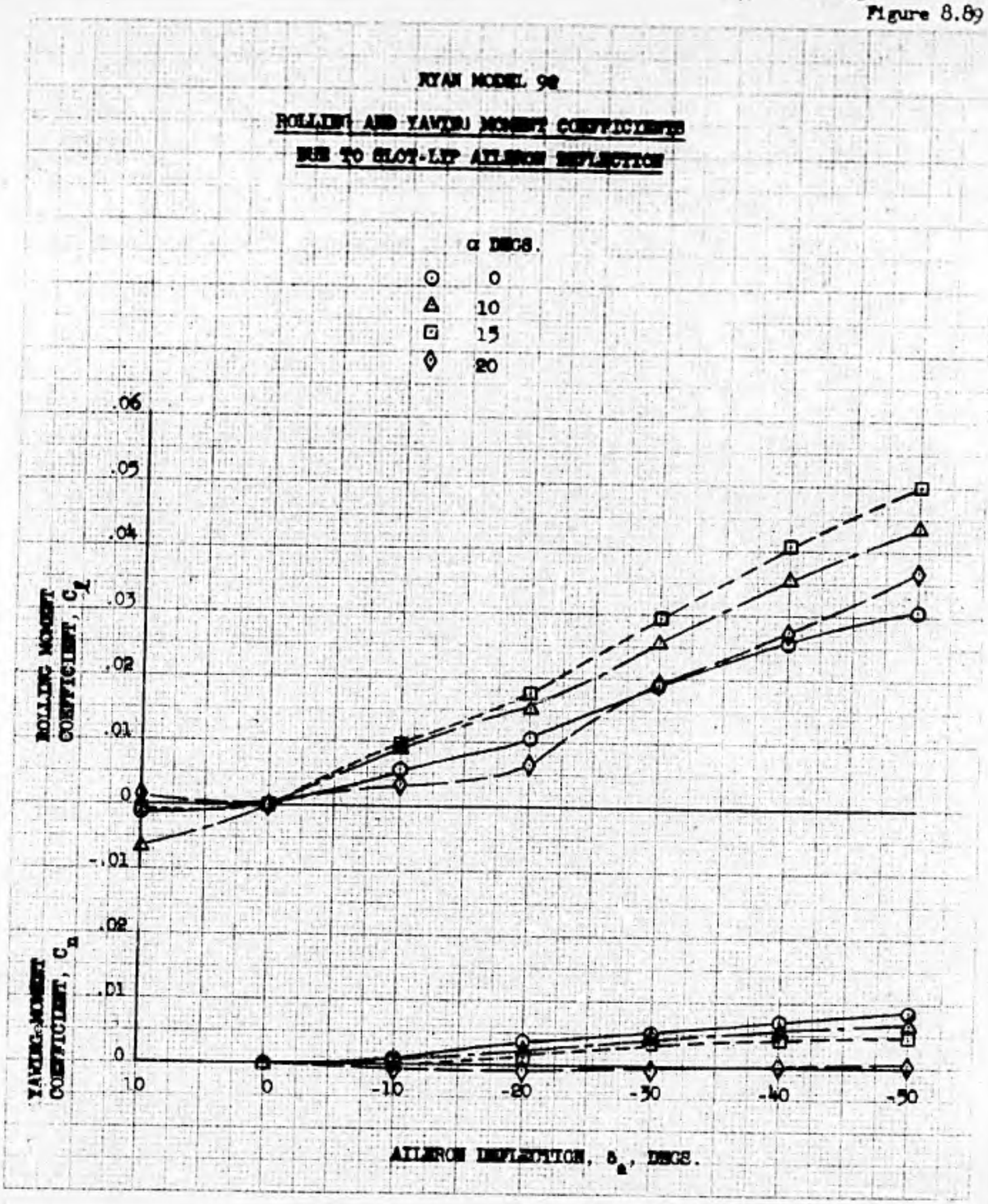

Figure 8.90

RYAN MODEL 92

HINGE MOMENT COEFFICIENT DUE TO SLOT-LIP AILERON DEFLECTION

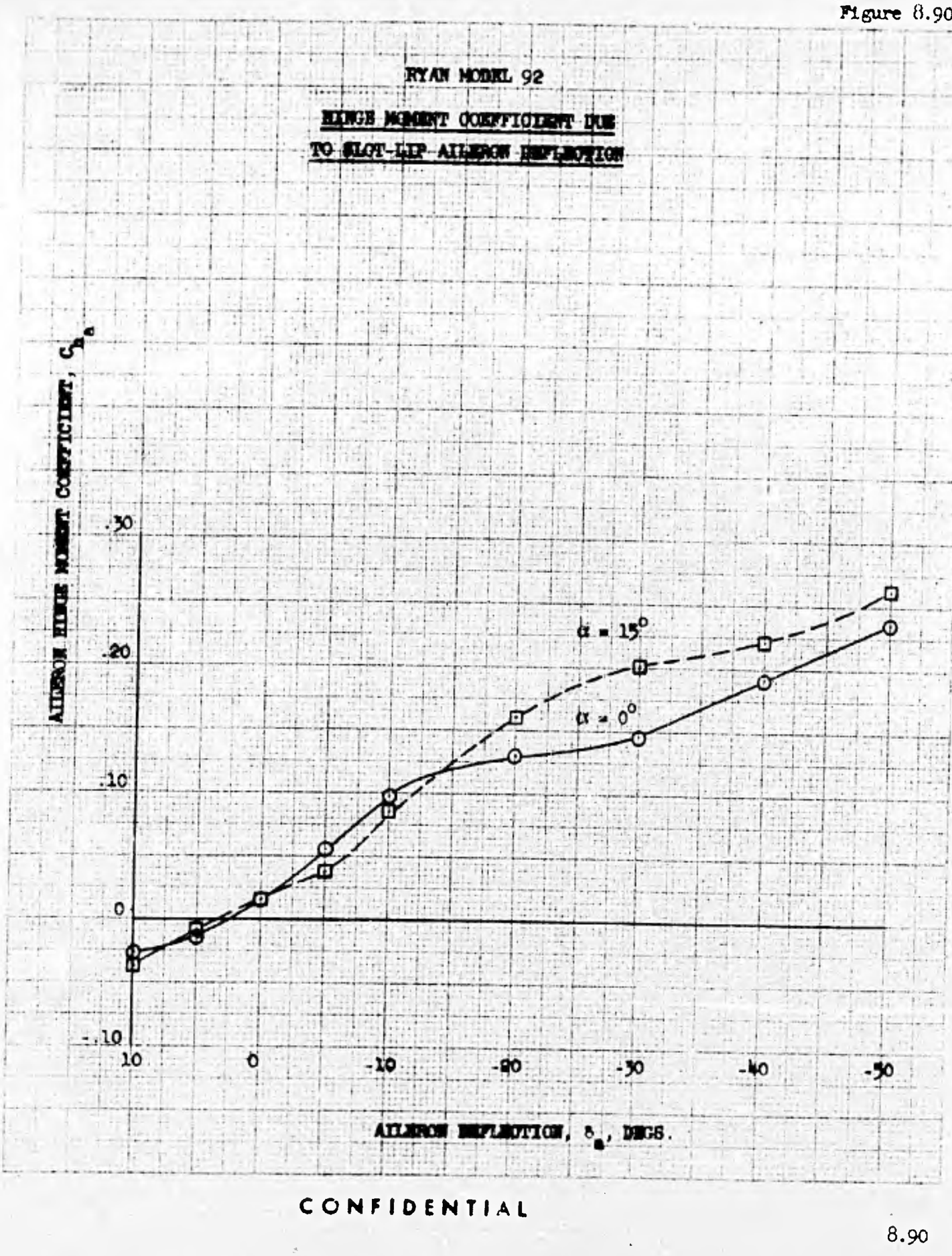

Figure 8.91

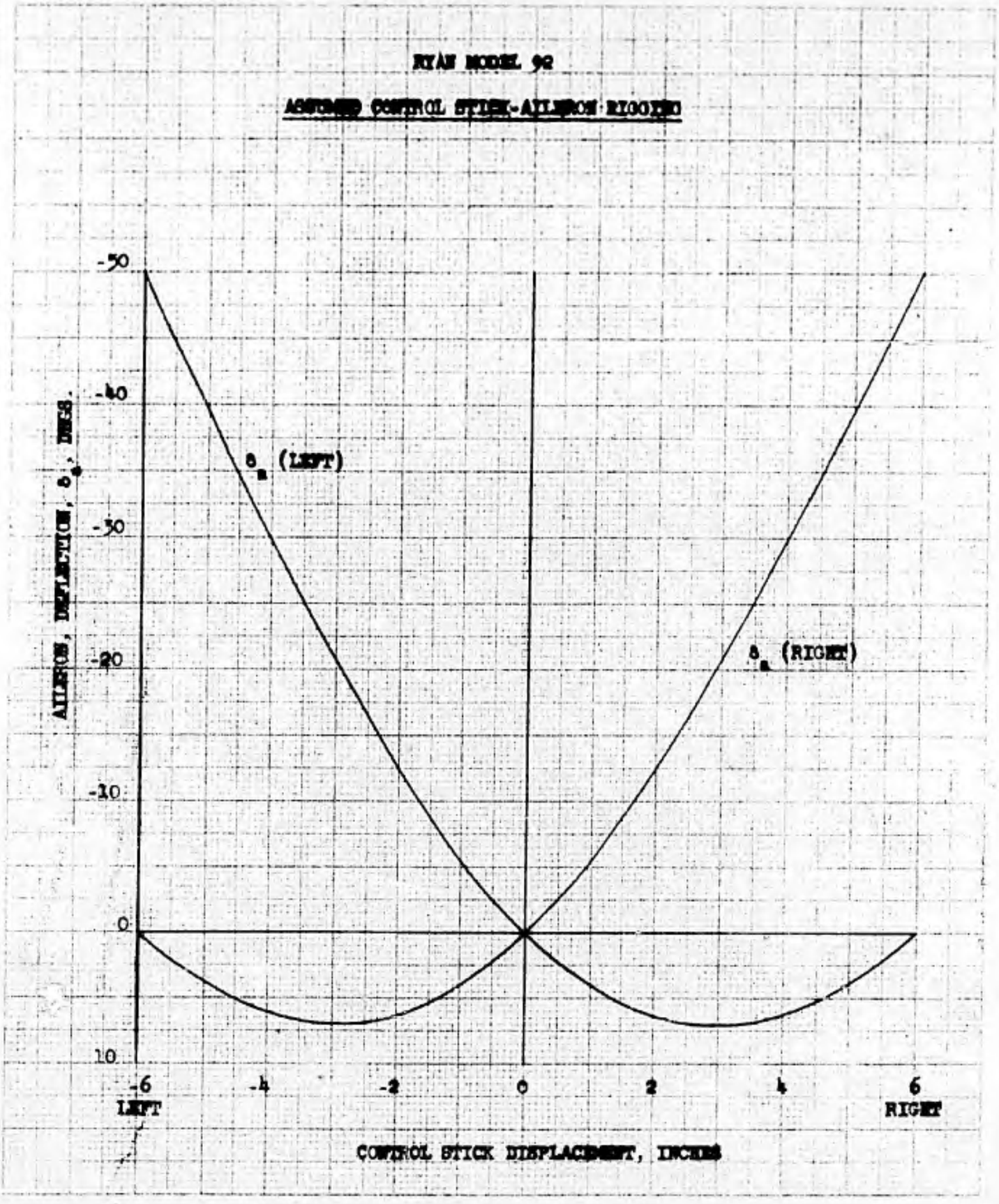
RYAN MODEL 92
ASSUMED CONTROL STICK-AILERON RIGGING
-50
-40
-30
-20
-10
0
10
AILERON DEFLECTION, δa, DEGS.
δa (LEFT)
δa (RIGHT)
-6
LEFT
-4
-2
0
2
4
6
RIGHT
CONTROL STICK DISPLACEMENT, INCHES

Figure 8.92

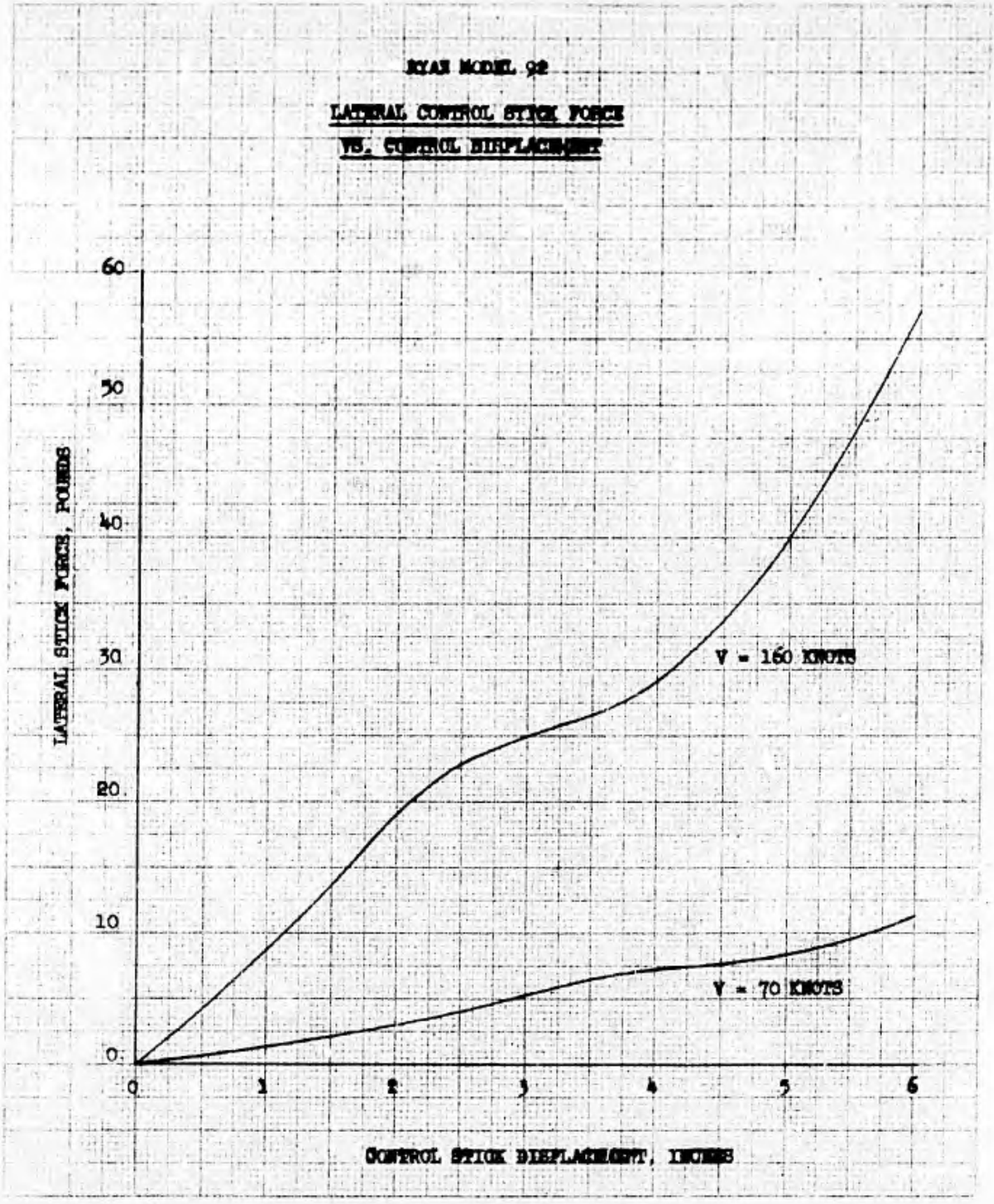
RYAN MODEL 92
LATERAL CONTROL STICK FORCE
VS. CONTROL DISPLACEMENT
LATERAL STICK FORCE, POUNDS
60
50
40
30
20
10
0
V = 160 KNOTS
V = 70 KNOTS
0
1
2
3
4
5
6
CONTROL STICK DISPLACEMENT, INCHES

Figure 8.93

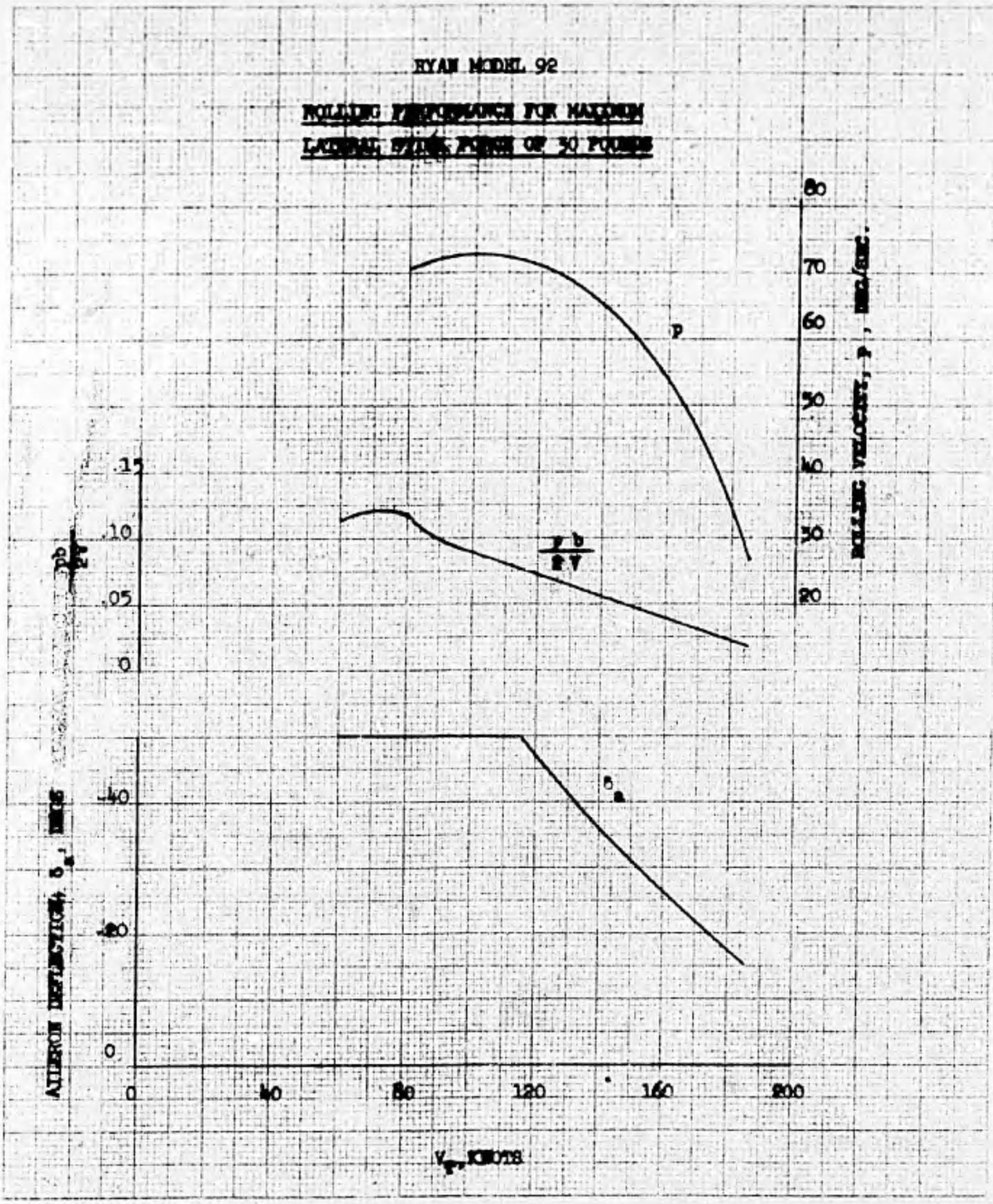
RYAN MODEL 92
ROLLING PERFORMANCE FOR MAXIMUM
LATERAL STICK FORCE OF 50 POUNDS
80
70
60
50
40
30
20
ROLLING VELOCITY, p, DEG/SEC.
p
$\frac{pb}{2V}$
.15
.10
.05
0
-40
-80
0
AILERON DEFLECTION, δ_a, DEG
δ_a
0
40
80
120
160
200
V_E, KNOTS

Figure 8.94

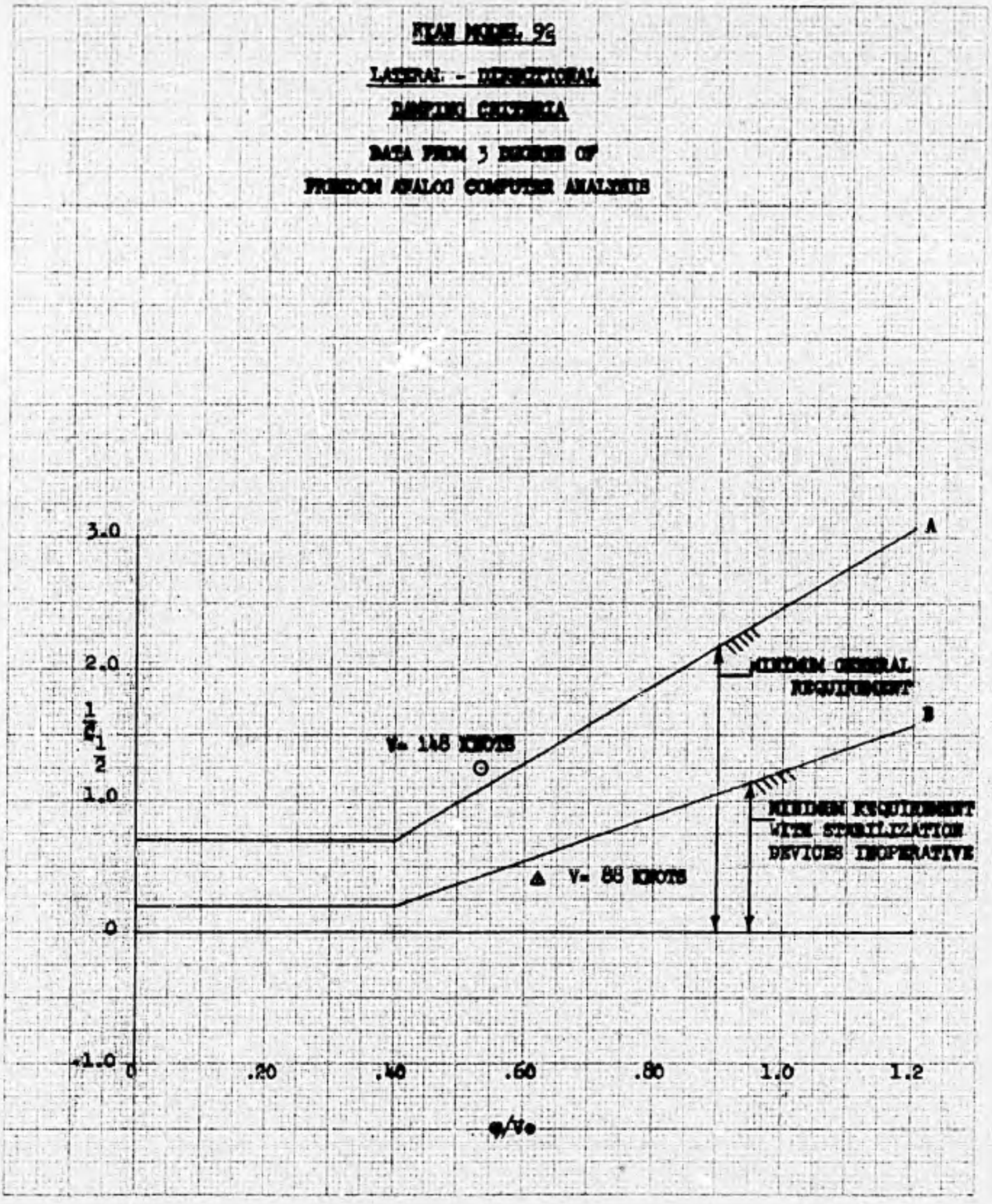
RYAN MODEL 92
LATERAL - DIRECTIONAL
DAMPING CRITERIA
DATA FROM 3 DEGREE OF
FREEDOM ANALOG COMPUTER ANALYSIS
3.0
2.0
1.0
0
-1.0
0
.20
.40
.60
.80
1.0
1.2
A
B
MINIMUM GENERAL
REQUIREMENT
V= 148 KNOTS
MINIMUM REQUIREMENT
WITH STABILIZATION
DEVICES INOPERATIVE
V= 88 KNOTS

Figure 8.95

RYAN MODEL 92

EFFECT OF SPEED ON LATERAL-DIRECTIONAL

DYNAMIC STABILITY

DATA FROM 5 DEGREE OF FREEDOM

ANALOG COMPUTER ANALYSIS

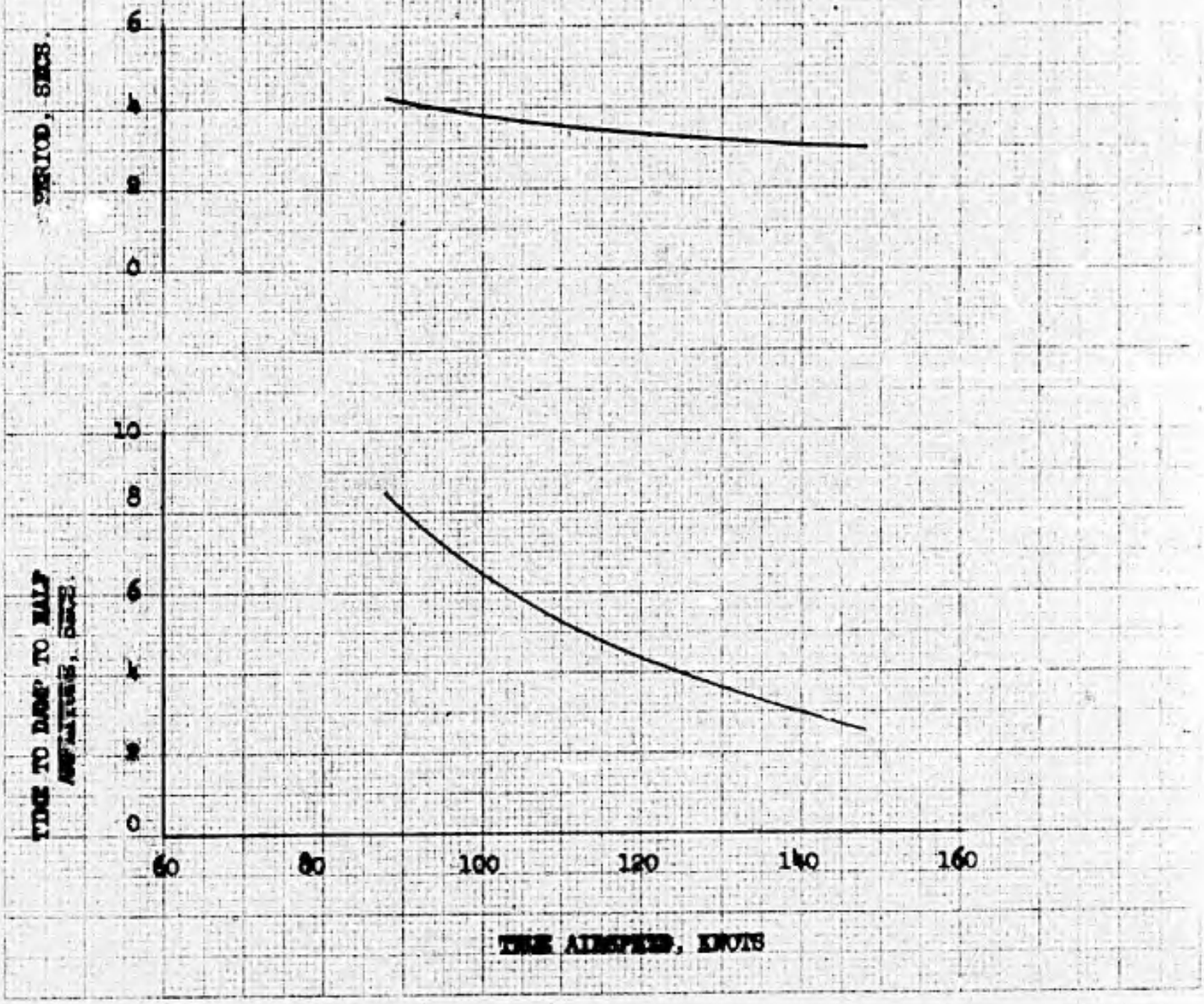

Figure 8.96

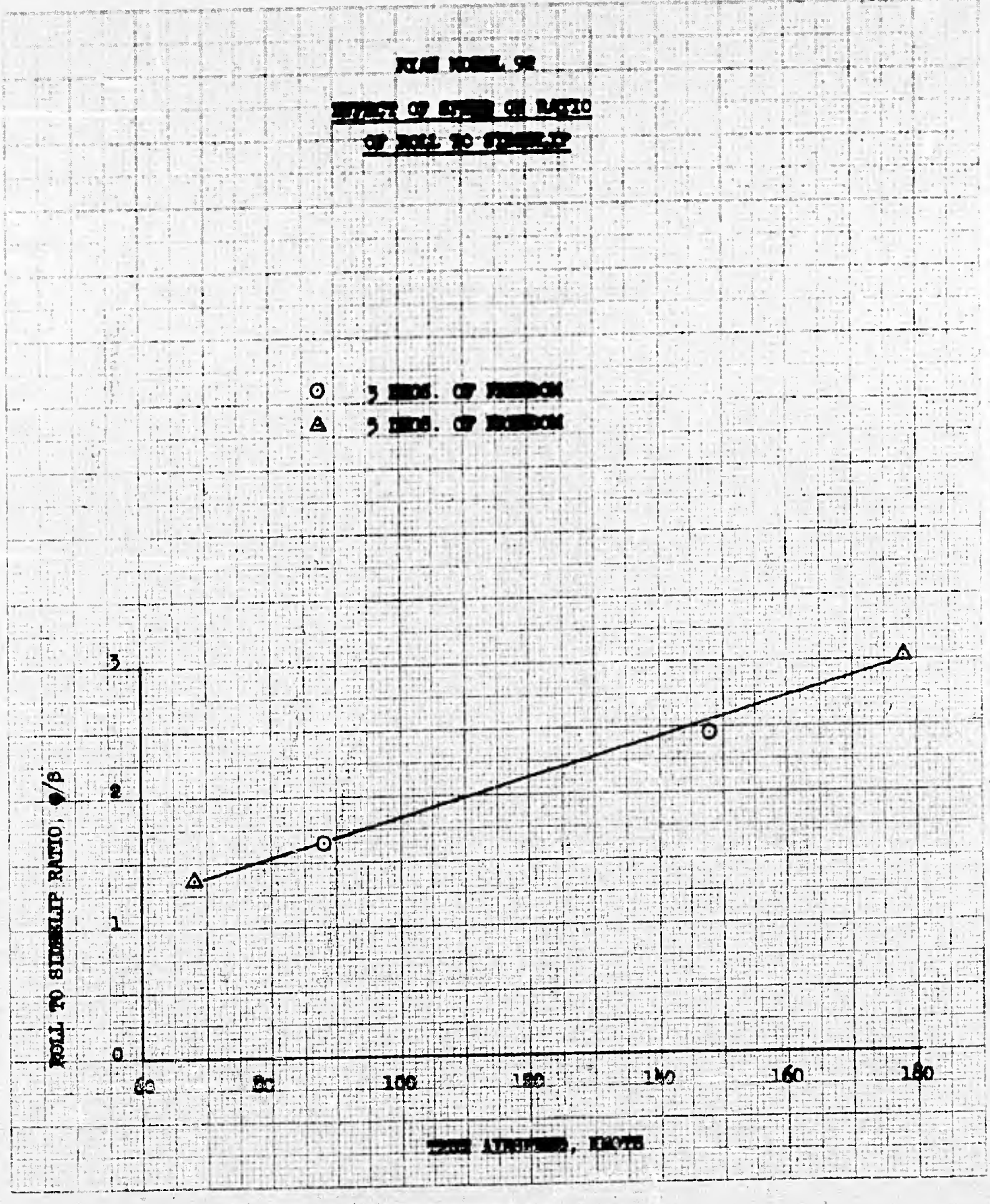
XL-80 MODEL SR
EFFECT OF SIDESLIP ON RATIO
OF ROLL TO SIDESLIP
○ 5 DEGS. OF FREEDOM
△ 5 DEGS. OF FREEDOM
ROLL TO SIDESLIP RATIO, ℓ/β
3
2
1
0
60
80
100
120
140
160
180

Figure 8.97

ANALOG SIMULATION TIME HISTORIES

5 Degrees of Freedom
V = 68 KNOTS

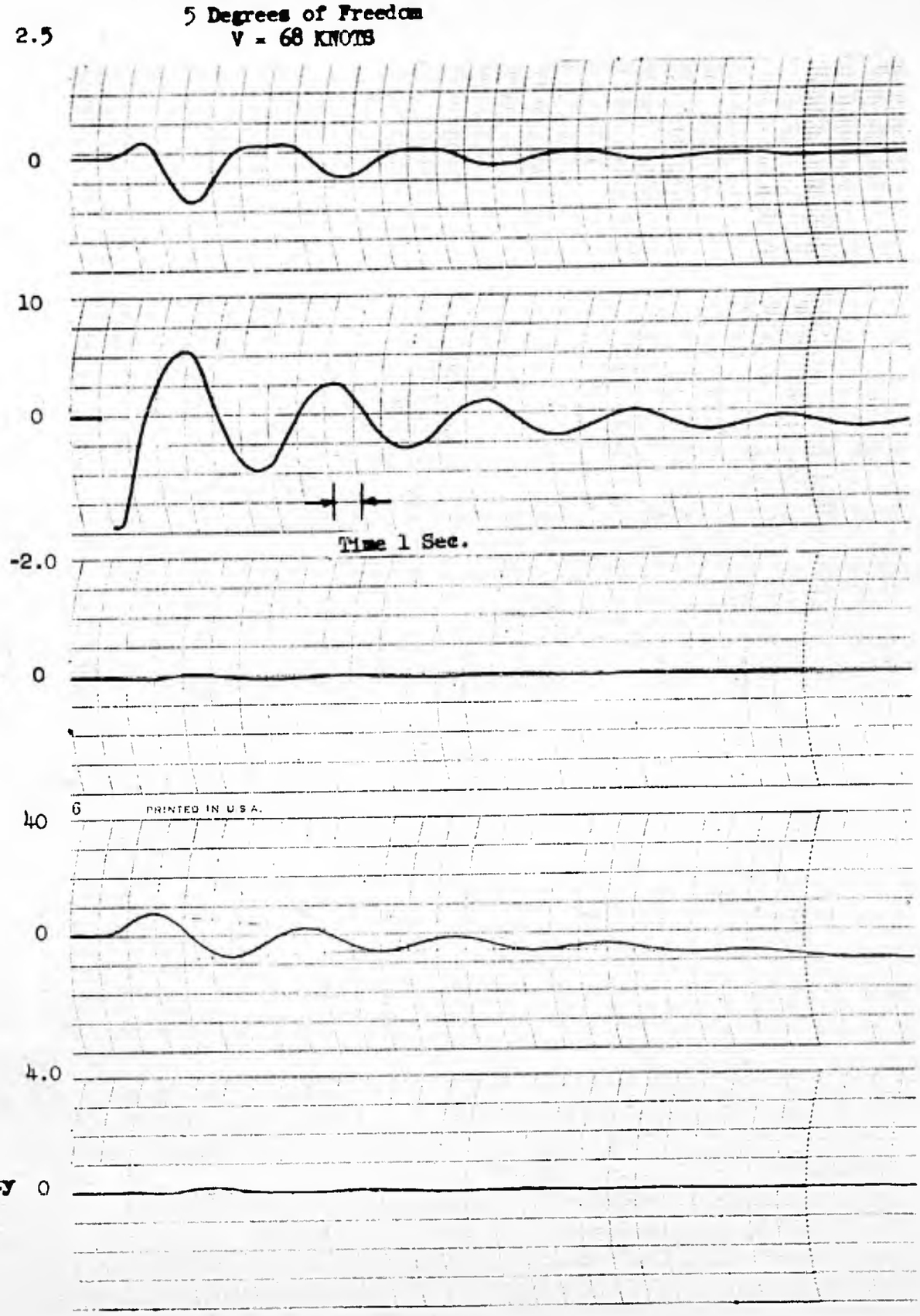

Figure 8.98

AFALCO SIMULATION TIME HISTORIES

5 Degrees of Freedom

V = 178 KNOTS

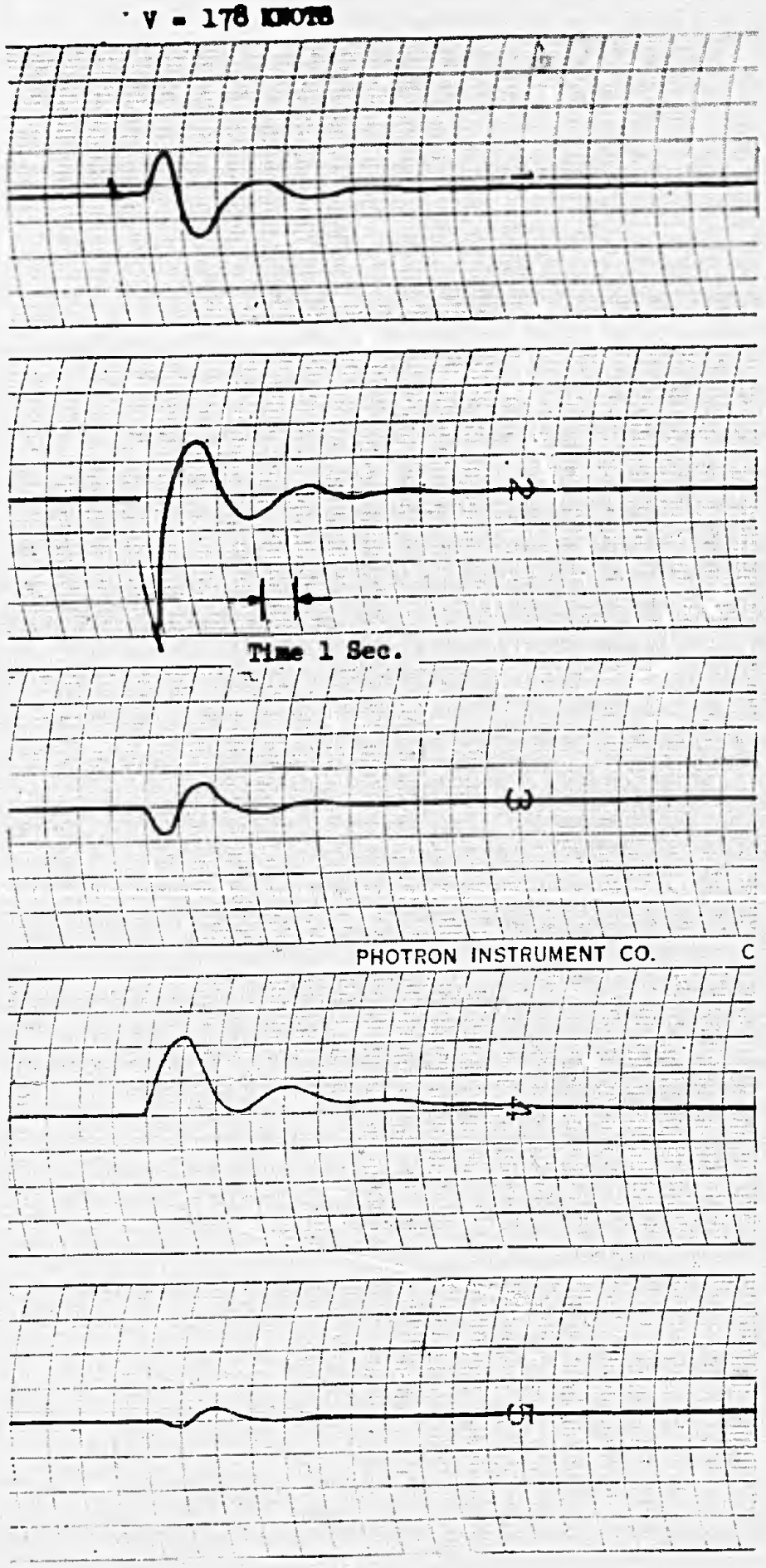

8.98

Figure 8.99

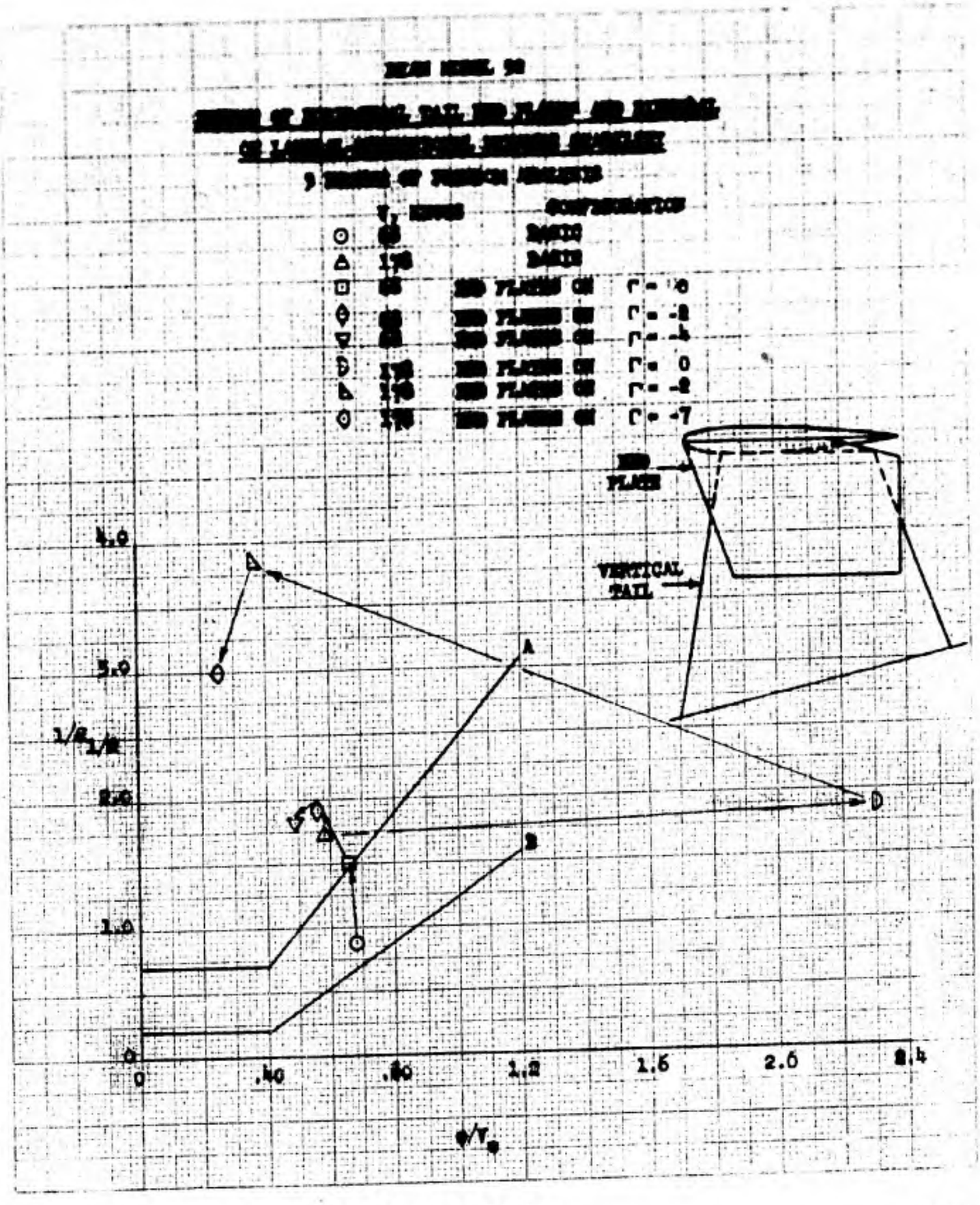

Figure 8.100

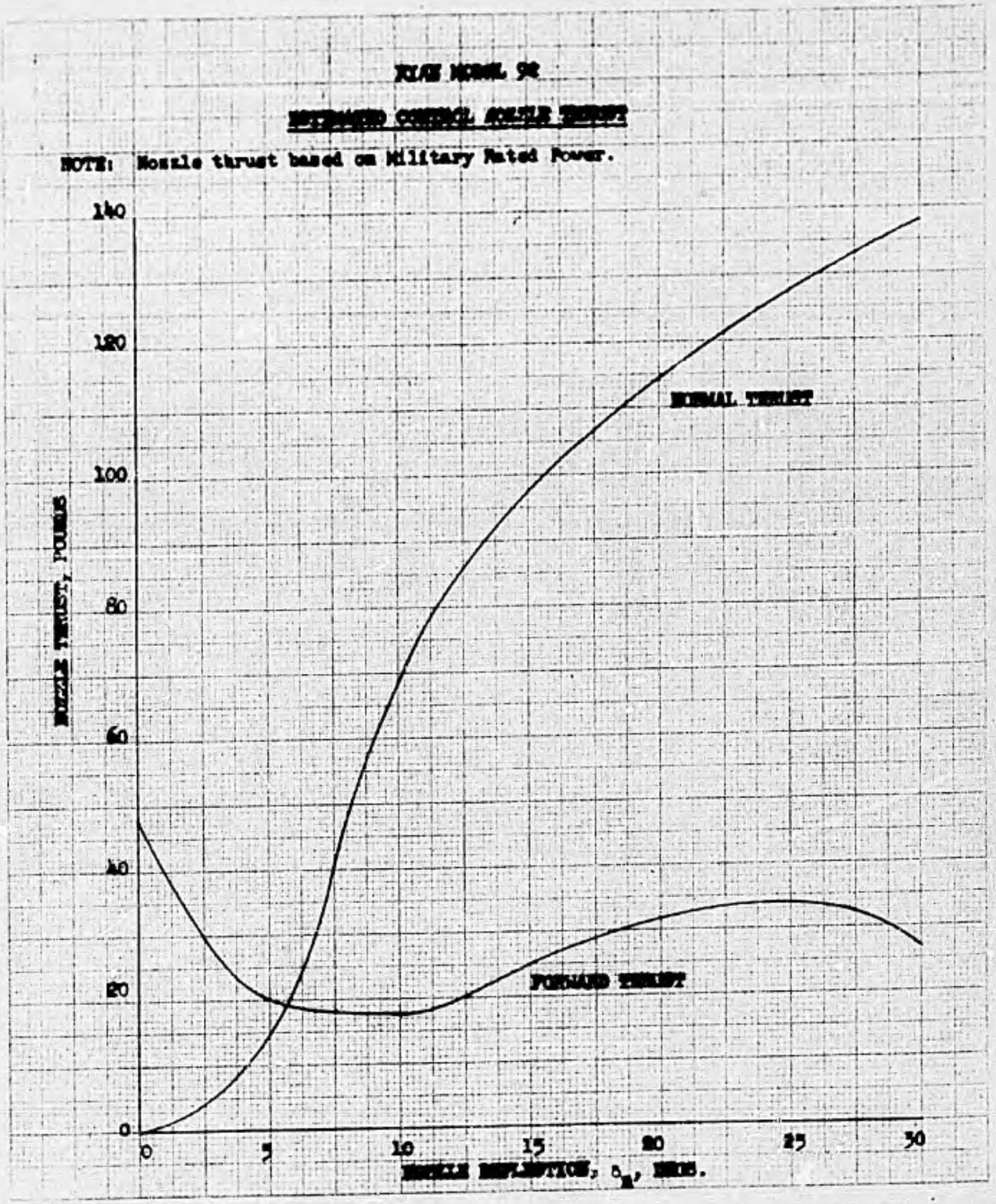
NOTE: Nozzle thrust based on Military Rated Power.
140
120
100
80
60
40
20
0
NOZZLE THRUST, POUNDS
NOMINAL THRUST
REVERSE THRUST
0
5
10
15
20
25
30
NOZZLE DEFLECTION, δ_N, DEG.

Figure 8.101

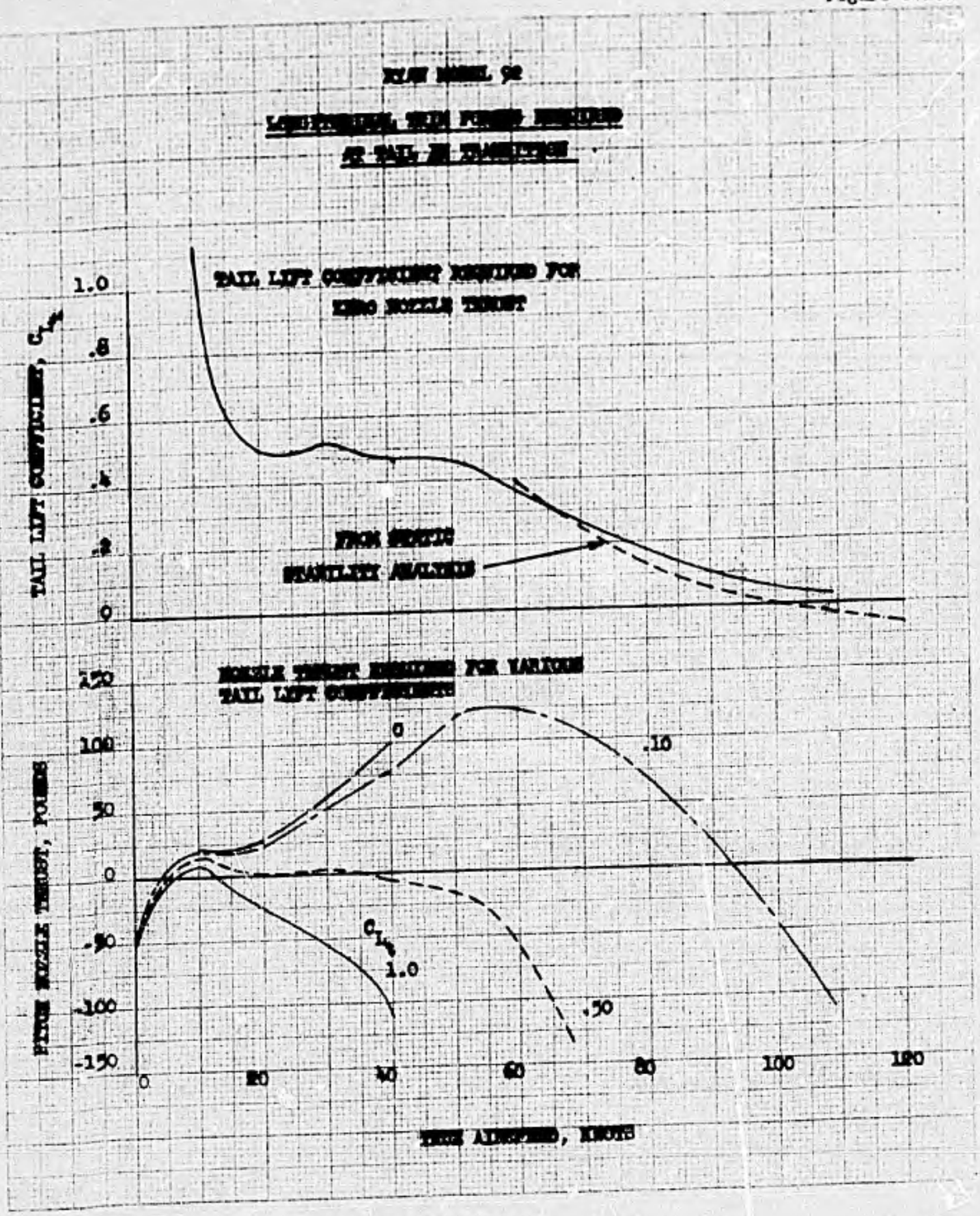
TAIL LIFT COEFFICIENT REQUIRED FOR
ZERO NOZZLE THRUST
FROM STATIC
STABILITY ANALYSIS
NOZZLE THRUST REQUIRED FOR VARIOUS
TAIL LIFT COEFFICIENTS
TAIL LIFT COEFFICIENT, C_{L_t}
1.0
.8
.6
.4
.2
0
200
100
50
0
-50
-100
-150
0
.10
C_{L_t}
1.0
.50
20
40
60
80
100
120
TRUE AIRSPEED, KNOTS

Figure 8.102

XIAN MODEL 92

YAW ENGINE THRUST REQUIRED TO TRIM YAWING MOMENT
DUE TO DIFFERENTIAL PITCH CONTROL

$\Delta i_p = 1.5°$

FULL RUDDER CONTROL IN

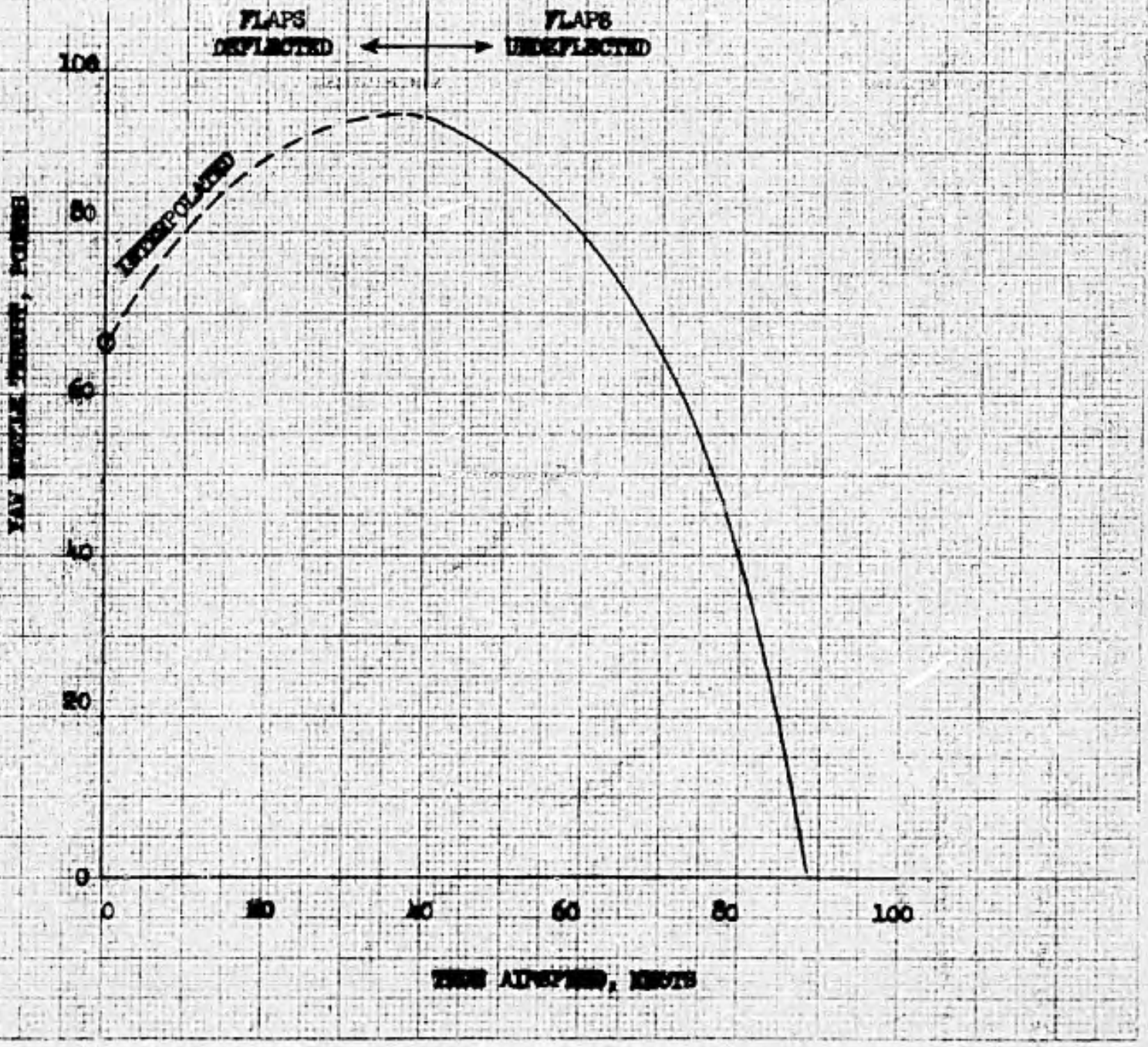

AD 301870